

AD-R141 046

MULTIVARIABLE DIGITAL CONTROL LAWS FOR THE UH-60A BLACK

1/3

HAWK HELICOPTER(U) AIR FORCE INST OF TECH

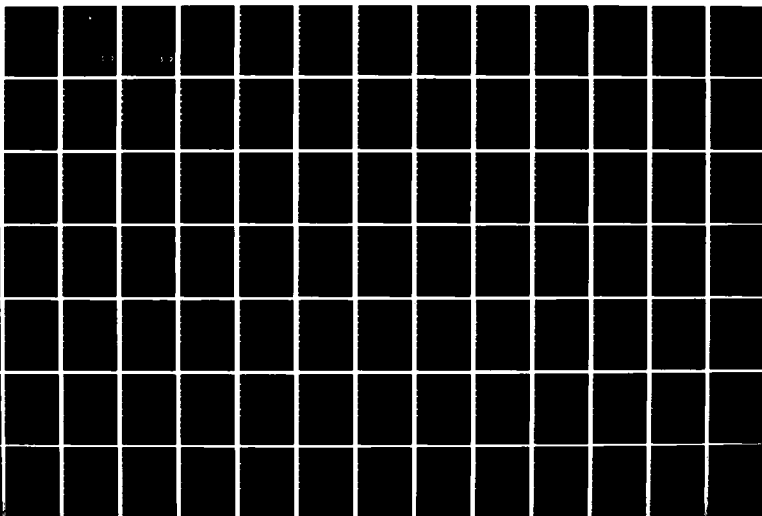
WRIGHT-PATTERSON AFB OH SCHOOL OF ENGINEERING

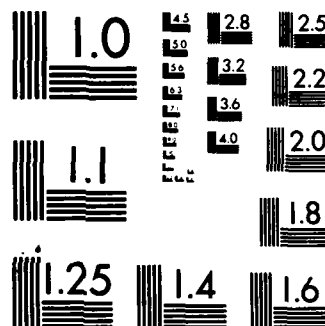
UNCLASSIFIED

B H MAYHEW MAR 84 AFIT/GE/EE/84M-6

F/G 1/3

NL





MICROCOPY RESOLUTION TEST CHART  
NATIONAL BUREAU OF STANDARDS-1963-A

AD-A141 046



MULTIVARIABLE DIGITAL CONTROL LAWS FOR THE  
UH-60A BLACK HAWK HELICOPTER

THESIS

AFIT/GE/EE/84M-6 Brian H. Mayhew  
2nd Lt USAF

DTIC FILE COPY

DTIC  
ELECTE  
MAY 15 1984

DEPARTMENT OF THE AIR FORCE  
AIR UNIVERSITY (ATC)

**AIR FORCE INSTITUTE OF TECHNOLOGY**

Wright-Patterson Air Force Base, Ohio

**DISTRIBUTION STATEMENT A**

Approved for public release

84 05 14 120

AFIT/GE/EE/84M-6

MULTIVARIABLE DIGITAL CONTROL LAWS FOR THE  
UH-60A BLACK HAWK HELICOPTER

THESIS

AFIT/GE/EE/84M-6 Brian H. Mayhew  
2nd Lt USAF

DTIC  
ELECTE  
MAY 15 1984  
S B D

Approved for public release; distribution unlimited.



AFIT/GE/EE/84M-6

MULTIVARIABLE DIGITAL CONTROL LAWS FOR THE  
UH-60A BLACK HAWK HELICOPTER

THESIS

Presented to the Faculty of the School of Engineering  
of the Air Force Institute of Technology

Air University

in Partial Fulfillment of the  
Requirements for the Degree of  
Master of Science

by

Brian H. Mayhew, B.S.

2nd Lt

USAF

Graduate Electrical Engineer

March 1984

Approved for public release; distribution unlimited.

## Preface

This thesis topic was chosen for two main reasons. First, it is in an area which parallels my graduate studies in flight control and advanced control theory. Second, I wanted an aircraft, in this case a helicopter, that would test the limits of the design technique as well as an aircraft that had not previously been designed for with this method. I would like to thank Duane P. Rubertus of the Flight Dynamics Laboratory and E. Robert Lemble of the Flight Control Division, Ames Research Center for generating and sponsoring this thesis topic.

The theoretical background is based on multivariable control law techniques developed by Professor Brian Porter from the University of Salford, England. I would like to express my appreciation to Professor John J. D'Azzo of the Department of Electrical Engineering at the Air Force Institute of Technology. The thesis would not have been possible without his guidance and suggestions.

This research was accomplished with four fellow students. I would like to thank Capt. Bill Locken, 2Lt Mark Hoffman, 1Lt Jeffrey Simmers, and 2Lt Scott Feldmann for their assistance and guidance.

Finally, I want to express my love and appreciation to my wife, Ellen, for her patience and understanding during this research effort.

2Lt Brian H. Mayhew

## Contents

	Page
Preface . . . . .	ii
List of Figures . . . . .	v
List of Tables . . . . .	xvi
List of Symbols . . . . .	xviii
Abstract . . . . .	xxvi
I. Introduction . . . . .	1
Background . . . . .	1
Problem . . . . .	2
Approach . . . . .	2
Assumptions . . . . .	3
Presentation . . . . .	4
II. UH-60A Black Hawk Model . . . . .	5
Actuator Models . . . . .	13
Trim Conditions . . . . .	15
III. Multivariable Control Law Theory . . . . .	22
Overview . . . . .	22
Regular Versus Irregular Design . . . . .	24
Asymptotic Characteristics . . . . .	29
Transmission Zones . . . . .	35
Measurement Matrix Elements . . . . .	36
Closed-Loop Roots . . . . .	37
MULTI Computer-Aided Design . . . . .	39
IV. Individual Multivariable Digital Control	
Laws and Results . . . . .	41
Requirements . . . . .	41
Inputs and Outputs . . . . .	41
Controllability and Observability . . . . .	42
Transmission Zeros . . . . .	42
Integral Plus Proportional Compensation . . . . .	44
A Design Procedure . . . . .	46
Open Loop Stability . . . . .	48
Yaw Rate Command System . . . . .	51
Coordinated Turn Command System . . . . .	78
Vertical Rate Command System . . . . .	106

V. Robust Controller Design . . . . .	144
Design Methodology . . . . .	145
Yaw Rate Command System . . . . .	146
Coordinated Turn Command System . . . . .	157
Vertical Rate Command System . . . . .	170
VI. Conclusions and Recommendations . . . . .	192
Thesis Summary . . . . .	192
Conclusions . . . . .	193
Recommendations . . . . .	194
Bibliography . . . . .	196
Appendix A: Nonlinear Simulation of a Symmetrical Aircraft . . .	A-1
Appendix B: Coordinated Turn With Computation Delay . . . . .	B-1
Vita . . . . .	232

Accession For	
NTIS GRA&I	<input checked="checked" type="checkbox"/>
DTIC TAB	<input type="checkbox"/>
Unannounced	<input type="checkbox"/>
Justification	
By	
Distribution/	
Availability Codes	
Dist	Avail and/or Special
A-1	



# List of Figures

<u>Figure</u>		<u>Page</u>
1	Helicopter Lift Vectors . . . . .	11
2	System Block Diagram - Continuous Design . . . . .	26
3	System Block Design - Discrete Design . . . . .	27
4a	Output Responses, $w_B$ (ft/sec) and $r_B$ (rad/sec), for the Yaw Rate Command System ( $V_{EAS} = 20$ knots). . . . .	55
4b	Output Response, $p_B$ , for the Yaw Rate Command System ( $V_{EAS} = 20$ knots). . . . .	56
4c	Output Response, $\theta$ , for the Yaw Rate Command System ( $V_{EAS} = 20$ knots). . . . .	56
4d	State Responses, $\phi$ (rad.) and $q_B$ (rad/sec) for the Yaw Rate Command System ( $V_{EAS} = 20$ knots) . . . . .	57
4e	State Responses, $u_B$ and $v_B$ , for the Yaw Rate Command System ( $V_{EAS} = 20$ knots). . . . .	57
4f	Longitudinal Control Surface Responses, $\Delta\delta_e$ and $\Delta\delta_c$ , for the Yaw Rate Command System ( $V_{EAS} = 20$ knots). . . . .	58
4g	Lateral Control Surface Responses, $\Delta\delta_a$ and $\Delta\delta_p$ , for the Yaw Rate Command System ( $V_{EAS} = 20$ knots). . . . .	58
5a	Output Responses, $\theta$ (rad.) and $p_B$ (rad/sec), for the Yaw Rate Command System With Actuators ( $V_{EAS} = 40$ knots) . . . . .	63
5b	Output Responses, $w_B$ (ft/sec) and $r_B$ (rad/sec), for the Yaw Rate Command System With Actuators ( $V_{EAS} = 40$ knots) . . . . .	63
5c	State Responses, $\phi$ (rad.) and $q_B$ (rad/sec) for the Yaw Rate Command System With Actuators ( $V_{EAS} = 40$ knots) . . . . .	64
5d	State Responses, $u_B$ and $v_B$ , for the Yaw Rate Command System With Actuators ( $V_{EAS} = 40$ knots) . . . . .	64
5e	Longitudinal Control Surface Responses, $\Delta\delta_e$ and $\Delta\delta_c$ , for the Yaw Rate Command System ( $V_{EAS} = 40$ knots) . . . . .	65
5f	Lateral Control Surface Responses, $\Delta\delta_a$ and $\Delta\delta_p$ , for the Yaw Rate Command System With Actuators ( $V_{EAS} = 40$ knots) . . . . .	65

6a	Output Response, $\theta$ , for the Yaw Rate Command System ( $V_{EAS} = 60$ knots) . . . . .	68
6b	Output Response, $p_B$ , for the Yaw Rate Command System ( $V_{EAS} = 60$ knots) . . . . .	68
6c	Output Response, $w_B$ , for the Yaw Rate Command System ( $V_{EAS} = 60$ knots) . . . . .	69
6d	Output Response, $r_B$ , for the Yaw Rate Command System ( $V_{EAS} = 60$ knots) . . . . .	69
6e	State Responses, $u_B$ and $v_B$ , for the Yaw Rate Command System ( $V_{EAS} = 60$ knots) . . . . .	70
6f	State Responses, $\phi$ (rad.) and $q_B$ (rad/sec) for the Yaw Rate Command System ( $V_{EAS} = 60$ knots) . . . . .	70
6g	Longitudinal Control Surface Responses, $\Delta\delta_e$ and $\Delta\delta_c$ , for the Yaw Rate Command System ( $V_{EAS} = 60$ knots). . . . .	71
6h	Lateral Control Surface Responses, $\Delta\delta_a$ and $\Delta\delta_p$ , for the Yaw Rate Command System ( $V_{EAS} = 60$ knots) . . . . .	71
7a	Output Response, $\theta$ , for the Yaw Rate Command System With Actuators ( $V_{EAS} = 60$ knots) . . . . .	74
7b	Output Response, $p_B$ , for the Yaw Rate Command System With Actuators ( $V_{EAS} = 60$ knots) . . . . .	74
7c	Output Response, $w_B$ , for the Yaw Rate Command System With Actuators ( $V_{EAS} = 60$ knots) . . . . .	75
7d	Output Response, $r_B$ , for the Yaw Rate Command System With Actuators ( $V_{EAS} = 60$ knots) . . . . .	75
7e	State Responses, $\phi$ (rad.) and $q_B$ (rad/sec) for the Yaw Rate Command System With Actuators ( $V_{EAS} = 60$ knots). . . . .	76
7f	State Responses, $u_B$ and $v_B$ , for the Yaw Rate Command System ( $V_{EAS} = 60$ knots) . . . . .	76
7g	Longitudinal Control Surface Responses, $\Delta\delta_e$ and $\Delta\delta_c$ , for the Yaw Rate Command System With Actuators ( $V_{EAS} = 60$ knots) . . . . .	77
7h	Lateral Control Surface Responses, $\Delta\delta_a$ and $\Delta\delta_p$ , for the Yaw Rate Command System With Actuators ( $V_{EAS} = 60$ knots) . . . . .	77
8a	Output Response, $\phi$ , for the Coordinated Turn Command System ( $V_{EAS} = 60$ knots) . . . . .	82

8b	Output Response, $\theta$ , for the Coordinated Turn Command System ( $V_{EAS} = 60$ knots) . . . . .	83
8c	Output Responses, $v_B$ and $w_B$ , for the Coordinated Turn Command System ( $C_{EAS} = 60$ knots) . . . . .	83
8d	State Response, $u_B$ , for the Coordinated Turn Command System ( $V_{EAS} = 60$ knots) . . . . .	84
8e	State Responses, $p_B$ , $q_B$ , and $r_B$ , for the Coordinated Turn Command System ( $V_{EAS} = 60$ knots) . . . . .	84
8f	Longitudinal Control Surface Responses $\Delta\delta_e$ and $\Delta\delta_c$ , for the Coordinated Turn Command System ( $V_{EAS} = 60$ knots) . . . . .	85
8g	Lateral Control Surface Responses, $\Delta\delta_a$ and $\Delta\delta_p$ , for the Coordinated Turn Command System ( $V_{EAS} = 60$ knots) . . . . .	85
9a	Output Response, $\phi$ , for the Coordinated Turn Command System ( $V_{EAS} = 100$ knots) . . . . .	90
9b	Output Response, $\theta$ , for the Coordinated Turn Command System ( $V_{EAS} = 100$ knots) . . . . .	91
9c	Output Responses, $v_B$ and $w_B$ , for the Coordinated Turn Command System ( $V_{EAS} = 100$ knots) . . . . .	91
9d	State Response, $u_B$ , for the Coordinated Turn Command System ( $V_{EAS} = 100$ knots) . . . . .	92
9e	State Responses, $p_B$ , $q_B$ , and $r_B$ , for the Coordinated Turn Command System ( $V_{EAS} = 100$ knots) . . . . .	92
9f	Longitudinal Control Surface Responses, $\Delta\delta_e$ and $\Delta\delta_c$ , for the Coordinated Turn Command System ( $V_{EAS} = 100$ knots) . . . . .	93
9g	Lateral Control Surface Responses, $\Delta\delta_a$ and $\Delta\delta_p$ , for the Coordinated Turn Command System ( $V_{EAS} = 100$ knots) . . . . .	93
10a	Output Response, $\phi$ , for the Coordinated Turn Command System ( $V_{EAS} = 140$ knots) . . . . .	96
10b	Output Response, $\theta$ , for the Coordinated Turn Command System ( $V_{EAS} = 140$ knots) . . . . .	97
10c	Output Responses, $v_B$ and $w_B$ , for the Coordinated Turn Command System ( $V_{EAS} = 140$ knots) . . . . .	97
10d	State Response, $u_B$ , for the Coordinated Turn Command System ( $V_{EAS} = 140$ knots) . . . . .	98

10e	State Responses, $p_B$ , $q_B$ , and $r_B$ , for the Coordinated Turn Command System ( $V_{EAS} = 140$ knots) . . . . .	98
10f	Longitudinal Control Surface Responses $\Delta\delta_e$ and $\Delta\delta_c$ , for the Coordinated Turn Command System ( $V_{EAS} = 140$ knots) . . . . .	99
10g	Lateral Control Surface Responses, $\Delta\delta_a$ and $\Delta\delta_p$ , for the Coordinated Turn Command System ( $V_{EAS} = 140$ knots) . . . . .	99
11a	Output Response, $\theta$ , for the Coordinated Turn Command System With Actuators ( $V_{EAS} = 140$ knots) . . . . .	101
11b	Output Response, $\phi$ , for the Coordinated Turn Command System With Actuators ( $V_{EAS} = 140$ knots) . . . . .	101
11c	Output Responses, $v_B$ and $w_B$ , for the Coordinated Turn Command System With Actuators ( $V_{EAS} = 140$ knots) . . . . .	102
11d	State Response, $u_B$ , and Output Response, $v_B$ , for the Coordinated Turn Command System With Actuators ( $V_{EAS} = 140$ knots) . . . . .	102
11e	State Response, $u_B$ , for the Coordinated Turn Command System With Actuators ( $V_{EAS} = 140$ knots) . . . . .	103
11f	State Responses, $p_B$ , $q_B$ , and $r_B$ , for the Coordinated Turn Command System With Actuators ( $V_{EAS} = 140$ knots) . . . . .	103
11g	Longitudinal Control Surface Responses $\Delta\delta_e$ and $\Delta\delta_c$ , for the Coordinated Turn Command System With Actuators ( $V_{EAS}=140$ knots) . . . . .	104
11h	Lateral Control Surface Responses, $\Delta\delta_a$ and $\Delta\delta_p$ , for the Coordinated Turn Command System With Actuators ( $V_{EAS} = 140$ knots) . . . . .	104
12a	Output Responses, $h_E$ and $w_B$ , and State Responses, $u_B$ and $v_B$ , for the Vertical Rate Command System ( $V_{EAS} = 20$ knots) . . . . .	112
12b	Output Responses, $\theta$ and $\phi(\text{rad})$ and $r_B(\text{rad/sec})$ for the Vertical Rate Command System ( $V_{EAS} = 20$ knots) . . . . .	113
12c	State Responses, $p_B$ and $q_B$ , for the Vertical Rate Command System ( $V_{EAS} = 20$ knots) . . . . .	113
12d	Longitudinal Control Surface Responses, $\Delta\delta_e$ and $\Delta\delta_c$ , for the Vertical Rate Command System ( $V_{EAS} = 20$ knots) . . . . .	114



12e	Lateral Control Surface Responses, $\Delta\delta_a$ and $\Delta\delta_p$ , for the Vertical Rate Command System ( $V_{EAS} = 20$ knots) . . . . .	114
13a	Output Responses, $h_E$ and $w_B$ , and State Responses, $u_B$ and $v_B$ , for the Vertical Rate Command System ( $V_{EAS} = 40$ knots) . . . . .	117
13b	Output Responses, $\theta$ and $\phi$ (rad) and $r_B$ (rad/sec) for the Vertical Rate Command System ( $V_{EAS} = 40$ knots) . . . .	118
13c	State Responses, $p_B$ and $q_B$ , for the Vertical Rate Command System ( $V_{EAS} = 40$ knots) . . . . .	118
13d	Longitudinal Control Surface Responses, $\Delta\delta_e$ and $\Delta\delta_c$ , for the Vertical Rate Command System ( $V_{EAS} = 40$ knots) . . . . .	119
13e	Lateral Control Surface Responses, $\Delta\delta_a$ and $\Delta\delta_p$ for the Vertical Rate Command System ( $V_{EAS} = 40$ knots) . . . .	119
14a	Output Response, $h_E$ , for the Vertical Rate Command System With Actuators ( $V_{EAS} = 40$ knots) . . . . .	121
14b	Output Response, $w_B$ , for the Vertical Rate Command System With Actuators ( $V_{EAS} = 40$ knots) . . . . .	121
14c	Output Responses, $\theta$ and $\phi$ , for the Vertical Rate Command System With Actuators ( $V_{EAS} = 40$ knots) . . . . .	122
14d	Output Response, $r_B$ , for the Vertical Rate Command System With Actuators ( $V_{EAS} = 40$ knots) . . . . .	122
14e	State Responses, $u_B$ and $v_B$ for the Vertical Rate Command System With Actuators ( $V_{EAS} = 40$ knots) . . . . .	123
14f	State Responses, $p_B$ and $q_B$ , for the Vertical Rate Command System With Actuators ( $V_{EAS} = 40$ knots) . . . .	123
14g	Longitudinal Control Surface Responses, $\Delta\delta_e$ and $\Delta\delta_c$ , for the Vertical Rate Command System With Actuators ( $V_{EAS} = 40$ knots) . . . . .	124
14h	Lateral Control Surface Responses, $\Delta\delta_a$ and $\Delta\delta_p$ , for the Vertical Rate Command System With Actuators ( $V_{EAS} = 40$ knots) . . . . .	124
15a	Output Response, $h_E$ , for the Vertical Rate Command System ( $V_{EAS} = 60$ knots) . . . . .	127
15b	Output Response, $w_B$ , for the Vertical Rate Command System ( $V_{EAS} = 60$ knots) . . . . .	127

15c	Output Responses, $\theta$ and $\phi$ , for the Vertical Rate Command System ( $V_{EAS} = 60$ knots) . . . . .	128
15d	Output Response, $r_B$ , for the Vertical Rate Command System ( $V_{EAS} = 60$ knots) . . . . .	128
15e	State Responses, $p_B$ and $q_B$ , for the Vertical Rate Command System ( $V_{EAS} = 60$ knots) . . . . .	129
15f	State Responses, $u_B$ and $v_B$ for the Vertical Rate Command System ( $V_{EAS} = 60$ knots) . . . . .	129
15g	Longitudinal Control Surface Responses, $\Delta\delta_e$ and $\Delta\delta_c$ , for the Vertical Rate Command System ( $V_{EAS} = 60$ knots) . .	130
15h	Lateral Control Surface Responses, $\Delta\delta_a$ and $\Delta\delta_p$ , for the Vertical Rate Command System ( $V_{EAS} = 60$ knots) . .	130
16a	Output Response, $h_F$ , for the Vertical Rate Command System ( $V_{EAS} = 100$ knots) . . . . .	133
16b	Output Response, $w_B$ , for the Vertical Rate Command System ( $V_{EAS} = 100$ knots) . . . . .	133
16c	Output Responses, $\theta$ and $\phi$ , for the Vertical Rate Command System ( $V_{EAS} = 100$ knots) . . . . .	134
16d	Output Response, $r_B$ , for the Vertical Rate Command System ( $V_{EAS} = 100$ knots) . . . . .	134
16e	State Responses, $p_B$ and $q_B$ , for the Vertical Rate Command System ( $V_{EAS} = 100$ knots) . . . . .	135
16f	State Responses, $u_B$ and $v_B$ for the Vertical Rate Command System ( $V_{EAS} = 100$ knots) . . . . .	135
16g	Longitudinal Control Surface Responses, $\Delta\delta_e$ and $\Delta\delta_c$ , for the Vertical Rate Command System ( $V_{EAS} = 100$ knots). .	136
16h	Lateral Control Surface Responses, $\Delta\delta_a$ and $\Delta\delta_p$ , for the Vertical Rate Command System ( $V_{EAS} = 100$ knots) . . .	136
17a	Output Response, $h_F$ , for the Vertical Rate Command System ( $V_{EAS} = 140$ knots) . . . . .	139
17b	Output Response, $w_B$ , for the Vertical Rate Command System ( $V_{EAS} = 140$ knots) . . . . .	139
17c	Output Responses, $\theta$ and $\phi$ , for the Vertical Rate Command System ( $V_{EAS} = 140$ knots) . . . . .	140

17d	Output Response, $r_B$ , for the Vertical Rate Command System ( $V_{EAS} = 140$ knots) . . . . .	140
17e	State Responses, $p_B$ and $q_B$ , for the Vertical Rate Command System ( $V_{EAS} = 140$ knots) . . . . .	141
17f	State Responses, $u_B$ and $v_B$ for the Vertical Rate Command System ( $V_{EAS} = 140$ knots) . . . . .	141
17g	Longitudinal Control Surface Responses, $\Delta\delta_e$ and $\Delta\delta_c$ , for the Vertical Rate Command System ( $V_{EAS} = 140$ knots). .	142
17h	Lateral Control Surface Responses, $\Delta\delta_a$ and $\Delta\delta_p$ , for the Vertical Rate Command System ( $V_{EAS} = 140$ knots) . . .	142
18a	Robust Controller Output Responses, $\Theta(\text{rad})$ and $p_B(\text{rad/sec})$ , for the Yaw Rate Command System ( $V_{EAS} = 20$ knots) . . . . .	149
18b	Robust Controller Output Responses, $w_B(\text{ft/sec})$ and $r_B(\text{rad/sec})$ , for the Yaw Rate Command System ( $V_{EAS} = 20$ knots) . . . . .	149
18c	Robust Controller State Responses, $u_B$ and $v_B$ , for the Yaw Rate Command System ( $V_{EAS} = 20$ knots) . . . . .	150
18d	Robust Controller State Responses, $\phi(\text{rad})$ and $q_B(\text{rad/sec})$ for the Yaw Rate Command System ( $V_{EAS} = 20$ knots) . . . . .	150
18e	Robust Controller Longitudinal Control Surface Responses, $\Delta\delta_e$ and $\Delta\delta_c$ , for the Yaw Rate Command System ( $V_{EAS} = 20$ knots) . . . . .	151
18f	Robust Controller Lateral Control Surface Responses, $\Delta\delta_a$ and $\Delta\delta_p$ for the Yaw Rate Command System ( $V_{EAS} = 20$ knots) . . . . .	151
19a	Robust Controller Output Responses, $\Theta(\text{rad})$ and $p_B(\text{rad/sec})$ , for the Yaw Rate Command System ( $V_{EAS} = 40$ knots) . . . . .	153
19b	Robust Controller Output Responses, $w_B(\text{ft/sec})$ and $r_B(\text{rad/sec})$ , for the Yaw Rate Command System ( $V_{EAS} = 40$ knots) . . . . .	153
19c	Robust Controller State Responses, $\phi(\text{rad})$ and $q_B(\text{rad/sec})$ , for the Yaw Rate Command System ( $V_{EAS} = 40$ knots) . . . . .	154
19d	Robust Controller State Responses, $u_B$ and $v_B$ , for the Yaw Rate Command System ( $V_{EAS} = 40$ knots) . . . . .	154

19e	Robust Controller Longitudinal Control Surface Responses, $\Delta\delta_e$ and $\Delta\delta_c$ , for the Yaw Rate Command System ( $V_{EAS} = 40$ knots) . . . . .	155
19f	Robust Controller Lateral Control Surface Responses, $\Delta\delta_a$ and $\Delta\delta_p$ , for the Yaw Rate Command System ( $V_{EAS} = 40$ knots) . . . . .	155
20a	Robust Controller Output Response, $\phi$ , for the Coordinated Turn Command System ( $V_{EAS} = 60$ knots) . .	159
20b	Robust Controller Output Response, $\theta$ , for the Coordinated Turn Command System ( $V_{EAS} = 60$ knots) . .	160
20c	Robust Controller Output Responses, $v_B$ and $w_B$ , for the Coordinated Turn Command System ( $V_{EAS} = 60$ knots) . . . . .	160
20d	Robust Controller State Response, $u_B$ , for the Coordinated Turn Command System ( $V_{EAS} = 60$ knots) . .	161
20e	Robust Controller State Responses, $p_B$ , $q_B$ , and $r_B$ , for the Coordinated Turn Command System ( $V_{EAS} = 60$ knots) . . . . .	161
20f	Robust Controller Longitudinal Control Surface Responses, $\Delta\delta_e$ and $\Delta\delta_c$ , for the Coordinated Turn Command System ( $V_{EAS} = 60$ knots) . . . . .	162
20g	Robust Controller Lateral Control Surface Responses, $\Delta\delta_a$ and $\Delta\delta_p$ , for the Coordinated Turn Command System ( $V_{EAS} = 60$ knots) . . . . .	162
21a	Robust Controller Output Response, $\phi$ , for the Coordinated Turn Command System ( $V_{EAS} = 100$ knots) . .	164
21b	Robust Controller Output Response, $\theta$ , for the Coordinated Turn Command System ( $V_{EAS} = 100$ knots) . .	165
21c	Robust Controller Output Responses, $v_B$ and $w_B$ , for the Coordinated Turn Command System ( $V_{EAS} = 100$ knots) . . . . .	165
21d	Robust Controller State Response, $u_B$ , for the Coordinated Turn Command System ( $V_{EAS} = 100$ knots) . .	166
21e	Robust Controller State Responses, $p_B$ , $q_B$ , and $r_B$ , for the Coordinated Turn Command System ( $V_{EAS} = 100$ knots) . . . . .	166

21f	Robust Controller Longitudinal Control Surface Responses, $\Delta\delta_e$ and $\Delta\delta_c$ , for the Coordinated Turn Command System ( $V_{EAS} = 100$ knots) . . . . .	167
21g	Robust Controller Lateral Control Surface Responses, $\Delta\delta_a$ and $\Delta\delta_p$ , for the Coordinated Turn Command System ( $V_{EAS} = 100$ knots) . . . . .	167
22a	Robust Controller Output Responses, $h_E$ and $w_B$ , and State Responses, $u_B$ and $v_B$ , for the Vertical Rate Command System ( $V_{EAS} = 20$ knots) . . . . .	172
22b	Robust Controller Output Responses, $\theta$ and $\phi$ (rad), and $r_B$ (rad/sec) for the Vertical Rate Command System ( $V_{EAS} = 20$ knots) . . . . .	173
22c	Robust Controller State Responses, $p_B$ and $q_B$ , for the Vertical Rate Command System ( $V_{EAS} = 20$ knots) . . . . .	173
22d	Robust Controller Longitudinal Control Surface Responses, $\Delta\delta_e$ and $\Delta\delta_c$ , for the Vertical Rate Command System ( $V_{EAS} = 20$ knots) . . . . .	174
22e	Robust Controller Lateral Control Surface Responses, $\Delta\delta_a$ and $\Delta\delta_p$ , for the Vertical Rate Command System ( $V_{EAS} = 20$ knots) . . . . .	174
23a	Robust Controller Output Responses, $h_E$ and $w_B$ , for the Vertical Rate Command System ( $V_{EAS} = 40$ knots) . . . . .	175
23b	Robust Controller Output Responses, $\theta$ and $\phi$ (rad), and $r_B$ (rad/sec) for the Vertical Rate Command System ( $V_{EAS} = 40$ knots) . . . . .	175
23c	Robust Controller State Responses, $u_B$ and $v_B$ , for the Vertical Rate Command System ( $V_{EAS} = 40$ knots) . . . . .	176
23d	Robust Controller State Responses, $p_B$ and $q_B$ , for the Vertical Rate Command System ( $V_{EAS} = 40$ knots) . . . . .	176
23e	Robust Controller Longitudinal Control Surface Responses, $\Delta\delta_e$ and $\Delta\delta_c$ , for the Vertical Rate Command System ( $V_{EAS} = 40$ knots) . . . . .	177
23f	Robust Controller Lateral Control Surface Responses, $\Delta\delta_a$ and $\Delta\delta_p$ , for the Vertical Rate Command System ( $V_{EAS} = 40$ knots) . . . . .	177
24a	Robust Controller Output Response, $h_E$ , for the Vertical Rate Command System ( $V_{EAS} = 60$ knots) . . . . .	179

24b	Robust Controller Output Response, $w_B$ , for the Vertical Rate Command System ( $V_{EAS} = 60$ knots) . . . . .	179
24c	Robust Controller Output Responses, $\theta$ and $\phi$ , for the Vertical Rate Command System ( $V_{EAS} = 60$ knots) . .	180
24d	Robust Controller Output Response, $r_B$ , for the Vertical Rate Command System ( $V_{EAS} = 60$ knots) . . . . .	180
24e	Robust Controller State Responses, $u_B$ and $v_B$ , for the Vertical Rate Command System ( $V_{EAS} = 60$ knots) . . . .	181
24f	Robust Controller State Responses, $p_B$ and $q_B$ , for the Vertical Rate Command System ( $V_{EAS} = 60$ knots) . . . .	181
24g	Robust Controller Longitudinal Control Surface Responses, $\Delta\delta_e$ and $\Delta\delta_c$ , for the Vertical Rate Command System ( $V_{EAS} = 60$ knots) . . . . .	182
24h	Robust Controller Lateral Control Surface Responses $\Delta\delta_a$ and $\Delta\delta_p$ , for the Vertical Rate Command System ( $V_{EAS} = 60$ knots) . . . . .	182
25a	Robust Controller Output Response, $h_E$ , for the Vertical Rate Command System ( $V_{EAS} = 100$ knots) . . .	184
25b	Robust Controller Output Response, $w_B$ , for the Vertical Rate Command System ( $V_{EAS} = 100$ knots) . . . . .	184
25c	Robust Controller Output Responses, $\theta$ and $\phi$ , for the Vertical Rate Command System ( $V_{EAS} = 100$ knots) . . .	185
25d	Robust Controller Output Response, $r_B$ , for the Vertical Rate Command System ( $V_{EAS} = 100$ knots) . . . . .	185
25e	Robust Controller State Responses, $u_B$ and $v_B$ , for the Vertical Rate Command System ( $V_{EAS} = 100$ knots) . . .	186
25f	Robust Controller State Responses, $p_B$ and $q_B$ , for the Vertical Rate Command System ( $V_{EAS} = 100$ knots) . . .	186
25g	Robust Controller Longitudinal Control Surface Responses, $\Delta\delta_e$ and $\Delta\delta_c$ , for the Vertical Rate Command System ( $V_{EAS} = 100$ knots) . . . . .	187
25h	Robust Controller Lateral Control Surface Responses, $\Delta\delta_a$ and $\Delta\delta_p$ , for the Vertical Rate Command System ( $V_{EAS} = 100$ knots) . . . . .	187
B-1a	State Responses, $p_B$ , $q_B$ , and $r_B$ , for the Coordinated Turn Command System With Computational Delay ( $V_{EAS}=60$ knots) . . . . .	B-2

B-1b	Output Response, $\Theta$ , for the Coordinated Turn Command System With Computational Delay ( $V_{EAS} = 60$ knots) . . .	B-3
B-1c	Output Response, $\phi$ , for the Coordinated Turn Command System With Computational Delay ( $V_{EAS}=60$ knots) . . .	B-3
B-1d	Output Responses, $v_B$ and $w_B$ , for the Coordinated Turn Command System with Computational Delay ( $V_{EAS}=60$ knots) . . . . .	B-4
B-1e	Cyclic Roll Control Response, $\Delta\delta_a$ , for the Coordinated Turn Command System With Computational Delay ( $V_{EAS}=60$ knots) . . . . .	B-4
B-1f	Longitudinal Control Surface Responses, $\Delta\delta_e$ and $\Delta\delta_c$ , for the Coordinated Turn Command System With Computational Delay ( $V_{EAS} = 60$ knots. . . . .	B-5
B-1g	Tail Rotor Yaw Control Response, $\Delta\delta_p$ , for the Coordinated Turn Command System With Computational Delay ( $V_{EAS} = 60$ knots) . . . . .	B-5

# List of Tables

<u>Table</u>		<u>Page</u>
1	Asymptotic Equations for Zero- $B_2$ Form . . . . .	32
IV-1	Yaw Rate Results for $V_{EAS} = 20$ knots . . . . .	59
IV-2	Yaw Rate Results for $V_{EAS} = 40$ knots . . . . .	61
IV-3	Yaw Rate Response With Actuators for $V_{EAS} = 60$ knots . . . . .	72
IV-4	Yaw Rate Response for $V_{EAS} = 60$ knots . . . . .	72
IV-5	Expected Values of $r_B$ and $q_B$ for the Coordinated Turn Command System . . . . .	80
IV-6	Coordinated Turn Responses for $V_{EAS} = 60$ knots . . . . .	86
IV-7	Coordinated Turn Responses for $V_{EAS} = 100$ knots . . . . .	83
IV-8	Coordinated Turn Results for $V_{EAS} = 140$ knots . . . . .	94
IV-9	Coordinated Turn Results With Actuators for $V_{EAS} = 140$ knots . . . . .	105
IV-10	Vertical Rate Response for $V_{EAS} = 20$ knots . . . . .	110
IV-11	Vertical Rate Responses for $V_{EAS} = 40$ knots . . . . .	115
IV-12	Vertical Rate Responses With Actuators for $V_{EAS} = 40$ knots . . . . .	125
IV-13	Vertical Rate Responses for the $V_{EAS} = 60$ knots . . . . .	131
IV-14	Vertical Rate Responses for the $V_{EAS} = 100$ knots . . . . .	137
IV-15	Vertical Rate Responses for the $V_{EAS} = 140$ knots . . . . .	143
V-1	Yaw Rate Results ( $V_{EAS} = 20$ knots) for the Robust Controller . . . . .	148
V-2	Yaw Rate Results ( $V_{EAS} = 40$ knots) for the Robust Controller . . . . .	152
V-3	Yaw Rate Results for the Output Response, $\theta$ . . . . .	152
V-4	Yaw Rate Results for the Output Response, $p_B$ . . . . .	156



V-5	Yaw Rate Results for the Output Response, $w_B$ . . . . .	156
V-6	Yaw Rate Results for the Output Response, $r_B$ . . . . .	156
V-7	Coordinated Turn Results ( $V_{EAS} = 60$ knots) for the Robust Controller . . . . .	158
V-8	Coordinated Turn Results ( $V_{EAS} = 100$ knots) for the Robust Controller . . . . .	163
V-9	Coordinated Turn Results for the Output Response, $\theta$ . . . . .	168
V-10	Coordinated Turn Results for the Output Response, $\phi$ . . . . .	168
V-11	Coordinated Turn Results for the Output Response, $v_B$ . . . . .	169
V-12	Coordinated Turn Results for the Output Response, $w_B$ . . . . .	169
V-13	Vertical Rate Results ( $V_{EAS} = 20$ knots) for the Robust Controller . . . . .	171
V-14	Vertical Rate Results ( $V_{EAS} = 40$ knots) for the Robust Controller . . . . .	178
V-15	Vertical Rate Results ( $V_{EAS} = 60$ knots) for the Robust Controller . . . . .	183
V-16	Vertical Rate Results ( $V_{EAS} = 100$ knots) for the Robust Controller . . . . .	188
V-17	Vertical Rate Results for the Output Response, $\theta$ . . . . .	189
V-18	Vertical Rate Results for the Output Response, $\phi$ . . . . .	189
V-19	Vertical Rate Results for the Output Response, $w_B$ . . . . .	190
V-20	Vertical Rate Results for the Output Response, $r_B$ . . . . .	190

### List of Symbols

$\underline{A}$	Continuous-time plant matrix
$\alpha$	Angle of attack, perturbation angle of attack in perturbation equations
$\alpha_0$	Equilibrium (trim) angle of attack
$\alpha$	Ratio of proportional to integral feedback
$R$	Aspect Ratio
$\underline{B}$	Continuous-time control input matrix
$b$	Wing span
$\beta$	Sideslip angle
$\beta_0$	Equilibrium (trim) sideslip angle
$C$	Complex plane
$\underline{C}$	Continuous-time output matrix
$c$	Wing mean aerodynamic chord
$C_D$	Nondimensional coefficient of drag (along velocity vector)
$C_{D_\alpha}$	Nondimensional variation of drag with angle of attack
$C_{D_0}$	Nondimensional bias coefficient of drag at zero angle of attack
$C_L$	Nondimensional coefficient of lift (normal to velocity vector)
$C_{L_\alpha}$	Nondimensional variation of lift with angle of attack
$C_{L_{\dot{\alpha}}}$	Nondimensional variation of lift with the rate of change of angle of attack
$C_{L_\delta}$	Nondimensional variation of lift with elevator ( $\delta_e$ ) or flaperon ( $\delta_f$ )
$C_{L_0}$	Nondimensional bias coefficient of lift at zero angle of attack
$C_{L_q}$	Nondimensional variation of lift with pitch rate

$C_{L_v}$	Nondimensional variation of lift with total velocity
$C_{l_\beta}$	Nondimensional variation of rolling moment with sideslip angle
$C_{l_\delta}$	Nondimensional variation of rolling moment with aileron ( $\delta_a$ ), rudder ( $\delta_r$ ), canard ( $\delta_c$ ) or differential tail ( $\delta_{DT}$ )
$C_{l_p}$	Nondimensional variation of rolling moment with roll rate
$C_{l_r}$	Nondimensional variation of rolling moment with yaw rate
$C_m$	Nondimensional coefficient of pitching moment
$C_{m_\alpha}$	Nondimensional coefficient of pitching moment with angle of attack
$C_{m_\delta}$	Nondimensional coefficient of pitching moment with elevator ( $\delta_e$ ) or flaperon ( $\delta_f$ )
$C_{m_0}$	Nondimensional bias coefficient of pitching moment at zero angle of attack
$C_{m_q}$	Nondimensional variation of pitching moment with pitch rate
$C_{m_v}$	Nondimensional variation of pitching moment with total velocity
cmd	Command
$C_{n_\beta}$	Nondimensional variation of yawing moment with sideslip angle
$C_{n_\delta}$	Nondimensional variation of yawing moment with aileron ( $\delta_a$ ), rudder ( $\delta_r$ ), canard ( $\delta_c$ ), or differential tail ( $\delta_{DT}$ )
$C_{n_p}$	Nondimensional variation of yawing moment with roll rate
$C_{n_r}$	Nondimensional variation of yawing moment with yaw rate
cos	Cosine

$C_{y_\beta}$	Nondimensional variation of y-force with sideslip angle
$C_{y_\delta}$	Nondimensional variation of y-force with aileron ( $\delta_a$ ), canard ( $\delta_c$ ), or differential tail ( $\delta_{DT}$ )
$C_{y_p}$	Nondimensional variation of y-force with roll rate
$C_{y_r}$	Nondimensional variation of y-force with yaw rate
deg	Degree
$\delta_a$	Aileron deflection
$\delta_c$	Canard deflection
$\delta_{DT}$	Differential horizontal tail deflection
$\delta_e$	Elevator deflection
$\delta_f$	Flap deflection
$\Delta\delta_a$	Cyclic roll control perturbation
$\Delta\delta_c$	Collective lift control perturbation
$\Delta\delta_e$	Cyclic pitch control perturbation
$\Delta\delta_p$	Tail rotor yaw control perturbation
$\mathbf{e}$	Configuration constant
$\underline{\mathbf{e}}$	Error vector
$\underline{\mathbf{e}}(kT)$	Discrete error vector
$\epsilon, \epsilon$	Epsilon scalar multiplier; "element of" symbol (depends on context)
$\underline{\mathbf{F}}$	Augmented continuous-time output matrix
ft	Feet
f	Sampling frequency
g	Gravity, gain constant (depends on context)
$\underline{\mathbf{G}}(s)$	Transfer function matrix
$h_E$	Perturbation -z- earth axis velocity

$h$  Altitude  
 $I_{xx}, I_x$  Moment of inertia about x body axis  
 $I_{yy}, I_y$  Moment of inertia about y body axis  
 $I_{zz}, I_z$  Moment of inertia about z body axis  
 $I_{xz}$  Product of inertia about xz body axis  
 $I$  Identity matrix  
 $\underline{K}_0$  Proportional control law feedback matrix  
 $\underline{K}_1$  Integral control law feedback matrix  
 $\ell$  Number of inputs = number of outputs variable  
 $L_\delta$  Dimensional variation of pitching moment with cyclic roll control ( $\Delta\delta_a$ ), collective lift control ( $\Delta\delta_c$ ), cyclic pitch control ( $\Delta\delta_e$ ), and tail rotor yaw control ( $\Delta\delta_p$ )  
 $L$  Dimensional rolling moment  
 $L_p$  Dimensional variation of rolling moment with roll rate  
 $L_q$  Dimensional variation of rolling moment with pitch rate  
 $L_r$  Dimensional variation of rolling moment with yaw rate  
 $L_u$  Dimensional variation of rolling moment with x-body velocity  
 $L_v$  Dimensional variation of rolling moment with y-body velocity  
 $L_w$  Dimensional variation of rolling moment with z-body velocity  
 $\underline{M}$  Measurement matrix  
 $m$  Aircraft mass, number of inputs  
 $M$  Dimensional pitching moment  
 $\underline{M}_c$  Controllability matrix  
 $\underline{M}_o$  Observability matrix  
 $M_p$  Dimensional variation of pitching moment with roll rate  
 $M_q$  Dimensional variation of pitching moment with pitch rate  
 $M_r$  Dimensional variation of pitching moment with yaw rate

$M_u$	Dimensional variation of pitching moment with x-body velocity
$M_v$	Dimensional variation of pitching moment with y-body velocity
$M_w$	Dimensional variation of pitching moment with z-body velocity
$n$	Number of states
$N$	Dimensional yawing moment
$N_p$	Dimensional variation of yawing moment with roll rate
$N_q$	Dimensional variation of yawing moment with pitch rate
$N_r$	Dimensional variation of yawing moment with yaw rate
$N_u$	Dimensional variation of yawing moment with x-body velocity
$N_v$	Dimensional variation of yawing moment with y-body velocity
$N_w$	Dimensional variation of yawing moment with z-body velocity
$p$	Number of outputs, roll rate
$\phi$	Roll angle
$\phi_e$	Equilibrium (trim) roll angle
$\phi$	Perturbation roll angle
$q$	Pitch rate
$q_B$	Perturbation pitch rate in the body axis
$q$	Dynamic pressure
$\psi$	Yaw angle
$\psi_e$	Equilibrium (trim) yaw angle
$R$	Real number plane
rad	Radians
$S$	Surface area
$s$	Laplace operator
sec	Seconds
sin	Sine

$\sigma$	Element of the ( $\Sigma$ ) matrix
$\Sigma$	Sigma gain weighting matrix
$\underline{T}$	Transformation matrix
$T$	Sampling period
$\theta$	Pitch angle
$\theta_e$	Equilibrium (trim) pitch angle
$\theta$	Perturbation pitch angle
$T_{x_B}$	Thrust along x-body axis
$T_{y_B}$	Thrust along y-body axis
$T_{z_B}$	Thrust along z-body axis
$u$	Velocity along the x-body axis
$u_{B_e}, u_0$	Equilibrium (trim) velocity along the x-body axis
$\underline{u}$	Input vector
$u_B$	Perturbation velocity along the x-body axis
$v$	Velocity along the y-body axis
$v_{B_e}, v_0$	Equilibrium (trim) velocity along the y-body axis
$\underline{v}$	Command input vector
$v_B$	Perturbation velocity along the y-body axis
$V, V_T$	Total (true) velocity
$W$	Aircraft weight
$w$	velocity along the z-body axis
$w_{B_e}, w_0$	Equilibrium (trim) velocity along the z-body axis
$\underline{w}$	Controller output vector

$w_B$  Perturbation velocity along the z-body axis  
 $\underline{x}$  State vector  
 $X_a$  Aerodynamic forces along the x-body axis  
 $X_p$  Dimensional variation of x-force with roll rate  
 $X_q$  Dimensional variation of x-force with pitch rate  
 $X_r$  Dimensional variation of x-force with yaw rate  
 $X_u$  Dimensional variation of x-force with x-body axis velocity  
 $X_v$  Dimensional variation of x-force with y-body axis velocity  
 $X_w$  Dimensional variation of x-force with z-body axis velocity  
 $\underline{y}$  Output vector  
 $Y_a$  Aerodynamic forces along the y-body axis  
 $Y_p$  Dimensional variation of y-force with roll rate  
 $Y_q$  Dimensional variation of y-force with pitch rate  
 $Y_r$  Dimensional variation of y-force with yaw rate  
 $Y_u$  Dimensional variation of y-force with x-body axis velocity  
 $Y_v$  Dimensional variation of y-force with y-body axis velocity  
 $Y_w$  Dimensional variation of y-force with z-body axis velocity  
 $\underline{z}$  Integral of error vector  
 $\underline{z}(kT)$  Discrete integral of error vector  
 $Z_a$  Aerodynamic forces along the z-body axis  
 $Z_p$  Dimensional variation of z-force with roll rate  
 $Z_q$  Dimensional variation of z-force with pitch rate  
 $Z_r$  Dimensional variation of z-force with yaw rate  
 $Z_u$  Dimensional variation of z-force with x-body axis velocity  
 $Z_v$  Dimensional variation of z-force with y-body axis velocity  
 $Z_w$  Dimensional variation of z-force with z-body axis velocity



$z_t$       Transmission zeros  
 $z_{1,2}$     Finite system roots  
 $z_3$       Infinite system roots

Abstract

This thesis investigates the application of multivariable design techniques developed by Professor Brian Porter of the University of Salford, England to design digital control laws for the UH-60A Black Hawk helicopter. In the study, designs were developed for five longitudinally and laterally, strongly coupled plants with control inputs of cyclic roll control, cyclic pitch control, collective lift control, and tail rotor yaw control. An improved computer-aided design package called "MULTI" was used in refining the control laws.

Separate controllers were developed to perform three flight maneuvers. The maneuvers performed were a coordinated turn, a yaw rate response, and a vertical rate response. Since each maneuver is flown at a different airspeed, a uniquely specified linearized plant model was required.

The methods employed to obtain a design are presented along with the evaluations of the final control laws. After successful designs of the individual control laws for the three maneuvers were developed, tests were performed to find a single controller to perform each maneuver for its applicable flight conditions. Finally, the evaluation of the robustness of the single controllers is presented.

## I. INTRODUCTION

The advent of digital fly-by-wire control systems has hastened the need for the design of multivariable techniques to handle large complex systems. The advantages of digital fly-by-wire control systems are faster response times to inputs, the elements of the control laws are just numbers stored in the flight computer, and the vast reduction of hardware due to mechanical systems which would be replaced by smaller electrical networks. With this reduction in hardware, more weapon and navigational systems can be stored in the aircraft.

This thesis addresses the development of digital multivariable control laws for the UH-60A Black Hawk helicopter. The results of this thesis are to be incorporated in a survey of multivariable control law techniques for multiple input/multiple output (MIMO) systems in order to develop the best optical fly-by-wire control system for the UH-60D Night Hawk helicopter. This first chapter presents the background, problem statement, assumptions, and the sequence of presentation.

### Background

Classical methods, which worked well for simple single input/single output control systems are no longer easily applied. As aircraft become more complex, especially for aircraft which have strongly coupled longitudinal and lateral modes, a single input may not cause just one output. With this added complexity, the need for multivariable control law techniques to handle MIMO systems is apparent. Professor Porter and his associates have suggested four direct design techniques to be implemented as digital flight control systems. These techniques provide

for the design of fast sampling error-actuated digital controllers for highly interactive linear multivariable systems. Professor Porter proposed that to obtain tight tracking of commanded step inputs, an integral plus portional controller actuated by the error between the commanded input and the desired output must be employed. This control technique, he suggested, would result in greater decoupling of the outputs than other previous multivariable control law methods. Even though other design techniques have been used successfully on other aircraft, the subject of this thesis is applying Porter's method to the Black Hawk helicopter.

#### Problem

The purpose of this thesis is to investigate the development of tight tracking multivariable digital control laws for the UH-60A Black Hawk helicopter. After individual control laws are developed for each maneuver at its applicable flight conditions, the design of a robust controller that will perform at all flight conditions for a particular maneuver, is investigated. These controllers are developed and simulated by the use of an existing computer aided design (C.A.D.) software package called MULTI (Ref 13).

#### Approach

This thesis is limited to the design of digital multivariable control laws using the control law techniques developed by Professor Porter. All designs are completed using the interactive computer program MULTI. In this thesis, five steps are taken

1. Development of the equations of motion and actuator dynamics for five separate flight conditions.
2. Development of the control law theory as proposed by Professor Porter.
3. Design of digital multivariable control laws using the irregular design method (see Chapter III) for three maneuvers at their applicable flight conditions.
4. Design of a robust controller to perform tight tracking of the commanded inputs for all flight conditions of a particular maneuver.
5. Development of a nonlinear simulation of a symmetrical aircraft to be implemented in MULTI.

#### Assumptions

Basic assumptions are established to reduce the model complexity. These assumptions are listed below.

1. The helicopter is a rigid body, and its mass is constant.
2. The rotation speed of the helicopter blades remains constant as designed by the manufacturer.
3. The earth's surface is an inertial reference frame.
4. The atmosphere is assumed fixed with respect to the earth.
5. Linearization about an operating point is acceptable for point designs.
6. Aerodynamics are fixed for each flight condition.
7. The initial angular velocities,  $p_0$ ,  $q_0$ , and  $r_0$  in the body-axis frame are equal to zero.

## Presentation

Six chapters are included in this thesis. Chapter II presents the helicopter's equations of motion in the required state-space representation. The regular and irregular design approaches developed by Professor Porter are presented in Chapter III. The development and results of the individual digital control laws for the three maneuvers at their applicable flight conditions are presented in Chapter IV. Chapter V describes the development and results of the robust controller for each maneuver at the applicable flight conditions. Finally, Chapter VI offers conclusions from the design effort and recommendations for further studies and improvements to MULTI.

## II. UH-60A Black Hawk Model

The linear, first-order set of differential equations describing the rigid body motion of the UH-60A Black Hawk helicopter are of the form:

$$\dot{\underline{x}} = \underline{A}\underline{x} + \underline{B}\underline{u} \quad (2.1)$$

where the state vector  $\underline{x}$  represents the perturbations from trim of the body axis variables:  $u, v, w, p, q, r, \theta$ , and  $\phi$ . The control vector  $\underline{u}$  represents the deviations from the trim positions of the controls  $\delta_e, \delta_c, \delta_a$ , and  $\delta_p$ . The linear representation is valid only if the initial angular velocities  $p_0, q_0$  and  $r_0$  are zero.

The elements of the plant matrix  $\underline{A}$  and control matrix  $\underline{B}$  are of two types. The first type consists of inertial and gravitational terms that can be obtained analytically from the equations of motion. The second type consists of partial derivatives arising from aerodynamic forces and moments.

The output equation is of the form

$$\underline{y} = \underline{C} \underline{x} \quad (2.2)$$

which gives a relationship between the desired outputs and the linear combinations of states to obtain those outputs. The elements of the  $\underline{C}$  matrix reflect the desired maneuver to be performed.

In this chapter, an attempt is made to understand the perturbation state equations, the control surfaces, the actuator dynamics, and the trim conditions for the UH-60A Black Hawk helicopter. The first step is to take a careful look at the state equations described by Equation (2.1).

The full linearized set of state equations can be described by the following matrix equations:

$$\begin{bmatrix} \dot{u}_B \\ \dot{w}_B \\ \dot{q}_B \\ \dot{\theta} \\ \dot{v}_B \\ \dot{p}_B \\ \dot{\phi} \\ \dot{r}_B \end{bmatrix} = \begin{bmatrix} \frac{X_u}{m} & \frac{X_w}{m} & \frac{X_q}{m} & -g \cos \theta_0 & \frac{X_v}{m} & \frac{X_p}{m} & 0 & \frac{X_r + v_0}{m} \\ \frac{Z_u}{m} & \frac{Z_w}{m} & \frac{Z_q}{m} & -g \cos \theta_0 \sin \theta_0 & \frac{Z_v}{m} & \frac{Z_p + v_0}{m} & -g \sin \theta_0 \cos \theta_0 & \frac{Z_r}{m} \\ \frac{M_u}{I_y} & \frac{M_w}{I_y} & \frac{M_q}{I_y} & 0 & \frac{M_v}{I_y} & \frac{M_p}{I_y} & 0 & \frac{M_r}{I_y} \\ 0 & 0 & \cos \phi_0 & 0 & 0 & 0 & 0 & -\sin \phi_0 \\ \frac{Y_u}{m} & \frac{Y_w}{m} & \frac{Y_q}{m} & -g \sin \phi_0 \sin \theta_0 & \frac{Y_v}{m} & \frac{Y_p + w_0}{m} & g \cos \phi_0 \cos \theta_0 & \frac{Y_r - u_0}{m} \\ \frac{I_{xz} L_u + I_{xz}^2 u}{I_{xz}^2 - I_{xz}^2} & \frac{I_{xz} L_w + I_{xz}^2 w}{I_{xz}^2 - I_{xz}^2} & \frac{I_{xz} L_q + I_{xz}^2 q}{I_{xz}^2 - I_{xz}^2} & 0 & \frac{I_{xz} L_v + I_{xz}^2 v}{I_{xz}^2 - I_{xz}^2} & \frac{I_{xz} L_p + I_{xz}^2 p}{I_{xz}^2 - I_{xz}^2} & 0 & \frac{I_{xz} L_r + I_{xz}^2 r}{I_{xz}^2 - I_{xz}^2} \\ 0 & 0 & \sin \phi_0 \tan \theta_0 & 0 & 0 & 1 & 0 & \cos \phi_0 \tan \theta_0 \\ \frac{I_{xz} L_u + I_{xz}^2 u}{I_{xz}^2 - I_{xz}^2} & \frac{I_{xz} L_w + I_{xz}^2 w}{I_{xz}^2 - I_{xz}^2} & \frac{I_{xz} L_q + I_{xz}^2 q}{I_{xz}^2 - I_{xz}^2} & 0 & \frac{I_{xz} L_v + I_{xz}^2 v}{I_{xz}^2 - I_{xz}^2} & \frac{I_{xz} L_p + I_{xz}^2 p}{I_{xz}^2 - I_{xz}^2} & 0 & \frac{I_{xz} L_r + I_{xz}^2 r}{I_{xz}^2 - I_{xz}^2} \end{bmatrix}$$



(2.3)

$$\begin{bmatrix}
 \frac{X_{\delta e}}{m} & \frac{X_{\delta c}}{m} & \frac{X_{\delta a}}{m} & \frac{X_{\delta p}}{m} \\
 \frac{Z_{\delta e}}{m} & \frac{Z_{\delta c}}{m} & \frac{Z_{\delta a}}{m} & \frac{Z_{\delta p}}{m} \\
 \frac{N_{\delta e}}{I_y} & \frac{N_{\delta c}}{I_y} & \frac{N_{\delta a}}{I_y} & \frac{N_{\delta p}}{I_y} \\
 0 & 0 & 0 & 0 \\
 \frac{Y_{\delta e}}{m} & \frac{Y_{\delta c}}{m} & \frac{Y_{\delta a}}{m} & \frac{Y_{\delta p}}{m}
 \end{bmatrix}
 +
 \begin{bmatrix}
 \frac{I_z L_{\delta e} + I_{xz} N_{\delta e}}{I_x I_z - I_{xz}^2} & \frac{I_z L_{\delta c} + I_{xz} N_{\delta c}}{I_x I_z - I_{xz}^2} & \frac{I_z L_{\delta a} + I_{xz} N_{\delta a}}{I_x I_z - I_{xz}^2} & \frac{I_z L_{\delta p} + I_{xz} N_{\delta p}}{I_x I_z - I_{xz}^2} \\
 0 & 0 & 0 & 0 \\
 \frac{I_{xz} L_{\delta e} + I_x N_{\delta e}}{I_x I_z - I_{xz}^2} & \frac{I_{xz} L_{\delta c} + I_x N_{\delta c}}{I_x I_z - I_{xz}^2} & \frac{I_{xz} L_{\delta a} + I_x N_{\delta a}}{I_x I_z - I_{xz}^2} & \frac{I_{xz} L_{\delta p} + I_x N_{\delta p}}{I_x I_z - I_{xz}^2}
 \end{bmatrix}
 \begin{bmatrix}
 \Delta \delta_e \\
 \Delta \delta_c \\
 \Delta \delta_a \\
 \Delta \delta_p
 \end{bmatrix}$$

where

$$\underline{x} = \begin{bmatrix} u_B \\ w_B \\ q_B \\ \theta \\ v_B \\ p_B \\ \phi \\ r_B \end{bmatrix} \quad (2.4)$$

is the state perturbation vector which can be further decomposed into the longitudinal perturbation states  $\underline{x}_1$  and the lateral perturbation states  $\underline{x}_2$  as shown below.

$$\underline{x}_1 = \begin{bmatrix} u_B \\ w_B \\ q_B \\ \theta \end{bmatrix} \text{ and } \underline{x}_2 = \begin{bmatrix} v_B \\ p_B \\ \phi \\ r_B \end{bmatrix} \quad (2.5)$$

The longitudinal perturbation vector consists of four states defined as follows:

$u_B$  = velocity along the x-body axis (ft/sec)  
 $w_B$  = velocity along the z-body axis (ft/sec)  
 $q_B$  = body axis pitch rate (rad/sec)  
 $\theta$  = Euler angle pitch attitude (rad)

The lateral perturbation vector consists of four states defined as follows:

$v_B$  = velocity along the y-body axis (ft/sec)  
 $p_B$  = body axis roll rate (rad/sec)  
 $r_B$  = body axis yaw rate (rad/sec)  
 $\phi$  = Euler angle roll attitude (rad)

The state equations for a sample flight condition,  $V_{EAS}=20$  knots, is presented below:

$$\frac{d}{dt} \begin{bmatrix} u_B \\ w_B \\ q_B \\ \theta \\ v_B \\ p_B \\ \phi \\ r_B \end{bmatrix} = \begin{bmatrix} -.0104 & .0374 & -.608 & -32.0 & -.0223 & -.188 & 0 & -.195 \\ -.146 & -.383 & 35.8 & -3.27 & -.0254 & .422 & .748 & -.300 \\ .00108 & .00343 & -.89 & 0 & .0111 & .289 & 0 & -.0298 \\ 0 & 0 & 1.00 & 0 & 0 & 0 & 0 & .0234 \\ -.0181 & .00692 & -.00138 & .0765 & -.0582 & 1.46 & 32.0 & -33.0 \\ .0218 & .0166 & -1.98 & 0 & -.0375 & -3.74 & 0 & -.0653 \\ 0 & 0 & -.00239 & 0 & 0 & 1.00 & 0 & .102 \\ -.00464 & -.00295 & -.845 & 0 & .00688 & -.453 & 0 & -.369 \end{bmatrix} \begin{bmatrix} u_B \\ w_B \\ q_B \\ \theta \\ v_B \\ p_B \\ \phi \\ r_B \end{bmatrix} + \begin{bmatrix} -1.58 & .97 & .0329 & .913 \\ -1.04 & -7.33 & .0461 & 1.07 \\ .351 & .0273 & -.00384 & -.00644 \\ 0 & 0 & 0 & 0 \\ .05 & .0626 & .953 & -1.34 \\ .0472 & -.0126 & 1.36 & -.619 \\ 0 & 0 & 0 & 0 \\ -.00692 & .0593 & .0881 & .527 \end{bmatrix} \begin{bmatrix} \Delta \delta_e \\ \Delta \delta_c \\ \Delta \delta_a \\ \Delta \delta_p \end{bmatrix} \quad (2.6)$$

These state equations can be partitioned into four  $4 \times 4$  matrices as shown by the dashed lines in Equation (2.6). A notational

$$\dot{\underline{x}} = \begin{bmatrix} \underline{A}_{11} & \underline{A}_{12} \\ \underline{A}_{21} & \underline{A}_{22} \end{bmatrix} \underline{x} + \begin{bmatrix} \underline{B}_1 \\ \underline{B}_2 \end{bmatrix} \underline{u} \quad (2.7)$$

expression for the state equations with partitioning is shown in Equation (2.7). Ideally, the cross matrices  $\underline{A}_{12}$  and  $\underline{A}_{21}$  are set equal to  $\underline{0}$  and the state equations are then decoupled into the longitudinal and lateral state equations. However, a close examination of the cross matrices reveals that the cross matrix elements are not approximately equal to zero. In fact, some of them are quite large compared to elements in the diagonal matrices. Therefore, a reduced-order controller design is not practical as it would ignore the effects of coupling between the longitudinal and lateral modes.

Since decoupling of states is not practical, a more workable set of equations is needed. The new state vector that is used in this thesis is

$$\underline{z} = \begin{bmatrix} \theta \\ \phi \\ u_B \\ v_B \\ w_B \\ p_B \\ q_B \\ r_B \end{bmatrix} \quad (2.8)$$

This new vector,  $\underline{z}$  has three advantages over the old vector  $\underline{x}$ . The first is that it is easy to remember in that the Euler angles, the body velocities, and the body axis angular rates are grouped together. The second reason is that a relatively simple method for calculating transmission zeros is available for  $\underline{B}$  matrices in the zero- $\underline{B}_2$  format. The dimension of  $\underline{B}_2$  is equal to the number of inputs. This second reason requires that the  $\underline{B}_1$  matrix be a zero matrix. The third reason is that in order to pick a measurement matrix  $\underline{M}$ , the method requires the feedback of rates of states that are unaffected by the control inputs. Therefore the zero- $\underline{B}_2$  format is desirable, or at least all the  $\underline{B}$  matrix zero rows should occupy the top rows. The measurement matrix is covered in Chapter III.

The transformation matrix that transforms the  $\underline{x}$  vector to the desired  $\underline{z}$  vector is

$$\underline{T} = \begin{bmatrix} 0 & 0 & 0 & 1 & 0 & 0 & 0 & 0 \\ 0 & 0 & 0 & 0 & 0 & 0 & 1 & 0 \\ 1 & 0 & 0 & 0 & 0 & 0 & 0 & 0 \\ 0 & 0 & 0 & 0 & 1 & 0 & 0 & 0 \\ 0 & 1 & 0 & 0 & 0 & 0 & 0 & 0 \\ 0 & 0 & 0 & 0 & 0 & 1 & 0 & 0 \\ 0 & 0 & 1 & 0 & 0 & 0 & 0 & 0 \\ 0 & 0 & 0 & 0 & 0 & 0 & 0 & 1 \end{bmatrix} \quad (2.9)$$

The complete set of equations is transformed using  $\underline{x} = \underline{T}^{-1} \underline{z}$ . Thus

$$\dot{\underline{x}} = \underline{A} \underline{x} + \underline{B} \underline{u} \quad (2.10)$$

$$\underline{T}^{-1} \dot{\underline{z}} = \underline{A} \underline{T}^{-1} \underline{z} + \underline{B} \underline{u} \quad (2.11)$$

$$\dot{\underline{z}} = \underline{T} \underline{A} \underline{T}^{-1} \underline{z} + \underline{T} \underline{B} \underline{u} \quad (2.12)$$

$$\underline{y} = \underline{C} \underline{x} \quad (2.13)$$

$$\underline{y} = \underline{C} \underline{T}^{-1} \underline{z} \quad (2.14)$$

Transformation of the output equation is actually not needed. It gives the relationship for expressing the old states as a linearized combination of the new states. Since, an output matrix has not been specified yet, a new  $\underline{C}$  that reflects the commanded maneuver is developed when needed.

The new set of state equations for the  $V_{EAS}=20$  knots flight condition can be expressed by the equation below.

$$\frac{d}{dt} \begin{bmatrix} \theta \\ \phi \\ u_B \\ v_B \\ w_B \\ p_B \\ q_B \\ r_B \end{bmatrix} = \begin{bmatrix} 0 & 0 & 0 & 0 & 0 & 0 & 0 & 1 & .0234 \\ 0 & 0 & 0 & 0 & 0 & 0 & 1 & -.00239 & .102 \\ -31.0 & 0 & -.0104 & -.0223 & .0374 & -.188 & -.608 & -.195 & \\ -.0765 & -32.0 & .0181 & -.0582 & .00692 & 1.46 & -.00138 & -33.0 & \\ -3.27 & .748 & -.146 & -.0254 & -.383 & .422 & 35.8 & -.3 & \\ 0 & 0 & .0218 & -.0375 & .0166 & -3.74 & -1.98 & -.0655 & \\ 0 & 0 & .00108 & .0111 & .00343 & .289 & -.89 & -.0298 & \\ 0 & 0 & -.00464 & .00688 & -.00295 & -.453 & -.845 & -.350 & \end{bmatrix} \begin{bmatrix} \theta \\ \phi \\ u_B \\ v_B \\ w_B \\ p_B \\ q_B \\ r_B \end{bmatrix} + \begin{bmatrix} 0 & 0 & 0 & 0 \\ 0 & 0 & 0 & 0 \\ -1.58 & .97 & .0329 & .913 \\ .05 & .0626 & .953 & -1.34 \\ -1.04 & -7.38 & .0461 & 1.07 \\ .0472 & -.0126 & 1.36 & -.619 \\ .351 & .0273 & -.00384 & -.00644 \\ -.00692 & .0593 & .0881 & .527 \end{bmatrix} \begin{bmatrix} \Delta \delta_e \\ \Delta \delta_c \\ \Delta \delta_a \\ \Delta \delta_p \end{bmatrix} \quad (2.15)$$

Examining this set of state equations reveals that the  $\underline{B}$  matrix is not in zero- $\underline{B}_2$  form. Therefore, another transformation that would

change two of the rows to rows of zeroes is needed. However, this transformation would result in a new set of states. This transformation was deemed impractical due to the altering of the states. As a result, all the flight condition state equations are not in zero- $\underline{B}_2$  form.

The control input vector,  $\underline{\Delta\delta}$ , shown below, consists of four control surfaces. It is assumed that the rotational speed of the helicopter blades is constant

$$\underline{\Delta\delta} = \begin{bmatrix} \Delta\delta_e \\ \Delta\delta_c \\ \Delta\delta_a \\ \Delta\delta_p \end{bmatrix} \quad (2.16)$$

as designed by the manufacturer. The longitudinal control surfaces consist of the cyclic pitch control,  $\Delta\delta_e$ , and the collective lift control,  $\Delta\delta_c$ . The cyclic pitch control is analogous to the elevator of an aircraft. The cyclic pitch control controls the thrust of a helicopter. By increasing the angle-of-attack of the blades as a whole, the helicopter experiences an increase in thrust in the forward direction. This deflection is illustrated in the figure below. If the

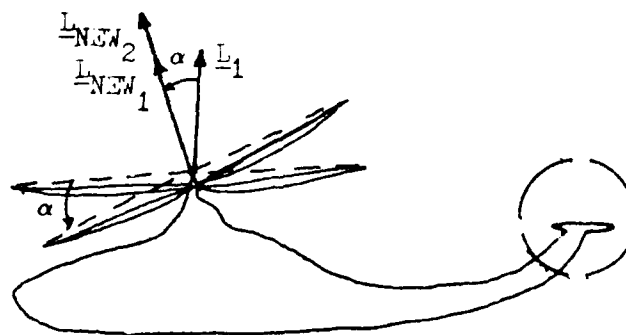


Figure 1. Helicopter Lift Vectors

helicopter is initially in hover, the lift expressed in the earth-axis

system  $(\hat{x}_E, \hat{y}_E, \hat{z}_E)$  is

$$L_{OLD} = -L_1 \hat{z}_E \quad (2.17)$$

By increasing the angle-of-attack, the new lift expressed in the earth-axis system is

$$L_{NEW_1} = L_1 \sin \alpha \hat{x}_E - L_1 \cos \alpha \hat{z}_E \quad (2.18)$$

Therefore, by increasing the angle of attack, the pilot increases the force or thrust along the  $\hat{x}_E$  coordinate by  $L_1 \sin \alpha$ . This increased force causes a forward velocity.

The collective lift control,  $\Delta \delta_c$ , is analogous to a power control. By changing the angle of attack of each blade by the same amount, the lift vector either increases or decreases in magnitude but not in direction. Again, if the helicopter is in hover, and the pilot decreases the angle-of-attack of each blade, the new lift is expressed by

$$L_{NEW_2} = -L_2 \hat{z}_E \quad (2.19)$$

where  $L_2 < L_1$ . This deflection of the collective lift control results in a loss of altitude. If instead, the pilot increases the angle-of-attack of each blade while at lift vector,  $L_{NEW_1}$ , the new lift vector is

$$L_{NEW_2} = L_2 \sin \alpha \hat{x}_E - L_2 \cos \alpha \hat{z}_E \quad (2.20)$$

where  $L_2 > L_1$ . The helicopter experiences an increase in lift, altitude, and forward velocity.

The lateral control surfaces consist of the cyclic roll control,  $\Delta \delta_a$ , and the tail rotor yaw control,  $\Delta \delta_p$ . The cyclic roll control is

analogous to an aileron for an aircraft and operates like the cyclic pitch control except that a change in angle-of-attack of the blades as a whole results in a lift vector in the  $(\hat{y}_E, \hat{z}_E)$  plane instead of the  $(\hat{x}_E, \hat{z}_E)$  plane. The tail rotor yaw control,  $\Delta\delta_p$ , is analogous to the rudder of an aircraft. The tail rotor yaw control maintains the orientation of the helicopter, especially during changes in the lift vector, by acting as a counter-torque to the torque produced by the rotation of the main rotor.

The control limits for the UH-60A Black Hawk helicopter, listed below, are for pedal deflections or stick displacements. The units of the control surface deflections are in inches. Even though the control limits are

$$\begin{aligned} -5.00 &\leq \Delta\delta_e \leq 5.00 \\ 0.0 &\leq \Delta\delta_c \leq 8.75 \\ -5.00 &\leq \Delta\delta_a \leq 5.00 \\ -2.75 &\leq \Delta\delta_p \leq 2.75 \end{aligned} \tag{2.21}$$

listed, the actual amount of control deflection depends on the trim condition of the helicopter.

#### Actuator Models

The actuator dynamics for the cyclic pitch control, cyclic roll control, and tail rotor yaw control can be modelled as a first-order transfer function  $[500/(s+500)]$ . The following equations are simulated with the flight dynamics model. It should be noted that the actuator dynamics are not incorporated into the A matrix, but they are included in simulating the complete system.



$$\delta_i(s) = \frac{500}{s+500} \delta_{i\_cmd}(s) \quad (2.22)$$

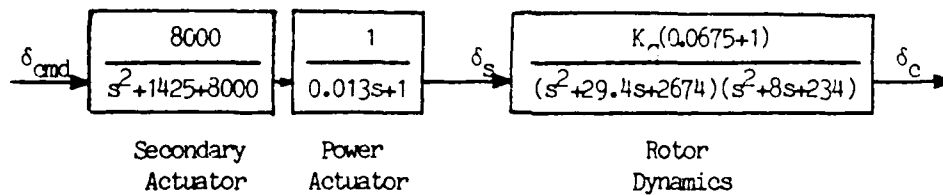
where  $i = e, a, \text{ and } p$

$$\delta_i(s) [s+500] = 500 \delta_{i\_cmd}(s) \quad (2.23)$$

$$\dot{\delta}_i(t) + 500 \delta_i(t) = 500 \delta_{i\_cmd}(t) \quad (2.24)$$

$$\dot{\delta}_i(t) = -500 \delta_i(t) + 500 \delta_{i\_cmd}(t) \quad (2.25)$$

The actuator dynamics for the collective lift control can be modelled by the following block diagram:



where  $K_G = (2674)(234) = 625,716$ . For a step input, the following figures of merit are obtained:

Rise time	$(t_r) = 0.0481706$	
Peak time	$(t_p) = 0.184195$	
Settling time	$(t_s) = 1.08044$	(2.26)
Peak value	$(M_p) = 1.70024$	
Final value	$(FV) = 1.00000$	

In order to simulate the actuator dynamics in MULTI, a second-order transfer function is needed. The proposed second-order collective lift control actuator dynamics model is shown in the following block diagram:

This transfer function can be represented in terms of phase variable

notation. The resulting state and output equations are

$$\dot{\underline{x}} = \begin{bmatrix} 0 & 1 \\ -241 & -8 \end{bmatrix} \underline{x} + \begin{bmatrix} 0 \\ 1 \end{bmatrix} \delta_{c_{cmd}} \quad (2.28)$$

$$\delta_c = [ 241 \quad 16.06 ] \underline{x} \quad (2.29)$$

This model for the collective lift control yields the following figures of merit for a unit step input

Rise time	$(t_r) = 0.0470176$	
Peak time	$(t_p) = 0.146900$	
Settling time	$(t_s) = 1.02511$	(2.30)
Peak value	$(M_p) = 1.68905$	
Final value	$(FV) = 1.00000$	

Comparing the figures of merit for the original actuator dynamics model with the approximate dynamics model reveals that the second-order collective lift control actuator dynamics model is a good match.

### Trim Conditions

The perturbation state equations were developed by linearizing the nonlinear aerodynamic equations for the helicopter around an equilibrium condition. For the UH-60A Black Hawk's mission to be completed, it must perform different maneuvers at six different trim equilibrium flight conditions. The flight conditions are specified by the total velocity in the earth-axis-system ( $V_{EAS}$ ). For the three maneuvers to be performed: a coordinated turn, a yaw rate response, and a vertical rate response, the flight conditions for  $V_{EAS} = 20, 40, 60, 100$  and  $140$  knots were used. For each flight condition, a set of trim equilibrium values

were supplied by the sponsor. The trim equilibrium values are given for  $\theta$ ,  $\phi$ ,  $w_B$ ,  $\delta_e$ ,  $\delta_a$ ,  $\delta_c$ , and  $\delta_p$ . The remaining equilibrium values can be found, if desired, by using the following equations:

$$\text{True Velocity } (V_T) = V_{EAS} \times \frac{6080 \text{ ft/nautical mile}}{3600 \text{ sec}} \quad (2.31)$$

$$V_T = [u_B + v_B + w_B]^{1/2} \quad (2.32)$$

$$\beta = \sin^{-1}(v_B/v_T) \quad (2.33)$$

$$\alpha = \tan^{-1}(w_B/u_B) \quad (2.34)$$

$$\gamma = \theta - \alpha \quad (2.35)$$

From the trimmed surface deflections, the new control limits can be derived. For instance, if  $(\delta_a)_e = -0.758$ , then the cyclic roll control can only deflect another 4.242 inches in the negative direction and 5.758 inches in the positive direction. Therefore, the new control limits for the cyclic roll control are

$$-4.242 \leq \delta_a \leq 5.758 \quad (2.36)$$

For the  $V_{EAS} = 20$  knots flight condition (see Equation (2.15) for the state equations), the equilibrium trim values are:

$$\begin{aligned} \theta_e &= 5.83 \text{ deg} \\ \phi_e &= -1.34 \text{ deg} \\ w_{Be} &= 3.42 \text{ ft/sec} \\ (\delta_a)_e &= -0.994 \text{ inches} \\ (\delta_e)_e &= -0.368 \text{ inches} \\ (\delta_c)_e &= 5.35 \text{ inches} \\ (\delta_p)_e &= -1.06 \text{ inches} \\ V_T &= 33.5 \text{ ft/sec} \end{aligned} \quad (2.37)$$

For the trimmed values of the control surfaces, the new control surface limits are:

$$\begin{array}{cccc}
 & \delta_e & \delta_c & \delta_a & \delta_p \\
 \text{MIN.} & -4.632 & -5.35 & -4.006 & -1.69 \\
 \text{MAX.} & 5.368 & 3.40 & 5.994 & 3.81
 \end{array} \quad (2.38)$$

It should be noted that all simulation results are perturbations from the equilibrium conditions. The following pages contain the other four flight conditions with the appropriate perturbation state equations and trim equilibrium values.

States Equations for the Flight Condition:  $V_{EAS} = 40$  knots

$$\frac{d}{dt} \begin{bmatrix} \theta \\ \phi \\ u_B \\ v_B \\ w_B \\ p_B \\ q_B \\ r_B \end{bmatrix} = \begin{bmatrix} 0 & 0 & 0 & 0 & 0 & 0 & 1 & .0176 \\ 0 & 0 & 0 & 0 & 0 & 1 & -.00133 & .0759 \\ -32.1 & 0 & -.0112 & -.00985 & .0429 & -.0583 & -1.88 & -.107 \\ .0428 & 32.1 & .0026 & -.0819 & .00808 & 2.72 & .213 & -60.3 \\ -2.44 & .564 & -.125 & -.0153 & -.562 & .955 & 70.2 & -.417 \\ 0 & 0 & -.00963 & -.0312 & .0268 & -3.94 & -1.76 & .116 \\ 0 & 0 & -.00023 & .00783 & .00675 & .247 & -1.07 & -.0896 \\ 0 & 0 & -.00623 & .011 & -.00522 & -.408 & -.663 & -.528 \end{bmatrix} \begin{bmatrix} \theta \\ \phi \\ u_B \\ v_B \\ w_B \\ p_B \\ q_B \\ r_B \end{bmatrix}$$

$$+ \begin{bmatrix} 0 & 0 & 0 & 0 \\ 0 & 0 & 0 & 0 \\ -1.5 & .701 & .0181 & .866 \\ -.0395 & .196 & .94 & -1.36 \\ -2.03 & -7.48 & .0994 & 1.63 \\ .097 & .205 & 1.35 & -.636 \\ .372 & .0635 & -.00149 & -.0297 \\ -.0133 & .0255 & .0868 & .542 \end{bmatrix} \begin{bmatrix} \Delta \delta_e \\ \Delta \delta_c \\ \Delta \delta_a \\ \Delta \delta_p \end{bmatrix} \quad (2.39)$$

Equilibrium Trim Values for the Flight Condition:  $V_{EAS} = 40$  knots

True Velocity ( $V_T$ ) = 67.55 ft/sec

$$\theta_e = 4.34 \text{ deg}$$

$$\phi_e = -1.01 \text{ deg}$$

$$w_{B_e} = 5.11 \text{ ft/sec} \quad (2.40)$$

$$(\delta_a)_e = -0.758 \text{ inches}$$

$$(\delta_e)_e = -0.208 \text{ inches}$$

$$(\delta_c)_e = 4.58 \text{ inches}$$

$$(\delta_p)_e = -0.583 \text{ inches}$$

For the trimmed values of the control surfaces, the new control surface limits are:

	$\delta_e$	$\delta_c$	$\delta_a$	$\delta_p$	
MIN.	-4.792	-4.58	-4.242	-2.167	(2.41)
MAX.	5.208	4.17	5.758	3.333	

States Equations for the Flight Condition:  $V_{EAS} = 60$  knots

$$\frac{d}{dt} \begin{bmatrix} \theta \\ \phi \\ u_B \\ v_B \\ w_B \\ p_B \\ q_B \\ r_B \end{bmatrix} = \begin{bmatrix} 0 & 0 & 0 & 0 & 0 & 0 & 1 & 0 \\ 0 & 0 & 0 & 0 & 0 & 0 & 1 & 0.061 \\ -32.1 & 0 & -.019 & -.00227 & .0481 & .0155 & -2.77 & 9.91 \\ 0 & 32.1 & -.00342 & -.104 & .0102 & 3.52 & .461 & -99.3 \\ -1.96 & 0 & -.0475 & -.0205 & -.67 & -8.64 & 104. & -.497 \\ 0 & 0 & -.0076 & -.0329 & .0229 & 4.05 & -1.69 & .246 \\ 0 & 0 & .00193 & .00602 & .00891 & .201 & -1.23 & -.113 \\ 0 & 0 & -.00409 & .0138 & -.00977 & -.333 & -.563 & -.644 \end{bmatrix} \begin{bmatrix} \theta \\ \phi \\ u_B \\ v_B \\ w_B \\ p_B \\ q_B \\ r_B \end{bmatrix} + \begin{bmatrix} 0 & 0 & 0 & 0 \\ 0 & 0 & 0 & 0 \\ -1.41 & .593 & -.0108 & .872 \\ .0208 & .246 & .93 & -1.59 \\ -3.27 & -8.32 & .3744 & 2.37 \\ .113 & .197 & 1.34 & -.75 \\ .400 & .0892 & .0053 & -.0334 \\ -.0261 & -.0385 & .0872 & .645 \end{bmatrix} \begin{bmatrix} \Delta \delta_e \\ \Delta \delta_c \\ \Delta \delta_a \\ \Delta \delta_p \end{bmatrix} \quad (2.42)$$

Equilibrium Trim Values for the Flight Condition:  $V_{EAS} = 60$  knots

True Velocity ( $V_T$ ) = 101.33 ft/sec

$$\theta_e = 3.49 \text{ deg}$$

$$\phi_e = 0 \text{ deg}$$

$$w_{B_e} = 6.13 \text{ ft/sec} \quad (2.43)$$

$$(\delta_a)_e = -0.237 \text{ inches}$$

$$(\delta_e)_e = -0.425 \text{ inches}$$

$$(\delta_c)_e = 4.20 \text{ inches}$$

$$(\delta_p)_e = -0.581 \text{ inches}$$

For the trimmed values of the control surfaces, the new control surface limits are:

	$\delta_e$	$\delta_c$	$\delta_a$	$\delta_p$	
MIN.	-4.575	-4.20	-4.763	-2.169	(2.44)
MAX.	5.425	4.55	5.237	3.331	

States Equations for the Flight Condition:  $V_{EAS} = 100$  knots

$$\frac{d}{dt} \begin{bmatrix} \theta \\ \phi \\ u_B \\ v_B \\ w_B \\ p_B \\ q_B \\ r_B \end{bmatrix} = \begin{bmatrix} 0 & 0 & 0 & 0 & 0 & 0 & 1 & 0 \\ 0 & 0 & 0 & 0 & 0 & 1 & 0 & 0.0432 \\ -32.2 & 0 & -0.0324 & -0.000582 & 0.0643 & -0.113 & -4.48 & 7.93 \\ 0 & 32.2 & -0.000714 & -0.143 & 0.0102 & 4.66 & 0.752 & -167.3 \\ -1.39 & 0 & -0.00879 & -0.0174 & -0.79 & -5.32 & 173. & -0.505 \\ 0 & 0 & -0.00304 & -0.0324 & 0.0191 & -4.00 & -1.58 & 0.356 \\ 0 & 0 & 0.00251 & 0.00164 & 0.00921 & 0.103 & -1.61 & -0.104 \\ 0 & 0 & -0.00304 & 0.0168 & -0.0117 & -0.294 & -0.513 & -0.836 \end{bmatrix} \begin{bmatrix} \theta \\ \phi \\ u_B \\ v_B \\ w_B \\ p_B \\ q_B \\ r_B \end{bmatrix} + \begin{bmatrix} 0 & 0 & 0 & 0 \\ 0 & 0 & 0 & 0 \\ -1.08 & 0.646 & -0.0166 & 0.7 \\ -0.0167 & 0.34 & 0.932 & -1.94 \\ -6.14 & -9.63 & 0.5634 & 4.0 \\ 0.138 & 0.228 & 1.34 & -0.924 \\ 0.46 & 0.095 & 0.0283 & -0.0752 \\ -0.0411 & -0.0994 & 0.0861 & 0.805 \end{bmatrix} \begin{bmatrix} \Delta \delta_e \\ \Delta \delta_c \\ \Delta \delta_a \\ \Delta \delta_p \end{bmatrix} \quad (2.45)$$

Equilibrium Trim Values for the Flight Condition:  $V_{EAS} = 100$  knots

True Velocity ( $V_T$ ) =

$$\begin{aligned}
 \theta_e &= 2.47 \text{ deg} \\
 \phi_e &= 0.0 \text{ deg} \\
 w_{B_e} &= 7.27 \text{ ft/sec} \\
 (\delta_a)_e &= 0.179 \text{ inches} \\
 (\delta_e)_e &= -1.06 \text{ inches} \\
 (\delta_c)_e &= 4.43 \text{ inches} \\
 (\delta_p)_e &= -0.260 \text{ inches}
 \end{aligned} \tag{2.46}$$

For the trimmed values of the control surfaces, the new control surface limits are:

	$\delta_e$	$\delta_c$	$\delta_a$	$\delta_p$	
MIN.	-3.94	-4.43	-5.179	-2.49	(2.47)
MAX.	6.06	4.32	4.821	3.01	

States Equations for the Flight Condition:  $V_{EAS} = 140$  knots

$$\frac{d}{dt} \begin{bmatrix} \theta \\ \phi \\ u_B \\ v_B \\ w_B \\ p_B \\ q_B \\ r_B \end{bmatrix} = \begin{bmatrix} 0 & 0 & 0 & 0 & 0 & 0 & 1 & 0 \\ 0 & 0 & 0 & 0 & 0 & 1 & 0 & -0.0161 \\ -32.2 & 0 & -.0402 & -.00206 & .0726 & -.336 & 5.55 & 8.81 \\ 0 & 32.2 & .00185 & -.184 & .00698 & -.603 & 1.01 & -.234 \\ 0.518 & 0 & -.00798 & -.0424 & -.871 & -4.94 & 243. & -.354 \\ 0 & 0 & .000609 & 0.0338 & .0152 & -3.73 & -1.44 & .519 \\ 0 & 0 & .00509 & -.00707 & .00944 & .0038 & -2.02 & -.0252 \\ 0 & 0 & -.00381 & .0184 & -.00653 & -.35 & -.541 & -.992 \end{bmatrix} \begin{bmatrix} \theta \\ \phi \\ u_B \\ v_B \\ w_B \\ p_B \\ q_B \\ r_B \end{bmatrix}$$

$$+ \begin{bmatrix} 0 & 0 & 0 & 0 \\ 0 & 0 & 0 & 0 \\ -.808 & .489 & -.00579 & .567 \\ -.0771 & .38 & .97 & -2.18 \\ -9.12 & -11.1 & .849 & 5.54 \\ 0.143 & .247 & 1.36 & -1.04 \\ 0.53 & 0.00436 & .0647 & -.175 \\ .0117 & -.0785 & .0840 & .882 \end{bmatrix} \begin{bmatrix} \Delta \delta_e \\ \Delta \delta_c \\ \Delta \delta_a \\ \Delta \delta_p \end{bmatrix} \tag{2.48}$$

Equilibrium Trim Values for the Flight Condition:  $V_{EAS} = 140$  knots

True Velocity ( $V_T$ ) =

$$\theta_e = -0.921 \text{ deg}$$

$$\phi_e = 0.0 \text{ deg}$$

$$w_{B_e} = -3.79 \text{ ft/sec} \quad (2.49)$$

$$(\delta_a)_e = 0.388 \text{ inches}$$

$$(\delta_e)_e = -1.64 \text{ inches}$$

$$(\delta_c)_e = 5.74 \text{ inches}$$

$$(\delta_p)_e = -.0260 \text{ inches}$$

For the trimmed values of the control surfaces, the new control surface limits are:

	$\delta_e$	$\delta_c$	$\delta_a$	$\delta_p$	
MIN.	-3.36	-5.74	-5.388	-2.724	(2.50)
MAX.	6.64	3.01	4.612	2.776	



### III. Multivariable Control Law Theory Overview

The multivariable digital control law designs in this thesis are the result of the application of control law methods developed by Professor Brian Porter of the University of Salford, England. The techniques are presented in Reference 14. This chapter summarizes the techniques used in the design of high performance tracking systems for aircraft control. The theoretical discussions cover the continuous-time case as well as the corresponding discrete-time case. A better insight into the design process can be obtained by examining the s-plane root locations and their migrations as the gains  $\rightarrow \infty$  than the corresponding z-plane analysis. Finally, an understanding of the effects of transmission zeroes, especially unstable ones, is considered.

The plant to be controlled can be described by a first-order set of linear differential equations. These equations written in state-space format are of the form:

$$\dot{\underline{x}} = \underline{A}\underline{x} + \underline{B}u \quad (3.1)$$

$$\underline{y} = \underline{C}\underline{x} \quad (3.2)$$

where

$\underline{A}$  = a continuous-time plant matrix (nxn)

$\underline{B}$  = a continuous-time control matrix (nxm)

$\underline{C}$  = a continuous-time output matrix (pxn)

The dimensions n, m, and p are defined as the number of states, inputs, and outputs.

The  $\underline{A}$ ,  $\underline{B}$ , and  $\underline{C}$  matrices are partitioned to yield the following equations:

$$\begin{bmatrix} \dot{\underline{x}}_1 \\ \dot{\underline{x}}_2 \end{bmatrix} = \begin{bmatrix} \underline{A}_{11} & \underline{A}_{12} \\ \underline{A}_{21} & \underline{A}_{22} \end{bmatrix} \begin{bmatrix} \underline{x}_1 \\ \underline{x}_2 \end{bmatrix} + \begin{bmatrix} \underline{B}_1 \\ \underline{B}_2 \end{bmatrix} \underline{u} \quad (3.3)$$

$$\underline{y} = [\underline{C}_1 \quad \underline{C}_2] \begin{bmatrix} \underline{x}_1 \\ \underline{x}_2 \end{bmatrix} \quad (3.4)$$

In equations (3.3) and (3.4),  $\underline{x}_1 \in \mathbb{R}^{n-m}$ ,  $\underline{x}_2 \in \mathbb{R}^m$ ,  $\underline{u} \in \mathbb{R}^p$ ,  $\underline{y} \in \mathbb{R}^p$ ,  $\underline{A}_{11} \in \mathbb{R}^{(n-m) \times (n-m)}$ ,  $\underline{A}_{12} \in \mathbb{R}^{(n-m) \times m}$ ,  $\underline{A}_{21} \in \mathbb{R}^{m \times (n-m)}$ ,  $\underline{A}_{22} \in \mathbb{R}^{m \times m}$ ,  $\underline{B}_1 \in \mathbb{R}^{(n-m) \times p}$ ,  $\underline{B}_2 \in \mathbb{R}^{m \times p}$ ,  $\underline{C}_1 \in \mathbb{R}^{p \times (n-m)}$ , and  $\underline{C}_2 \in \mathbb{R}^{p \times p}$ . The matrix  $\underline{B}_2$  is a square matrix with a row and column size equal to the number of inputs in the vector  $\underline{u}$ . The matrix  $\underline{C}_2$  is also square with the number of rows and columns equal to the number of outputs. The designation of "inputs" for the aircraft model usually refers to the control surfaces, such as elevator or ailerons for a fixed wing aircraft, or cyclic pitch control and cyclic roll control for a helicopter. However, in designs which incorporate the surface actuator states into the  $\underline{A}$  matrix, the "inputs" then denote the surface actuator input commands. Outputs are states or combinations of states of the aircraft such as pitch rate, roll angle, and flight path angle.

A requirement of the design method is that the number of inputs equal the number of outputs, thus  $\underline{B}_2$ ,  $\underline{C}_2$  and  $\underline{A}_{22}$  have the same row and column dimensions. The input and output dimensions,  $m$  and  $p$ , are then replaced by a new dimension  $\ell$ , since  $m=p=\ell$ . Knowing these dimension requirements allows the system matrices to be easily partitioned as shown above.

Two design methods are applicable to the vehicle under study using the regular or irregular designs. The design method used is determined by the type of plant being considered.

### Regular Versus Irregular Design

To be considered as a "regular design", the matrix representing the first Markov parameter,  $[CB]$ , must have rank equal to the number of outputs, i.e.  $\text{rank } [CB] = l$ . The gain matrix is formed using the inverse of  $[CB]$ ; therefore, a rank deficient  $[CB]$  will cause an indefinite gain matrix to be formed.

Plants in which the first Markov parameter,  $[CB]$ , is rank deficient are designated as "irregular". To allow a design to be accomplished, the output to be controlled is changed to  $\underline{w}(t) = \underline{y}(t) + \underline{M}x_1(t)$ . The new output matrix  $F$  is formed as shown and used in place of the  $\underline{C}$  matrix:

$$\underline{F} = [\underline{F}_1 \quad \underline{F}_2] \quad (3.5)$$

where

$$\underline{F}_1 = [\underline{C}_1 + \underline{M}A_{11}] \quad (3.6)$$

$$\underline{F}_2 = [\underline{C}_2 + \underline{M}A_{12}] \quad (3.7)$$

The elements of the  $\underline{M}$  matrix are selected to obtain a matrix  $[\underline{FB}]$  having full rank and thus being invertible.

The fast-sampling error-actuated digital control law governed on the discrete-time set  $T_T = \{0, T, 2T, \dots\}$  is a proportional plus integral feedback law expressed as:

$$\underline{u}(kT) = (1/T)\{\underline{K}_0 \underline{e}(kT) + \underline{K}_1 \underline{z}(kT)\} \quad (3.8)$$

where

$1/T$  is the sampling frequency

$\underline{K}_0$  is the proportional gain matrix for the error signal  $\underline{e}(kT)$ ,  $\underline{K}_0 \in R^{l \times l}$

$\underline{K}_1$  is the gain matrix for the backward difference of the error signal, which is designated  $\underline{z}(kT)$ ,  $\underline{K}_1 \in R^{l \times l}$ .

The  $\ell$  discrete-time vector integrators which generate the  $\underline{z}(kT)$  vectors are defined by the equation:

$$\underline{z}\{(k+1)T\} = \underline{z}(kT) + T\mathbf{e}(kT) \quad (3.9)$$

For the continuous case, the control law governed on the set  $T = [0, t]$  can be expressed as

$$\begin{aligned} \underline{u} &= g(\underline{K}_0 \mathbf{e}(t) + \underline{K}_1 \int \mathbf{e}(t) dt) \\ &= g(\underline{K}_0 \mathbf{e}(t) + \underline{K}_1 \underline{z}(t)) \end{aligned} \quad (3.10)$$

where

$g$  is the forward path gain

$\underline{K}_0$  is the proportional gain for the error signal

$\underline{K}_1$  is the gain for the integral of the error signal.

The control input vector  $\underline{u}$  is required to cause the output vector  $\underline{y}$  to track any constant command input vector  $\underline{v}$  on  $T$  (or  $T_T$ ) in the sense that the error vector  $\mathbf{e}(t) = \underline{v}(t) - \underline{y}(t)$  assumes the steady-state value

$$\lim_{t \rightarrow \infty} \mathbf{e}(t) = \lim_{t \rightarrow \infty} \{\underline{v}(t) - \underline{y}(t)\} = 0 \quad (3.11)$$

for arbitrary initial conditions.

A block diagram of the system with this control law is presented in Figures 2 and 3 for both the continuous and discrete cases. The portion in broken lines is present only for irregular designs.

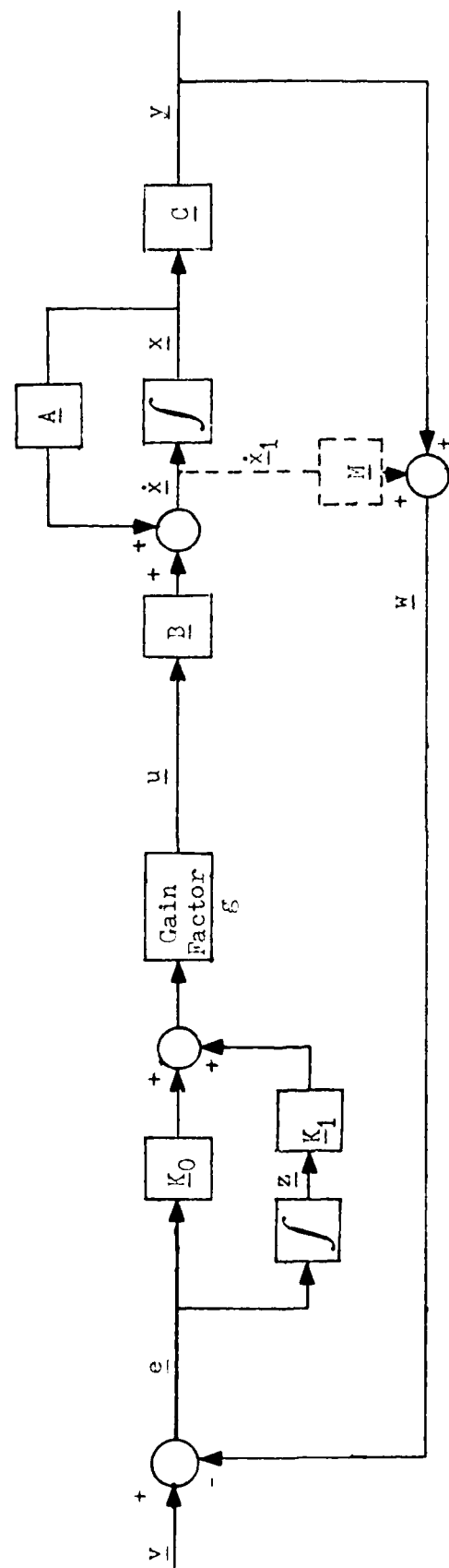


Figure 2. System Block Diagram - Continuous Design

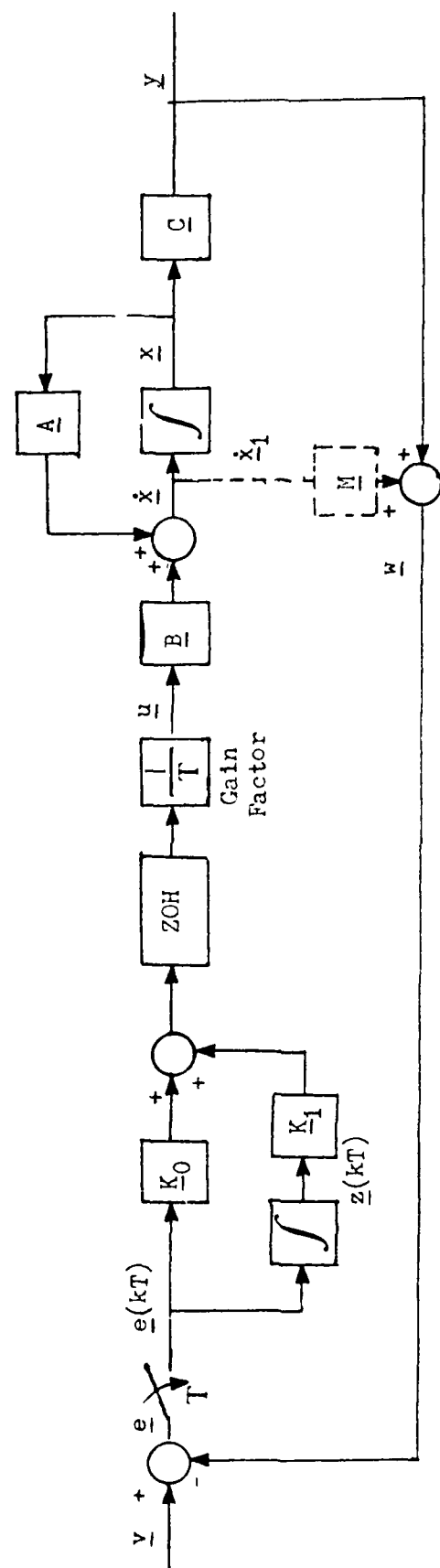


Figure 3. System Block Diagram - Discrete Design

The gain factor in the figures is the sampling frequency ( $1/T$ ) for the discrete system or a gain constant ( $g$ ) for the inuous system. For the regular design the error vector  $\underline{e}$  is expressed as  $\underline{e} = \underline{v} - \underline{y}$ . The dimension of  $\underline{e}$  is equal to  $l$ . Each command in the vector  $\underline{v}$  is summed with the negative of its corresponding output element in the  $\underline{y}$  vector and is the input for the proportional plus integral gain paths. For the discrete case, the control law is

$$\underline{u}(kT) = (1/T)[K_0(\underline{v}(kT) - \underline{y}(kT)) + K_1 \underline{z}(kT)] \quad (3.12)$$

where  $\underline{v}(kT) = \underline{v} = \text{constant command vector during the simulation}$ . For the integral forward path there exists a bank of integrators, one for each error signal developed, that insure that the error signals are always driven to zero, thus resulting in the final value of the output equal to the input for the step type commands.

In the irregular design, the  $\underline{e}$  vector is defined by

$$\underline{e} = \underline{v} - \underline{w} \quad (3.13)$$

where

$$\underline{w} = \underline{y} + \underline{M}\dot{\underline{x}}_1 \quad (3.14)$$

These outputs  $\underline{w}$  are developed with the measurement matrix  $\underline{M} \in \mathbb{R}^{l \times (n-l)}$  and the derivatives  $\dot{\underline{x}}_1$  of the system states. Again, for step inputs, the error signal is driven to zero. Rates of the system states,  $\dot{\underline{x}}_1$ , go to zero because there is no input signal to these state equations if the  $\underline{B}$  matrix is in zero- $\underline{B}_2$  form. The one exception to the state derivatives,  $\dot{\underline{x}}_1$  always going to zero is when a state derivative in  $\dot{\underline{x}}_1$  is a function of a state in  $\underline{x}_2$ . If the state in  $\underline{x}_2$  is commanded to a

constant, the state derivative in  $\dot{\underline{x}}_1$  will also be a constant in steady state. A simple example is if the rate of change of the roll angle ( $\dot{\phi}$ ) is a function of the roll rate ( $\Delta p_B$ ) and the yaw rate ( $\Delta r_B$ ), specifically,  $\dot{\phi} = a_1 \Delta p_B + a_2 \Delta r_B$  where  $a_1 \gg a_2$ , then if  $\Delta r_B$  is commanded to a constant ( $k_1$ ) and the  $\Delta p_B$  to zero, the rate of change of roll angle will be equal to  $a_2 k_1$  in steady-state. Therefore, to obtain zero steady-state error, the measurement matrix elements must be chosen so that the system does not feedback the  $\dot{\phi}$  state derivative.

### Asymptotic Characteristics

For the design shown in Figure 2, as the gain factor  $g$  increases, the system transfer function  $\underline{G}(s) = \underline{C}(s\underline{I} - \underline{A})^{-1}\underline{B}$  approaches the asymptotic form

$$\underline{\Gamma}(\lambda) = \underline{\tilde{\Gamma}}(\lambda) + \underline{\hat{\Gamma}}(\lambda) \quad (3.5)$$

where

$$\underline{\tilde{\Gamma}}(\lambda) = \underline{C}_0 (\lambda \underline{I}_n - \underline{A}_0)^{-1} \underline{B}_0 \quad (3.16)$$

$$\underline{\hat{\Gamma}}(\lambda) = \underline{C}_2 (\lambda \underline{I}_\ell - g \underline{A}_4)^{-1} g \underline{B}_2 \underline{K}_0 \quad (3.17)$$

$$\underline{A}_0 = \left[ \begin{array}{c|c} -\underline{K}_0^{-1} \underline{K}_1 & \underline{0} \\ \hline \underline{A}_{12} \underline{C}_2^{-1} \underline{K}_0^{-1} \underline{K}_1 & \underline{A}_{11} - \underline{A}_{12} \underline{C}_2^{-1} \underline{C}_1 \end{array} \right] \quad (3.18)$$

$$\underline{B}_0 = \left[ \begin{array}{c} \underline{0} \\ \hline \underline{A}_{12} \underline{C}_2^{-1} \end{array} \right] \quad (3.19)$$

$$\underline{C}_0 = [\underline{K}_0^{-1} \underline{K}_1 \mid \underline{0}] \quad (3.20)$$

and

$$\underline{A}_4 = -\underline{B}_2 \underline{K}_0 \underline{C}_2 \quad (3.21)$$



The matrix  $\tilde{\Gamma}(\lambda)$  is the "slow" transfer function matrix and  $\hat{\Gamma}(\lambda)$  is the "fast" transfer function matrix. The poles of these transfer functions fall into three groups designated  $Z_1$ ,  $Z_2$ , and  $Z_3$ . The "slow" modes  $Z_s$  of the tracking system correspond as  $g \rightarrow \infty$  to the poles  $Z_1 \cup Z_2$  of  $\tilde{\Gamma}(\lambda)$  where

$$Z_1 = \{\lambda \in \mathbb{C} : |\lambda \underline{K}_0 + \underline{K}_1| = 0\} \quad (3.22)$$

and

$$Z_2 = \{\lambda \in \mathbb{C} : |\lambda \underline{I}_{n-l} - \underline{A}_{11} + \underline{A}_{12} \underline{C}_2^{-1} \underline{C}_1| = 0\}. \quad (3.23)$$

The poles of  $Z_1$  are called the assignable finite eigenvalues while the poles of  $Z_2$  contain all of the transmission zeroes in the system. The "fast" modes  $Z_f$  of the tracking system correspond as  $g \rightarrow \infty$  to the poles of  $\hat{\Gamma}(\lambda)$  where

$$Z_3 = \{\lambda \in \mathbb{C} : |\lambda \underline{I}_l + g \underline{C}_2 \underline{B}_2 \underline{K}_0| = 0\}. \quad (3.24)$$

The poles  $Z_3$  are called the fast eigenvalues of the system.

From the matrix partitions of  $\underline{B}_0$  and  $\underline{C}_0$ , it follows that as  $g \rightarrow \infty$ , the "slow" transfer function matrix

$$\tilde{\Gamma}(\lambda) = \underline{0} \quad (3.25)$$

Therefore, from equation (3.15), the transfer function matrix  $\underline{G}(\lambda)$  of the continuous-time closed-loop tracking system assumes the asymptotic form

$$\Gamma(\lambda) = (\lambda \underline{I}_l + g \underline{C}_2 \underline{B}_2 \underline{K}_0)^{-1} g \underline{C}_2 \underline{B}_2 \underline{K}_0 \quad (3.26)$$

in consonance with the fact that only the "fast" modes corresponding to the poles  $Z_3$  remain both controllable and observable as  $g \rightarrow \infty$ . The "slow" transfer function modes corresponding to the poles  $Z_1$  become asymptotically uncontrollable as  $g \rightarrow \infty$  in view of the block structure of

the matrices  $A_0$  and  $B_0$ . The rank of the controllability matrix is

$$\text{rank } \underline{M}_c = \text{rank} \begin{bmatrix} \underline{B}_0 & \underline{A}_0 \underline{B}_0 & \underline{A}_0^2 \underline{B}_0 & \dots & \underline{A}_0^{n-1} \underline{B}_0 \end{bmatrix} = n-l \quad (3.27)$$

which indicates that there are  $l$  uncontrollable finite assignable poles in  $Z_1$ . The number of poles in  $Z_1$  agrees with Equation (3.22). The values of the  $Z_1$  poles are equal to the ratio of integral to proportional gain values. (This can be shown by substituting Equation (3.31) into Equation (3.22).)

The "slow modes" corresponding to the poles of  $Z_2$  become asymptotically unobservable as  $g \rightarrow \infty$  in view of the block structure of the matrices  $\underline{A}_0$  and  $\underline{C}_0$ . The rank of the observability matrix

$$\text{rank } \underline{M}_o = \text{rank} \begin{bmatrix} \underline{C}_0^T & \underline{A}_0^T \underline{C}_0^T & (\underline{A}_0^T)^2 \underline{C}_0^T & \dots & (\underline{A}_0^T)^{n-1} \underline{C}_0^T \end{bmatrix} = l \quad (3.28)$$

which indicates that there are  $n-l$  unobservable finite poles in  $Z_2$ . The number of poles in  $Z_2$  agrees with Equation (3.23) and they are located at the transmission zero locations. The number of  $Z_3$  infinite poles equals the number ( $l$ ) of outputs of the system. Expressions for the asymptotic modes are given in Table 1.

As the gain factor  $g$  is increased, tracking of the system's output to input commands ( $\underline{v}$ ) becomes increasingly "tight". Reference 14 shows that only moderate increases in gain factor are needed for the output to resemble an extremely fast first-order response. Although the dominant finite (fast) roots can be made complex, much of the experience to date has been with real roots.

The gain  $\underline{K}_0$  is chosen such that

$$\underline{CBK}_0 = \text{diagonal } \{\sigma_1, \sigma_2, \dots, \sigma_l\} \quad (3.29)$$

Table 1  
Asymptotic Equations for Zero-B<sub>2</sub> Form

System is represented by:

$$\begin{bmatrix} \dot{x}_1 \\ \dot{x}_2 \end{bmatrix} = \begin{bmatrix} A_{11} & A_{12} \\ A_{21} & A_{22} \end{bmatrix} \begin{bmatrix} x_1 \\ x_2 \end{bmatrix} + \begin{bmatrix} 0 \\ B_2 \end{bmatrix} \bar{u} \quad \text{and} \quad y = \begin{bmatrix} C_1 & C_2 \end{bmatrix} \begin{bmatrix} x_1 \\ x_2 \end{bmatrix}$$

### Continuous Case

Gain Factor = g

(Poles are in the s-plane)

$$\tilde{\Gamma}(\lambda) = \underline{C}_0(\lambda \underline{I}_n - \underline{A}_0)^{-1} \underline{B}_0 = 0$$

$$\Gamma(\lambda) = (\lambda \underline{I}_\ell + g \underline{C}_2 \underline{B}_2 \underline{K}_0)^{-1} g \underline{C}_2 \underline{B}_2 \underline{K}_0$$

(Finite roots)

$$Z_1 = |\lambda \underline{K}_0 + \underline{K}_1| = 0$$

$$Z_2 = |\lambda \underline{I}_{n-\ell} - \underline{A}_{11} + \underline{A}_{12} \underline{C}_2^{-1} \underline{C}_1| = 0$$

(Infinite roots)

$$Z_3 = |\lambda \underline{I}_\ell + g \underline{C}_2 \underline{B}_2 \underline{K}_0| = 0$$

### Discrete Case

Gain Factor = 1/T

(Poles are in the z-plane)

$$\tilde{\Gamma}(\lambda) = \underline{C}_0(\lambda \underline{I}_n - \underline{A}_0)^{-1} \underline{B}_0$$

$$\Gamma(\lambda) = (\lambda \underline{I}_\ell - \underline{I}_\ell + \underline{C}_2 \underline{B}_2 \underline{K}_0)^{-1} \underline{C}_2 \underline{B}_2 \underline{K}_0$$

$$Z_1 = |\lambda \underline{I}_\ell - \underline{I}_\ell + \underline{T} \underline{K}_0^{-1} \underline{C}_1| = 0$$

$$Z_2 = |\lambda \underline{I}_{n-\ell} - \underline{T} \underline{A}_{11} + \underline{A}_{12} \underline{C}_2^{-1} \underline{C}_1| = 0$$

$$Z_3 = |\lambda \underline{I}_\ell - \underline{I}_\ell + \underline{C}_2 \underline{B}_2 \underline{K}_0| = 0$$

Table 1 (continued)

where:

$$\underline{A}_0 = \left[ \begin{array}{c|c} -\underline{\bar{K}}_0^{-1} \underline{\bar{K}}_1 & \underline{0} \\ \hline \underline{A}_{12} \underline{\bar{C}}_2^{-1} \underline{\bar{K}}_0^{-1} \underline{\bar{K}}_1 & \underline{A}_{11}^{-1} \underline{\bar{A}}_{12} \underline{\bar{C}}_2^{-1} \underline{\bar{C}}_1 \end{array} \right]$$

$$\underline{B}_0 = \left[ \begin{array}{c} \underline{0} \\ \hline \underline{A}_{12} \underline{\bar{C}}_2^{-1} \end{array} \right]$$

$$\underline{C}_0 = \left[ \underline{\bar{K}}_0^{-1} \underline{\bar{K}}_1 \mid \underline{0} \right]$$

where  $\sigma_j \in \mathbb{R}^+$  ( $j=1,2,3,\dots,l$ ). By using Equation (3.29), the proportional gain matrix can be found by

$$\underline{K}_0 = [\underline{CB}]^{-1} \underline{\Sigma} \quad (3.30)$$

The elements of the  $\underline{\Sigma}$  matrix, which is selected as a diagonal matrix, are chosen by the designer. These values determine respective gains or the weighting of each error signal on the control surface or the system input being commanded by the control law. The integral gain matrix  $\underline{K}_1$  is often determined by a scalar multiplication of the  $\underline{K}_0$  matrix.

$$\underline{K}_1 = \bar{\alpha} \underline{K}_0 \quad (3.31)$$

It follows from Equation (3.26) that the transfer function  $\underline{g}(\lambda)$  of the continuous-time tracking system assumes the diagonal asymptotic form

$$\underline{g}(\lambda) = \text{diagonal} \left\{ \frac{g\sigma_1}{\lambda+g\sigma_1}, \frac{g\sigma_2}{\lambda+g\sigma_2}, \dots, \frac{g\sigma_l}{\lambda+g\sigma_l} \right\} \quad (3.32)$$

For the digital system the asymptotic transfer function has the form:

$$\underline{g}(\lambda) = \text{diagonal} \left\{ \frac{\sigma_1}{\lambda-1+\sigma_1}, \frac{\sigma_2}{\lambda-1+\sigma_2}, \dots, \frac{\sigma_l}{\lambda-1+\sigma_l} \right\} \quad (3.33)$$

Therefore as  $g \rightarrow \infty$ , or  $T \rightarrow 0$ , the transfer matrix  $\underline{g}(\lambda)$  approaches a diagonal asymptotic form of increasingly noninteracting control. As can be seen from Equations (3.32) and (3.33), the  $Z_3$  infinite roots are located on the real axis equal to  $-g\sigma_1$  for the continuous case and at  $1-\sigma_1$ , which is near the z-plane origin for the discrete case.

For the irregular plant, the above equations are applied by replacing the  $\underline{C}$  matrix with an  $\underline{F}$  matrix. The component  $\underline{C}_1$  is replaced

by  $\underline{F}_1$  and  $\underline{C}_2$  is replaced by  $\underline{F}_2$  as calculated in Equations (3.6) and (3.7).

In the equations of Table 1, the gain values  $\underline{K}_0$  and  $\underline{K}_1$  are the same as those developed from the equations that are not in zero- $\underline{B}_2$  form. This is because

$$[\underline{CB}] = [\underline{C}_2 \underline{B}_2] \text{ or } [\underline{FB}] = [\underline{F}_2 \underline{B}_2] \quad (3.34)$$

### Transmission Zeros

Transmission zeros are considered as regions in either the s-plane or the z-plane. These regions are asymptotic locations for certain finite or slow poles of the system. Output feedback does not alter the locations of transmission zeros (Ref 20) for regular systems. Such locations coincide with conventional single input/single output transfer function zeroes; or for MIMO systems, they may simply be regions that attract finite poles as  $g \rightarrow \infty$ . For the basic system transmission zeros cannot be altered by the controller design and, since infinite gain cannot be attained, the location of roots migrating towards these zeros do contribute to the system response.

Designing for a system with an unstable transmission zero is possible, but it means an upper gain limit for stability must be established. Stable operation is possible only below that limit. Increasing gain eventually results in a pole migrating to an unstable location. Establishing an upper control limit is a necessary but not sufficient condition for stable operation. Another condition that must be considered is the effect the system responses have on the control limits. Even though the closed-loop denominator contains stable poles,

the system responses can cause saturation of the control surfaces. Saturation for long periods of time can cause windup. This situation is especially prevalent when a closed-loop zero is located to the right of the closed-loop pole located closest to the origin. Designing for a stable system within the given control limits with two unstable transmission zeros has not been possible since the transmission zero regions are always in the right-half plane.

Using the zero- $B_2$  form, the transmission zeros can be calculated from Equation (3.23). Although they cannot be altered by output feedback, transmission zeros can be changed in two ways. First, should the location of the system be unacceptable, it is sometimes possible to select another  $C$  matrix that is acceptable for the design and yields different zero locations. Second, the measurement matrix modifies the transmission zeros, and it may be possible to alter the matrix elements to give both acceptable performance and acceptable transmission zero locations.

#### Measurement Matrix Elements

Some guidelines are available for the selection of the measurement matrix. Reference 19 presents a systematic approach to their selection for optimum decoupling. In addition the following suggestions are offered:

1. Make the measurement matrix as sparse as possible, adding only enough non-zero elements to yield an  $F$  matrix and an  $[FB]$  matrix of full rank.
2. Select values for the non-zero elements that give acceptable transmission zeros. In most cases, the values of the measurement

elements result in transmission zero locations that are equal to the reciprocal of the element value.

3. Select the location of the non-zero elements to use a state derivative that can be easily obtained and is zero for steady-state step commands as discussed previously.

### Closed-Loop Roots

The design technique does not guarantee stability of the system unless it has stable transmission zeros and infinite gain. Even with stable transmission zeros, the pole migrations can cross into the unstable region as the gain increases, and then return to the stable transmission zero. Therefore, the closed-loop system poles are evaluated after each design parameter variation to check if the closed-loop system has crossed into the unstable region. The equations for computing the closed-loop poles are presented below.

Partitioning of the A and B system matrices is accomplished as before to yield B<sub>2</sub> and A<sub>22</sub> of order (lxl), where l is the number of inputs.

$$\dot{\underline{x}} = \begin{bmatrix} \underline{A}_{11} & \underline{A}_{12} \\ \underline{A}_{21} & \underline{A}_{22} \end{bmatrix} \underline{x} + \begin{bmatrix} \underline{B}_1 \\ \underline{B}_2 \end{bmatrix} \underline{u} \quad (3.35)$$

$$\underline{y} = [\underline{C}_1 \mid \underline{C}_2] \underline{x}$$

or

$$\dot{\underline{x}}_1 = \underline{A}_{11} \underline{x}_1 + \underline{A}_{12} \underline{x}_2 + \underline{B}_1 \underline{u} \quad (3.36)$$

$$\underline{x}_2 = \underline{A}_{21} \underline{x}_1 + \underline{A}_{22} \underline{x}_2 + \underline{B}_2 \underline{u} \quad (3.37)$$

$$\underline{y} = \underline{C}_1 \underline{x}_1 + \underline{C}_2 \underline{x}_2 \quad (3.38)$$

$$\underline{e} = \underline{v} - \underline{y} \quad (3.39)$$

$$\underline{u} = g\underline{K}_2 \underline{e} + g\underline{K}_1 \int \underline{e} dt \quad (3.40)$$



$$\text{let } \dot{\underline{z}} = \underline{e} \text{ and } z f e d t \quad (3.41)$$

$$\text{then } \dot{\underline{z}} = \underline{v} - \underline{y} \quad (3.42)$$

$$\dot{\underline{z}} = -\underline{C}_1 \underline{x}_1 - \underline{C}_2 \underline{x}_2 + \underline{v} \quad (3.43)$$

$$\underline{u} = g_{K_0} \dot{\underline{z}} + g_{K_1} \underline{z} = g_{K_0} [-\underline{C}_1 \underline{x}_1 - \underline{C}_2 \underline{x}_2 + \underline{v}] + g_{K_1} \underline{z} \quad (3.44)$$

$$\underline{u} = -g_{K_0} \underline{C}_1 \underline{x}_1 - g_{K_0} \underline{C}_2 \underline{x}_2 + g_{K_0} \underline{v} + g_{K_1} \underline{z} \quad (3.45)$$

$$\dot{\underline{x}}_1 = (\underline{A}_{11} - g_{B_1 K_0} \underline{C}_1) \underline{x}_1 + (\underline{A}_{12} - g_{B_1 K_0} \underline{C}_2) \underline{x}_2 + g_{B_1 K_0} \underline{v} + g_{B_1 K_1} \underline{z} \quad (3.46)$$

$$\dot{\underline{x}}_2 = (\underline{A}_{21} - g_{B_2 K_0} \underline{C}_1) \underline{x}_1 + (\underline{A}_{22} - g_{B_2 K_0} \underline{C}_2) \underline{x}_2 + g_{B_2 K_0} \underline{v} + g_{B_2 K_1} \underline{z} \quad (3.47)$$

Writing Equations (3.42), (3.45), and (3.46) in matrix notation provides the description of the closed-loop system where  $\underline{v}$  is the input command vector to the control system.

$$\begin{bmatrix} \dot{\underline{z}} \\ \dot{\underline{x}}_1 \\ \dot{\underline{x}}_2 \end{bmatrix} = \begin{bmatrix} 0 & -\underline{C}_1 & -\underline{C}_2 \\ g_{B_1 K_1} & \underline{A}_{11} - g_{B_1 K_0} \underline{C}_1 & \underline{A}_{12} - g_{B_1 K_0} \underline{C}_2 \\ g_{B_2 K_1} & \underline{A}_{21} - g_{B_2 K_0} \underline{C}_1 & \underline{A}_{22} - g_{B_2 K_0} \underline{C}_2 \end{bmatrix} \begin{bmatrix} \underline{z} \\ \underline{x}_1 \\ \underline{x}_2 \end{bmatrix} + \begin{bmatrix} \underline{I} \\ g_{B_1 K_0} \\ g_{B_2 K_0} \end{bmatrix} \underline{v} \quad (3.48)$$

Note that  $\underline{z}$  is a vector of dimension  $l \times 1$ . For irregular designs replace  $\underline{C}_1$  by  $\underline{F}_1$  and  $\underline{C}_2$  by  $\underline{F}_2$ .

Some caution should be exercised in using these closed-loop equations. For the digital system, the control is piecewise continuous between samples and thus, by letting  $g=1/T$ , these equations can be used to evaluate stability in general. Effects that are not considered are quantization and the zero-order hold when sampling and computational time delays.

### MULTI Computer-Aided Design

The MULTI program was created by previous AFIT thesis research (Ref 13) and allows real-time, on-line, computer-aided designs to be accomplished with the control law theories presented in this chapter. A user's guide is presented in Reference 13.

There are several differences between the MULTI program computations and the theoretical equations presented in this chapter. In the computation of the gain matrices, a number of flexibilities are provided. The actual MULTI computations are shown below.

For the regular design case:

$$\underline{K}_0 = \bar{\alpha}\epsilon[\underline{CB}]^{-1} \underline{\Sigma} \quad (3.49)$$

$$\underline{K}_1 = \epsilon[\underline{CB}]^{-1} \underline{\Sigma} \quad (3.50)$$

Both  $\bar{\alpha}$  and  $\epsilon$  are scalars, and  $\alpha$  is used to set the ratio of proportional to integral gain. Unfortunately, it is the inverse of the usual method of varying the relationship.  $\epsilon$  is a scalar that can be used to change all the gain elements by any desired amount. This design parameter is especially important in keeping the control surfaces from being saturated. For the digital design case, varying  $\epsilon$  proves useful for cases where the sampling frequency has been fixed by other design considerations. The system response can be altered by increasing  $\epsilon$ , resulting in the same effect as increasing  $1/T$ .

For the irregular design:

$$\underline{K}_0 = \bar{\alpha} \epsilon [\underline{F}_2 \underline{B}_2]^{-1} \underline{\Sigma} \quad (3.51)$$

$$\underline{K}_1 = \epsilon [\underline{F}_2 \underline{B}_2]^{-1} \underline{\Sigma} \quad (3.52)$$

It should be noted that the  $[\underline{FB}]$  matrix must be used for the calculations if  $\underline{B}$  is not in  $\begin{bmatrix} 0 \\ - \\ \underline{B}_2 \end{bmatrix}$  form.

#### IV. Individual Multivariable Digital Control Laws and Results

##### Requirements

The following requirements must be satisfied in applying the design method:

1. The number of inputs must equal the number of outputs.
2. The system must be controllable and observable.
3. All transmission zeros must be stable.
4. Integral plus proportional control is applied to all forward loop signals.

Each of these requirements is considered in detail in the following paragraphs.

##### Inputs and Outputs

The "inputs" refer to the number of control surfaces that can be commanded to alter the aircraft's states. These are inputs to the aerodynamic model (plant). For the UH-60A Black Hawk helicopter, the inputs consist of cyclic pitch control, collective lift control, cyclic roll control, and tail rotor yaw control. These are designated by  $\underline{u}$  in the state equations. The "outputs" are the variables contained in the  $\underline{y}$  vector and are the responses to be controlled. For this system, there must be four controlled outputs. The outputs can be states of the plant or linear combinations of states. The commanded maneuver determines the output responses,  $\underline{y}$ , to be controlled. In this study, three output command vectors are selected to perform three maneuvers consisting of yaw rate response, a coordinated turn, and a vertical rate response. An explanation of the selection of each  $\underline{y}$  vector is given in the design

procedure section.

### Controllability and Observability

Controllability and observability are properties of the state-space representation of a system. Controllability implies that the inputs can affect each mode of the system. For a linear, time-invariant system, controllability of the plant can be checked by evaluating the rank of the matrix  $\underline{M}_C$  (Ref.4) where

$$\text{Rank } \underline{M}_C = \text{Rank}[\underline{B} \quad \underline{AB} \quad \underline{A^{n-1}B}] = n \quad (4.1)$$

For the augmented system containing integrators, an additional requirement is that (Ref 12)

$$\text{Rank} \begin{bmatrix} \underline{A} & \underline{B} \\ -\underline{C} & \underline{0} \end{bmatrix} = n+l$$

Observability implies that the outputs are affected by every mode. It also implies that the effects on the outputs of one state variable can be distinguished from the effects of the other state variables. For a time-invariant system, this property of the plant can be determined by evaluating the rank of the observability matrix,  $\underline{M}_O$ , (Ref 4) where

$$\text{Rank } \underline{M}_O = \text{Rank} \begin{bmatrix} \underline{C}^T & \underline{A}^T \underline{C}^T & \underline{A}^{T(n-1)} \underline{C}^T \end{bmatrix} = n \quad (4.2)$$

Controllability and observability are evaluated for each design. In trials where the criteria are not met, the system model is redefined until controllability and observability are achieved.

### Transmission Zeros

As discussed in Chapter III, transmission zeros of the system are considered as regions toward which some system roots migrate with

increasing gain. As gain approaches infinity, or the sampling time approaches zero, for a discrete system the affected roots asymptotically approach the transmission zero locations. Output feedback does not alter transmission zeros. In the strictest sense, it is desired that all such zeros be stable to insure system stability with high gain. Such a selection does not guarantee stability for all system gain values since the locus of system roots may journey into the unstable region before arriving in the vicinity of the transmission zeros. Thus for stable transmission zeros, stable operation is only assured for gain values approaching infinity. A controller design for a system with unstable transmission zeros can be developed with these techniques, but in such cases an upper gain boundary is established to prevent system roots from moving into the unstable region. Thus, the restriction is not absolute; however, failing to meet it does impose additional design considerations.

For irregular designs the CB matrix does not have full rank, and additional transmission zeros are introduced by the measurement matrix M. These transmission zeros can be altered by changing the measurement matrix elements. If the measurement matrix is very sparse, the location of the additional transmission zeros in the s-plane is the inverse of the values of the elements in the measurement matrix. Thus, a 0.25 element in the measurement matrix produces a transmission zero at -4.0 in the s-plane. This simple relationship breaks down as the number of matrix elements increases or if the B matrix is not in zero-B<sub>2</sub> form. Reference 19 provides a guide to the selection of the measurement matrix.

### Integral Plus Proportional Compensation

The fast-sampling error-actuated controller is governed by a control law equation of the form

$$\underline{u}(kT) = f\{\underline{K}_0 \underline{e}(kT) + \sum_{j=1}^q \underline{K}_j \underline{z}_j(kT)\} \quad (4.3)$$

where  $\underline{K}_j \in R^{l \times l}$  ( $j=0,1,2, \dots, q$ ),  $f=1/T$  is a scalar gain equal to the sampling frequency, and the control input vector  $\underline{u}(t)$  is piecewise-constant on the intervals  $kT \leq t < (k+1)T$  ( $k=0,1,2, \dots$ ). Since only tight tracking of step inputs is required, higher order vector integrators ( $j>2$ ) needed to follow ramp, parabolic, and higher order inputs are not used in this study. Therefore, the error-actuated controller reduces to

$$\underline{u}(kT) = f\{\underline{K}_0 \underline{e}(kT) + \underline{K}_1 \underline{z}(kT)\} \quad (4.4)$$

which is applied on all forward loops. This error-actuated controller contains a vector comparator,  $\underline{e}(kT)$ , which compares the commanded maneuver,  $\underline{v}$ , with the desired output vector  $\underline{y}(kT)$ . It also contains an integral component. The vector integrator has the equation form

$$\underline{z}[(k+1)T] = \underline{z}(kT) + T \underline{e}(kT) \quad (4.5)$$

where  $\underline{z} \in R^l$  and  $k=0,1,2,3, \dots$ . The vector integrator can be also expressed as

$$\underline{z}(kT) = \underline{z}(0) + T \sum_{j=0}^{k-1} \underline{e}(jT) \quad (4.6)$$

where  $\underline{z}(0)$  is usually equal to zero. Assuming  $\underline{z}(0) = \underline{0}$ , Equation (4.2) can be rewritten as

$$\underline{u}(kT) = f\{\underline{K}_0 \underline{e}(kT) + \underline{K}_1 T \sum_{j=0}^{j=k-1} e(jT)\} \quad (4.7)$$

This equation expresses the error-actuated controller entirely in terms of the error vector,  $\underline{e}(kT)$ . Substituting Equation (3.31) gives the final form of the controller expressed as

$$\underline{u}(kT) = f\{\underline{K}_0 \underline{e}(kT) + \bar{\alpha} \underline{K}_0 \sum_{j=0}^{j=k-1} e(jT)\} \quad (4.8)$$

An inherent stability problem associated with proportional plus integral controllers applied to actuators which can saturate is windup. Consider a very large change in the desired setpoint (commanded maneuver is initiated): the proportional channel of the proportional plus integral controller can cause saturation of the system's actuators, and the integrator channel begins to integrate large errors and eventually reaches a commanded control level that would cause saturation by itself. As the tracking error signal decreases, the proportional channel output also decreases, but the already saturated integrator channel does not "discharge" its commanded control level until after the error has changed sign, causing the total proportional plus integral controller output to stay at or near a saturating value, even though the actual system output,  $y$ , may be very close to the desired value. This can cause very large and undesirable overshoots in the observed system behavior. An antiwindup compensation method might involve adding a limiter in series with the input to the controlled system in order to preclude the control law from commanding values outside the saturation limits of the actuators. MULTI currently has an option that sets the



control limits for the control surfaces. However, windup effects are still experienced if the control limits are saturated for lengthy periods of time. Therefore, the requirement for proportional plus integral control is that it is applied on all forward loops and that control surface limits are not exceeded by the control surface responses.

#### A Design Procedure

A procedure for developing a design is established, based on the efforts in this thesis. The basic steps in this procedure are outlined below and are then discussed in detail.

1. Formulate the aircraft design model into the proper format.
2. Select the outputs to be controlled.
3. Check controllability and observability.
4. Calculate the transmission zeros and select the measurement matrix if it is required.
5. Check the open loop-stability of the system.
6. Scale gains for stable response and to keep controls within allowable limits.
7. Vary weighting matrix elements for desired responses and to meet control input restraints.
8. Adjust the ratio of proportional plus integral gain for timely steady-state behavior.

Chapter II covers the formulation of an aircraft model in state-space format necessary for this design application. Time spent in developing a controller design requires that the models for the plant, actuators, and sensors are an adequate representation. If possible, the

models should be validated before proceeding with the control law design.

Selection of the outputs to be controlled is dependent on the maneuver to be commanded. For this study, the three maneuvers to be performed are the yaw rate command system, the coordinated turn command system, and the vertical rate command system. The three maneuvers are shown below as originally presented by the sponsor:

1. Yaw Rate Command System

$$r_B = \pm 10 \text{ deg/sec, step input}$$

$$p_B = 0$$

$$q_B = 0$$

2. Coordinated Turn Command System

$$p_B = \pm 10 \text{ deg/sec, step input - for a period of a few seconds.}$$

$$y_B = 0$$

3. Vertical Rate Response

$$h_E = \pm 20 \text{ ft/sec, step input}$$

$$\theta \approx \gamma$$

It should be noted that since there are four inputs, there must be four controlled outputs. The final selection of the output vectors is discussed later in this chapter.

Controllability and observability are checked for both the open-loop aircraft and the closed-loop design model prior to performing the design. This is an area prone to error due to the tedium of performing operations on matrices with realistic elements. Automation can significantly reduce the computational burden but is not employed in this thesis.

The selection of measurement matrix elements and the calculation of transmission zeros are steps that are interrelated in the design. An initial selection of the measurement matrix elements ( $m_{ij}$ ) is made with  $0 < m_{ij} < 1$ . After measurement matrix selection, the transmission zeros are calculated. Based on their locations, refinement of the measurement matrix elements is made. In some cases, unstable transmission zeros that are not created by the measurement matrix can be removed by redefining the output  $\underline{C}$  matrix.

#### Open Loop Stability

The five flight conditions that are used in this study are the low speed flight conditions,  $V_{EAS} = 20$  and 40 knots, and the forward flight conditions,  $V_{EAS} = 60, 100,$  and 140 knots. A preliminary insight into the stability of the UH-60A Black Hawk helicopter can be gained by examining the poles of the denominator of the open-loop transfer function. If the helicopter plant contains an unstable mode(s), greater care must be taken in the design process to insure that the right-half s-plane poles(s) or pole(s) outside the unit circle in the z-plane are brought back into their respective regions of stability for the closed-loop system. The denominator of the open-loop transfer functions for the five flight conditions are listed below.

The denominator of the open-loop transfer function for the  $V_{EAS} = 20$  knots flight condition is:

$$\begin{array}{ll}
 (.1000E+01) S^{**} 8 & (-.3595E+01) + J(0. \quad) \\
 (.5451E+01) S^{**} 7 & (-.1950E+00) + J(-.7487E+00) \\
 (.8000E+01) S^{**} 6 & (-.1950E+00) + J(.7487E+00) \\
 (.6033E+01) S^{**} 5 & (-.1474E+01) + J(0. \quad) \\
 (.4828E+01) S^{**} 4 & (.1497E+00) + J(.4652E+00) \quad (4.9) \\
 (.1373E+01) S^{**} 3 & (.1497E+00) + J(-.4652E+00) \\
 (.9037E+00) S^{**} 2 & (-.1898E+00) + J(0. \quad)
 \end{array}$$

(.2258E+00) S** 1	(-.1014E+00) + J(0. )
(.1459E-01) S** 0	DENOMINATOR GAIN = .1000E+01

It should be noted that there are two unstable open-loop poles at  $s=0.1497 \pm j0.4652$ .

The denominator of the open-loop transfer function for the  $V_{EAS} = 40$  knots flight condition is:

(.1000E+01) S** 8	(-.3902E+01) + J(0. )	
(.6193E+01) S** 7	(-.2371E+00) + J(-.9279E+00)	
(.1126E+02) S** 6	(-.2371E+00) + J(.9279E+00)	
(.1113E+02) S** 5	(-.1519E+01) + J(0. )	
(.8566E+01) S** 4	(-.1642E+00) + J(.3188E+00)	(4.10)
(.2219E+01) S** 3	(-.1642E+00) + J(-.3189E+00)	
(.3890E+00) S** 2	(.1723E+00) + J(0. )	
(-.8950E-01) S** 1	(-.1412E+00) + J(0. )	
(-.1702E-01) S** 0	DENOMINATOR GAIN = .1000E+01	

It should be noted that there is one unstable open-loop pole at  $s=0.1723$ .

The denominator of the open-loop transfer function for the  $V_{EAS} = 60$  knots flight condition is:

(.1000E+01) S** 8	(-.3833E+01) + J(0. )	
(.6717E+01) S** 7	(-.3881E+00) + J(-.1370E+01)	
(.1432E+02) S** 6	(-.3881E+00) + J(.1370E+01)	
(.1656E+02) S** 5	(-.2294E+01) + J(0. )	
(.1481E+02) S** 4	(.1877E+00) + J(.2468E+00)	(4.11)
(-.2496E+01) S** 3	(.1877E+00) + J(-.2468E+00)	
(.8405E+00) S** 2	(-.1676E+00) + J(0. )	
(.3070E+00) S** 1	(-.2195E-01) + J(0. )	
(.6304E-02) S** 0	DENOMINATOR GAIN = .1000E+01	

It should be noted that there are two unstable open-loop poles at  $s=0.1877 \pm j0.2468$ .

The denominator of the open-loop transfer function for the  $V_{EAS} =$   
100 knots flight condition is:

$$\begin{array}{ll}
 (.1000E+01) S^{**} 8 & (-.3910E+01) + J(0. \quad) \\
 (.7411E+01) S^{**} 7 & (-.4536E+00) + J(-.1807E+01) \\
 (.1920E+02) S^{**} 6 & (-.4536E+00) + J(.1807E+01) \\
 (.3033E+02) S^{**} 5 & (-.2712E+01) + J(0. \quad) \\
 (.3333E+02) S^{**} 4 & (.1988E+00) + J(.2632E+00) \quad (4.11) \\
 (-.3508E+01) S^{**} 3 & (.1988E+00) + J(-.2632E+00) \\
 (.1194E+01) S^{**} 2 & (-.2312E+00) + J(0. \quad) \\
 (.9960E+00) S^{**} 1 & (-.4890E-01) + J(0. \quad) \\
 (.4526E-01) S^{**} 0 & \text{DENOMINATOR GAIN} = .1000E+01
 \end{array}$$

It should be noted that there are two unstable open-loop poles at  
 $s = 0.1988 \pm j0.2632$ .

The denominator of the open-loop transfer function for the  $V_{EAS} =$   
140 knots flight condition is:

$$\begin{array}{ll}
 (.1000E+01) S^{**} 3 & (-.3663E+00) + J(.2169E+01) \\
 (.7837E+01) S^{**} 7 & (-.3663E+00) + J(-.2169E+01) \\
 (.2289E+02) S^{**} 6 & (-.4018E+01) + J(0. \quad) \\
 (.4565E+02) S^{**} 5 & (-.2937E+01) + J(0. \quad) \\
 (.6390E+02) S^{**} 4 & (.1391E+00) + J(.2929E+00) \quad (4.13) \\
 (.9718E+01) S^{**} 3 & (.1391E+00) + J(-.2929E+00) \\
 (.2127E+01) S^{**} 2 & (-.3701E+00) + J(0. \quad) \\
 (.2324E+01) S^{**} 1 & (-.5768E-01) + J(0. \quad) \\
 (.1282E+00) S^{**} 0 & \text{DENOMINATOR GAIN} = .1000E+01
 \end{array}$$

It should be noted there are two unstable open-loop poles at  $s = 0.1391 \pm$   
 $j0.2929$ . It should also be noted that all five flight conditions  
contain an unstable mode. As a result of these open-loop instabilities,  
the closed-loop poles must be checked for stability after each design  
trial. Even though the desired outputs might tightly track the desired  
maneuver over a specific time period, an unstable mode in a closed-loop  
system for an individual digital control law is unacceptable.

For the first design attempt, the  $\alpha$ ,  $\Sigma$ , and  $\epsilon$  parameters are set to  
one in MULTI. In most cases this results in an unstable system. This  
result can be checked from the denominator of the closed-loop transfer

function and therefore a simulation run is a waste of resources. For the unstable system, the gain is then reduced by decreasing  $\epsilon$  until stable operation is obtained. However, stable operation does not guarantee that the control limits are not exceeded. Once stable operation is reached, a simulation is run. If the control limits are exceeded,  $\epsilon$  must be reduced until the controls no longer reach saturation. The weighting matrix elements are then adjusted (ratioed with respect to one another) to achieve acceptable responses. Then, the proportional plus integral ratio ( $1/\bar{\alpha}$ ) is adjusted so that steady-state behavior is reached within a desired time. Again, system stability and control limit saturation must be checked after each parameter variation.

Finally, before any design can be attempted, a selection of the sampling frequency,  $f$ , must be made. Based on the current capabilities of current digital computers, a sampling frequency equal to 50 Hertz is selected for this study.

The following pages contain the results achieved for the three commanded maneuvers at the applicable flight conditions.

#### Yaw Rate Command System

The purpose of the yaw rate command system is to execute a flat turn about the z-body axis. As originally stated, the yaw rate command system commands  $r_B$  to  $\pm 10$  deg/sec with  $q_B = p_B = 0$ . The perturbation state,  $w_B$ , must also be commanded to zero to complete the output vector as well as to express the desire to have no z-body velocity while executing a flat turn. However, with this output vector incorporated into the  $\underline{C}$  matrix there are two transmission zeros at the origin. As mentioned in Chapter III, a stable design with two transmission zeros at the origin

is nearly impossible to design as the transmission zeros are approached from the unstable region of the s-plane with increasing gain.

Therefore, instead of commanding the perturbation pitch rate,  $q_B$ , to zero, the perturbation pitch angle,  $\theta$  is commanded to zero. Since  $\dot{\theta} = q_B$  in most cases, commanding  $\theta$  to zero results in  $q_B$  being zero. It is also possible to command the perturbation roll angle,  $\phi$ , to zero instead of the perturbation roll rate  $p_B$  to zero. With the appropriate measurement matrix, stable transmission zeros can be obtained. However, a constant roll rate due to the constant yaw rate results. Examining the  $p_B$  equation for any flight condition confirms this result. The magnitude of the constant roll rate is quite unacceptable. Commanding both  $\phi$  and  $p_B$  is impossible as it results in singular gain matrices. Therefore the final choice of output vector to be controlled for the yaw rate command system is

$$\underline{y} = \begin{bmatrix} \theta \\ p_B \\ w_B \\ r_B \end{bmatrix} \quad (4.14)$$

The selection of  $\theta$  requires that a measurement matrix be selected in order that the first Markov parameter,  $[\underline{CB}]$ , have full rank. Since the  $\underline{B}$  matrix is not in zero- $\underline{B}_2$  form, there is no current method for obtaining the  $\underline{M}$  matrix in order that the outputs are decoupled from each other. Therefore, the objective of selecting the  $\underline{M}$  matrix is to obtain full rank for the  $[\underline{FB}]$  matrix. A careful examination of the  $\underline{A}$  matrix reveals that unneeded complexity results if the  $\underline{M}$  matrix is not of the form

$$\underline{M} = \begin{bmatrix} m_{11} & m_{12} & 0 & 0 \\ m_{21} & m_{22} & 0 & 0 \\ 0 & 0 & 0 & 0 \\ 0 & 0 & 0 & 0 \end{bmatrix} \quad (4.15)$$

For this command system,  $m_{12} = m_{21} = m_{22} = 0$  and  $m_{11} = 0.25$ . With this choice of  $\underline{M}$  matrix, there is a transmission at the origin. One transmission zero at the origin can be handled by the design method; however, an upper stability limit must be established.

Successful designs have been obtained for the  $V_{EAS} = 20, 40$ , and  $60$  knots flight conditions. Designs for the yaw rate command system at  $V_{EAS} = 100$  and  $140$  knots have not been achieved. At these flight conditions, instabilities and control limit saturation problems are insurmountable. For the  $V_{EAS} = 20$  knots flight condition, the final denominator of the closed-loop transfer function is

(.1000E+01) S** 12	(-.3322E+01) + J(.3787E+01)	
(.2608E+02) S** 11	(-.3322E+01) + J(-.3787E+01)	
(.2712E+03) S** 10	(-.1208E+02) + J(0. )	
(.1701E+04) S** 9	(-.5012E+00) + J(.1498E+01)	
(.7196E+04) S** 8	(-.5012E+00) + J(-.1498E+01)	
(.2261E+05) S** 7	(-.4188E+01) + J(0. )	
(.5492E+05) S** 6	(-.3756E-01) + J(.3104E+01)	(4.16)
(.8951E+05) S** 5	(-.3756E-01) + J(-.3104E+01)	
(.9802E+05) S** 4	(-.2037E+01) + J(0. )	
(.6798E+05) S** 3	(-.3935E-04) + J(0. )	
(.3461E+04) S** 2	(-.1249E-01) + J(0. )	
(.3291E+02) S** 1	(-.4175E-01) + J(0. )	
(.1290E-02) S** 0	DENOMINATOR GAIN = .1000E+01	

It should be noted that the closed-loop system poles are all in the stable region. The figures of merit are listed in Table IV-1 and the time response plots in Figures 4a - 4g. The design data for each individual controller precedes the corresponding plots.



Design Data for the Yaw Rate Command System  
Flight Condition:  $V_{EAS} = 20$  knots

$T = 0.02$  seconds

$\alpha = 0.25$

$$\underline{\Sigma} = \begin{bmatrix} 0.2 & 0 & 0 & 0 \\ 0 & 2.0 & 0 & 0 \\ 0 & 0 & 0.1 & 0 \\ 0 & 0 & 0 & 1.0 \end{bmatrix}$$

$\varepsilon = 0.5$

$$\underline{M} = \begin{bmatrix} 0.25 & 0 & 0 & 0 \\ 0 & 0 & 0 & 0 \\ 0 & 0 & 0 & 0 \\ 0 & 0 & 0 & 0 \end{bmatrix}$$

$$\underline{K}_0 = \begin{bmatrix} 0.2881 & 0.001605 & 0.0001351 & -0.005827 \\ -0.03929 & -0.003245 & -0.001686 & 0.03288 \\ -0.006159 & 0.1709 & 0.00096213 & 0.0992 \\ 0.009233 & -0.02819 & 0.0001311 & 0.2168 \end{bmatrix}$$

$$\underline{K}_1 = \begin{bmatrix} 1.152 & 0.00642 & 0.0005406 & -0.02331 \\ -0.1572 & -0.01298 & -0.006745 & 0.1315 \\ -0.02464 & 0.6835 & 0.0002485 & 0.3968 \\ 0.03693 & -0.1127 & 0.0007245 & 0.8673 \end{bmatrix}$$

Input ramp input: 1.0 seconds

Input command:  $\theta = 0.0$

$p = 0.0$

$w = 0.0$

$r = 0.1745$  rad/sec step

NOTE: Step commands are ramped to steady state over a specified time. This time is designated as the "input ramp time" given above.

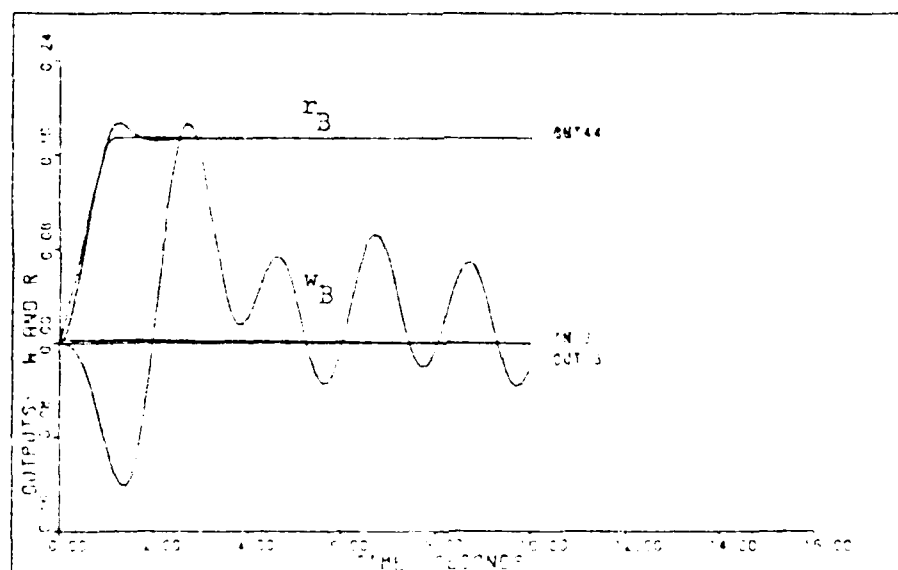


Figure 4a. Output Responses,  $w_B$ (ft/sec) and  $r_B$ (rad/sec), for the Yaw Rate Command System ( $V_{EAS} = 20$  Knots)

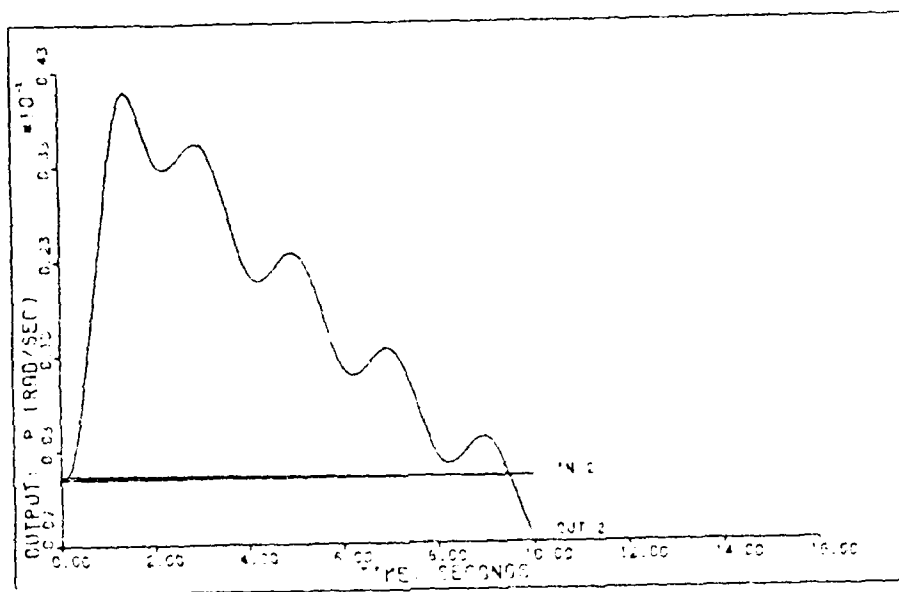


Figure 4b. Output Response,  $p_B$ , for the Yaw Rate Command System  
(VEAS = 20 Knots)

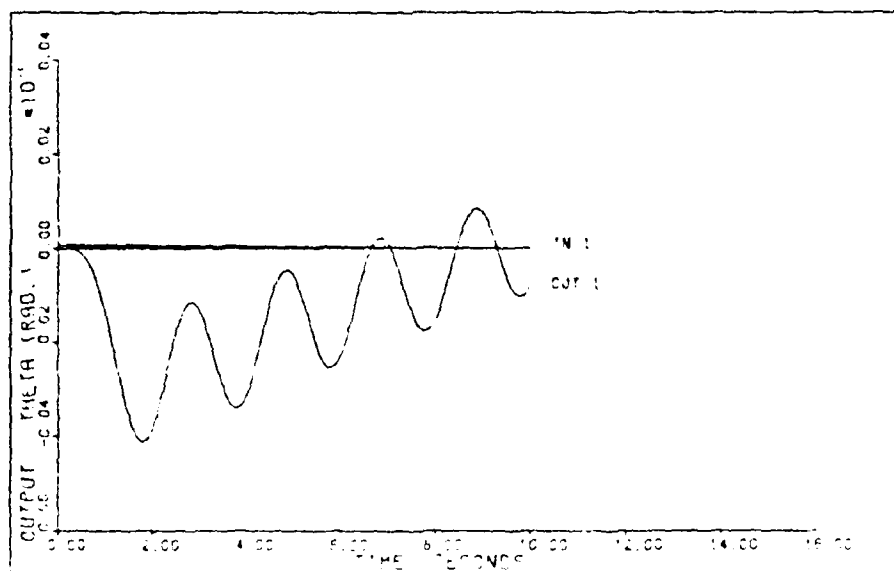


Figure 4c. Output Response,  $\theta$ , for the Yaw Rate Command System  
(VEAS = 20 Knots)

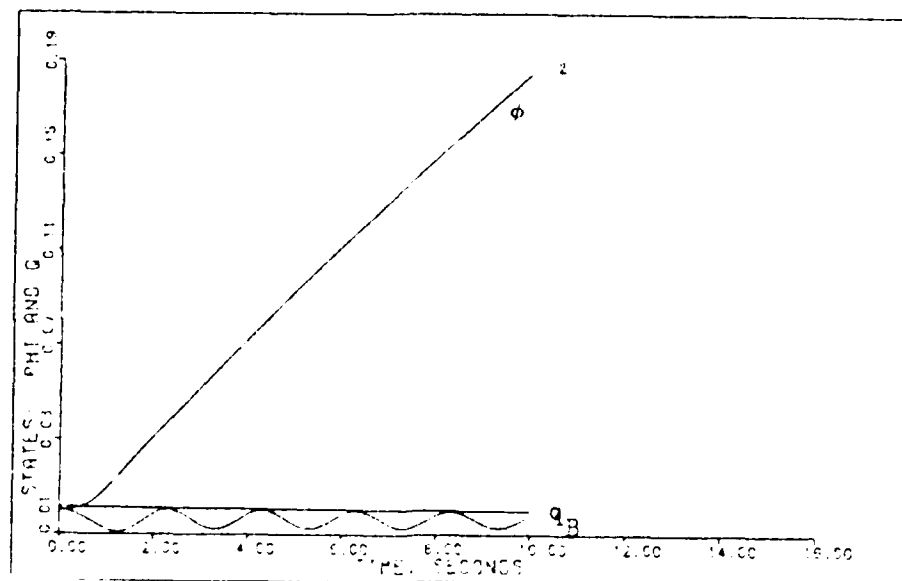


Figure 4d. State Responses,  $\phi$ (rad.) and  $q_B$ (rad/sec) for the Yaw Rate Command System ( $V_{EAS} = 20$  Knots)

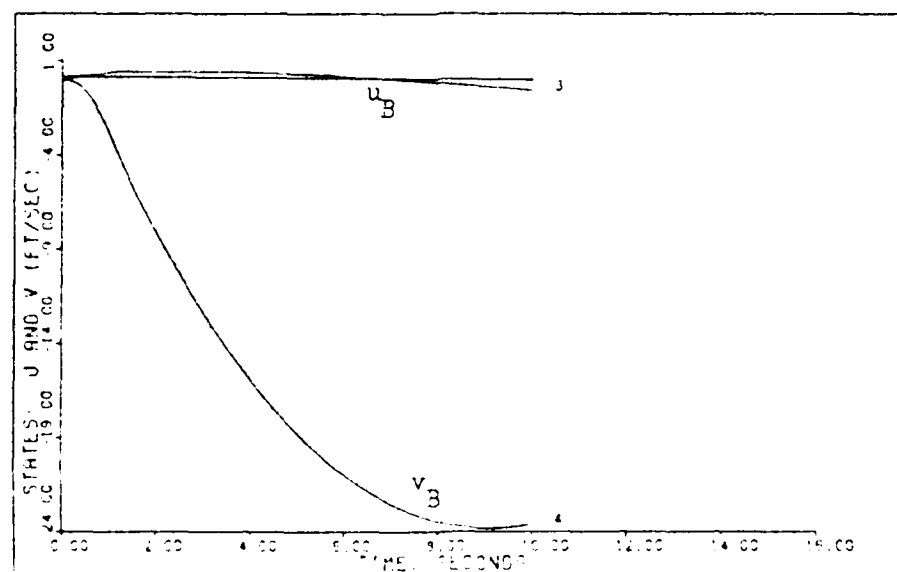


Figure 4e. State Responses,  $u_B$  and  $v_B$ , for the Yaw Rate Command System ( $V_{EAS} = 20$  Knots)

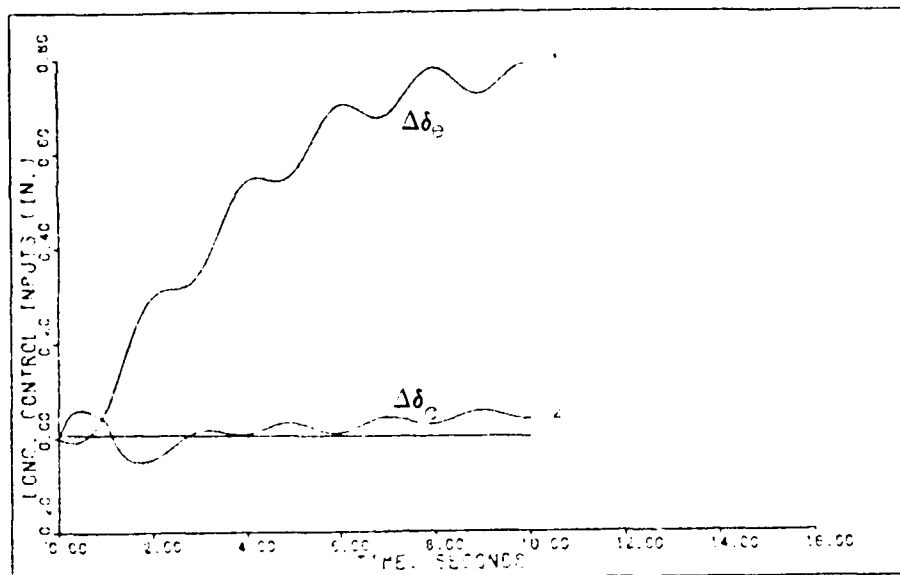


Figure 4f. Longitudinal Control Surface Responses,  $\Delta\delta_e$  and  $\Delta\delta_c$ , for the Yaw Rate Command System ( $V_{EAS} = 20$  Knots)

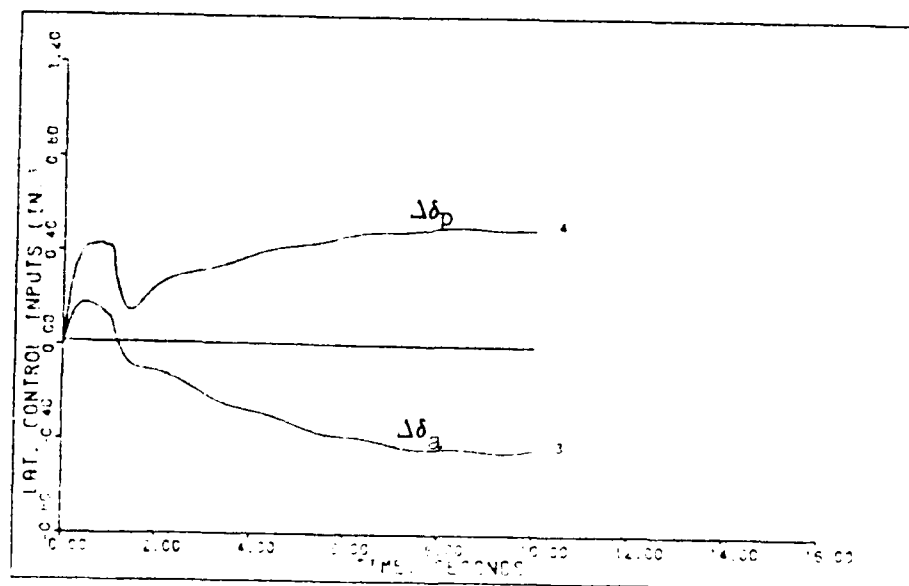


Figure 4g. Lateral Control Surface Responses,  $\Delta\delta_a$  and  $\Delta\delta_p$ , for the Yaw Rate Command System ( $V_{EAS} = 20$  Knots)

Table IV-1  
Yaw Rates Results for  $V_{EAS} = 20$  knots

Outputs	$M_p$	$t_p$	$M_m$	$t_m$	FV	$t_s$
$\theta$	0.00084723	8.9	-0.0041178	1.8	-0.000851	10
$p_B$	0.0040857	1.4	-0.000631	10	-0.000631	10
$w_B$	0.1865	2.7	-0.12069	1.4	-0.01753	10
$r_B$	0.18666	1.3	0	0	0.17435	1.6

In Table IV-1, the symbols representing the figures of merit are:

$M_p$  = the positive peak value

$t_p$  = the time to reach  $M_p$

$M_m$  = the negative peak value

$t_m$  = the time to reach  $M_m$

FV = final value

$t_s$  = the settling time

Since the simulation time equals 10 seconds, it should be noted that a settling time of 10 seconds does not indicate that the response has reached steady-state. It should be noted for the output responses that  $\theta$  is in radians and  $p_B$  and  $r_B$  are in radians/sec. An examination of the output time responses reveals relatively tight tracking of the commanded maneuver. However, problems exist in the state responses,  $\phi$  and  $v_B$ . The perturbation roll angle state equation is

$$\dot{\phi} = -0.00239 q_B + p_B + 0.102 r_B \quad (4.17)$$

For the commanded yaw rate,  $r_B = 0.1745$  rad/sec and  $q_B = p_B = 0$  in the steady-state. Therefore,  $\dot{\phi} = 0.0178$  rad/sec in the steady-state. It should be noted that the increasing roll angle is due to the yaw rate

and not the roll rate. A side-effect of this undesired roll angle is the y-body axis velocity,  $v_B$ . An examination of Figure 4e. reveals a slow, oscillatory, lightly-damped response with a magnitude comparable to the total velocity. It can be concluded that the yaw rate response has excited the dutch roll mode. This result is not totally satisfactory. Another problem exists in the pitch angle perturbation state equation described below

$$\dot{\theta} = q_B + 0.0234 r_B . \quad (4.18)$$

As shown above,  $\dot{\theta}$  also assumes a constant value in steady-state of  $\dot{\theta} = 0.0040833$  rad/sec. The output,  $\theta$ , is given by

$$\theta = \theta + 0.25 q_B + 0.00585 r_B \quad (4.19)$$

which violates the condition for zero steady-state error since

$$e = -0.25 q_B - 0.001021 \quad (4.20)$$

Examining Figure 4d. reveals that  $q_B$  oscillates around a negative-valued constant not equal to zero. The conclusion that can be reached about the yaw rate command system at  $V_{EAS} = 20$  knots is that there is relatively tight tracking for the desired outputs; however, the state responses,  $\phi$  and  $v_B$ , are undesirable. The main problem with the yaw rate command system is that only four outputs can be commanded. This limitation prevents taking into account all the effects caused by the helicopter executing a flat turn. Another output vector could be selected as long as a trade-off analysis is performed.

For the  $V_{EAS} = 40$  knots flight condition, the final denominator of the closed-loop transfer function is

```
(.1000E+01) S** 12      (-.2179E+02) + J(0.          )
(.3944E+02) S** 11      (-.4658E+01) + J(.3753E+01)
(.5367E+03) S** 10      (-.4658E+01) + J(-.3753E+01)
(.4116E+04) S** 9       (-.2409E+00) + J(.3501E+01)
(.2055E+05) S** 8       (-.2409E+00) + J(-.3501E+01)
(.7536E+05) S** 7       (-.7449E+00) + J(.1712E+01)
(.2066E+06) S** 6       (-.7449E+00) + J(-.1712E+01) (4.21)
(.3824E+06) S** 5       (-.4022E+01) + J(0.          )
(.4719E+06) S** 4       (-.2272E+01) + J(0.          )
(.3361E+06) S** 3       (-.1357E-02) + J(0.          )
(.2100E+05) S** 2       (-.1769E-01) + J(0.          )
(.2889E+03) S** 1       (-.4829E-01) + J(0.          )
(.3541E+00) S** 0       DENOMINATOR GAIN = .1000E+01
```

It should be noted that the closed-loop system poles are all in the stable region. For this flight condition, the simulation contains the actuators dynamics models developed in Chapter II. The figures of merit are listed in Table IV-2 and the time response plots in Figures 5a. - 5f.

Table IV-2  
Yaw Rate Results for  $V_{EAS}=40$  knots

Outputs	$M_p$	$t_p$	$M_m$	$t_m$	FV	$t_s$
$\theta$	0	0	-0.003705	1.6	-0.001085	10
$p_B$	0.003456	1.4	-0.0000607	0.1	0.0013465	10
$w_B$	0.180373	2.3	-0.151656	1.1	0.013948	10
$r_B$	0.18058	1.2	0	0	0.173435	1.5

An examination of the time responses reveals relatively tight tracking of the desired output responses. Again, there are unsatisfactory results for the state responses,  $\phi$  and  $v_B$ . The perturbation roll angle state equation is

$$\dot{\phi} = -0.00133 q_B + p_B + 0.0759 r_B . \quad (4.22)$$



Design Data for the Yaw Rate Command System

Flight Condition:  $V_{EAS} = 40$  knots with actuators

$T = 0.02$  seconds

$\alpha = 0.25$

$$\underline{\Sigma} = \begin{bmatrix} 0.2 & 0 & 0 & 0 \\ 0 & 2.5 & 0 & 0 \\ 0 & 0 & 0.1 & 0 \\ 0 & 0 & 0 & 1 \end{bmatrix}$$

$\epsilon = 0.70$

$$\underline{M} = \begin{bmatrix} 0.25 & 0 & 0 & 0 \\ 0 & 0 & 0 & 0 \\ 0 & 0 & 0 & 0 \\ 0 & 0 & 0 & 0 \end{bmatrix}$$

$$\underline{K}_0 = \begin{bmatrix} 0.3953 & -0.001604 & 0.0004224 & 0.004925 \\ -0.1040 & -0.006046 & -0.002435 & 0.06556 \\ -0.005336 & 0.3024 & 0.0003703 & 0.1306 \\ 0.01545 & -0.04818 & 0.00006562 & 0.299 \end{bmatrix}$$

$$\underline{K}_1 = \begin{bmatrix} 1.581 & -0.006415 & 0.001689 & 0.0197 \\ -0.4159 & -0.02419 & -0.00974 & 0.2622 \\ -0.02134 & 1.210 & 0.001481 & 0.5222 \\ 0.06179 & -0.1927 & 0.0001615 & 1.196 \end{bmatrix}$$

Input ramp input: 1.0 seconds

Input command:  $\theta = 0.0$

$p = 0.0$

$w = 0.0$

$r = 0.1745$  rad/sec step

Note: Step commands are ramped to steady state over a specified time. This time is designated as the "input ramp time" given above.

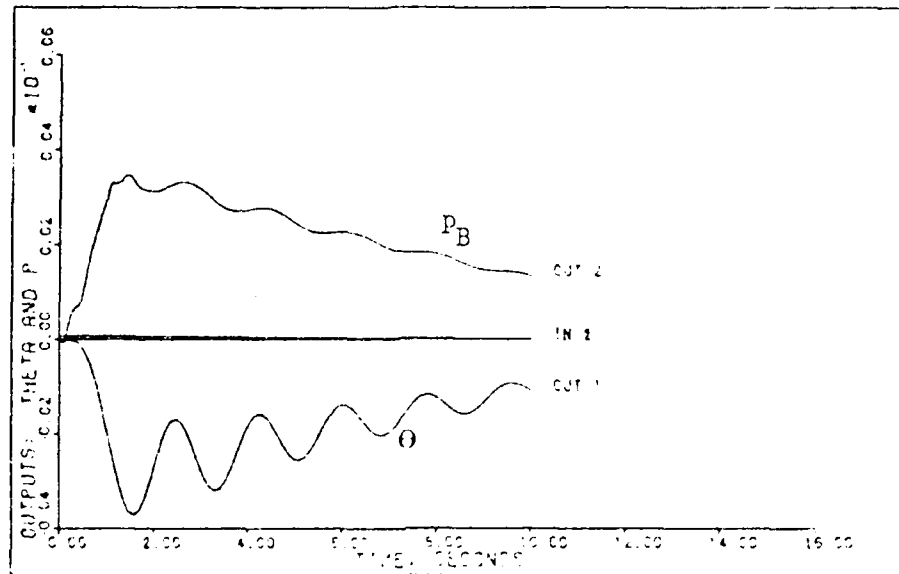


Figure 5a. Output Responses,  $\theta$ (rad.) and  $p_B$ (rad/sec), for the Yaw Rate Command System With Actuators ( $V_{EAS} = 40$  Knots)

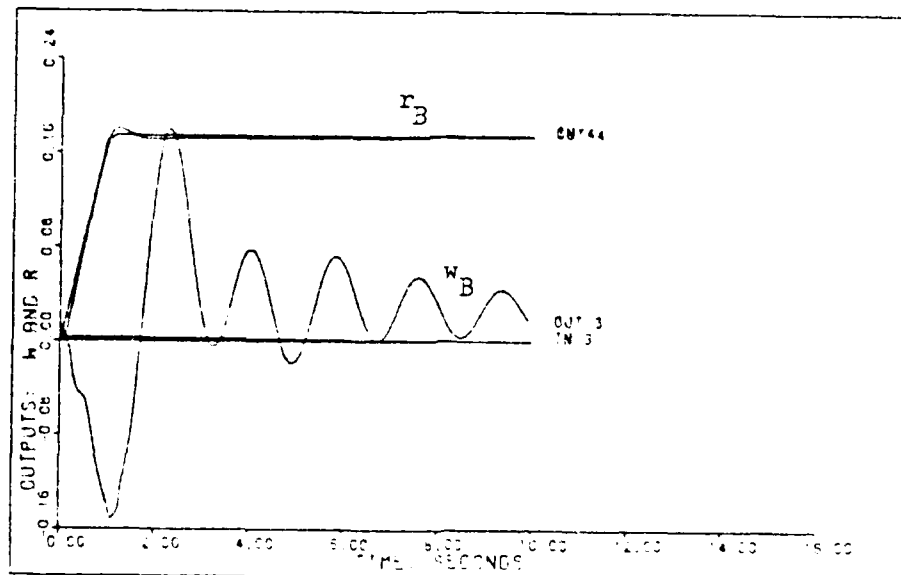


Figure 5b. Output Responses,  $w_B$ (ft/sec) and  $r_B$ (rad/sec), for the Yaw Rate Command System With Actuators ( $V_{EAS} = 40$  Knots)

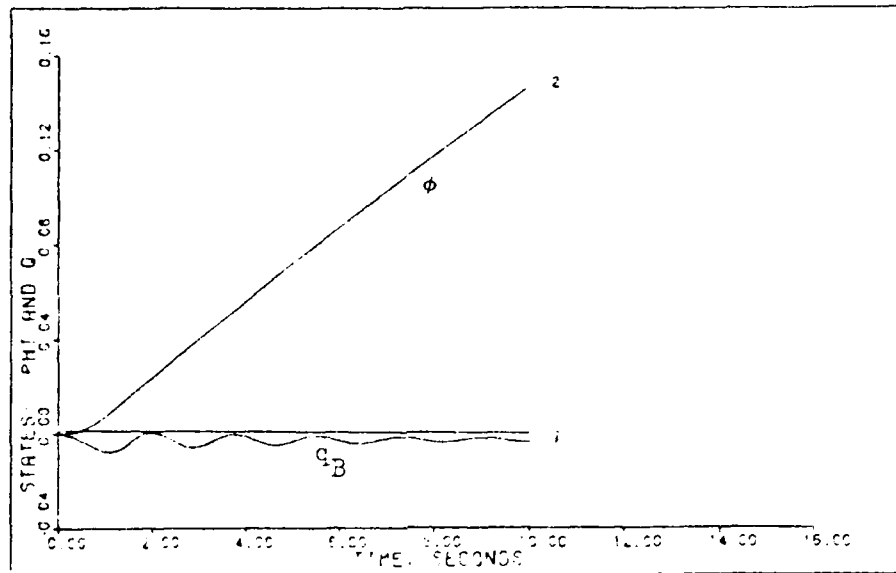


Figure 5c. State Responses,  $\phi$ (rad.) and  $q_B$  (rad/sec) for the Yaw Rate Command System With Actuators ( $V_{EAS} = 40$  Knots)

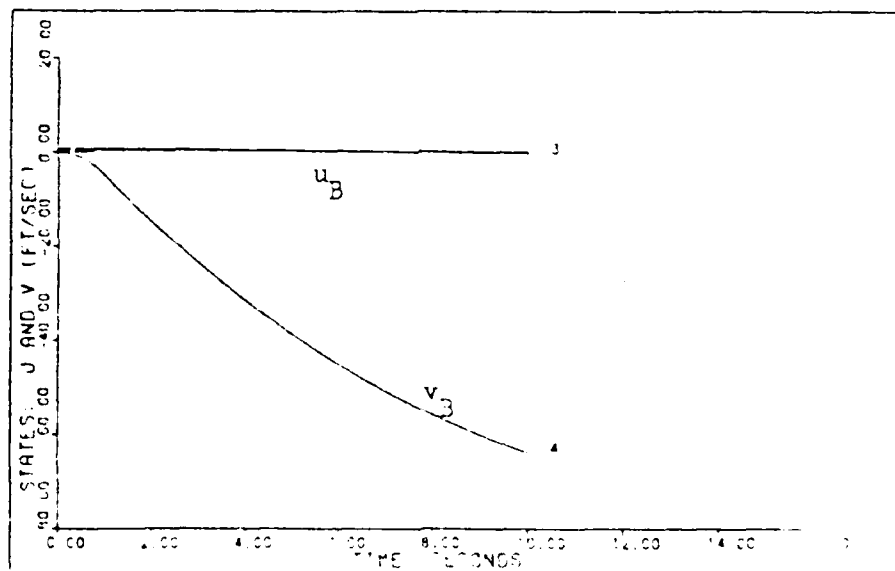


Figure 5d. State Responses,  $u_B$  and  $v_B$ , for the Yaw Rate Command System With Actuators ( $V_{EAS} = 40$  Knots)

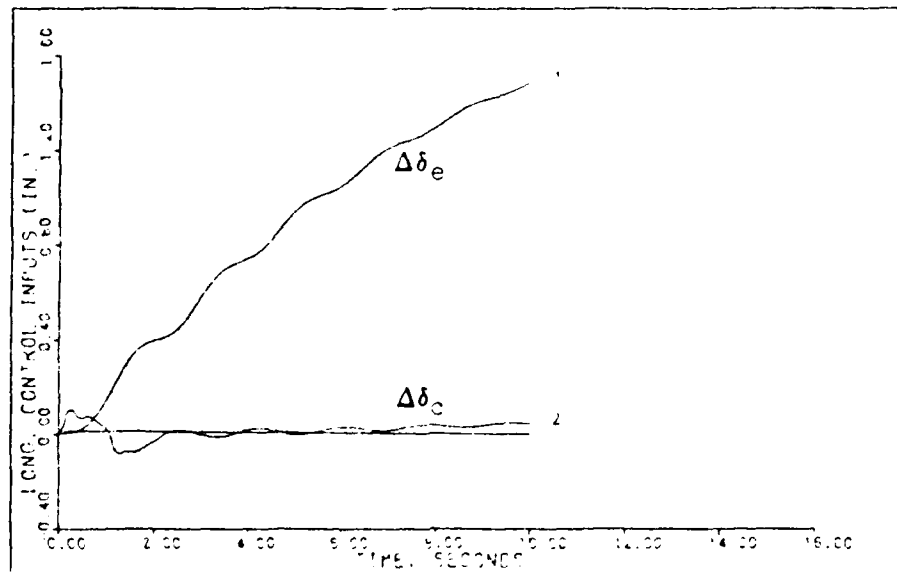


Figure 5e. Longitudinal Control Surface Responses,  $\Delta\delta_e$  and  $\Delta\delta_c$ , for the Yaw Rate Command System ( $V_{EAS} = 40$  Knots)

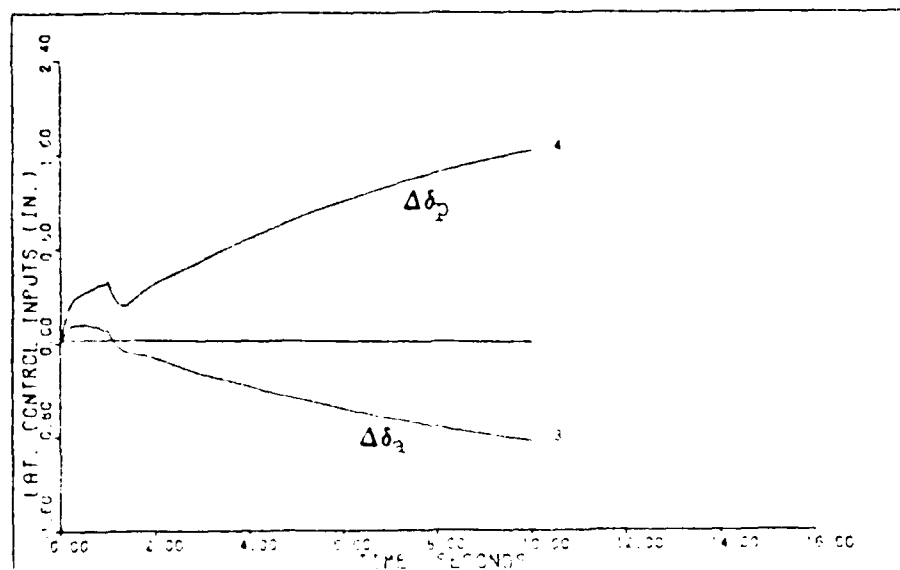


Figure 5f. Lateral Control Surface Responses,  $\Delta\delta_a$  and  $\Delta\delta_p$ , for the Yaw Rate Command System With Actuators ( $V_{EAS} = 40$  Knots)

In steady-state,  $\dot{\phi} = 0.01324$  rad/sec and results from the constant  $r_B$  command. The perturbation side velocity,  $v_B$ , again shows even greater effect of the dutch roll mode with respect to the total velocity. The same problem with  $\theta$  and the steady-state error again occur since

$$\dot{\theta} = q_B + 0.0176 r_B. \quad (4.23)$$

and the desired output response for  $\theta$  is

$$\theta = \theta + 0.25 q_B + 0.0044 r_B. \quad (4.24)$$

Even though tight tracking of the desired outputs is obtained, the uncontrolled states,  $\phi$  and  $v_B$ , exhibit unsatisfactory dutch roll mode effects.

The final denominator of the closed-loop transfer function for the  $V_{EAS}=60$  knots flight condition is

(.1000E+01) S** 12	(-.3506E+02) + J(0. )	
(.5472E+02) S** 11	(-.3275E+00) + J(-.3634E+01)	
(.8712E+03) S** 10	(-.3275E+00) + J(.3634E+01)	
(.7400E+04) S** 9	(-.5346E+01) + J(.3601E+01)	
(.3900E+05) S** 8	(-.5346E+01) + J(-.3601E+01)	
(.1562E+06) S** 7	(-.8954E+00) + J(.1767E+01)	
(.4525E+06) S** 6	(-.8954E+00) + J(-.1767E+01)	(4.25)
(.8888E+06) S** 5	(-.4019E+01) + J(0. )	
(.1140E+07) S** 4	(-.2433E+01) + J(0. )	
(.8204E+06) S** 3	(-.1987E-02) + J(.1808E01)	
(.5293E+05) S** 2	(-.1987E-02) + J(-.1808E01)	
(.4659E+03) S** 1	(-.6627E-01) + J(0. )	
(.1632E+02) S** 0	DENOMINATOR GAIN = .1000E+01	

It should be noted that the closed-loop system poles are all in the stable region. For this flight condition, the simulation is performed both with and without actuators. The figures of merit for the simulation with actuators are listed in Table IV-3 and the time response plots in Figures 6a.-6h. The figures of merit for the simulation without actuators are listed in Table IV-4 and the time response plots

Design Data for the Yaw Rate Command System

Flight Condition:  $V_{EAS} = 60$  knots

$T = 0.02$  seconds

$\alpha = 0.25$

$$\underline{\Sigma} = \begin{bmatrix} 0.2 & 0 & 0 & 0 \\ 0 & 3.5 & 0 & 0 \\ 0 & 0 & 0.1 & 0 \\ 0 & 0 & 0 & 1 \end{bmatrix}$$

$\epsilon = 0.8$

$$\underline{M} = \begin{bmatrix} 0.25 & 0 & 0 & 0 \\ 0 & 0 & 0 & 0 \\ 0 & 0 & 0 & 0 \\ 0 & 0 & 0 & 0 \end{bmatrix}$$

$$\underline{K}_0 = \begin{bmatrix} 0.4388 & -0.01382 & 0.0005775 & 0.00259 \\ -0.1703 & 0.008547 & -0.002668 & 0.08984 \\ -0.00717 & 0.4855 & 0.0002487 & 0.517 \\ 0.008557 & -0.06569 & -0.0001695 & 0.295 \end{bmatrix}$$

$$\underline{K}_1 = \begin{bmatrix} 1.755 & -0.0553 & 0.00231 & 0.01036 \\ -0.6814 & 0.03419 & -0.01067 & 0.3594 \\ -0.02868 & 1.942 & 0.0009946 & 0.6063 \\ 0.03423 & -0.2628 & -0.000678 & 1.18 \end{bmatrix}$$

Input ramp time: 1.0 second

Input command:  $\theta = 0.0$   
 $p = 0.0$   
 $w = 0.0$   
 $r = 0.1745$  rad/sec step

Note: Step commands are ramped to steady state over a specified time. This time is designated as the "input ramp time" given above.

AD-A141 046

MULTIVARIABLE DIGITAL CONTROL LAWS FOR THE UH-60A BLACK 2/3

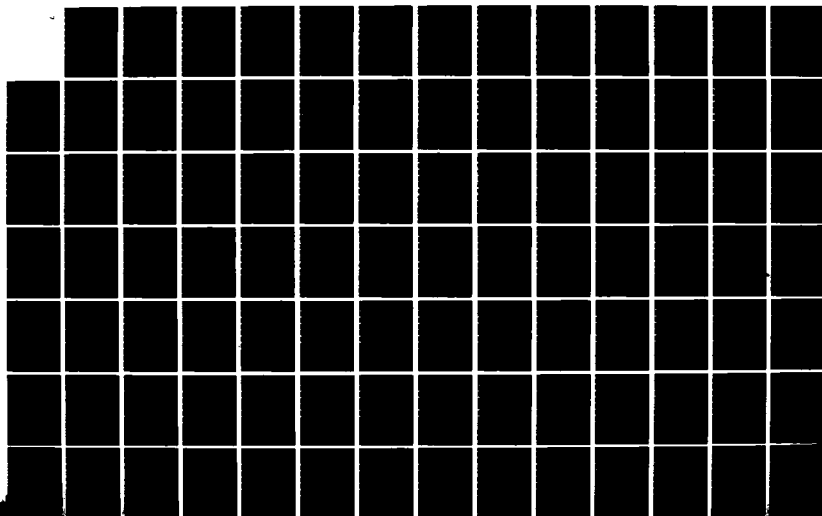
HAWK HELICOPTER(U) AIR FORCE INST OF TECH  
WRIGHT-PATTERSON AFB OH SCHOOL OF ENGINEERING

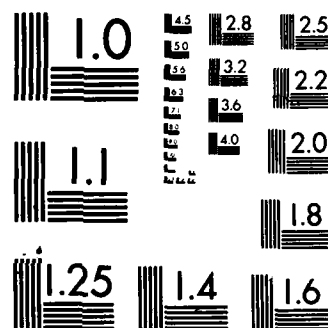
UNCLASSIFIED

B H MAYHEW MAR 84 AFIT/GE/EE/84M-6

F/G 1/3

NL





MICROCOPY RESOLUTION TEST CHART  
NATIONAL BUREAU OF STANDARDS-1963-A



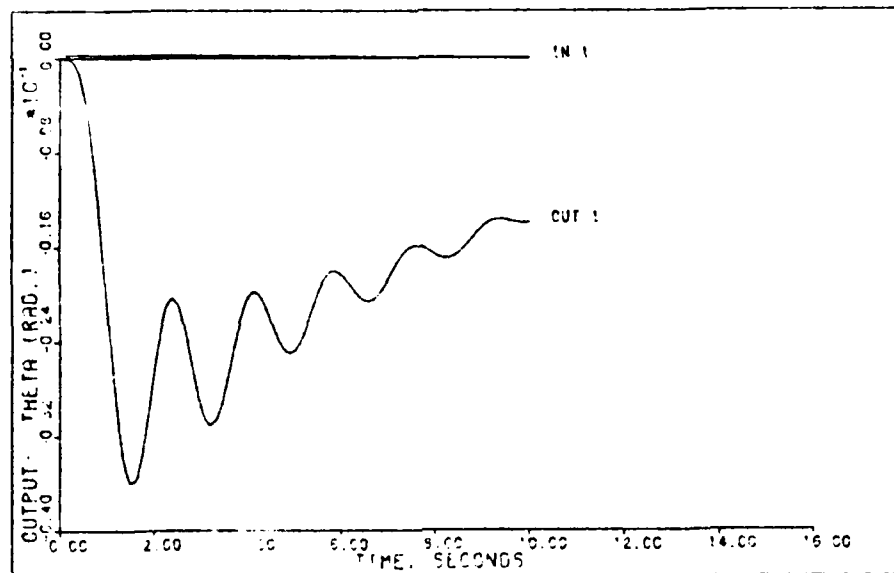


Figure 6a. Output Response,  $\Theta$ , for the Yaw Rate Command System ( $V_{EAS} = 60$  Knots)

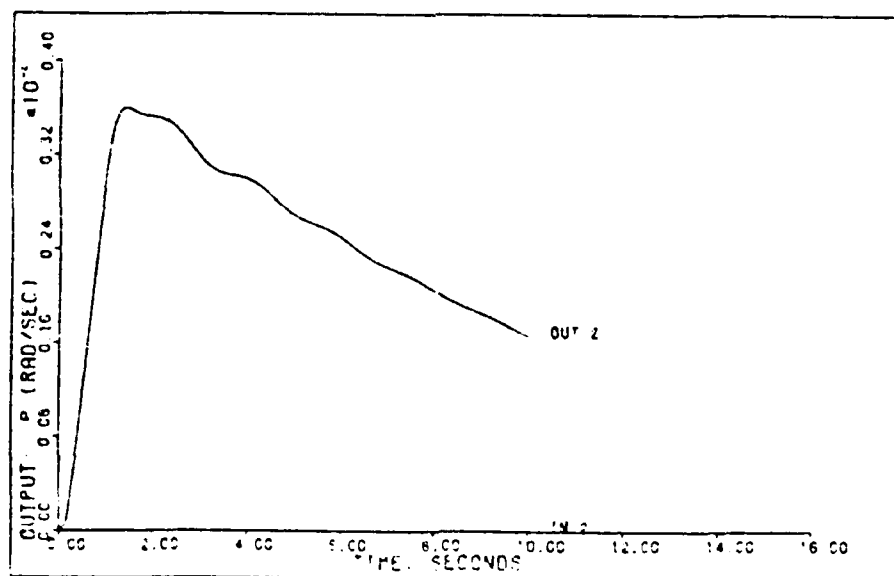


Figure 6b. Output Response,  $p_B$ , for the Yaw Rate Command System ( $V_{EAS} = 60$  Knots)

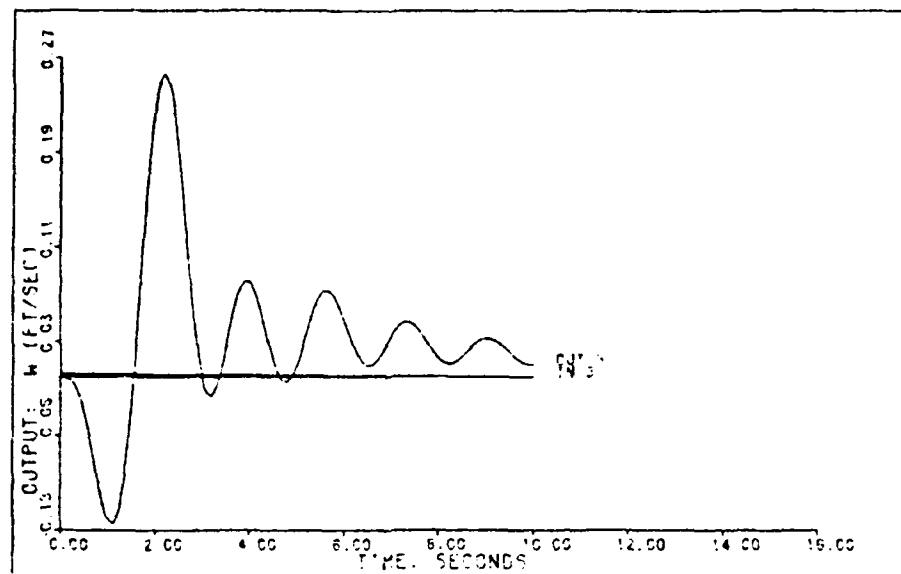


Figure 6c. Output Response,  $w_B$ , for the Yaw Rate Command System ( $V_{EAS} = 60$  Knots)

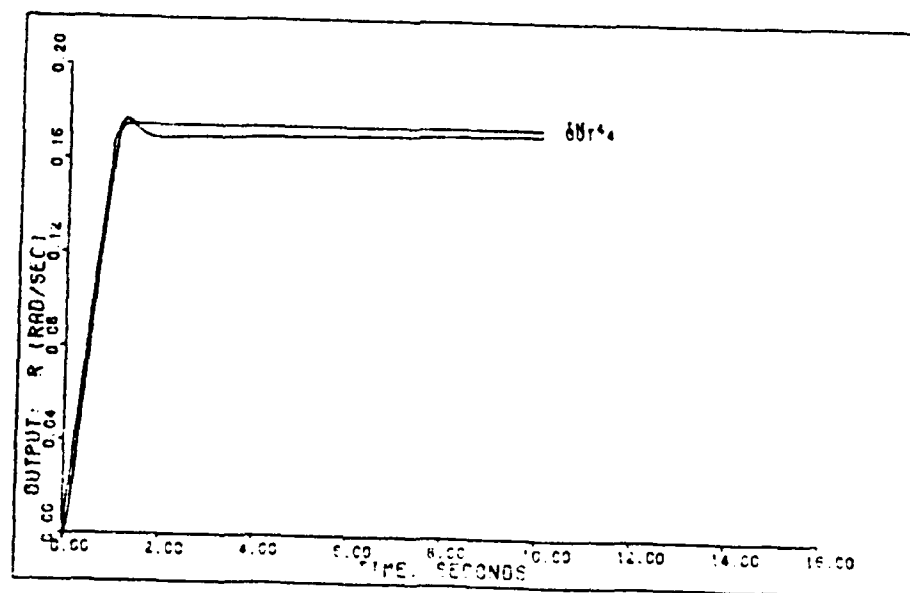


Figure 6d. Output Response,  $r_B$ , for the Yaw Rate Command System ( $V_{EAS} = 60$  Knots)

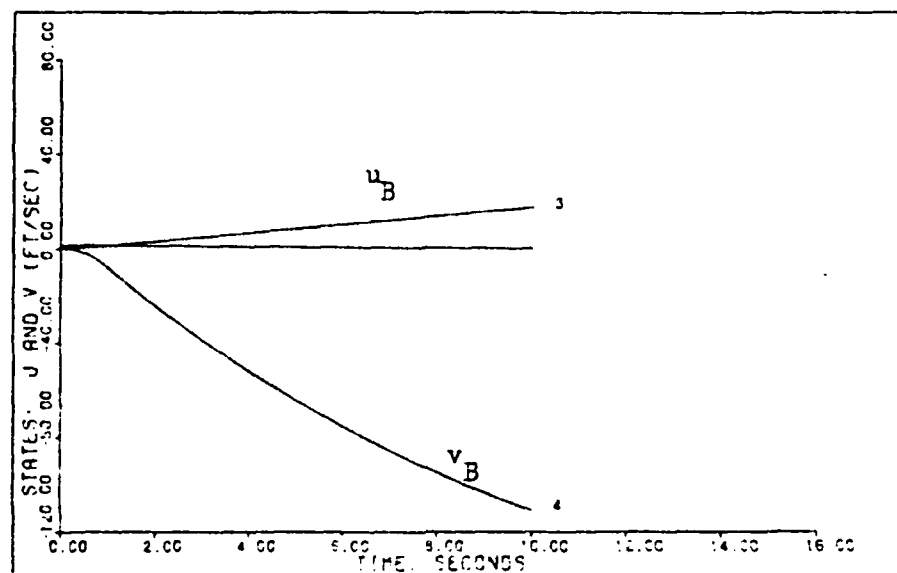


Figure 6e. State Responses,  $u_B$  and  $v_B$ , for the Yaw Rate Command System ( $V_{EAS} = 60$  Knots)

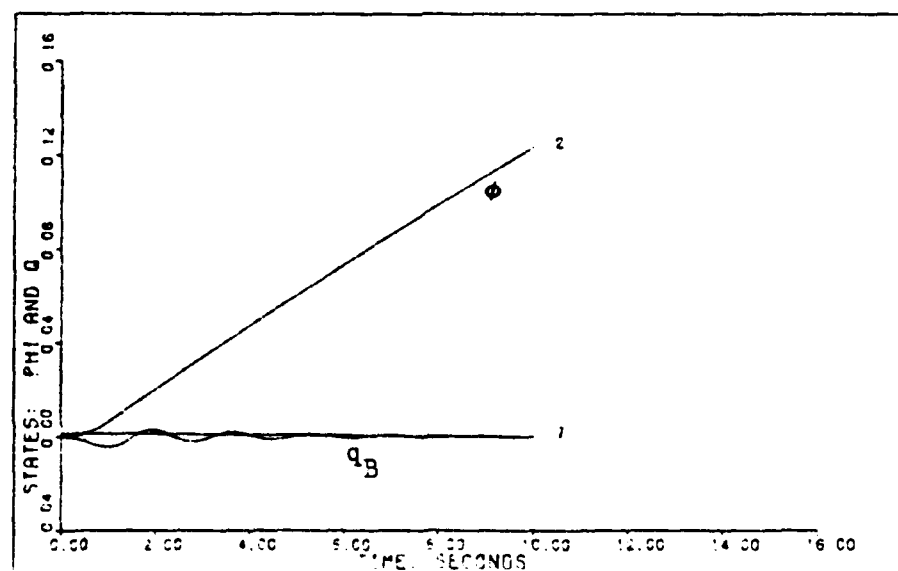


Figure 6f. State Responses,  $\phi$ (rad.) and  $q_B$ (rad/sec) for the Yaw Rate Command System ( $V_{EAS} = 60$  Knots)

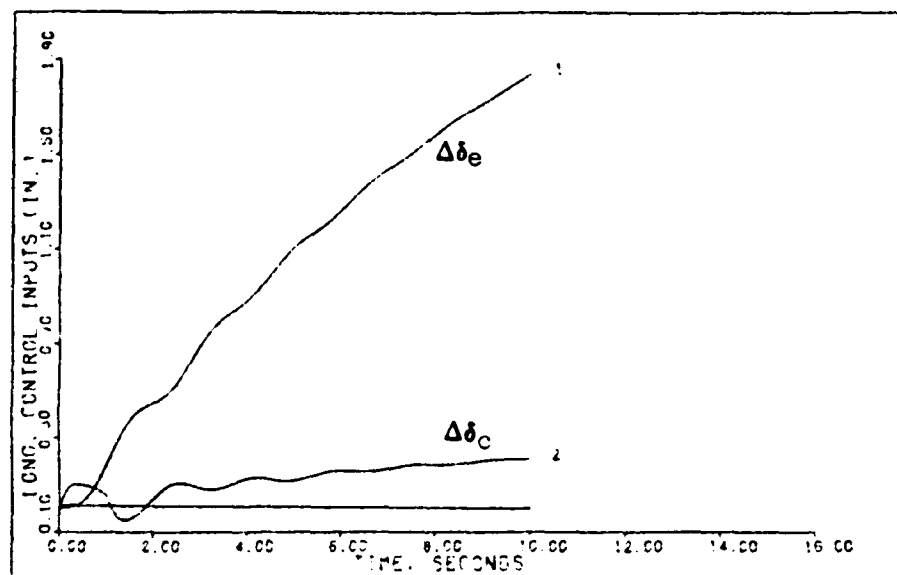


Figure 6g. Longitudinal Control Surface Responses,  $\Delta\delta_e$  and  $\Delta\delta_c$ , for the Yaw Rate Command System ( $V_{EAS} = 60$  Knots)

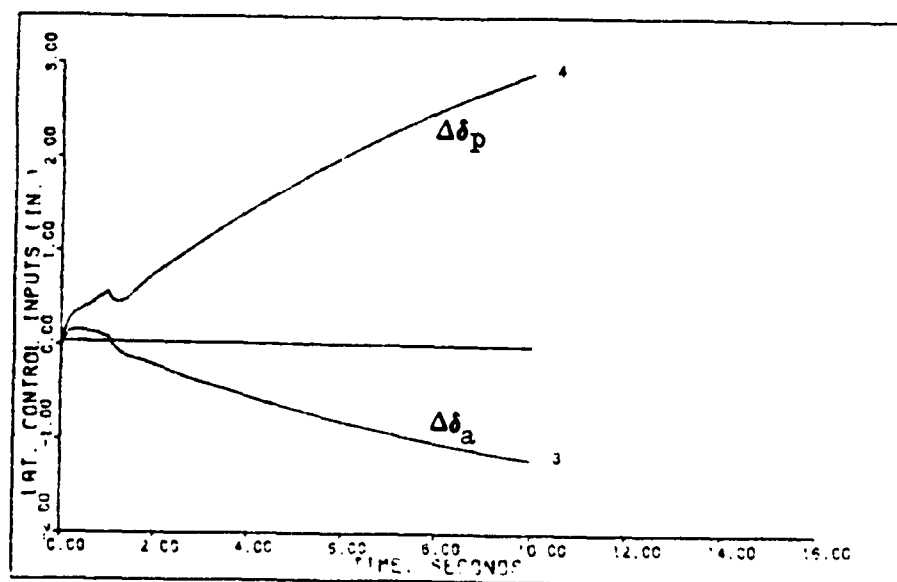


Figure 6h. Lateral Control Surface Responses,  $\Delta\delta_a$  and  $\Delta\delta_p$ , for the Yaw Rate Command System ( $V_{EAS} = 60$  Knots)

in Figures 7a.-7h.

Table IV-3  
Yaw Rate Response with Actuators for  $V_{EAS}=60$  knots

Outputs	$M_p$	$t_p$	$M_m$	$t_m$	FV	$t_s$
$\theta$	0	0	-0.00368698	1.5	-0.001453	9.7
$p_B$	0.00366367	1.4	-0.000014934	0.1	0.00165536	9.9
$w_B$	0.2426068	2.1	-0.1219128	1.1	0.007585	10
$r_B$	0.1767156	1.2	0	0	0.171732	1.4

Table IV-4  
Yaw Rate Response for  $V_{EAS}=60$  knots

Outputs	$M_p$	$t_p$	$M_m$	$t_m$	FV	$t_s$
$\theta$	0	0	-0.0035923	1.5	-0.001395	9.1
$p_B$	0.0035991	1.4	0	0	0.0016613	9.9
$w_B$	0.256420	2.2	-0.124232	1.2	0.0105276	9.9
$r_B$	0.1766397	1.2	0	0	0.1714144	1.4

From the figures of merit and the time response plots, it can be seen that there is little difference between the simulation with actuators and the simulation without actuators. Again, an examination of the output responses reveals relatively tight tracking of the desired output responses. The problems with  $\phi$  and  $v_B$  reappear as expected. The roll angle perturbation state equation is

$$\dot{\phi} = p_B + 0.061 r_B. \quad (4.26)$$

In steady-state,  $\dot{\phi}=0.01064$  rad/sec. Even though  $\dot{\phi}$  in steady-state improves with increasing total velocity,  $v_B$  becomes much worse. The non-zero steady-state error problem disappears since  $\dot{\theta} = q_B$ .

From the experience gained at the lower flight conditions, possible designs at  $V_{EAS} = 100$  and 140 knots would not be practical due to the increasingly unsatisfactory influence of the dutch roll mode on the perturbation y-body velocity,  $v_B$ .

Design Data for the Yaw Rate Command System With Actuators

Flight Condition:  $V_{EAS} = 60$  knots

$T = 0.00$  seconds

$\alpha = 0.25$

$$\underline{\Sigma} = \begin{bmatrix} 0.2 & 0 & 0 & 0 \\ 0 & 3.5 & 0 & 0 \\ 0 & 0 & 0.1 & 0 \\ 0 & 0 & 0 & 1 \end{bmatrix}$$

$\epsilon = 0.8$

$$\underline{M} = \begin{bmatrix} 0.25 & 0 & 0 & 0 \\ 0 & 0 & 0 & 0 \\ 0 & 0 & 0 & 0 \\ 0 & 0 & 0 & 0 \end{bmatrix}$$

$$\underline{K}_0 = \begin{bmatrix} 0.4388 & -0.01382 & 0.0005775 & 0.00259 \\ -0.1703 & 0.008547 & -0.002668 & 0.08984 \\ -0.00717 & 0.4855 & 0.0002487 & 0.517 \\ 0.008557 & -0.06569 & -0.0001695 & 0.295 \end{bmatrix}$$

$$\underline{K}_1 = \begin{bmatrix} 1.755 & -0.0553 & 0.00231 & 0.01036 \\ -0.6814 & 0.03419 & -0.01067 & 0.3594 \\ -0.02868 & 1.942 & 0.0009946 & 0.6068 \\ 0.03423 & -0.2628 & -0.000678 & 1.18 \end{bmatrix}$$

Input ramp time: 1.0 second

Input command:  $\theta = 0.0$

$p = 0.0$

$w = 0.0$

$r = 0.1745$  rad/sec step

Note: Step commands are ramped to steady state over a specified time. This time is designated as the "input ramp time" given above.

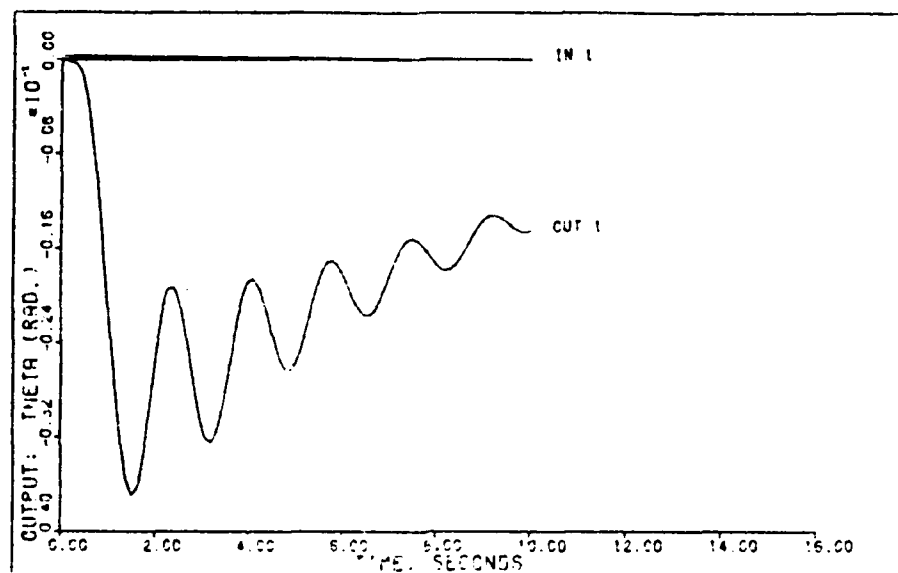


Figure 7a. Output Response,  $\Theta$ , for the Yaw Rate Command System With Actuators ( $V_{EAS} = 60$  Knots)

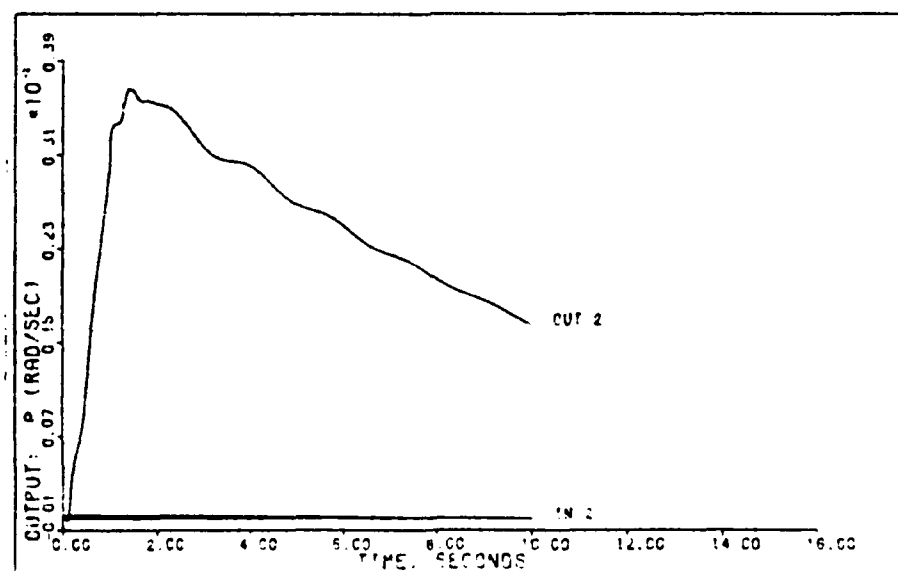


Figure 7b. Output Response,  $p_B$ , for the Yaw Rate Command System With Actuators ( $V_{EAS} = 60$  Knots)

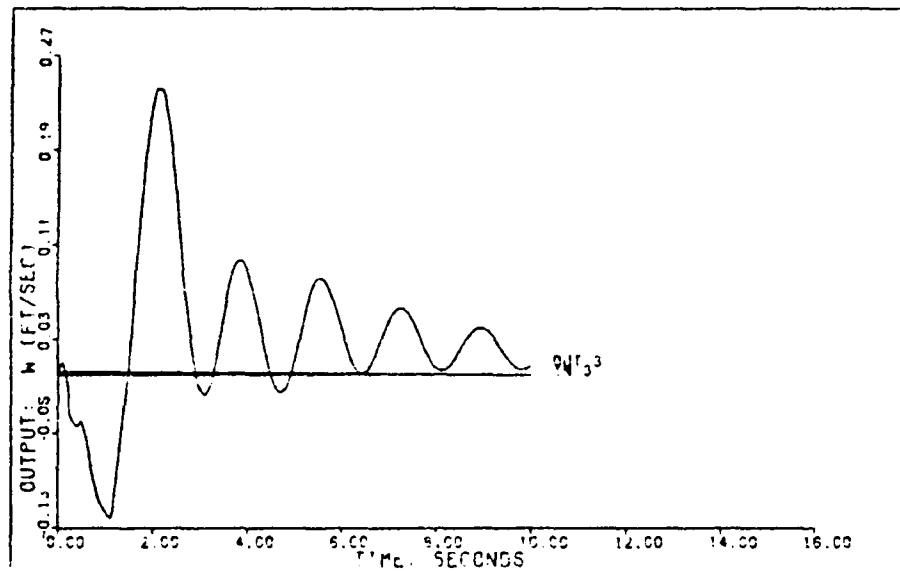


Figure 7c. Output Response,  $w_B$ , for the Yaw Rate Command System With Actuators ( $V_{EAS} = 60$  Knots)

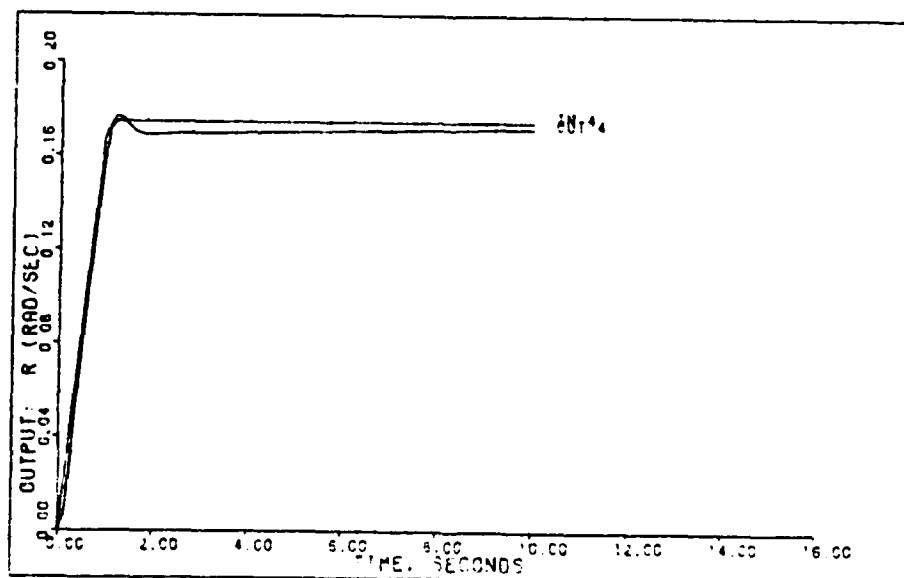


Figure 7d. Output Response,  $r_B$ , for the Yaw Rate Command System With Actuators ( $V_{EAS} = 60$  Knots)



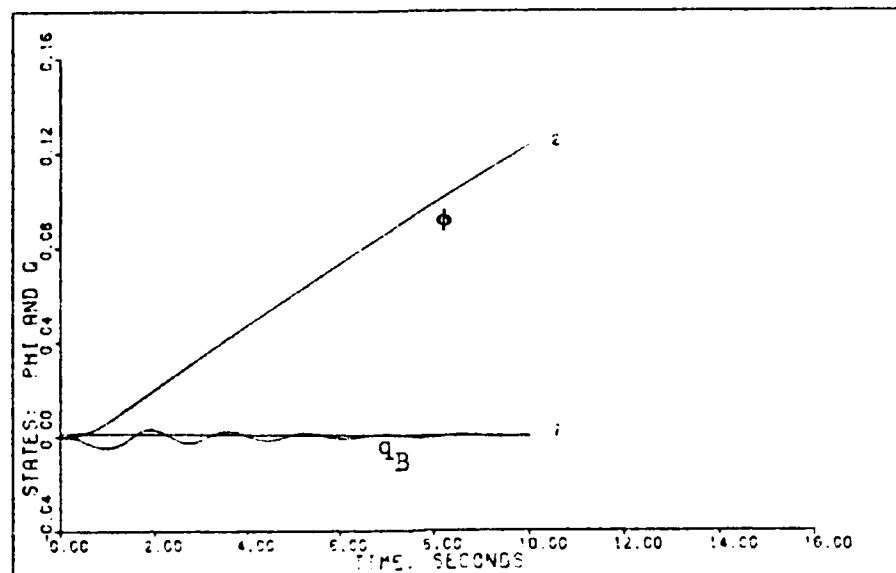


Figure 7e. State Responses,  $\phi$ (rad.) and  $q_B$ (rad/sec) for the Yaw Rate Command System With Actuators ( $V_{EAS} = 60$  Knots)

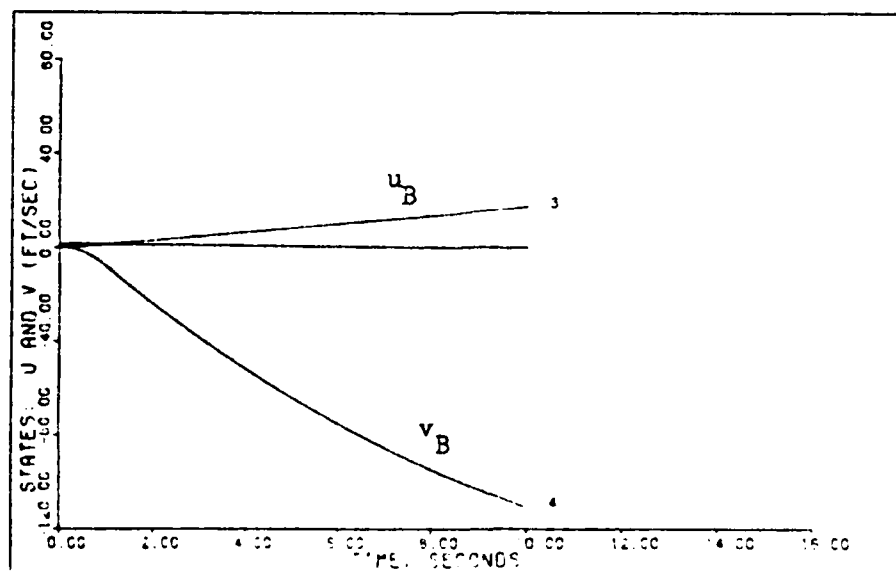


Figure 7f. State Responses,  $u_B$  and  $v_B$ , for the Yaw Rate Command System ( $V_{EAS} = 60$  Knots)

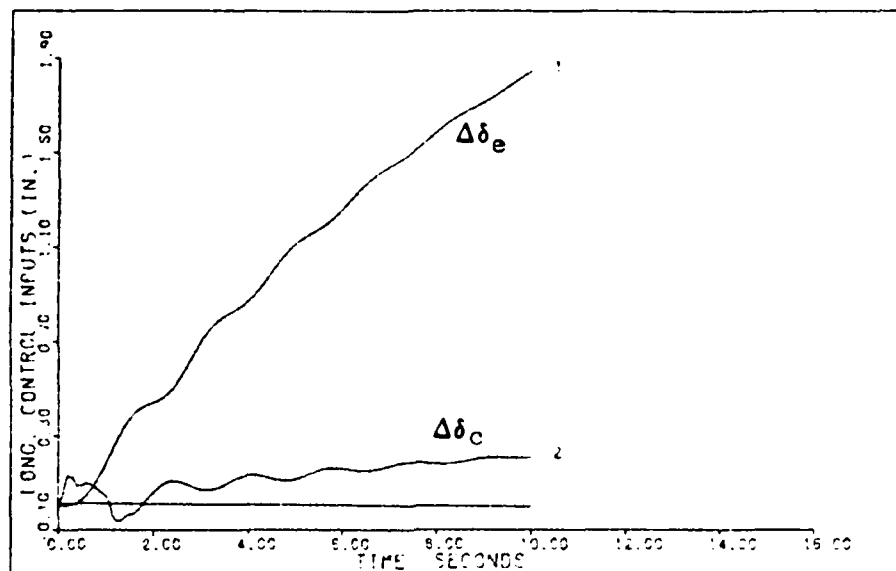


Figure 7g. Longitudinal Control Surface Responses,  $\Delta\delta_e$  and  $\Delta\delta_c$ , for the Yaw Rate Command System With Actuators ( $V_{EAS} = 60$  Knots)

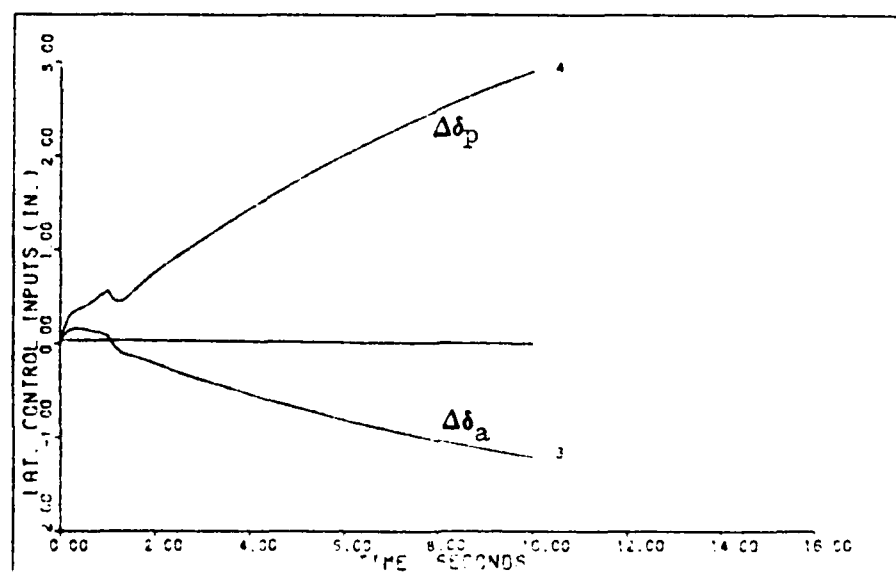


Figure 7h. Lateral Control Surface Responses,  $\Delta\delta_a$  and  $\Delta\delta_p$ , for the Yaw Rate Command System With Actuators ( $V_{EAS} = 60$  Knots)

### Coordinated Turn Command System

The purpose of the coordinated turn command system is to execute a coordinated turn. As originally stated, the coordinated turn command system commanded the perturbation roll rate,  $p_B = \pm 10$  deg/sec with the perturbation y-body acceleration,  $\ddot{y}_B = 0$ . The  $\ddot{y}_B = 0$  command indicates that there must be no sideslip ( $\beta=0$ ) while executing the coordinated turn. Since  $\ddot{y}_B = \dot{v}_B$ ,  $\dot{v}_B$  could be commanded to zero instead. However,  $\dot{v}_B$  contains inputs from the control surfaces. In order to command  $\dot{v}_B = 0$ , the output equation would require a D matrix. The current version of MULTI contains no implementation for a D matrix. As a result of this situation,  $v_B$  is commanded to zero. Since the sideslip angle,  $\beta$ , is defined by

$$\beta = \sin^{-1}(v_B/V_T) \quad (4.27)$$

commanding  $v_B=0$  is equivalent to having zero sideslip.

Since there are four control surfaces, two more outputs must be commanded. The perturbation state vectors,  $\theta$  and  $w_B$ , are added to include the requirement that the helicopter not pitch or have a z-body velocity.

Referring to Blakelock (Ref 3), a coordinated turn can be defined for a longitudinally and laterally coupled aircraft. For a given displacement of the roll angle, the yaw rate,  $r_B$ , and the pitch rate,  $q_B$ , can be found by the following equations

$$r_B = g \sin \phi \frac{\overline{V_T}}{V_T} \quad (4.28)$$

and

$$q_B = g \tan \phi \sin \phi \frac{\overline{V_T}}{V_T} \quad (4.29)$$

These two equations depend on the roll angle,  $\phi$ , and not the roll rate  $p_B$ . In order to stay within the small angle approximations of the linearized state equations,  $\phi$  is commanded instead of  $p_B$ . A second reason for selecting  $\phi$  over  $p_B$  is that stable transmission zeros are obtained. Using  $p_B$  results in a transmission zero at the origin. A final reason for selecting  $\phi$  is that the equations for a coordinated turn developed in Blakelock can be used to check the responses.

The final output vector selected for the coordinated turn command system is

$$\underline{y} = \begin{bmatrix} \theta \\ \phi \\ v_B \\ w_B \end{bmatrix} \quad (4.30)$$

Since  $p_B = \pm 10$  deg/sec,  $\phi$  is commanded to  $\pm 30$  deg in three seconds. It should be noted that  $\phi = \pm 30$  deg, is definitely straining the small angle approximations; however, this is ignored to expose the capabilities of the digital control law design method. Finally, it should be noted from Equation (4.29), that perturbation pitch rate results from a perturbation in the roll angle and not from a perturbation in the pitch angle.

Individual digital control laws have been developed at the  $V_{EAS} = 60, 100, \text{ and } 140$  knots flight condition. For these flight conditions, the expected values of  $r_B$  and  $q_B$  in rad/sec are listed in Table IV-5 for a perturbation roll angle,  $\phi = 30$  degrees.

Table IV-5  
Expected Values of  $r_B$  and  $q_B$  for the  
Coordinated Turn Command System

$V_{EAS}$	$r_B$	$q_B$
60	0.158882	0.0917303
100	0.0953289	0.055038
140	0.0680921	0.039313

The denominator of the closed-loop transfer function for the  $V_{EAS} =$   
60 knots flight condition is

$$\begin{aligned}
 & (.1000E+01) S^{**} 12 & (-.1262E+02) + J(.3797E+02) \\
 & (.1317E+03) S^{**} 11 & (-.1262E+02) + J(-.3797E+02) \\
 & (.8242E+04) S^{**} 10 & (-.4646E+02) + J(0. \quad \quad \quad) \\
 & (.3326E+06) S^{**} 9 & (-.2486E+02) + J(.3818E+00) \\
 & (.8307E+07) S^{**} 8 & (-.2486E+02) + J(-.3818E+00) \\
 & (.1111E+09) S^{**} 7 & (-.4274E+01) + J(0. \quad \quad \quad) \\
 & (.6773E+09) S^{**} 6 & (-.4001E+01) + J(0. \quad \quad \quad) \quad (4.29) \\
 & (.1892E+10) S^{**} 5 & (-.4104E+00) + J(.1003E+00) \\
 & (.2365E+10) S^{**} 4 & (-.4104E+00) + J(-.1003E+00) \\
 & (.1462E+10) S^{**} 3 & (-.9108E-02) + J(0. \quad \quad \quad) \\
 & (.4443E+09) S^{**} 2 & (-.5949E+00) + J(.8854E01) \\
 & (.5472E+08) S^{**} 1 & (-.5949E+00) + J(-.8854E01) \\
 & (.4626E+06) S^{**} 0 & \text{DENOMINATOR GAIN} = .1000E+01
 \end{aligned}$$

It is noted that the closed-loop poles are all within the stable region.  
The figures of merit are listed in Table IV-6 and the time response  
plots are given in Figures 8a.-8g.

# Design Data for the Coordinated Turn Command System

Flight Condition:  $V_{EAS} = 60$  knots

$T = 0.02$  seconds

$\alpha = 2.0$

$$\underline{\Sigma} = \begin{bmatrix} 1.0 & 0 & 0 & 0 \\ 0 & 0.5 & 0 & 0 \\ 0 & 0 & 0.5 & 0 \\ 0 & 0 & 0 & 0.5 \end{bmatrix}$$

$\epsilon = 0.5$

$$\underline{M} = \begin{bmatrix} 0.25 & 0 & 0 & 0 \\ 0 & 0.25 & 0 & 0 \\ 0 & 0 & 0 & 0 \\ 0 & 0 & 0 & 0 \end{bmatrix}$$

$$\underline{K}_0 = \begin{bmatrix} 10.96 & -0.0252 & -0.004485 & 0.01441 \\ -4.636 & 0.4774 & -0.1421 & 0.06772 \\ -0.7813 & 2.111 & -0.2269 & 0.004588 \\ -1.031 & 1.308 & -0.4693 & -0.007605 \end{bmatrix}$$

$$\underline{K}_1 = \begin{bmatrix} 5.479 & -0.0126 & -0.002243 & 0.007203 \\ -2.318 & 0.2387 & -0.07105 & -0.03386 \\ -0.3906 & 1.055 & -0.1135 & 0.002294 \\ -0.5154 & 0.654 & -0.2346 & -0.003803 \end{bmatrix}$$

Input ramp time: 3.0 seconds

Input command:  $\theta = 0.0$   
 $\phi = 0.5235$  rad/sec step  
 $v = 0.0$   
 $w = 0.0$

Note: Step commands are ramped to steady state over a specified time. This time is designated as the "input ramp time" given above.

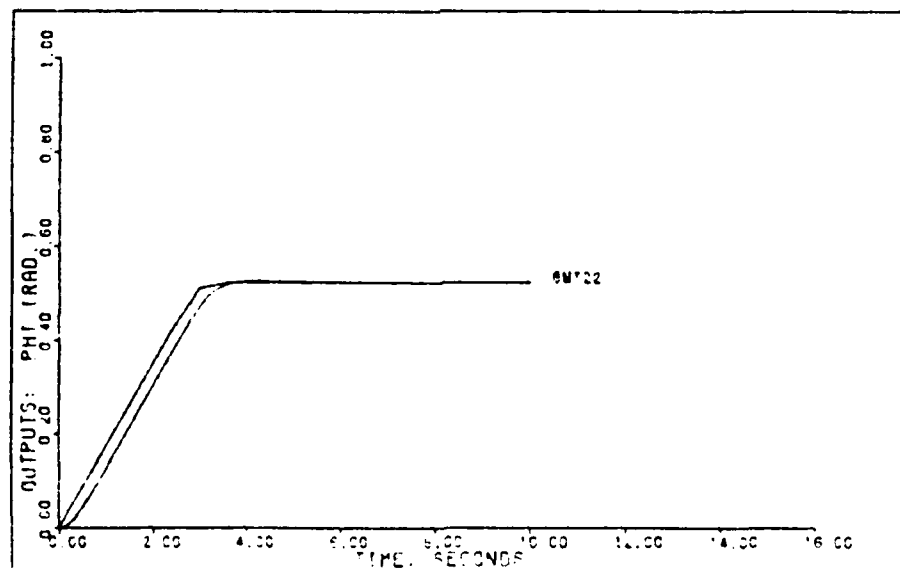


Figure 8a. Output Response,  $\phi$ , for the Coordinated Turn Command System  
( $V_{EAS} = 60$  Knots)

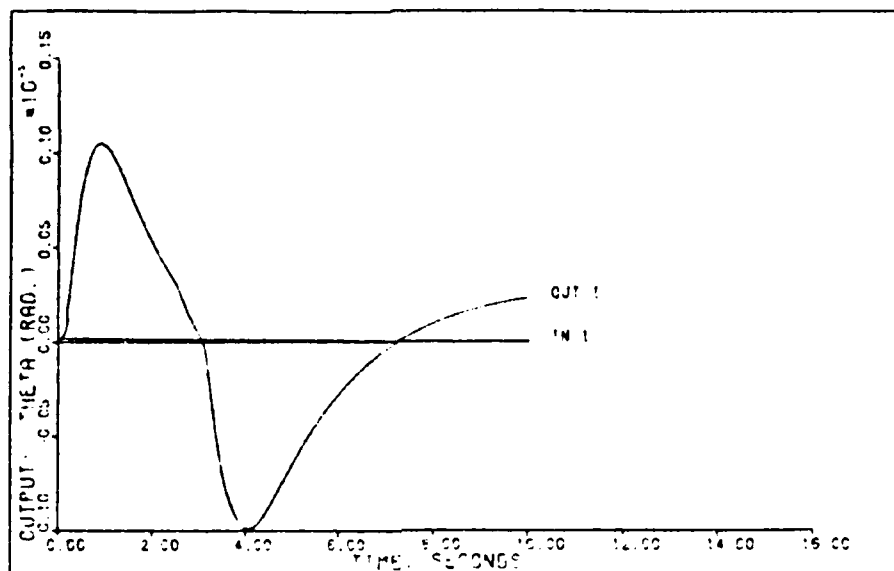


Figure 8b. Output Response,  $\Theta$ , for the Coordinated Turn Command System ( $V_{EAS} = 60$  Knots)

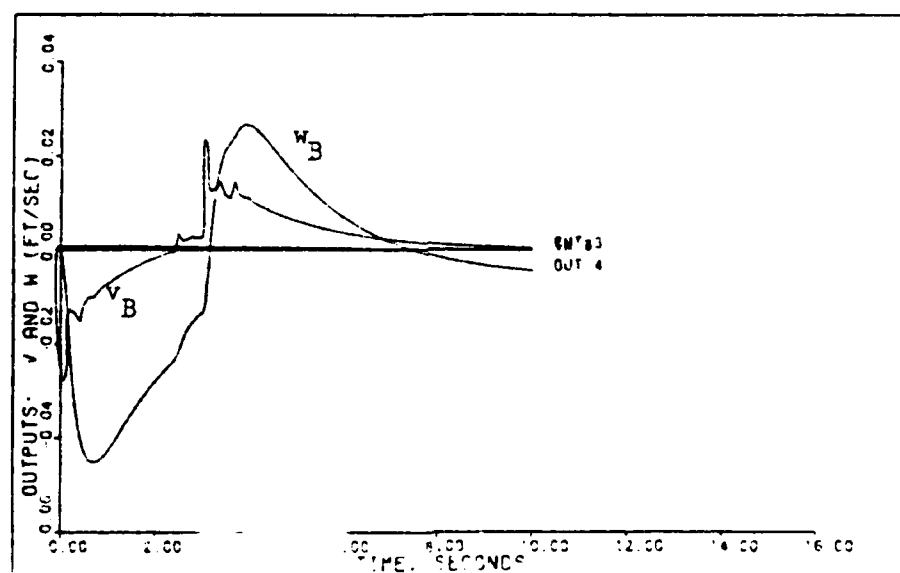


Figure 8c. Output Responses,  $v_B$  and  $w_B$ , for the Coordinated Turn Command System ( $C_{EAS} = 60$  Knots)



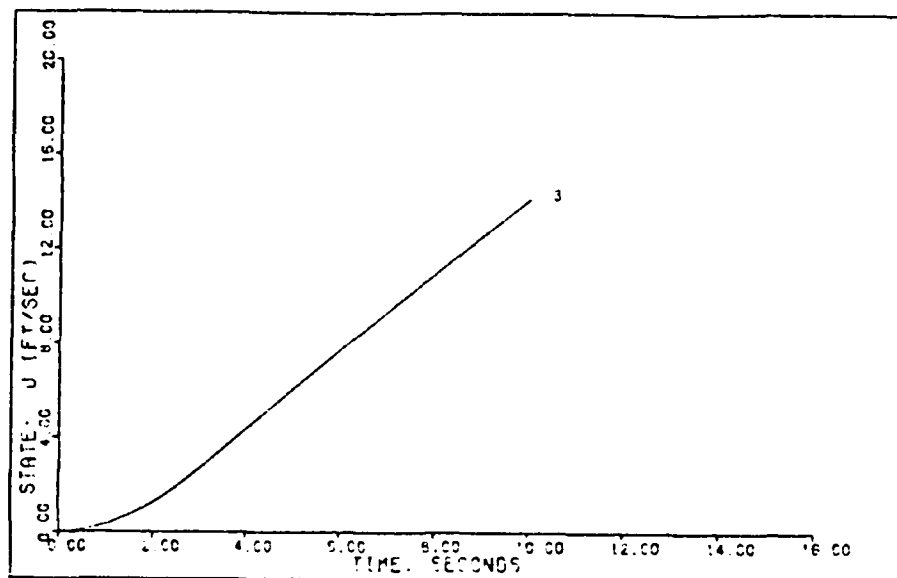


Figure 8d. State Response,  $u_B$ , for the Coordinated Turn Command System ( $V_{EAS} = 60$  Knots)

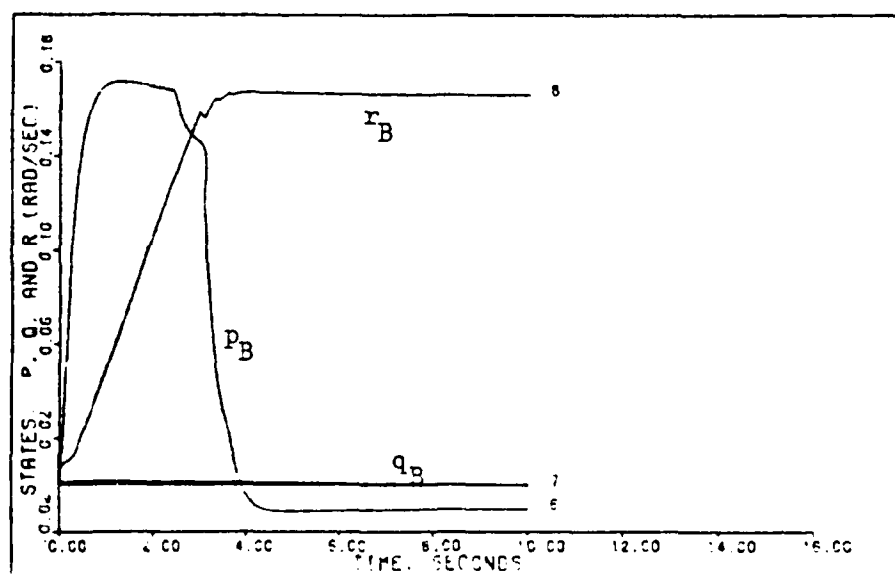


Figure 8e. State Responses,  $p_B$ ,  $q_B$ , and  $r_B$ , for the Coordinated Turn Command System ( $V_{EAS} = 60$  Knots)

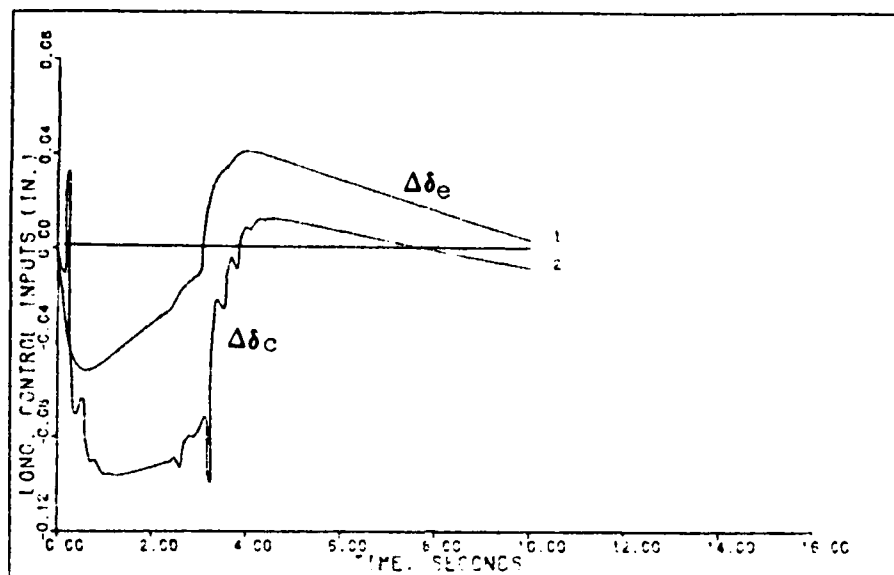


Figure 8f. Longitudinal Control Surface Responses  $\Delta\delta_e$  and  $\Delta\delta_c$ , for the Coordinated Turn Command System ( $V_{EAS} = 60$  Knots)

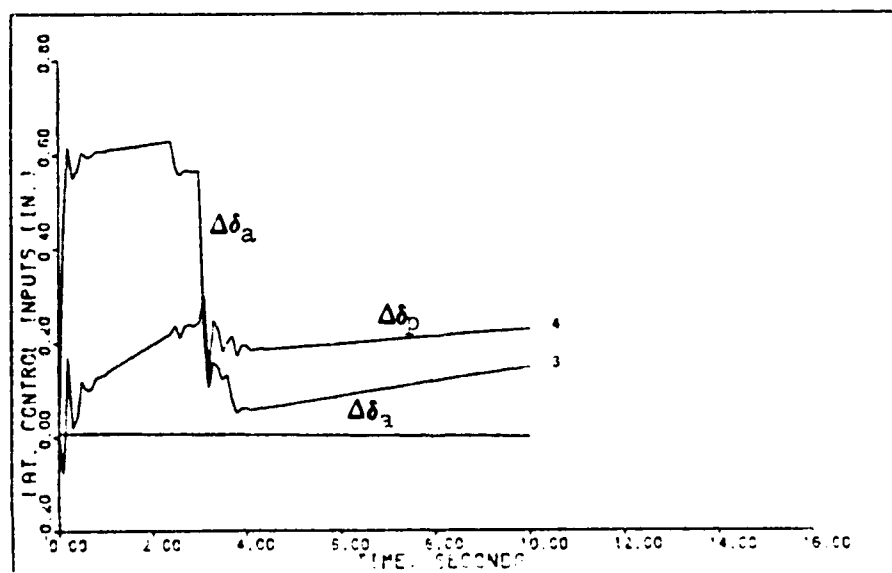


Figure 8g. Lateral Control Surface Responses,  $\Delta\delta_a$  and  $\Delta\delta_p$ , for the Coordinated Turn Command System ( $V_{EAS} = 60$  Knots)

Table IV-6  
Coordinated Turn Responses for  $V_{EAS} = 60$  knots

Outputs	$M_p$	$t_p$	$M_m$	$t_m$	FV	$t_s$
$\theta$	0.00010521	0.9	-0.00009911	4.1	0.00002301	9.9
$\phi$	0.52641322	4.4	0	0	0.5234557	3.5
$v_B$	0.0226923	3.1	-0.02664617	0.1	0.004735	10
$w_B$	0.02664741	3.9	-0.04513320	0.7	-0.0043384	9.9

The output responses,  $\theta$  and  $\phi$ , are in radians. Examining the time response plots reveals that extremely tight tracking of the desired outputs is obtained. The time response plots for the control surfaces are generated by a linear curve fit routine instead of the usual spline curve fit routine which smooths the responses between sample instances. The linear curve fit routine prevents the time responses from appearing to respond in negative time. An example of this is the  $v_B$  time response plot in Figure 8c. Problems with negative time responses occur when large perturbations are generated from the equilibrium conditions. The smoothing algorithm causes the response to occur during negative time, which of course is impossible.

From Figure 8e.,  $r_B$  is found to be equal to 0.16525 rad/sec which compares favorably to the expected value of 0.158882 rad/sec found in Table IV-5. The perturbation pitch rate,  $q_B$ , is approximately zero which does not compare to the value found in Table IV-5. It can be concluded that the original assumption of a coupled aircraft is not true, and that only the lateral modes are excited by the coordinated turn command system.

The final mystery of the coordinated turn command system is the perturbation x-body velocity,  $u_B$ , time response. From the state equations, it is found that

$$\begin{aligned}\dot{u}_B = & -32.1 \theta - 0.019 u_B - 0.00227 v_B + 0.0481 w_B \\ & + 0.0155 p_B - 2.77 q_B + 9.91 r_B - 1.41 \Delta \delta_e \\ & + 0.593 \Delta \delta_c - 0.0108 \Delta \delta_a + 0.872 \Delta \delta_p\end{aligned}\quad (4.32)$$

which can be further reduced to the following equation by examining the figures of merit and the time response plots.

$$\dot{u}_B = -0.019 u_B + 9.91 r_B + 0.872 \Delta \delta_p \quad (4.33)$$

In steady-state,  $r_B = 0.16525$  rad/sec and  $\Delta \delta_p = 0.22$  inches, therefore in steady-state

$$\dot{u}_B = -0.019 u_B + 1.8295 \quad (4.34)$$

From this equation, it can be seen that the increasing perturbation x-body velocity,  $u_B$ , is due to the perturbation yaw rate,  $r_B$ , and the perturbation tail rotor yaw control,  $\Delta \delta_p$ , attaining positive non-zero constants. Summarizing, the yawing of the helicopter in executing the coordinated turn causes an increase in the forward body velocity,  $u_B$ . From these results, a separate velocity control in addition to the individual digital control law must be implemented to perform the commanded turn command system.

The denominator of the closed-loop transfer function for the  $V_{EAS} = 100$  knots flight condition is

(.1000E+01) S** 12	(-.2381E+01) + J( .2186E+02)	
(.2929E+02) S** 11	(-.2381E+01) + J(-.2186E+02)	
(.8595E+03) S** 10	(-.4423E+01) + J( .2930E+01)	
(.1460E+05) S** 9	(-.4423E+01) + J(-.2930E+01)	
(.1378E+06) S** 8	(-.5083E+01) + J( .1015E+01)	
(.7664E+06) S** 7	(-.5083E+01) + J(-.1015E+01)	
(.2566E+07) S** 6	(-.3128E+01) + J(0. )	(4.33)
(.5063E+07) S** 5	(-.6797E+00) + J(0. )	
(.5660E+07) S** 4	(-.5425E+00) + J( .4646E-01)	
(.3521E+07) S** 3	(-.5425E+00) + J(-.4646E-01)	
(.1148E+07) S** 2	(-.2025E-01) + J(0. )	
(.1598E+06) S** 1	(-.5982E+00) + J(0. )	
(.2792E+04) S** 0	DENOMINATOR GAIN = .1000E+01	

It should be noted that closed-loop poles are all located in the stable region. The figures of merit are presented in Table IV-7 and the time responses are in Figures 9a.-9g.

Table IV-7  
Coordinated Turn Responses for  $V_{EAS} = 100$  knots

Outputs	$M_p$	$t_p$	$M_m$	$t_m$	FV	$t_s$
$\theta$	0.00029817	1.1	-0.0002789	4.2	0.0000785	10
$\phi$	0.545978	4.2	0	0	0.523831	5.6
$v_B$	0.116272	3.5	-0.1067917	0.5	0.051589	10
$w_B$	0.109392	4.4	-0.1465897	1.3	0.000985	10

Examining the time response plots reveals that relatively tight tracking of the desired output is obtained. However, it should be noted that there exists a high frequency oscillation in the time response plots for  $v_B$ ,  $r_B$ , and the control surfaces. Even though the magnitudes of these oscillations are relatively small, they cannot be totally ignored.

From Figure 8e,  $r_B$  is found approximately, due to the oscillation, to be slightly less than 0.10 rad/sec which compares favorably to the expected value of 0.0953289 rad/sec found in Table IV-5. The perturbation pitch rate,  $q_B$ , is again approximately zero which indicates a decoupling of the longitudinal and lateral modes. The magnitude of the x-body velocity,  $u_B$ , is smaller than the magnitude of  $u_B$  found for the  $V_{EAS} = 60$  knots flight condition. The smaller magnitude results from the smaller yaw rate and tail rotor yaw control displacements.

Design Data for the Coordinated Turn Command System

Flight Condition:  $V_{EAS} = 100$  knots

$T = 0.02$  seconds

$\alpha = 1.75$

$$\underline{\Sigma} = \begin{bmatrix} 1.0 & 0 & 0 & 0 \\ 0 & 0.5 & 0 & 0 \\ 0 & 0 & 0.5 & 0 \\ 0 & 0 & 0 & 0.5 \end{bmatrix}$$

$\epsilon = 0.1$

$$\underline{M} = \begin{bmatrix} 0.25 & 0 & 0 & 0 \\ 0 & 0.25 & 0 & 0 \\ 0 & 0 & 0 & 0 \\ 0 & 0 & 0 & 0 \end{bmatrix}$$

$$\underline{K}_0 = \begin{bmatrix} 1.739 & -0.01389 & -0.002782 & 0.001966 \\ -1.253 & 0.1141 & -0.02972 & -0.01102 \\ -0.1802 & 0.3756 & -0.4112 & 0.0005072 \\ -0.3211 & 0.2006 & -0.07004 & -0.001704 \end{bmatrix}$$

$$\underline{K}_1 = \begin{bmatrix} 0.9937 & -0.007936 & -0.00159 & 0.001123 \\ -0.7158 & 0.06521 & -0.01699 & -0.006296 \\ -0.1030 & 0.2146 & -0.0235 & 0.0002898 \\ -0.1835 & 0.1146 & -0.04003 & -0.0009738 \end{bmatrix}$$

Input ramp time: 3.0 seconds

Input command:  $\theta = 0.0$

$\phi = 0.5235$  rad/sec step

$v_B = 0.0$

$w_B = 0.0$

Note: Step commands are ramped to steady state over a specified time. This time is designated as the "input ramp time" given above.

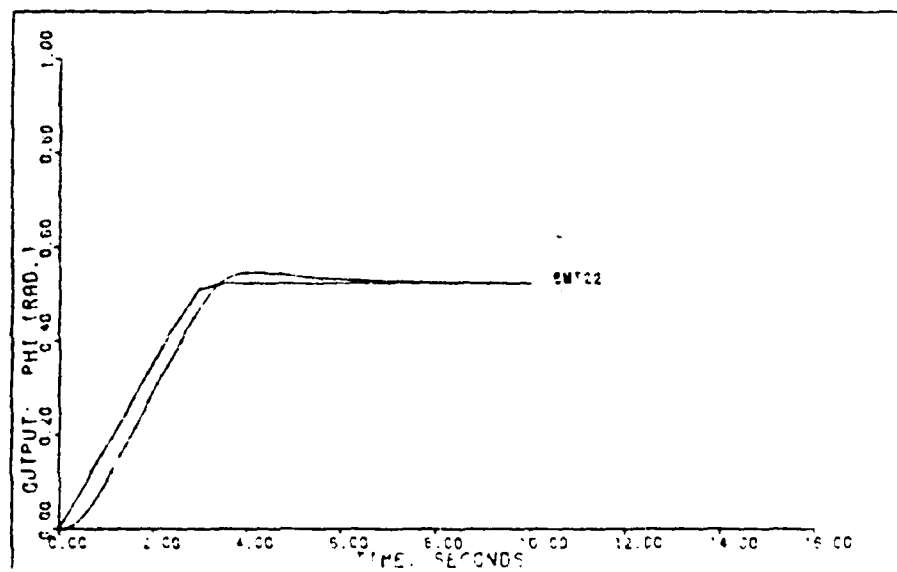


Figure 9a. Output Response,  $\phi$ , for the Coordinated Turn Command System  
( $V_{EAS} = 100$  Knots)

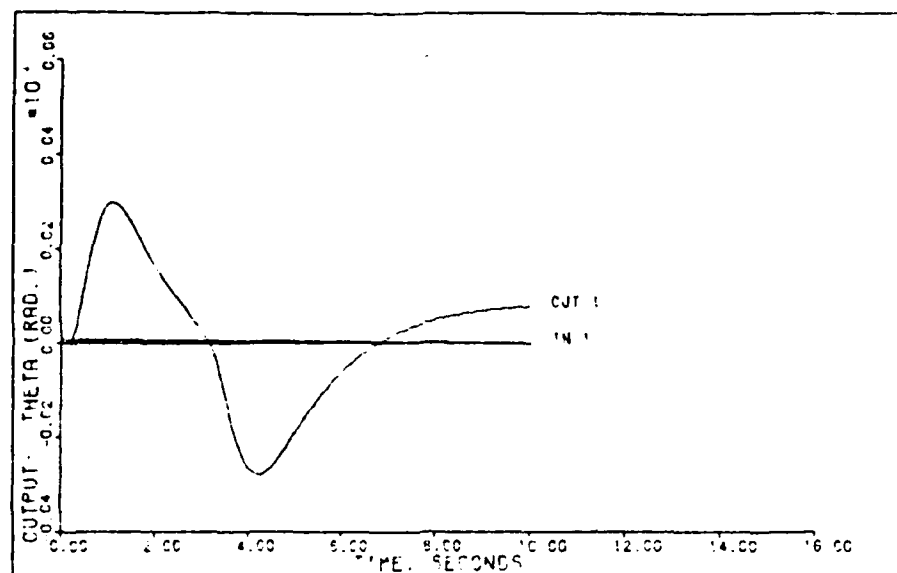


Figure 9b. Output Response,  $\Theta$ , for the Coordinated Turn Command System ( $V_{EAS} = 100$  Knots)

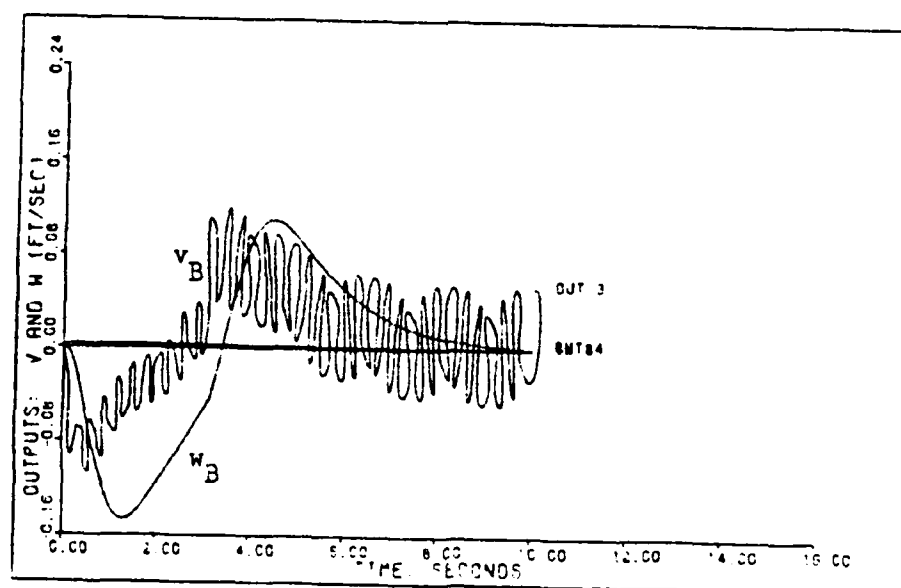


Figure 9c. Output Responses,  $v_B$  and  $w_B$ , for the Coordinated Turn Command System ( $V_{EAS} = 100$  Knots)



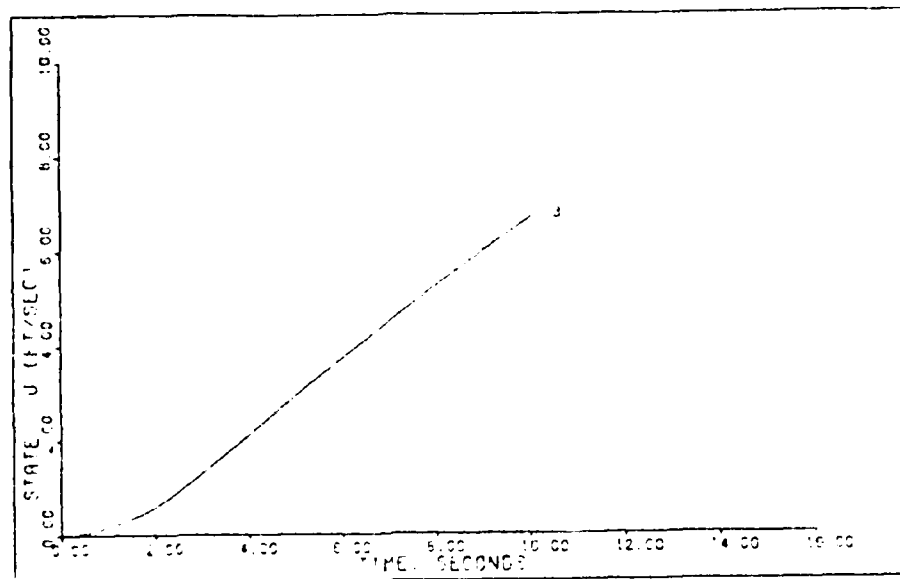


Figure 9d. State Response,  $u_B$ , for the Coordinated Turn Command System ( $V_{EAS} = 100$  Knots)

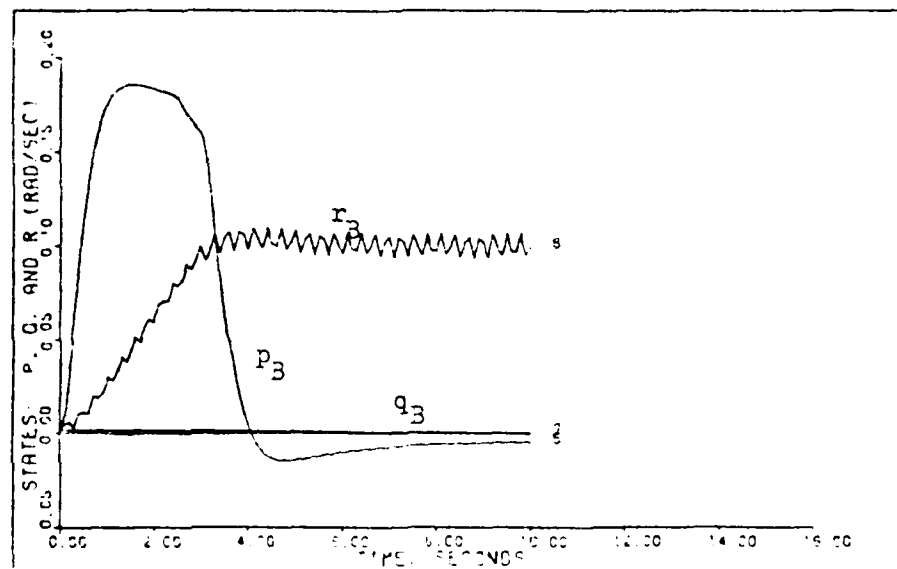


Figure 9e. State Responses,  $p_B$ ,  $q_B$ , and  $r_B$ , for the Coordinated Turn Command System ( $V_{EAS} = 100$  Knots)

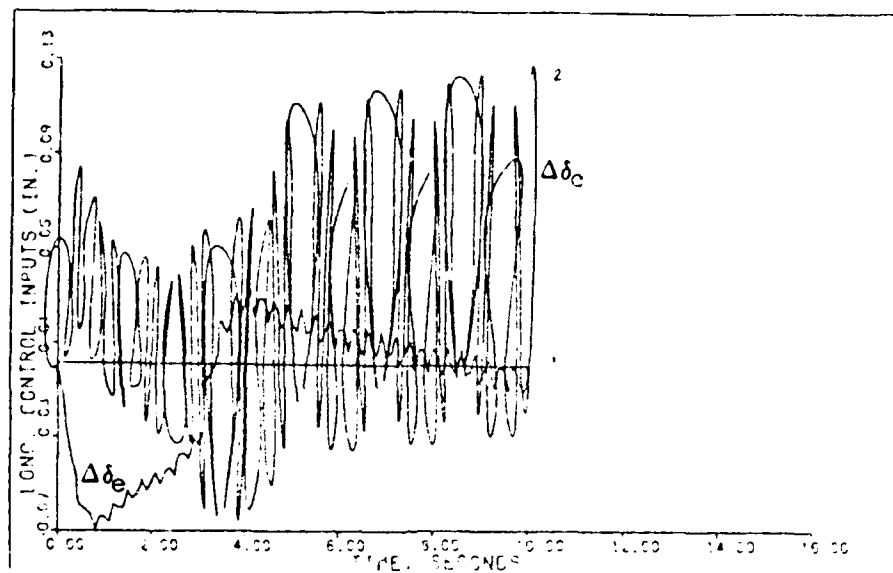


Figure 9f. Longitudinal Control Surface Responses,  $\Delta\delta_e$  and  $\Delta\delta_c$ , for the Coordinated Turn Command System ( $V_{EAS} = 100$  Knots)

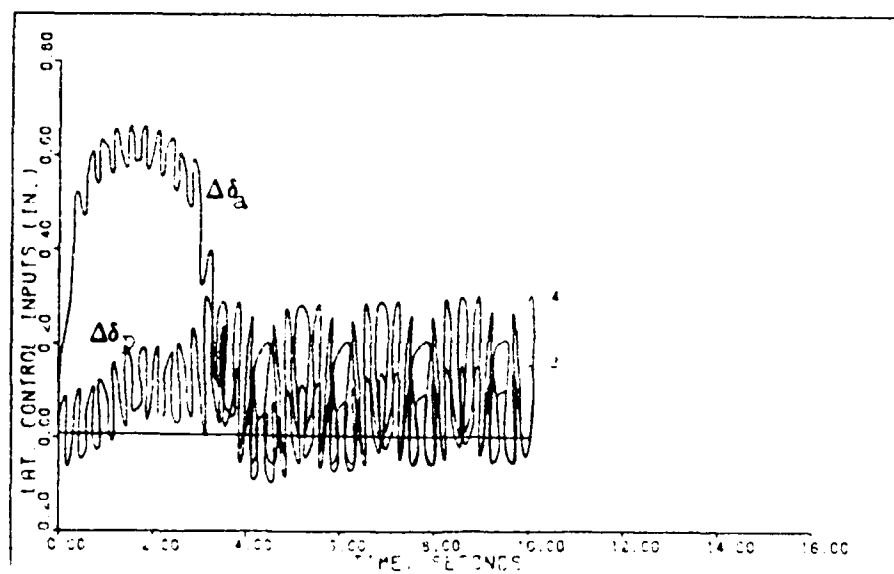


Figure 9g. Lateral Control Surface Responses,  $\Delta\delta_a$  and  $\Delta\delta_p$ , for the Coordinated Turn Command System ( $V_{EAS} = 100$  Knots)

The denominator of the closed-loop transfer function for the  $V_{EAS} = 140$  knots flight condition is

$$\begin{aligned}
 (.1000E+01) S^{**} 12 & \quad (-.1164E+01) + J(.1652E+02) \\
 (.2184E+02) S^{**} 11 & \quad (-.1164E+01) + J(-.1652E+02) \\
 (.4799E+03) S^{**} 10 & \quad (-.4765E+01) + J(.1990E+01) \\
 (.6429E+04) S^{**} 9 & \quad (-.4765E+01) + J(-.1990E+01) \\
 (.4738E+05) S^{**} 8 & \quad (-.3257E+01) + J(.5476E+00) \\
 (.2004E+06) S^{**} 7 & \quad (-.3257E+01) + J(-.5476E+00) \\
 (.5030E+06) S^{**} 6 & \quad (-.9295E+00) + J(.4506E+00) \quad (4.36) \\
 (.7603E+06) S^{**} 5 & \quad (-.9295E+00) + J(-.4506E+00) \\
 (.6986E+06) S^{**} 4 & \quad (-.5653E+00) + J(0) \\
 (.3809E+06) S^{**} 3 & \quad (-.2619E-01) + J(0) \\
 (.1141E+06) S^{**} 2 & \quad (-.5072E+00) + J(-.3903E-01) \\
 (.1519E+05) S^{**} 1 & \quad (-.5072E+00) + J(.3903E-01) \\
 (.3262E+03) S^{**} 0 & \quad \text{DENOMINATOR GAIN} = .1000E+01
 \end{aligned}$$

It should be noted that the closed-loop poles are located within the stable region. For this flight condition, the simulation is performed both with and without actuators. The figures of merit for the simulation without actuators are presented in Table IV-8 and the time response plots in Figures 10a.-10g. The figures of merit for the simulation with actuators are presented in Table IV-9 and the time response plots in Figures 11a.-11h.

Table IV-8  
Coordinated Turn Results for  $V_{EAS} = 140$  knots

Outputs	$M_p$	$t_p$	$M_m$	$t_m$	FV	$t_s$
$\theta$	0.0001663	6.1	-0.00002261	2.1	0.00013742	10
$\phi$	0.57912	4.5	0	0	0.523761	7.2
$v_B$	0.23351	3.9	-0.2035789	0.7	0.09211712	10
$w_B$	0.199289	5.1	-0.27393537	1.9	0.00613385	10

Design Data for the Coordinated Turn Command System

Flight Condition:  $V_{EAS} = 140$  knots

$T = 0.02$  seconds

$\alpha = 1.75$

$$\underline{\Sigma} = \begin{bmatrix} 1.0 & 0 & 0 & 0 \\ 0 & 0.2 & 0 & 0 \\ 0 & 0 & 0.2 & 0 \\ 0 & 0 & 0 & 0.2 \end{bmatrix}$$

$\epsilon = 0.1$

$$\underline{M} = \begin{bmatrix} 0.25 & 0 & 0 & 0 \\ 0 & 0.25 & 0 & 0 \\ 0 & 0 & 0 & 0 \\ 0 & 0 & 0 & 0 \end{bmatrix}$$

$$\underline{K}_0 = \begin{bmatrix} 1.243 & 0.005929 & -0.00609 & -0.0001509 \\ -1.197 & 0.04457 & -0.008789 & -0.003228 \\ -0.1649 & 0.1529 & -0.01716 & 0.0002646 \\ -0.3259 & 0.0756 & -0.02501 & -0.0004396 \end{bmatrix}$$

$$\underline{K}_1 = \begin{bmatrix} 0.7103 & -0.003388 & -0.00348 & 0.00008624 \\ -0.6838 & 0.02547 & -0.005022 & -0.001845 \\ -0.09423 & 0.0874 & -0.009803 & 0.0001512 \\ -0.1862 & 0.04321 & -0.01429 & -0.0002512 \end{bmatrix}$$

Input ramp time: 3.0 seconds

Input command:  $\theta = 0.0$

$\phi = 0.5235$  rad/sec step

$v_B = 0.0$

$w_B = 0.0$

Note: Step commands are ramped to steady state over a specified time. This time is designated as the "input ramp time" given above.

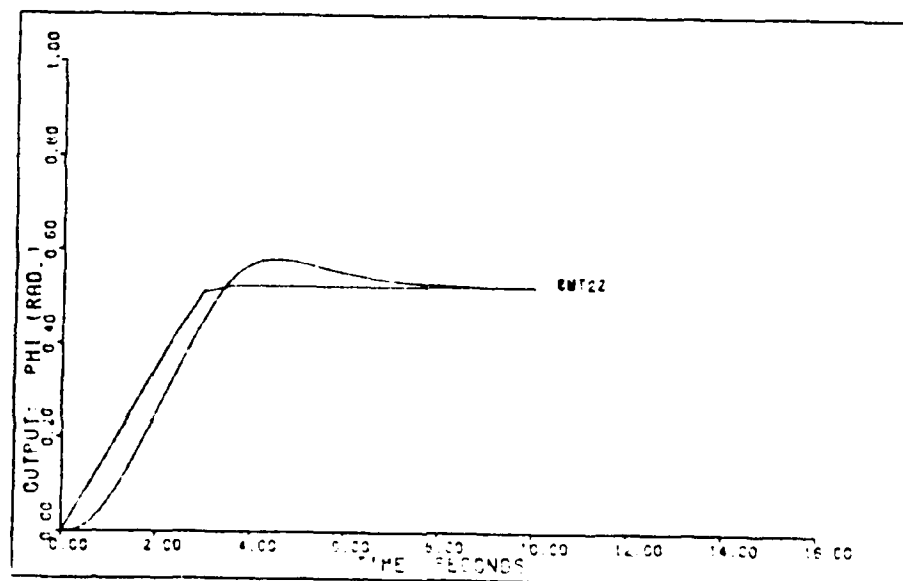


Figure 10a. Output Response,  $\phi$ , for the Coordinated Turn Command System  
( $V_{EAS} = 140$  Knots)

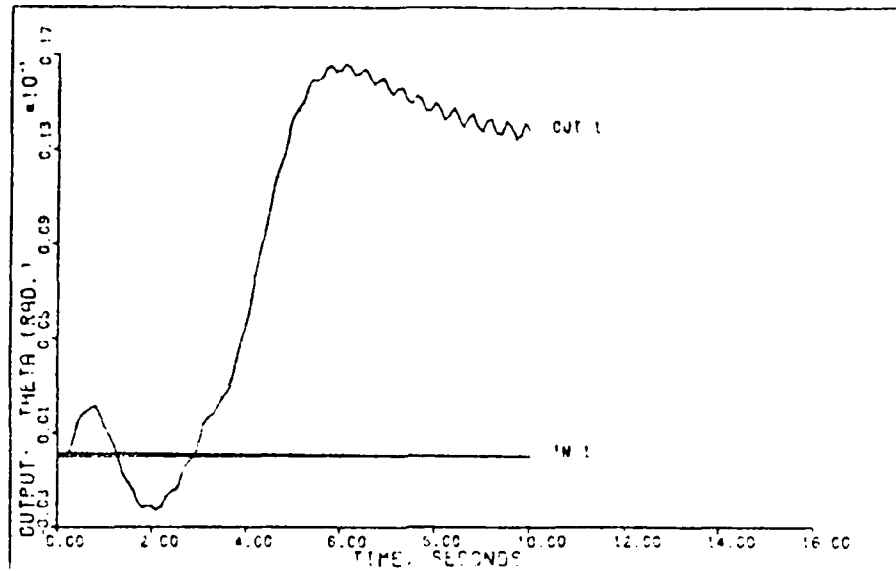


Figure 10b. Output Response,  $\Theta$ , for the Coordinated Turn Command System  
( $V_{EAS} = 140$  Knots)

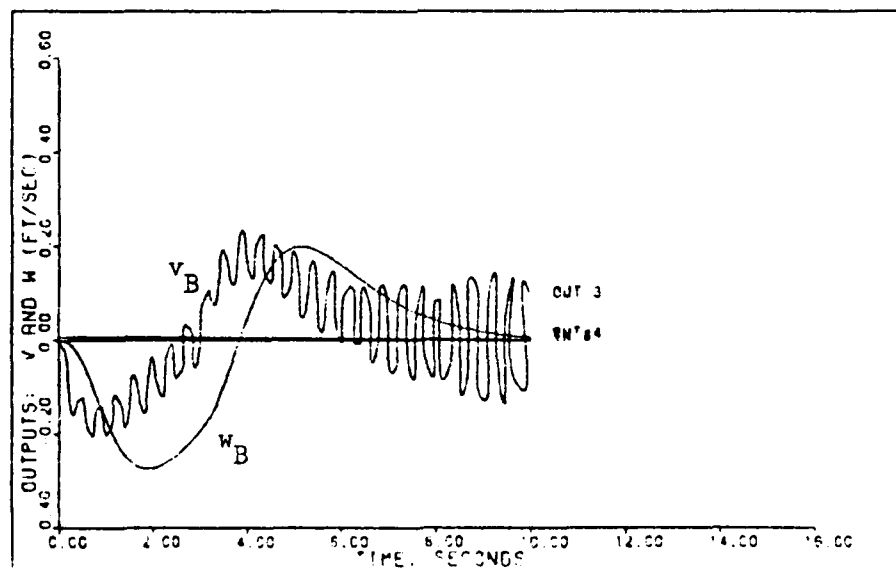


Figure 10c. Output Responses,  $v_B$  and  $w_B$ , for the Coordinated Turn Command System ( $V_{EAS} = 140$  Knots)

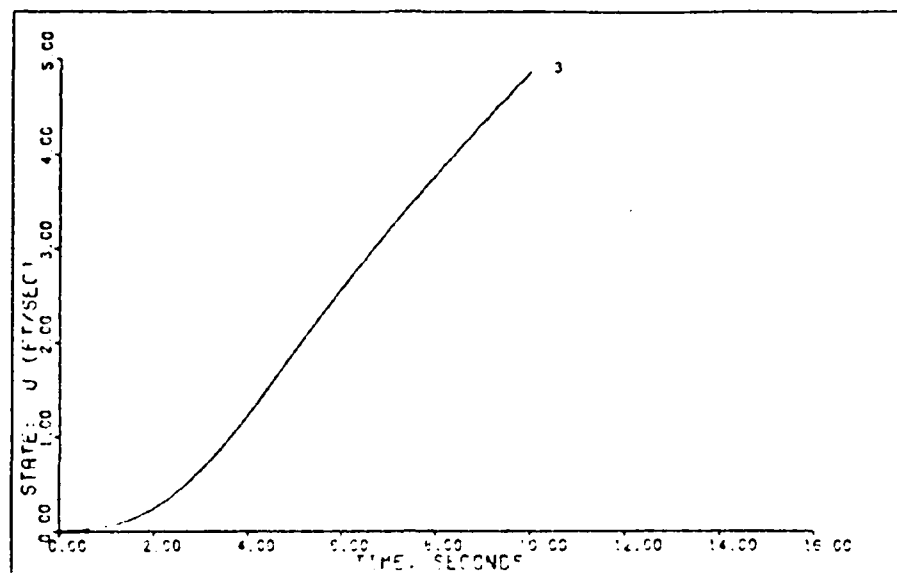


Figure 10d. State Response,  $u_B$ , for the Coordinated Turn Command System ( $V_{EAS} = 140$  Knots)

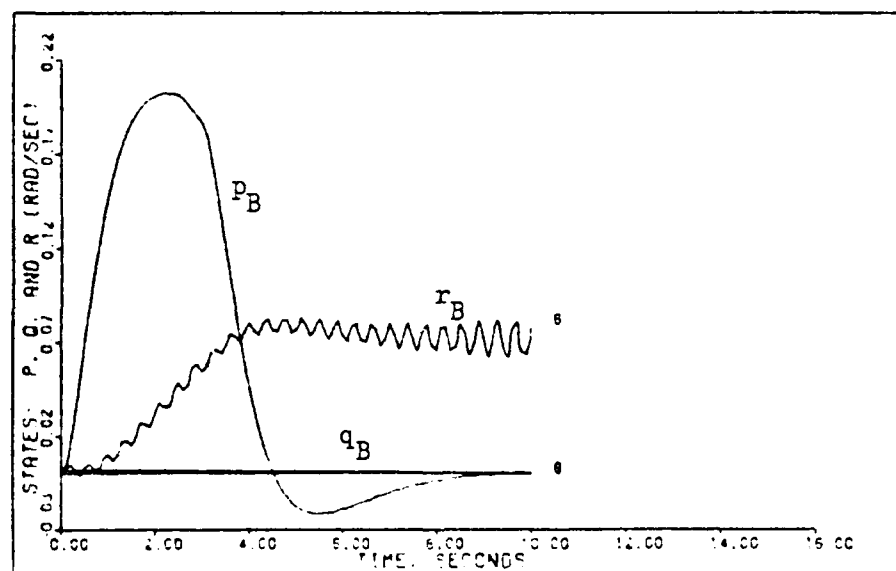


Figure 10e. State Responses,  $p_B$ ,  $q_B$ , and  $r_B$ , for the Coordinated Turn Command System ( $V_{EAS} = 140$  Knots)

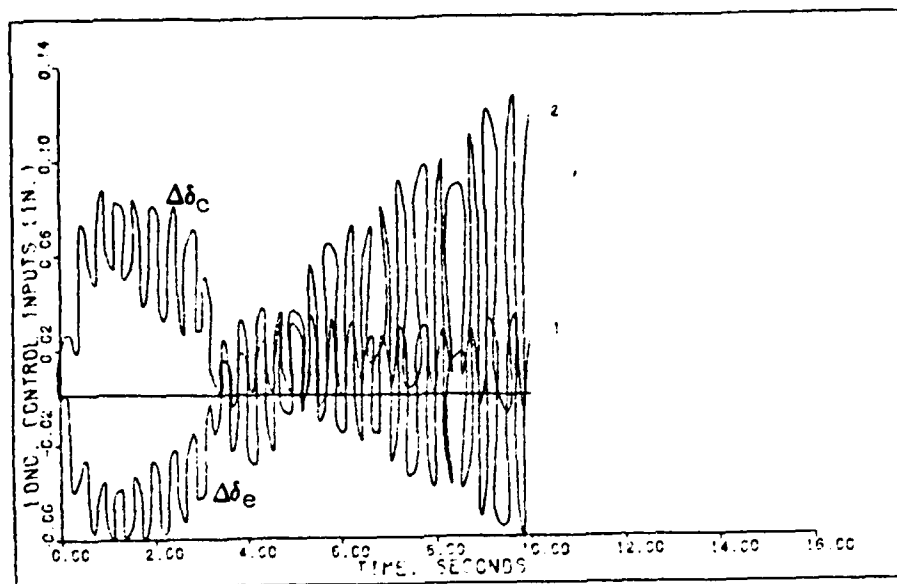


Figure 10f. Longitudinal Control Surface Responses  $\Delta\delta_e$  and  $\Delta\delta_c$ , for the Coordinated Turn Command System ( $V_{EAS} = 140$  Knots)

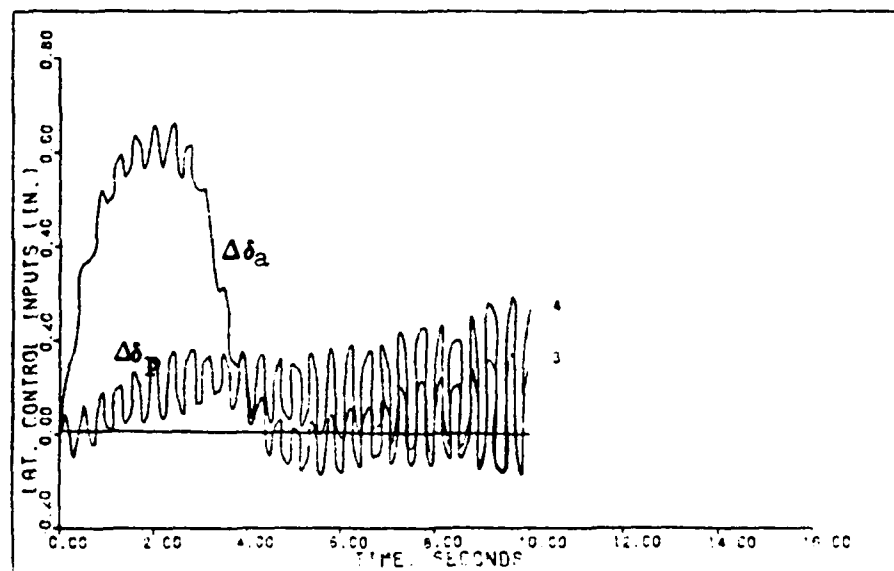


Figure 10g. Lateral Control Surface Responses,  $\Delta\delta_a$  and  $\Delta\delta_p$ , for the Coordinated Turn Command System ( $V_{EAS} = 140$  Knots)



Design Data for the Coordinated Turn Command System With Actuators

Flight Condition:  $V_{EAS} = 140$  knots

$T = 0.02$  seconds

$\alpha = 1.75$

$$\underline{\Sigma} = \begin{bmatrix} 1.0 & 0 & 0 & 0 \\ 0 & 0.2 & 0 & 0 \\ 0 & 0 & 0.2 & 0 \\ 0 & 0 & 0 & 0.2 \end{bmatrix}$$

$= 0.1$

$$\underline{M} = \begin{bmatrix} 0.25 & 0 & 0 & 0 \\ 0 & 0.25 & 0 & 0 \\ 0 & 0 & 0 & 0 \\ 0 & 0 & 0 & 0 \end{bmatrix}$$

$$\underline{K}_0 = \begin{bmatrix} 1.243 & 0.005929 & -0.00609 & -0.0001509 \\ -1.197 & 0.04457 & -0.008789 & -0.003228 \\ -0.1649 & 0.1529 & -0.01716 & 0.0002646 \\ -0.3259 & 0.0756 & -0.02501 & -0.0004396 \end{bmatrix}$$

$$\underline{K}_1 = \begin{bmatrix} 0.7103 & -0.003388 & -0.00348 & 0.00008624 \\ -0.6838 & 0.02547 & -0.005022 & -0.001845 \\ -0.09423 & 0.0874 & -0.009803 & 0.0001512 \\ -0.1862 & 0.04321 & -0.01429 & -0.0002512 \end{bmatrix}$$

Input ramp time: 3.0 seconds

Input command:  $\theta = 0.0$

$\phi = 0.5235$  rad/sec step

$v_B = 0.0$

$w_B = 0.0$

Note: Step commands are ramped to steady state over a specified time. This time is designated as the "input ramp time" given above.

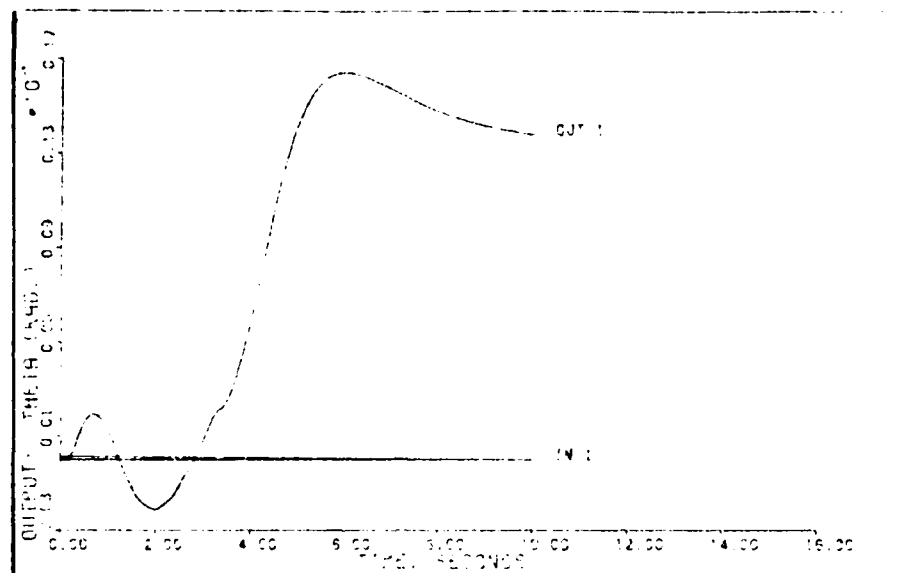


Figure 11a. Output Response,  $\Theta$ , for the Coordinated Turn Command System With Actuators ( $V_{EAS} = 140$  Knots)

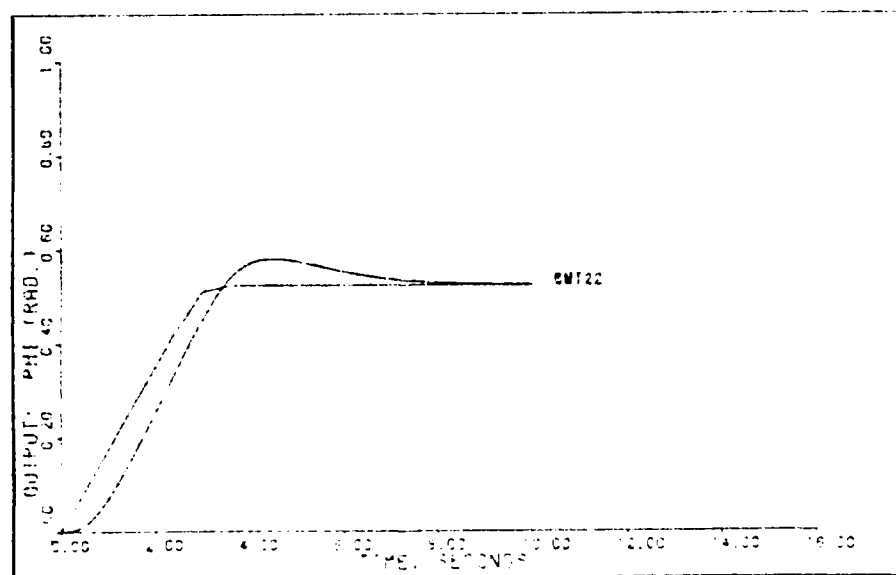


Figure 11b. Output Response,  $\phi$ , for the Coordinated Turn Command System With Actuators ( $V_{EAS} = 140$  Knots)

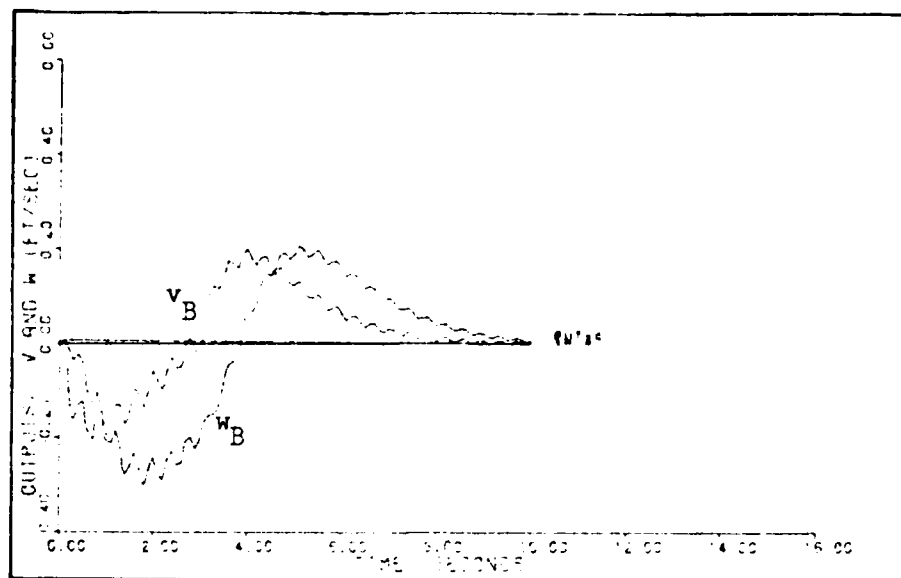


Figure 11c. Output Responses,  $v_B$  and  $w_B$ , for the Coordinated Turn Command System With Actuators ( $V_{EAS} = 140$  Knots)

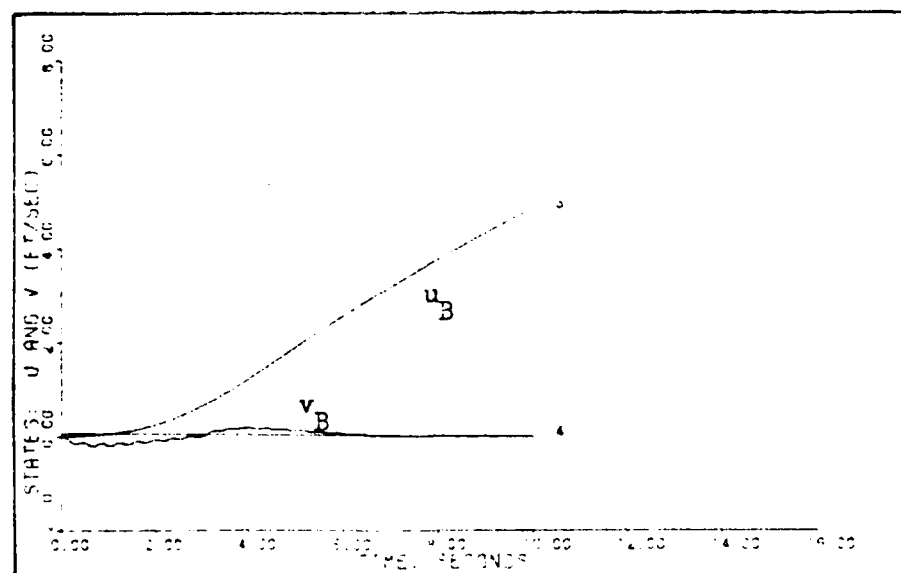


Figure 11d. State Response,  $u_B$ , and Output Response,  $v_B$ , for the Coordinated Turn Command System With Actuators ( $V_{EAS} = 140$  Knots)

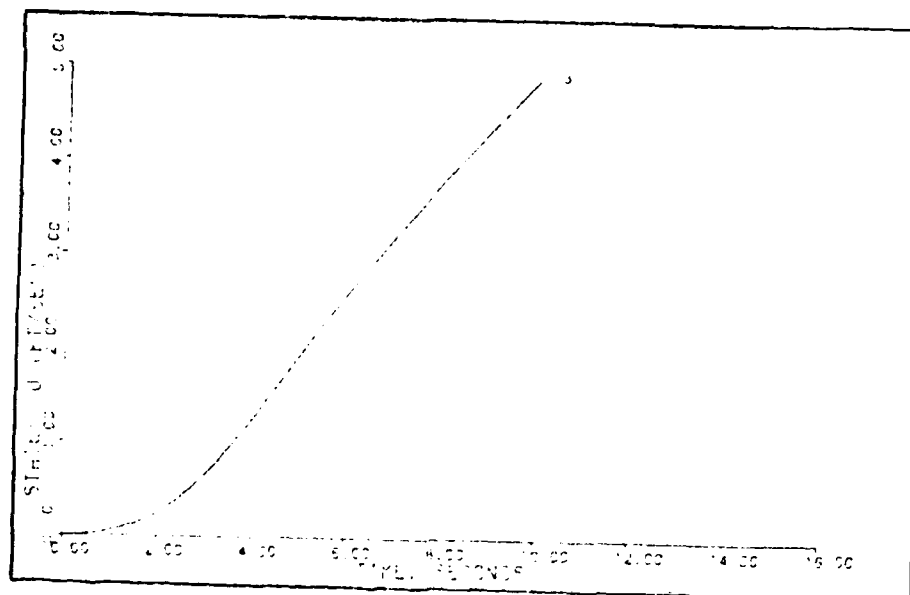


Figure 11e. State Response,  $u_B$ , for the Coordinated Turn Command System With Actuators ( $V_{EAS} = 140$  Knots)

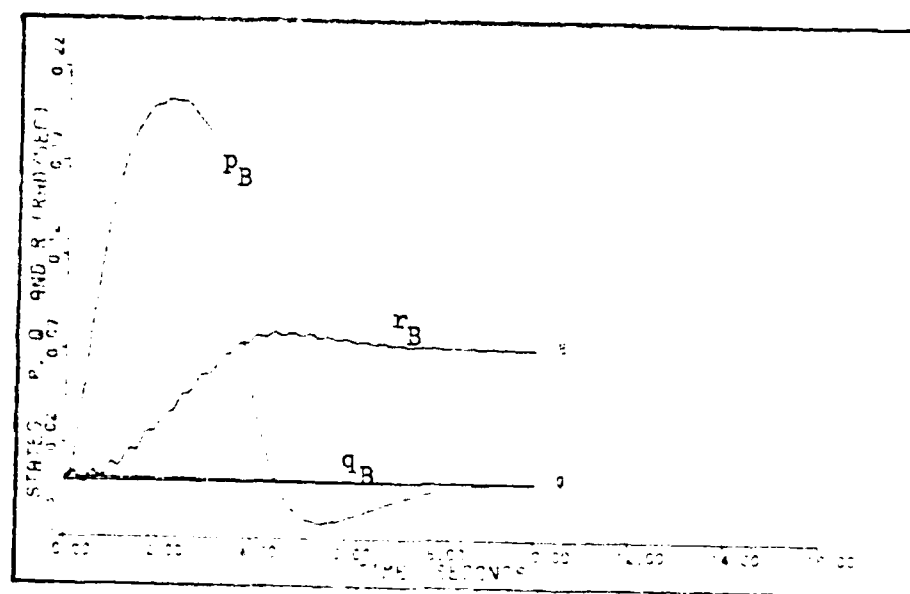


Figure 11f. State Responses,  $p_B$ ,  $q_B$ , and  $r_B$ , for the Coordinated Turn Command System With Actuators ( $V_{EAS} = 140$  Knots)

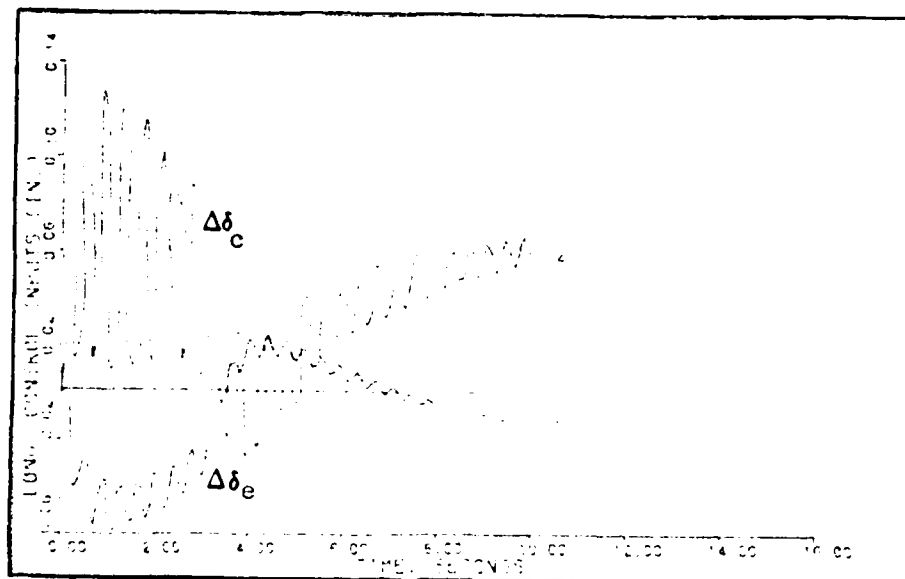


Figure 11g. Longitudinal Control Surface Responses  $\Delta\delta_e$  and  $\Delta\delta_c$ , for the Coordinated Turn Command System With Actuators ( $V_{EAS}=140$  Knots)

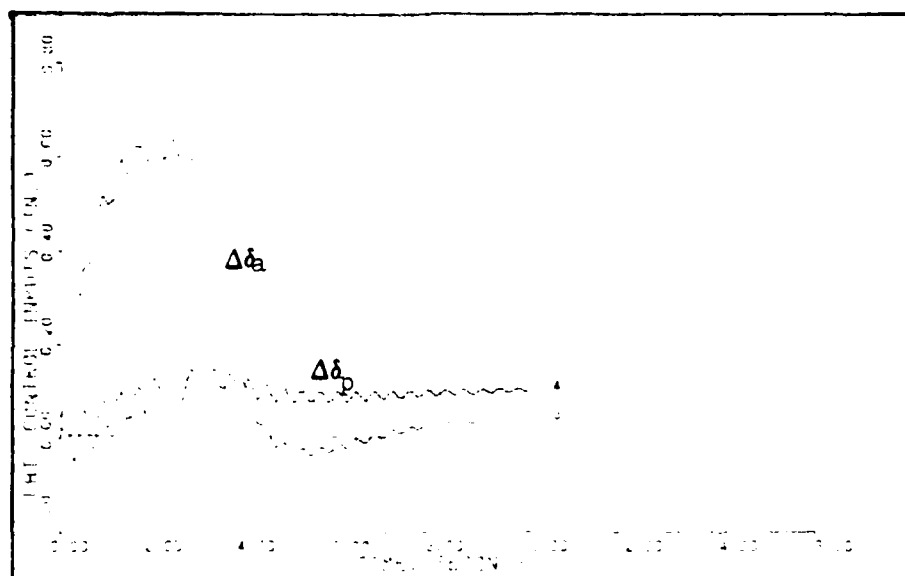


Figure 11h. Lateral Control Surface Responses,  $\Delta\delta_a$  and  $\Delta\delta_p$ , for the Coordinated Turn Command System With Actuators ( $V_{EAS} = 140$  Knots)

Table IV-9  
Coordinated Turn Results With Actuators for  $V_{EAS} = 140$  knots

Outputs	$M_p$	$t_p$	$M_m$	$t_m$	FV	$t_s$
$\theta$	0.0001639	6.1	-0.00002125	2.0	0.0001374	9.3
$\phi$	0.57918	4.5	0	0	0.523777	7.2
$v_B$	0.19958	4.0	-0.202249	0.7	0.002178	10
$w_B$	0.20630	5.1	-0.298619	1.8	0.006909	10

Examining the time response plots and the figures of merit reveals that relatively tight tracking of the desired outputs is obtained for the  $V_{EAS} = 140$  flight condition with or without actuators. Again, it should be noted that a high frequency oscillation of relatively small magnitude exists in some of the plots. An interesting point is noted when comparing the two simulations. It appears that the dynamics introduced by the actuators reduces the magnitudes of the oscillations without degradation in the output responses. An area of future research might be the effects of reducing the time constants of the actuator dynamics. It might be found that even though the oscillations still exist, they have small enough magnitudes to be ignored. A trade-off analysis must be performed between reducing the magnitudes of the oscillations and degradation of the output responses.

From Figure 10e,  $r_B$  is found approximately due to the oscillation, to be slightly less than 0.07 rad/sec which compares favorably to the expected value of 0.0680921 rad/sec found in Table IV-5. The perturbation pitch rate,  $q_B$ , is again approximately zero. The magnitude of  $u_B$  is further reduced by the smaller displacements of the perturbation yaw rate and perturbation tail rotor yaw control.

Overall, the three individual digital control laws developed for the coordinated turn command system at the  $V_{EAS} = 60, 100, \text{ and } 140$  knots

flight conditions perform relatively tight tracking of the desired outputs. Small magnitude high-frequency oscillations exist in some time responses for the  $V_{EAS} = 100$  and 140 knots flight condition. The expected value of the perturbation yaw rate,  $r_B$ , compared favorably with the results obtained for the three flight conditions. The expected value of the perturbation pitch rate,  $q_B$ , did not compare well with the values obtained. The expected value of  $q_B$  depends on the longitudinal and lateral models being coupled together which, is not the case considering the results. Finally, an increase in the x-body velocity,  $u_B$ , is experienced during the performance of a coordinated turn. The perturbation,  $u_B$ , is due to the displacements of the yaw rate and tail rotor yaw control and decreases in magnitude with increasing  $V_{EAS}$ .

#### Vertical Rate Command System

The purpose of the vertical rate command system is to perform an increase (decrease) in altitude of the helicopter without pitching the nose of the helicopter and without roll. An equivalent requirement is that the perturbation in the cyclic pitch control be zero. Without the cyclic pitch control, the maneuver reduces to a direct lift maneuver. As originally stated, the vertical rate command system commanded the perturbation z-earth axis velocity,  $\dot{h}_E = \pm 20$  ft/sec as well as the perturbation pitch angle being proportional to the perturbation flight path angle. After consultation with the sponsor, it was found that what was really desired was  $\theta = 0$ . Again, two more desired outputs are needed to complete the four element y vector. The perturbations,  $\phi$  and  $r_B$  are added to include the requirements that the helicopter not roll or yaw while performing a vertical rate command. Since the x vector

consists of body-axis states, an equation must be developed to express  $\dot{h}_E$  in body-axis states. Referring to Etkin (Ref 5), the following equation for  $\dot{h}_E$  is derived

$$\dot{h}_E = -\dot{z}_E = u_B \sin \Theta - v_B \sin \phi \cos \Theta - w_B \cos \phi \cos \Theta. \quad (4.37)$$

Since the longitudinal and lateral states are not decoupled,  $\phi$  cannot be set equal to zero. This nonlinear equation must be linearized around the equilibrium conditions  $h_{E_e}$ ,  $u_{B_e}$ ,  $v_{B_e}$ ,  $w_{B_e}$ ,  $\phi_e$  and  $\Theta_e$  to obtain the final perturbation equation for  $\dot{h}_E$  in terms of the body-axis perturbations states.

The equation  $h_E$  is linearized by using the following equations:

$$\begin{aligned} h_E &= h_{E_e} + \Delta h_E \\ \phi &= \phi_e + \phi \\ \Theta &= \Theta_e + \theta \end{aligned} \quad (4.38)$$

$$u_B = u_{B_e} + \Delta u_B$$

$$v_B = v_{B_e} + \Delta v_B$$

$$w_B = w_{B_e} + \Delta w_B$$

and perturbation approximations:

$$\begin{aligned} \cos(\theta) &\approx 1 \\ \sin(\theta) &\approx \theta \\ \Delta x \Delta y &\approx 0 \end{aligned} \quad (4.39)$$

The resulting equation after mathematical manipulations and the use of trigonometric identities is

$$\dot{h}_E = [u_{B_e} \cos \Theta_e + v_{B_e} \sin \phi_e \sin \Theta_e + w_{B_e} \cos \phi_e \sin \Theta_e] \theta$$



$$\begin{aligned}
& +[w_{B_e} \sin \phi_e \cos \theta_e - v_{B_e} \cos \phi_e \cos \theta_e] \dot{\phi} + [\sin \theta_e] u_B \\
& - [\sin \phi_e \cos \theta_e] v_B - [\cos \phi_e \cos \theta_e] w_B
\end{aligned} \tag{4.40}$$

as long as the following equilibrium condition is true

$$u_{B_e} \sin \theta_e - v_{B_e} \cos \theta_e \sin \phi_e - w_{B_e} \cos \phi_e \cos \theta_e = 0 \tag{4.41}$$

The commanded output,  $\dot{h}_E$ , depends on the body-axis states,  $\theta$ ,  $\phi$ ,  $v_B$ ,  $u_B$ ,  $w_B$ . The coefficients for  $\phi$ ,  $u_B$ , and  $v_B$  are quite small and do not have to be controlled. The coefficients for  $\theta$  and  $w_B$  are large, with the coefficient of  $\theta$  equal to the total velocity. Since  $\theta$  is already being commanded to zero, the z-earth axis velocity,  $\dot{h}_E$  essentially results from a negative perturbation of the z body-axis velocity,  $w_B$ . Since  $\dot{h}_E$  is a function of  $\theta$  and  $w_B$ , it cannot be commanded. However, there is an option in MULTI which obtains outputs as linear combinations of states. Therefore, the final output vector is

$$\underline{y} = \begin{bmatrix} \theta \\ \phi \\ w_B \\ r_B \end{bmatrix}. \tag{4.42}$$

After the design is completed, the desired output  $\dot{h}_E$  is formed by a linear combination of the states  $\theta$ ,  $\phi$ ,  $u_B$ ,  $v_B$ , and  $w_B$ . Since the states  $\phi$ ,  $u_B$  and  $v_B$  affect  $\dot{h}_E$ , they must be observed for undesired influences.

Individual digital control laws have been developed at the  $V_{EAS} = 20, 40, 60, 100$ , and 140 knots flight conditions. An interesting result occurred while the control laws were being developed. In commanding a direct lift maneuver, the lateral modes  $\phi$ ,  $r_B$  and  $v_B$  experienced large magnitudes. Since these unexpected results were undesirable, the

emphasis of the design changed to controlling the lateral modes first and performing the vertical rate response second. This new emphasis is reflected in the choice of the  $\underline{\Sigma}$  matrix. Each diagonal element of the  $\underline{\Sigma}$  matrix reflects the desire to control the corresponding output with respect to the other outputs in the  $\underline{y}$  vector. The  $\underline{\Sigma}$  matrix used in the designs for all five flight conditions is

$$\underline{\Sigma} = \begin{bmatrix} 0.25 & 0 & 0 & 0 \\ 0 & 1.0 & 0 & 0 \\ 0 & 0 & 0.25 & 0 \\ 0 & 0 & 0 & 1.0 \end{bmatrix} \quad (4.43)$$

The significance of the  $\underline{\Sigma}$  matrix elements is that the outputs  $\phi$  and  $r_B$ , are to be controlled equally but four times harder than the outputs,  $\theta$  and  $w_B$ .

The denominator of the closed-loop transfer function for the  $V_{EAS} = 20$  knots flight condition is

$$\begin{array}{ll} (.1000E+01) S^{**} 12 & (-.3652E+02) + J(.3560E+00) \\ (.9920E+02) S^{**} 11 & (-.3652E+02) + J(-.3560E+00) \\ (.3533E+04) S^{**} 10 & (-.4621E+01) + J(.3979E+01) \\ (.5772E+05) S^{**} 9 & (-.4621E+01) + J(-.3979E+01) \\ (.5183E+06) S^{**} 8 & (-.8697E+01) + J(0. ) \\ (.2775E+07) S^{**} 7 & (-.4056E+01) + J(0. ) \\ (.8867E+07) S^{**} 6 & (-.1040E+01) + J(.1317E+00) \\ (.1644E+08) S^{**} 5 & (-.1040E+01) + J(-.1317E+00) \\ (.1727E+08) S^{**} 4 & (-.1168E+01) + J(0. ) \\ (.9623E+07) S^{**} 3 & (-.8938E+00) + J(0. ) \\ (.2296E+07) S^{**} 2 & (-.1022E-01) + J(0. ) \\ (.6532E+05) S^{**} 1 & (-.2137E-01) + J(0. ) \\ (.4377E+03) S^{**} 0 & \text{DENOMINATOR GAIN} = .1000E+01 \end{array} \quad (4.44)$$

It should be noted that the closed-loop poles are all within the stable region. The figures of merit are presented in Table IV-10 and the time response plots in Figures 12a.-12e. The equation for  $\dot{h}_E$  is

$$\dot{h}_E = 33.50 + 2.223 \phi + 0.1016 u_B + 0.0233 v_B - 0.99456 w_B \quad (4.45)$$

Table IV-10  
Vertical Rate Response for  $V_{EAS} = 20$  knots

Outputs	$M_p$	$t_p$	$M_m$	$t_m$	FV	$t_s$
$\vartheta$	0.0000916	8.8	-0.000613	2.1	0.00009114	7.3
$\phi$	0	0	-0.0008251	2.2	-0.000104	9.0
$w_B$	0	0	-20.38037	2.5	-19.998275	2.1
$r_B$	0.0005902	2.0	0	0	0.0000805	9.1

Examining the time response plots and the figures of merit reveals extremely tight tracking of the desired outputs. From the time response plot of  $\dot{h}_E$ , it can be concluded that  $\dot{h}_E = -w_B$  as expected. The one problem with this flight condition is the large amount of collective lift control that is called for within a very small span of time. A large amount of collective control is required due to the low total velocity. It is possible that the rate limit of the actuator may be exceeded. A solution to the problem is to increase the ramp time or the time required for the commanded input to reach steady-state. By increasing the ramp time, the collective lift control is allowed more time to perform the maneuver. Of course, the other time responses will be likewise affected.

Design Data for the Vertical Rate Command System

Flight Condition:  $V_{EAS} = 20$  knots

$T = 0.02$  seconds

$\alpha = 1$

$$\underline{\Sigma} = \begin{bmatrix} 0.25 & 0 & 0 & 0 \\ 0 & 1.0 & 0 & 0 \\ 0 & 0 & 0.25 & 0 \\ 0 & 0 & 0 & 1.0 \end{bmatrix}$$

$\epsilon = 0.75$

$$\underline{M} = \begin{bmatrix} 0.25 & 0 & 0 & 0 \\ 0 & 0.25 & 0 & 0 \\ 0 & 0 & 0 & 0 \\ 0 & 0 & 0 & 0 \end{bmatrix}$$

$$\underline{K}_0 = \underline{K}_1 = \begin{bmatrix} 2.16 & 0.01926 & 0.002027 & -0.03545 \\ -0.2947 & -0.03894 & -0.02529 & 0.1983 \\ -0.04497 & 2.051 & 0.0009319 & 0.5429 \\ 0.06905 & -0.3382 & 0.002717 & 1.31 \end{bmatrix}$$

Input ramp time: 2.0 seconds

Input command:  $\theta = 0.0$

$\phi = 0.0$

$w_B = 20$  ft/sec step

$r_B = 0.0$

Note: Step commands are ramped to steady state over a specified time. This time is designated as the "input ramp time" given above.

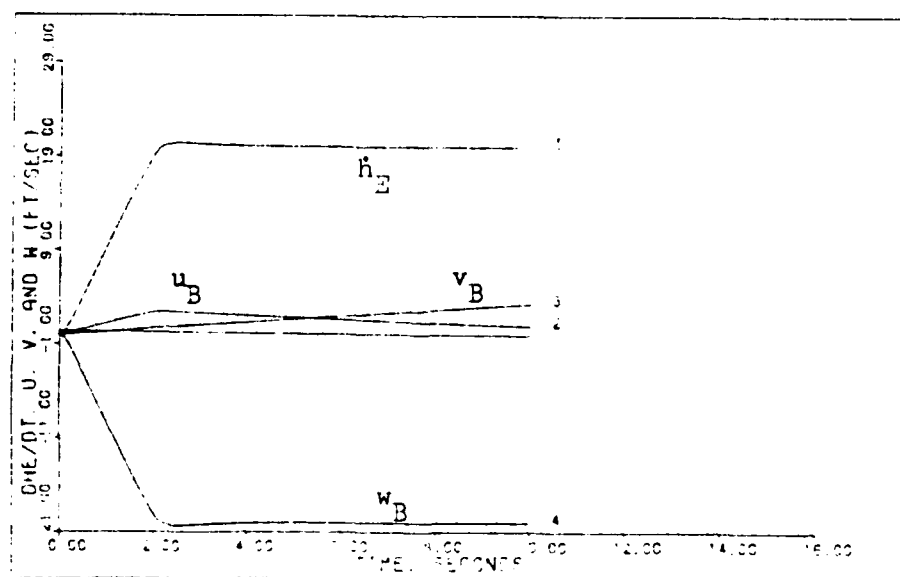


Figure 12a. Output Responses,  $\dot{h}_E$  and  $w_B$ , and State Responses,  $u_B$  and  $v_B$ , for the Vertical Rate Command System ( $V_{EAS} = 20$  Knots)

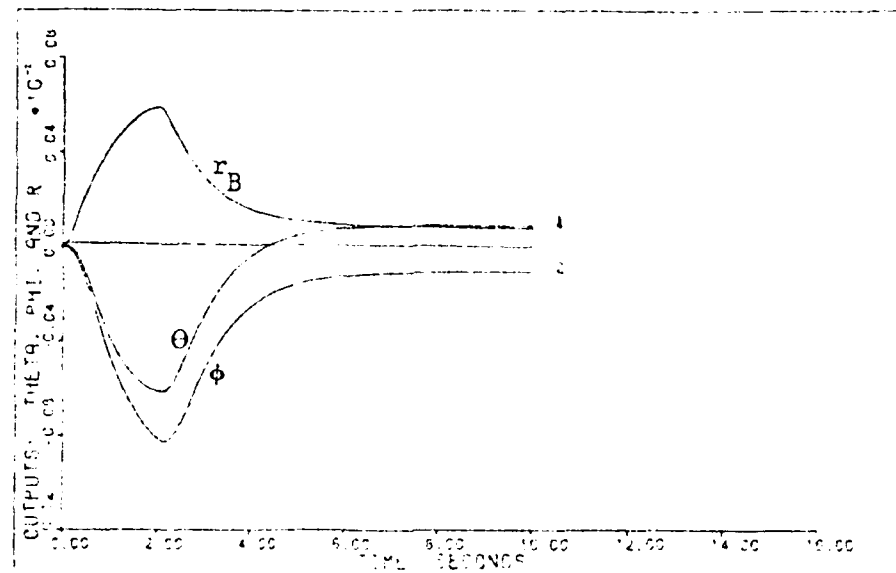


Figure 12b. Output Responses,  $\theta$  and  $\phi$ (rad) and  $r_B$ (rad/sec) for the Vertical Rate Command System ( $V_{EAS} = 20$  Knots)

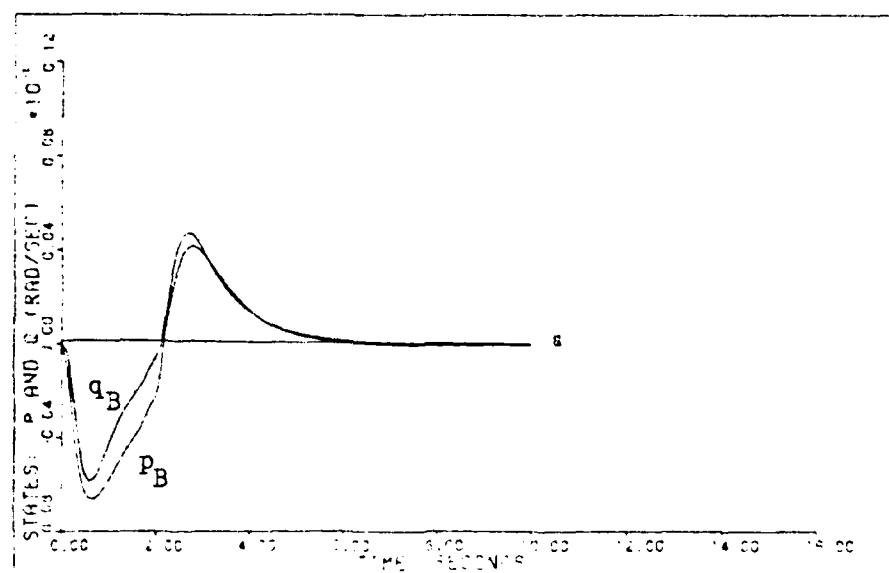


Figure 12c. State Responses,  $p_B$  and  $q_B$ , for the Vertical Rate Command System ( $V_{EAS} = 20$  Knots)

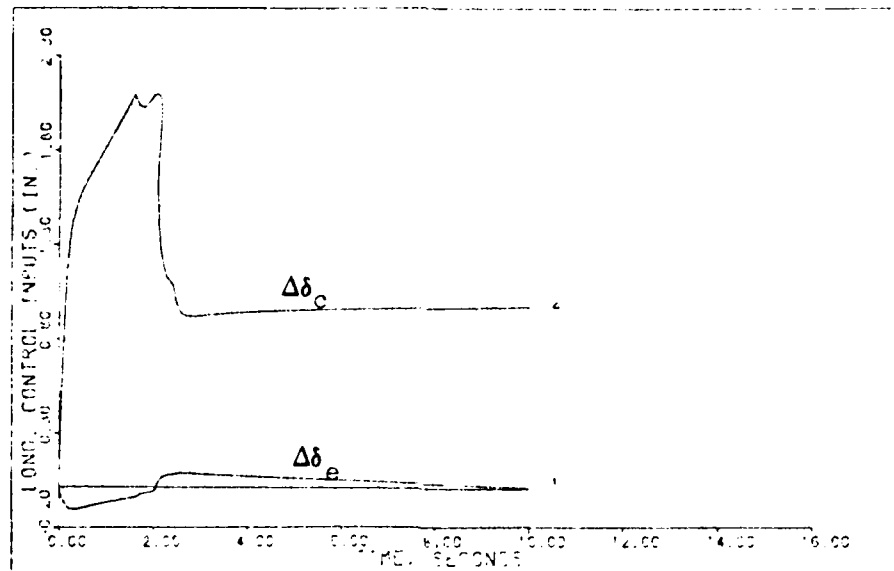


Figure 12d. Longitudinal Control Surface Responses,  $\Delta\delta_e$  and  $\Delta\delta_c$ , for the Vertical Rate Command System ( $V_{EAS} = 20$  Knots)

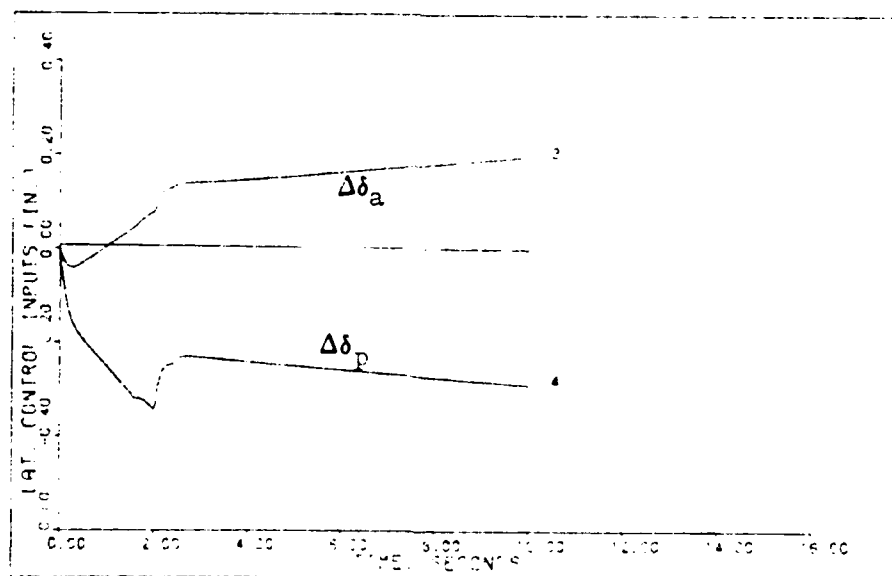


Figure 12e. Lateral Control Surface Responses,  $\Delta\delta_a$  and  $\Delta\delta_p$ , for the Vertical Rate Command System ( $V_{EAS} = 20$  Knots)

The denominator of the closed-loop transfer function for the  $V_{EAS} = 40$  knots flight condition is

(.1000E+01) S** 12	(-.3671E+02) + J( .3250E+00)	
(.9994E+02) S** 11	(-.3671E+02) + J(-.3250E+00)	
(.3589E+04) S** 10	(-.4648E+01) + J( .3886E+01)	
(.5913E+05) S** 9	(-.4648E+01) + J(-.3886E+01)	
(.5334E+06) S** 8	(-.9016E+01) + J(0. )	
(.2862E+07) S** 7	(-.4028E+01) + J(0. )	
(.9156E+07) S** 6	(-.9772E+00) + J( .6298E-01)	(4.46)
(.1702E+08) S** 5	(-.9772E+01) + J(-.6298E-01)	
(.1800E+08) S** 4	(-.1084E+01) + J( .5935E-01)	
(.1020E+08) S** 3	(-.1084E+01) + J(-.5935E-01)	
(.2562E+07) S** 2	(-.2060E-01) + J(0. )	
(.1215E+06) S** 1	(-.3593E-01) + J(0. )	
(.1501E+04) S** 0	DENOMINATOR GAIN = .1000E+01	

It should be noted that closed-loop system poles are all in the stable region. For this flight condition, the simulation is performed both with and without actuators. The figures of merit for the simulation without actuators are presented in Table IV-11 and the time response plots in Figures 13a.-13e. The figures of merit for the simulation with actuators are presented in Table IV-12 and the time response plots in Figures 14a.-14h. The equation for  $\dot{h}_E$  is

$$\dot{h}_E = 67.55 \theta + 3.468 \phi + 0.0757 u_B + 0.0176 v_B - 0.99698 w_B \quad (4.47)$$

Table IV-11  
Vertical Rate Responses for  $V_{EAS} = 40$  knots

Outputs	$M_p$	$t_p$	$M_m$	$t_m$	FV	$t_s$
$\theta$	0	0	-0.0014824	2.2	-0.000052	9.7
$\phi$	0.0014163	2.1	0	0	0.0000623	9.6
$w_B$	0	0	-20.253673	2.6	-19.99738	2.1
$r_B$	0.0009603	2.0	-0.00004467	7.9	-0.00004164	9.6



Design Data for the Vertical Rate Command System

Flight Condition:  $V_{EAS} = 40$  knots

$T = 0.02$  seconds

$\alpha = 1$

$$\underline{\Sigma} = \begin{bmatrix} 0.25 & 0 & 0 & 0 \\ 0 & 1.0 & 0 & 0 \\ 0 & 0 & 0.25 & 0 \\ 0 & 0 & 0 & 1.0 \end{bmatrix}$$

$= 0.1$

$$\underline{M} = \begin{bmatrix} 0.25 & 0 & 0 & 0 \\ 0 & 0.25 & 0 & 0 \\ 0 & 0 & 0 & 0 \\ 0 & 0 & 0 & 0 \end{bmatrix}$$

$$\underline{K}_0 = \underline{K}_1 = \begin{bmatrix} 2.118 & -0.011 & 0.004525 & 0.02132 \\ -0.5571 & -0.04146 & -0.02609 & 0.2817 \\ -0.02789 & 2.074 & 0.003968 & 0.5202 \\ 0.08264 & -0.3304 & 0.0007031 & 1.288 \end{bmatrix}$$

Input ramp time: 2.0 seconds

Input command:  $\theta = 0.0$

$\phi = 0.0$

$w_B = 20$  ft/sec step

$r_B = 0.0$

Note: Step commands are ramped to steady state over a specified time. This time is designated as the "input ramp time" given above.

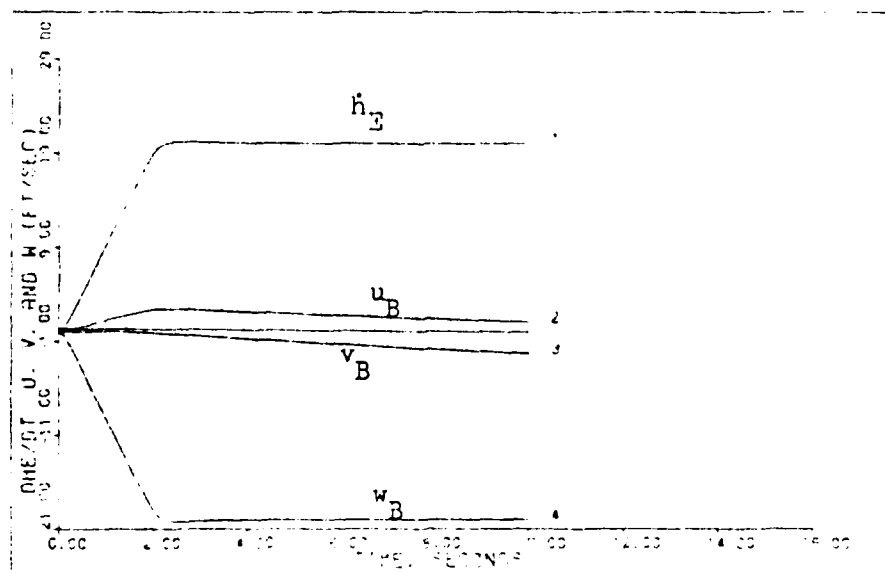


Figure 13a. Output Responses,  $\dot{h}_E$  and  $w_B$ , and State Responses,  $u_B$  and  $v_B$ , for the Vertical Rate Command System ( $V_{EAS} = 40$  Knots)

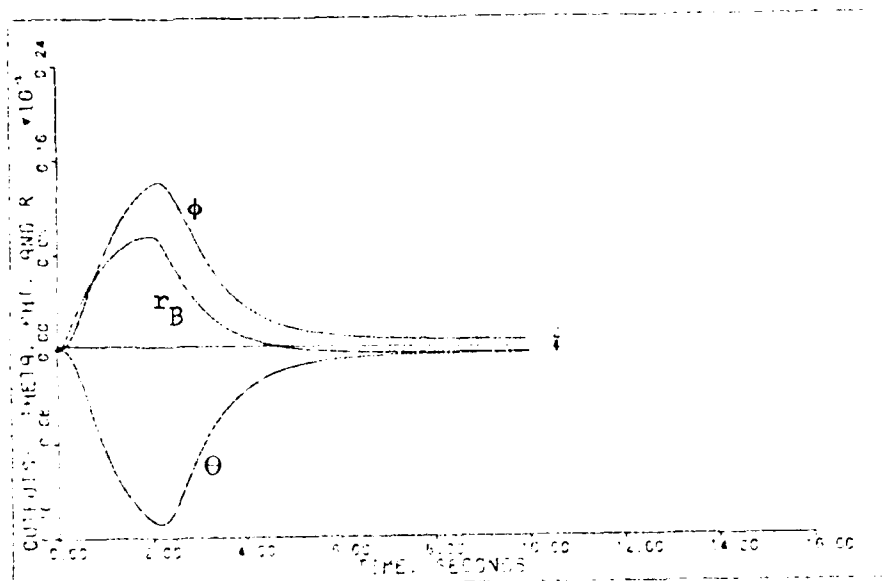


Figure 13b. Output Responses,  $\theta$  and  $\phi$ (rad) and  $r_B$ (rad/sec) for the Vertical Rate Command System ( $V_{EAS} = 40$  Knots)

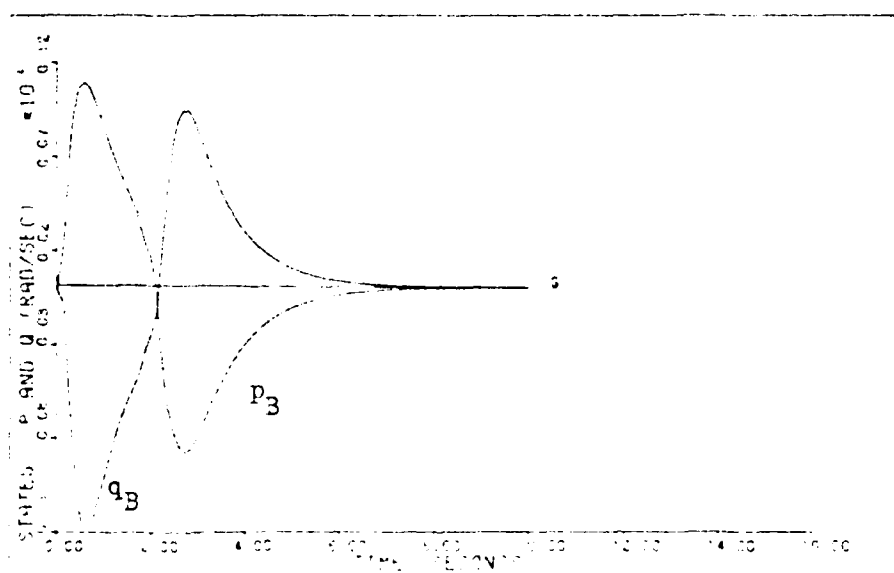


Figure 13c. State Responses,  $p_B$  and  $q_B$ , for the Vertical Rate Command System ( $V_{EAS} = 40$  Knots)

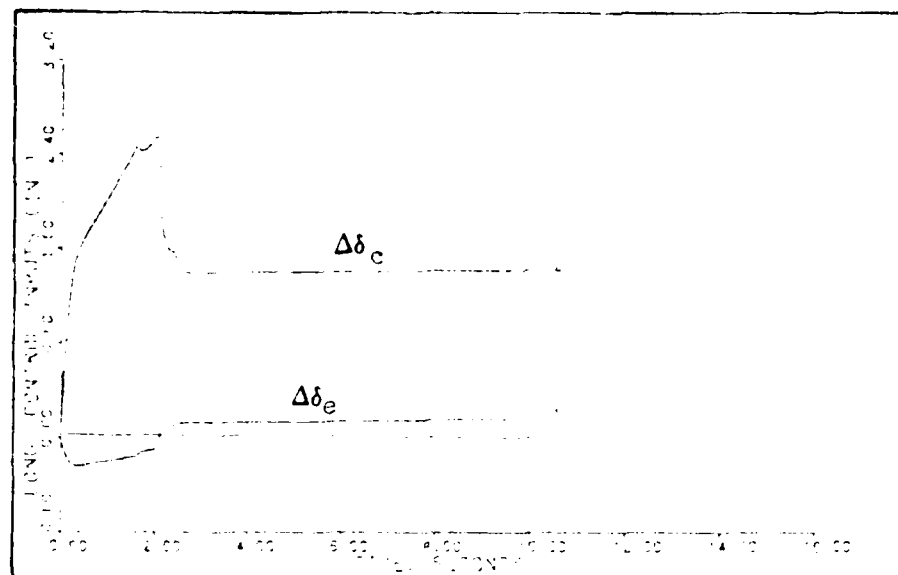


Figure 13d. Longitudinal Control Surface Responses,  $\Delta\delta_e$  and  $\Delta\delta_c$ , for the Vertical Rate Command System ( $V_{EAS} = 40$  Knots)

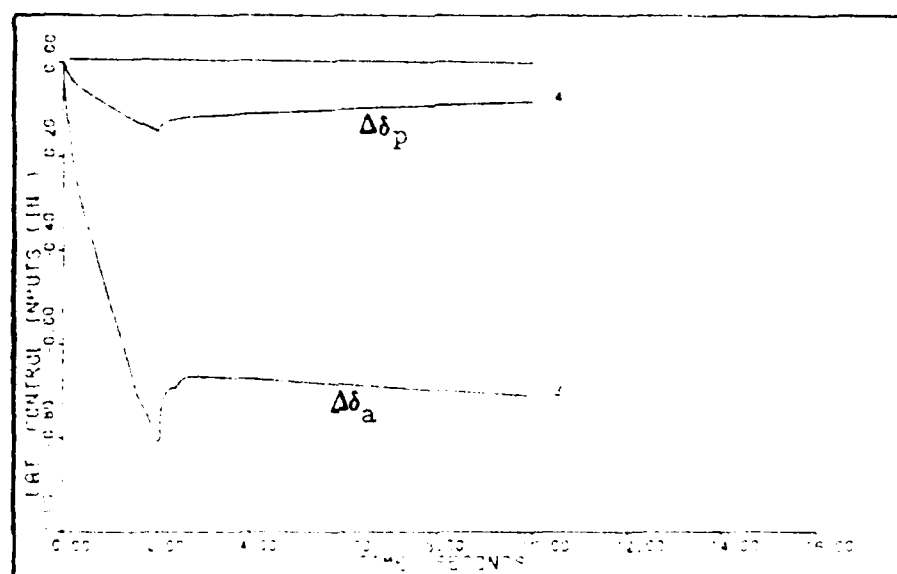


Figure 13e. Lateral Control Surface Responses,  $\Delta\delta_a$  and  $\Delta\delta_p$ , for the Vertical Rate Command System ( $V_{EAS} = 40$  Knots)

Design Data for the Vertical Rate Command System With Actuators  
Flight Condition:  $V_{EAS} = 40$  knots

$T = 0.02$  seconds

$\alpha = 1$

$$\underline{\Sigma} = \begin{bmatrix} 0.25 & 0 & 0 & 0 \\ 0 & 1.0 & 0 & 0 \\ 0 & 0 & 0.25 & 0 \\ 0 & 0 & 0 & 1.0 \end{bmatrix}$$

$= 0.1$

$$\underline{M} = \begin{bmatrix} 0.25 & 0 & 0 & 0 \\ 0 & 0.25 & 0 & 0 \\ 0 & 0 & 0 & 0 \\ 0 & 0 & 0 & 0 \end{bmatrix}$$

$$\underline{K}_0 = \underline{K}_1 = \begin{bmatrix} 2.118 & -0.011 & 0.004525 & 0.02132 \\ -0.5571 & -0.04146 & -0.02609 & 0.2817 \\ -0.02789 & 2.074 & 0.003968 & 0.5202 \\ 0.08264 & -0.3304 & 0.0007031 & 1.288 \end{bmatrix}$$

Input ramp time: 2.0 seconds

Input command:  $\theta = 0.0$

$\phi = 0.0$

$w_3 = 20$  ft/sec step

$r_3 = 0.0$

Note: Step commands are ramped to steady state over a specified time. This time is designated as the "input ramp time" given above.

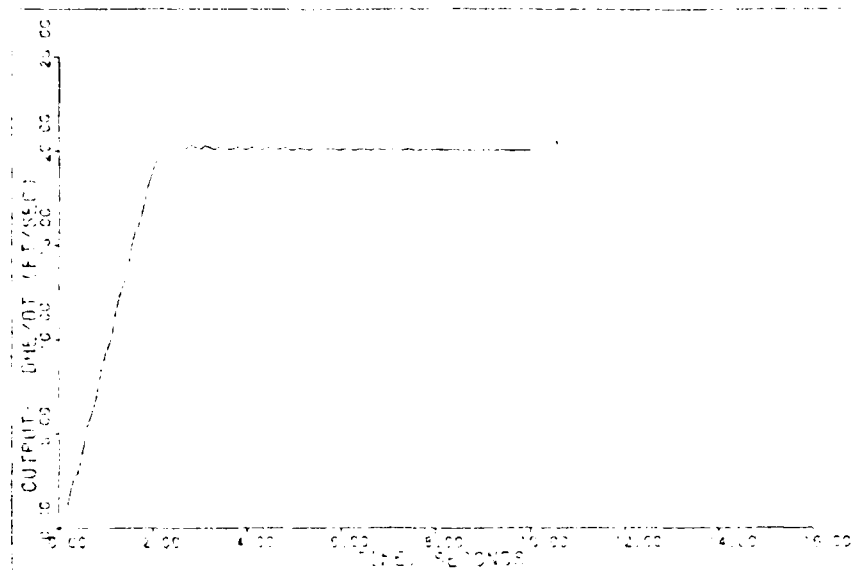


Figure 14a. Output Response,  $\dot{h}_E$ , for the Vertical Rate Command System With Actuators ( $V_{EAS} = 40$  Knots)

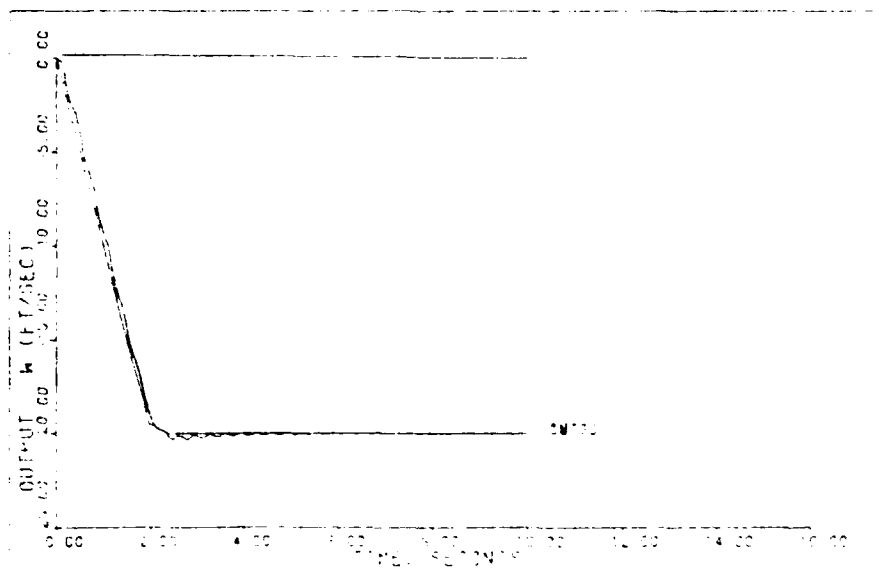


Figure 14b. Output Response,  $w_B$ , for the Vertical Rate Command System With Actuators ( $V_{EAS} = 40$  Knots)

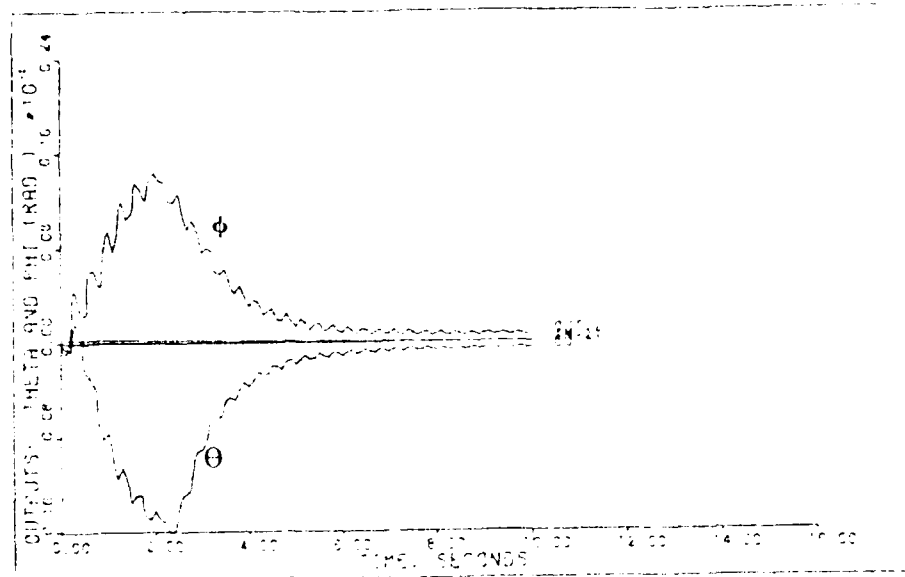


Figure 14c. Output Responses,  $\Theta$  and  $\phi$ , for the Vertical Rate Command System With Actuators ( $V_{EAS} = 40$  Knots)

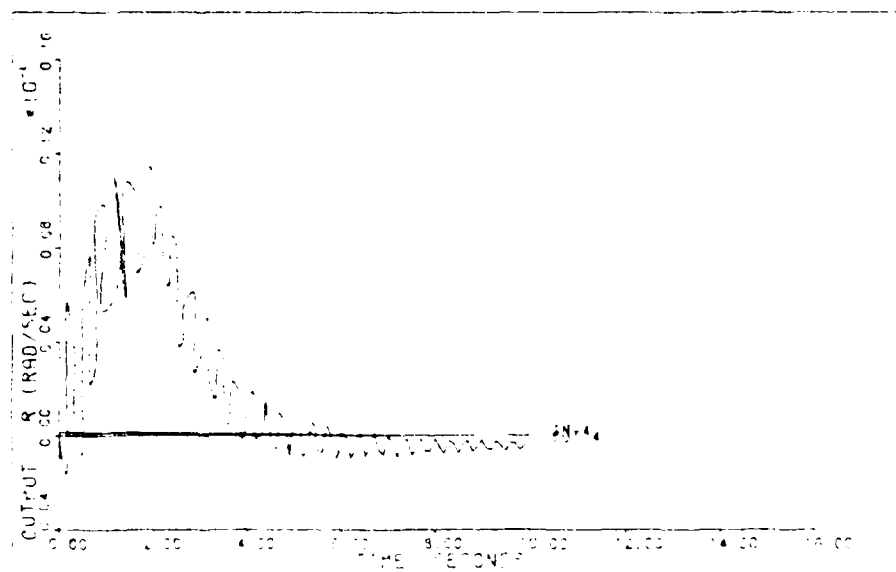


Figure 14d. Output Response,  $r_B$ , for the Vertical Rate Command System With Actuators ( $V_{EAS} = 40$  Knots)

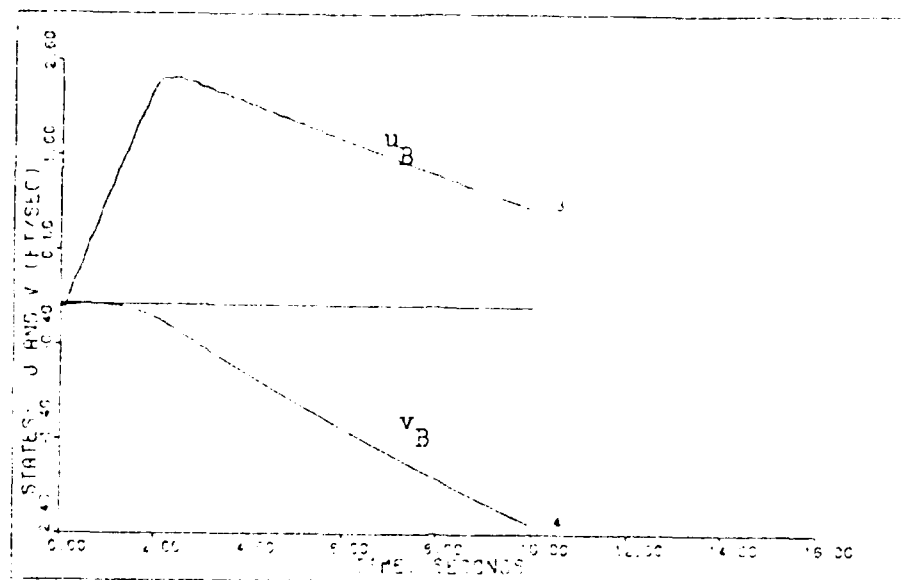


Figure 14e. State Responses,  $u_B$  and  $v_B$  for the Vertical Rate Command System With Actuators ( $V_{EAS} = 40$  Knots)

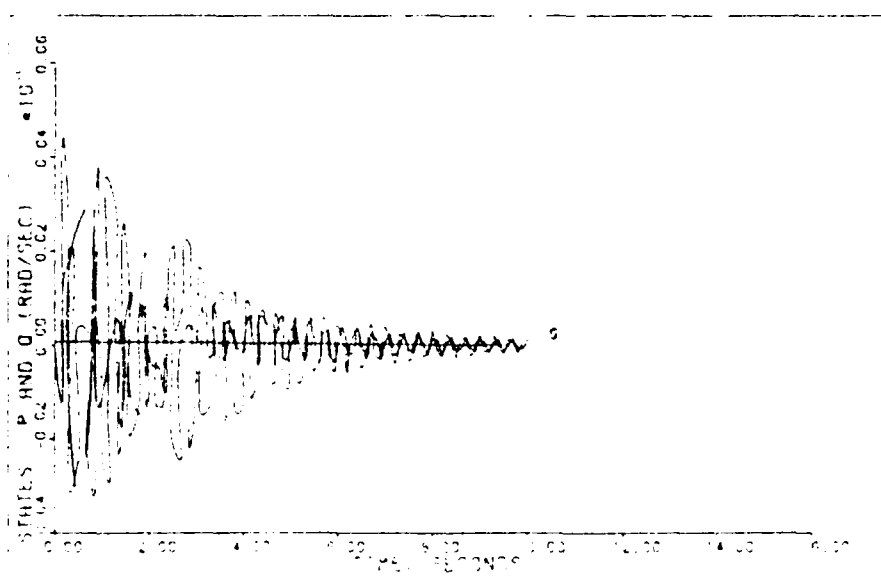


Figure 14f. State Responses,  $p_B$  and  $q_B$ , for the Vertical Rate Command System With Actuators ( $V_{EAS} = 40$  Knots)



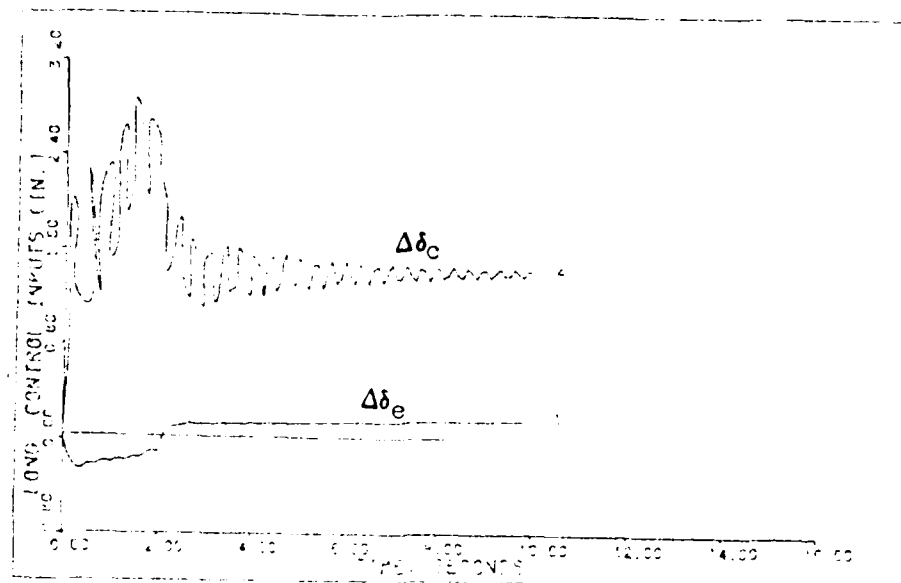


Figure 14g. Longitudinal Control Surface Responses,  $\Delta\delta_e$  and  $\Delta\delta_c$ , for the Vertical Rate Command System With Actuators ( $V_{EAS} = 40$  Knots)

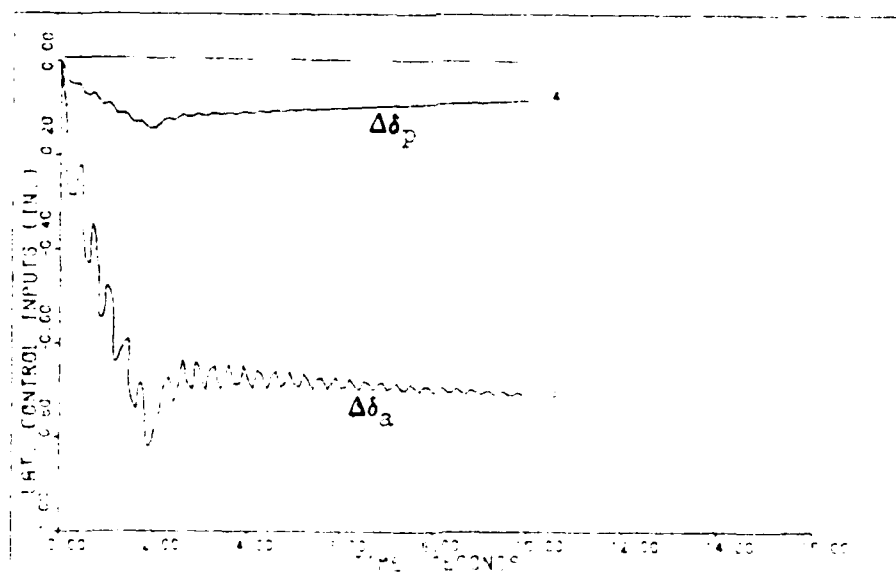


Figure 14h. Lateral Control Surface Responses,  $\Delta\delta_a$  and  $\Delta\delta_p$ , for the Vertical Rate Command System With Actuators ( $V_{EAS} = 40$  Knots)

Table IV-12  
Vertical Rate Responses With Actuators for  $V_{EAS} = 40$  knots

Outputs	$M_p$	$t_p$	$M_m$	$t_m$	FV	$t_s$
$\theta$	0.0001672	0.3	-0.0016025	2.4	-0.0000533	10
$\phi$	0.0014575	2.0	-0.0000897	0.1	0.0000674	10
$w_B$	0	0	-20.32646	2.8	-20.00837	2.2
$r_B$	0.0011397	1.9	-0.0001413	0.1	-0.0000252	10

Examining the time response plots and the figures of merit reveals extremely tight tracking of the desired outputs. From the time response plots of  $\dot{h}_E$ , it can be concluded that  $\dot{h}_E = -w_B$  as expected. The problem of a large amount of collective lift control in a short time is still evident. Again, the problem can be eliminated by increasing the ramp time. The interesting result that should be noted is the high frequency oscillations present in the simulation with actuators.

The denominator of the closed-loop transfer function for the  $V_{EAS} = 60$  knots flight condition is

$$\begin{aligned}
 & (.1000E+01) S^{**} 12 & (-.3683E+02) + J(.2783E+00) \\
 & (.1005E+03) S^{**} 11 & (-.3683E+02) + J(-.2783E+00) \\
 & (.3630E+04) S^{**} 10 & (-.4648E+01) + J(.3810E+01) \\
 & (.6017E+05) S^{**} 9 & (-.4648E+01) + J(-.3810E+01) \\
 & (.5446E+06) S^{**} 8 & (-.9338E+01) + J(0. \quad) \\
 & (.2925E+07) S^{**} 7 & (-.3983E+01) + J(0. \quad) \\
 & (.9361E+07) S^{**} 6 & (-.9357E+00) + J(.1143E+00) \quad (4.48) \\
 & (.1742E+08) S^{**} 5 & (-.9357E+00) + J(-.1143E+00) \\
 & (.1848E+08) S^{**} 4 & (-.1129E+01) + J(.9667E-01) \\
 & (.1053E+08) S^{**} 3 & (-.1129E+01) + J(-.9667E-01) \\
 & (.2678E+07) S^{**} 2 & (-.1545E-01) + J(0. \quad) \\
 & (.1498E+04) S^{**} 1 & (-.4663E-01) + J(0. \quad) \\
 & (.1498E+04) S^{**} 0 & \text{Denominator gain} = .1000E+01
 \end{aligned}$$

It should be noted that the closed-loop poles are all within the stable region. The figures of merit are presented in Table IV-13 and the time response plots are in Figures 15a.-15h. The equation for  $\dot{h}_E =$

$$\dot{h}_E = 101.33 \theta + 0.06087 u_B - 0.99815 w_B \quad (4.49)$$

Design Data for the Vertical Rate Command System

Flight Condition:  $V_{EAS} = 60$  knots

$T = 0.02$  seconds

$\alpha = 1.0$

$$\underline{\Sigma} = \begin{bmatrix} 0.25 & 0 & 0 & 0 \\ 0 & 1.0 & 0 & 0 \\ 0 & 0 & 0.25 & 0 \\ 0 & 0 & 0 & 1 \end{bmatrix}$$

$\varepsilon = 0.1$

$$\underline{M} = \begin{bmatrix} 0.25 & 0 & 0 & 0 \\ 0 & 0.25 & 0 & 0 \\ 0 & 0 & 0 & 0 \\ 0 & 0 & 0 & 0 \end{bmatrix}$$

$$\underline{K}_0 = \underline{K}_1 = \begin{bmatrix} 2.057 & -0.05925 & 0.005414 & 0.01062 \\ -0.7985 & 0.03663 & -0.02501 & 0.3364 \\ -0.03361 & 2.081 & 0.002331 & 0.5372 \\ 0.04011 & -0.2815 & -0.001589 & 1.111 \end{bmatrix}$$

Input ramp time: 2.0 seconds

Input command:  $\theta = 0.0$

$\phi = 0.0$

$w_3 = 20$  ft/sec step

$r_3 = 0.0$

Note: Step commands are ramped to steady state over a specified time. This time is designated as the "input ramp time" given above.

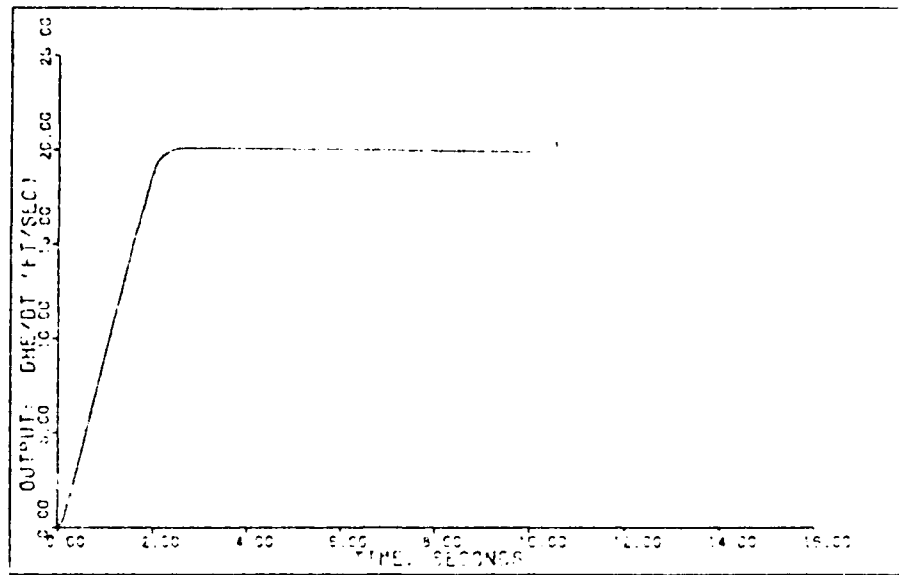


Figure 15a. Output Response,  $\dot{h}_E$ , for the Vertical Rate Command System  
( $V_{EAS} = 60$  Knots)

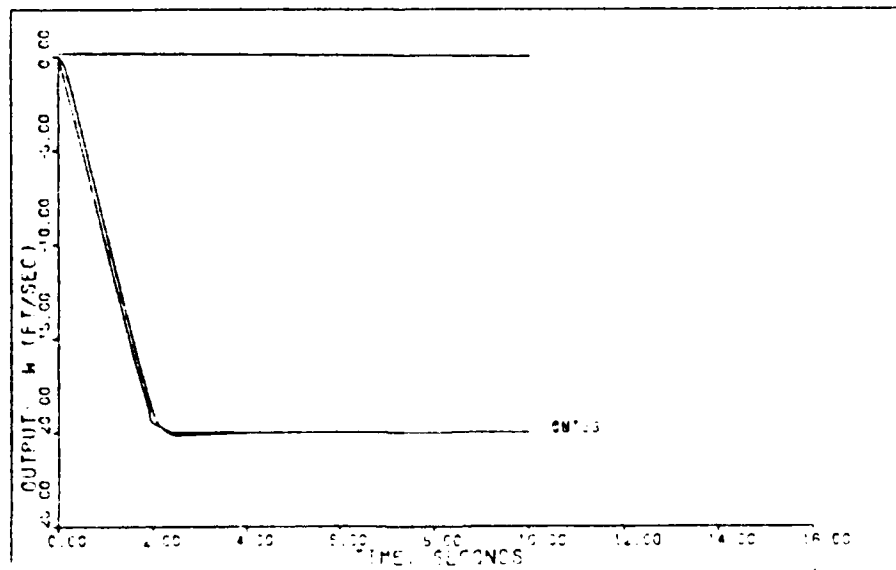


Figure 15b. Output Response,  $w_B$ , for the Vertical Rate Command System  
( $V_{EAS} = 60$  Knots)

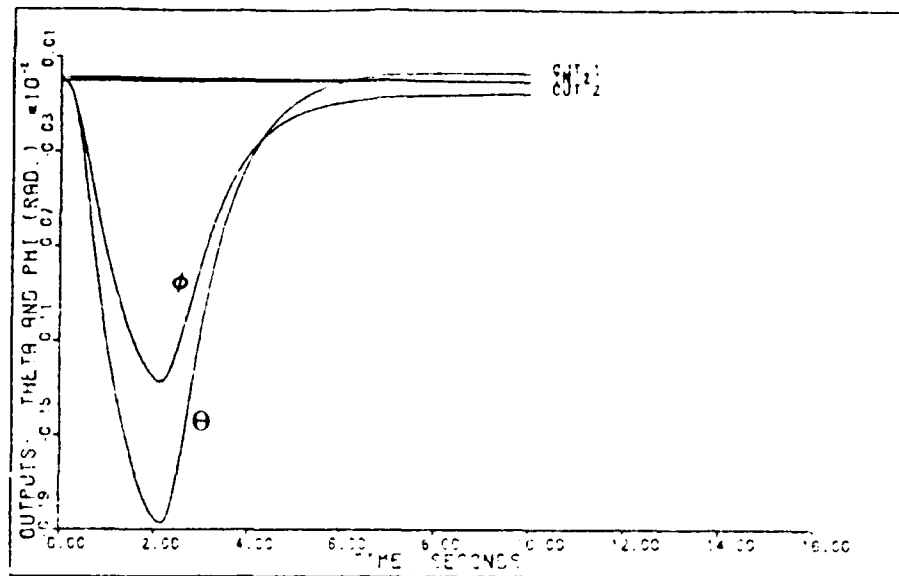


Figure 15c. Output Responses,  $\Theta$  and  $\phi$ , for the Vertical Rate Command System ( $V_{EAS} = 60$  Knots)

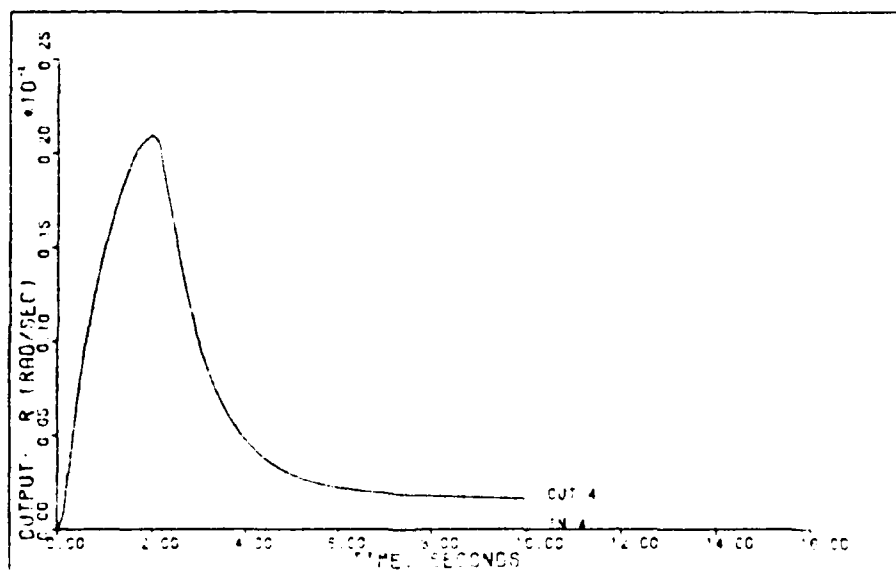


Figure 15d. Output Response,  $r_B$ , for the Vertical Rate Command System ( $V_{EAS} = 60$  Knots)

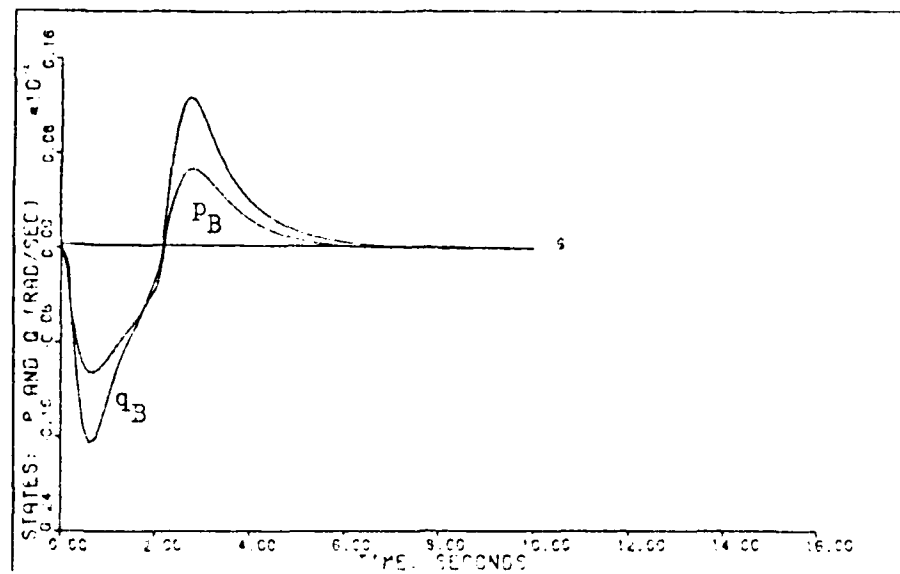


Figure 15e. State Responses,  $p_B$  and  $q_B$ , for the Vertical Rate Command System ( $V_{EAS} = 60$  Knots)

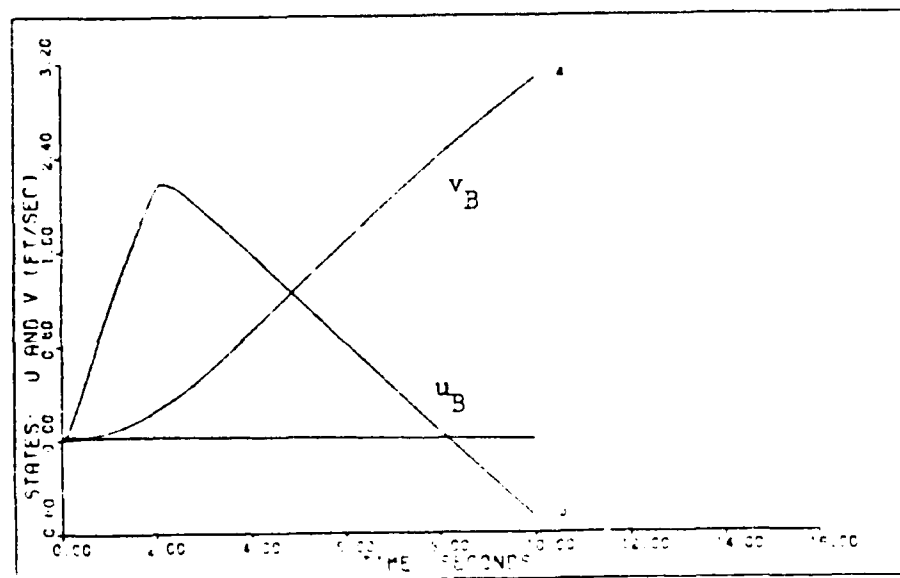


Figure 15f. State Responses,  $u_B$  and  $v_B$  for the Vertical Rate Command System ( $V_{EAS} = 60$  Knots)

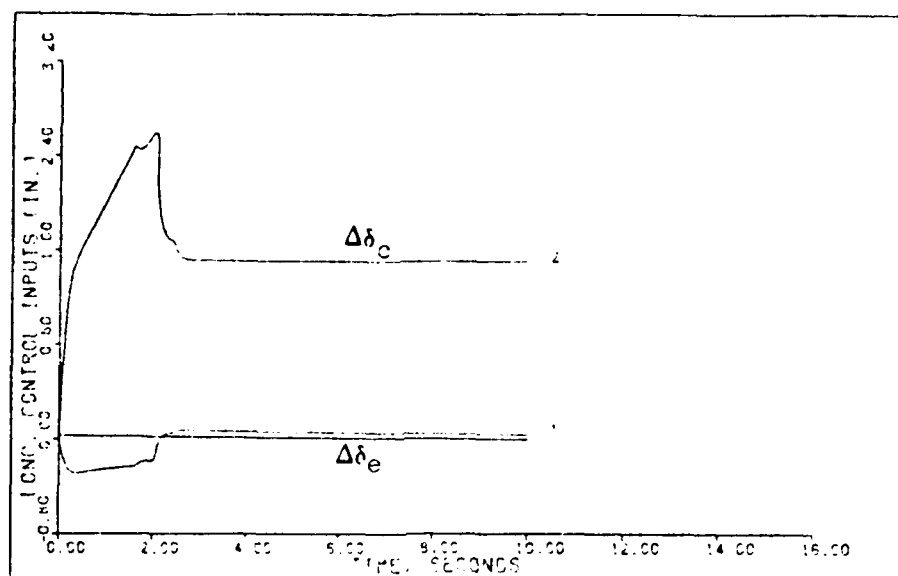


Figure 15g. Longitudinal Control Surface Responses,  $\Delta\delta_e$  and  $\Delta\delta_c$ , for the Vertical Rate Command System ( $V_{EAS} = 60$  Knots)

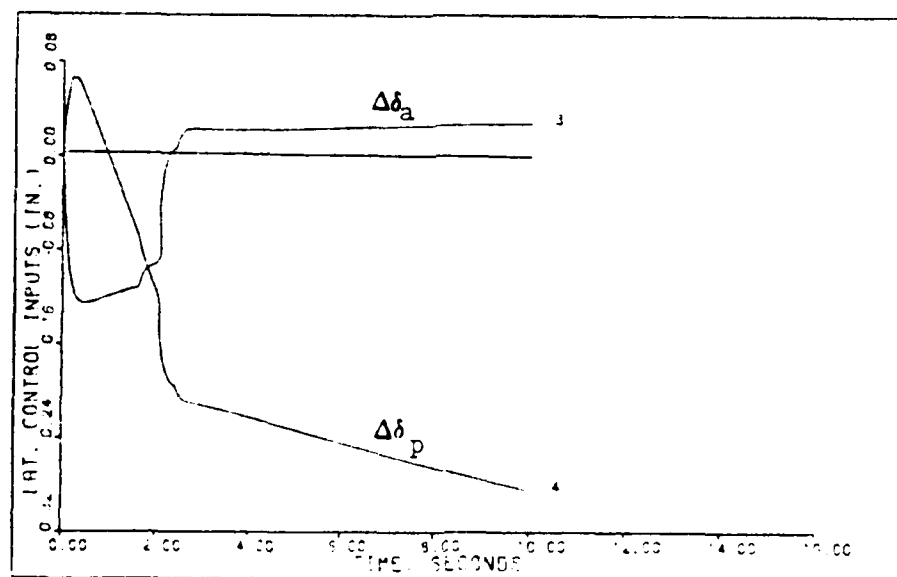


Figure 15h. Lateral Control Surface Responses,  $\Delta\delta_a$  and  $\Delta\delta_p$ , for the Vertical Rate Command System ( $V_{EAS} = 60$  Knots)

Table IV-13  
Vertical Rate Responses for the  $V_{EAS} = 60$  knots

Outputs	$M_p$	$t_p$	$M_m$	$t_m$	FV	$t_s$
$\theta$	0.0000345	8.9	-0.0018708	2.1	0.0000336	9.5
$\phi$	0	0	-0.0012733	2.1	-0.0000519	9.8
$w_B$	0	0	-20.173547	2.6	-19.999012	2.2
$r_B$	0.0020950	2.0	0	0	0.0001621	9.6

Examination of the figure of merits and the time response plots reveals tight tracking of the desired outputs. Figure 15g. shows that there still might be a problem with the control surface rate limit for  $\Delta\delta_c$ . Effects from the lateral modes are present but minimal.

The denominator of the closed-loop transfer function for the  $V_{EAS} = 100$  knots flight condition is

$$\begin{aligned}
 & (.1000E+01) S^{**} 12 & (-.3702E+02) + J(0. & ) \\
 & (.1012E+03) S^{**} 11 & (-.3675E+02) + J(0. & ) \\
 & (.3690E+04) S^{**} 10 & (-.4616E+01) + J(-.3579E+01) \\
 & (.6190E+05) S^{**} 9 & (-.4716E+01) + J(.3579E+01) \\
 & (.5645E+06) S^{**} 8 & (-.9710E+01) + J(0. & ) \\
 & (.3043E+07) S^{**} 7 & (-.3993E+01) + J(0. & ) \\
 & (.9776E+07) S^{**} 6 & (-.9952E+00) + J(.8466E-01) & (4.50) \\
 & (.1836E+08) S^{**} 5 & (-.9952E+00) + J(-.8466E-01) \\
 & (.1981E+08) S^{**} 4 & (-.1082E+01) + J(.3475E-01) \\
 & (.1166E+08) S^{**} 3 & (-.1082E+01) + J(-.3475E-01) \\
 & (.3206E+07) S^{**} 2 & (-.2005E-01) + J(0. & ) \\
 & (.2408E+06) S^{**} 1 & (-.8375E-01) + J(0. & ) \\
 & (.3629E+04) S^{**} 0 & \text{Denominator gain} = .1000E+01
 \end{aligned}$$

It should be noted that the closed-loop poles are all within the stable region. The figures of merit are presented in Table IV-14 and the time response plots are in Figures 16a.-16h. The equation for  $\dot{h}_E$  is

$$\dot{h}_E = 168.89 \theta + 0.0431 u_B - 0.9991 w_B \quad (4.51)$$



Design Data for the Vertical Rate Command System

Flight Condition:  $V_{EAS} = 100$  knots

$T = 0.02$  seconds

$\alpha = 1.0$

$$\underline{Z} = \begin{bmatrix} 0.25 & 0 & 0 & 0 \\ 0 & 1.0 & 0 & 0 \\ 0 & 0 & 0.25 & 0 \\ 0 & 0 & 0 & 1 \end{bmatrix}$$

$= 0.1$

$$\underline{M} = \begin{bmatrix} 0.25 & 0 & 0 & 0 \\ 0 & 0.25 & 0 & 0 \\ 0 & 0 & 0 & 0 \\ 0 & 0 & 0 & 0 \end{bmatrix}$$

$$\underline{K}_0 = \underline{K}_1 = \begin{bmatrix} 1.875 & -0.1958 & 0.004245 & 0.03670 \\ -1.218 & 0.1581 & -0.02326 & 0.3921 \\ -0.02189 & 2.085 & 0.001573 & 0.5424 \\ -0.05239 & -0.2135 & -0.002823 & 0.9239 \end{bmatrix}$$

Input ramp time: 2.0 seconds

Input command:  $\theta = 0.0$

$\phi = 0.0$

$w_B = 20$  ft/sec step

$r_B = 0.0$

Note: Step commands are ramped to steady state over a specified time. This time is designated as the "input ramp time" given above.

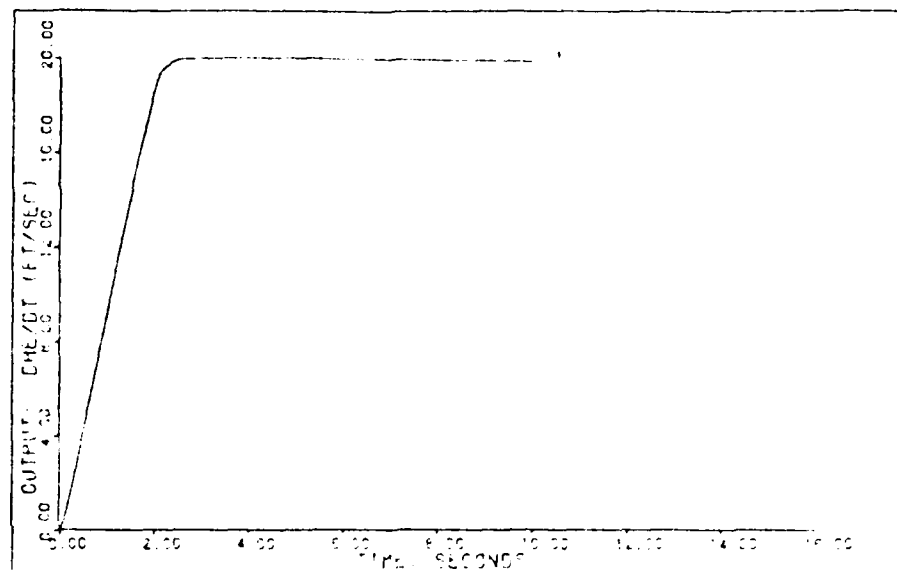


Figure 16a. Output Response,  $h_E$ , for the Vertical Rate Command System  
( $V_{EAS} = 100$  Knots)

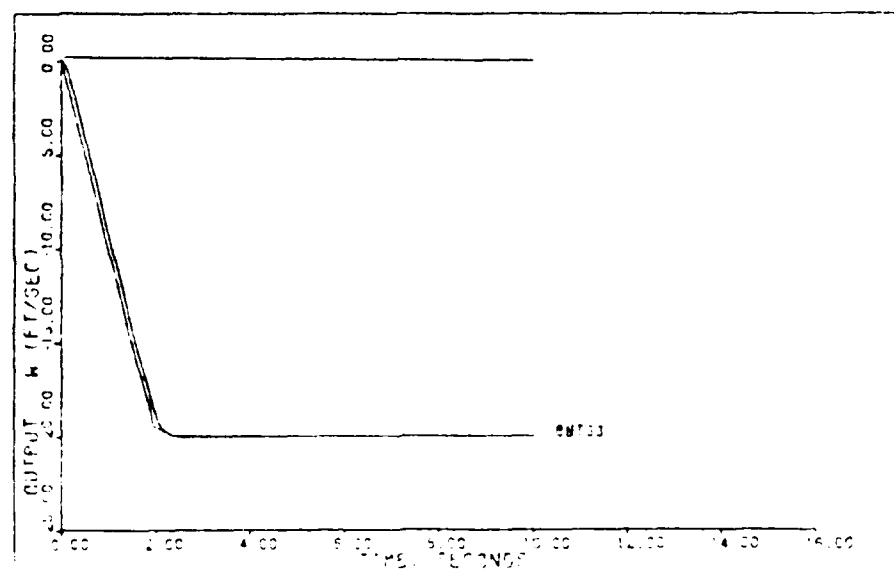


Figure 16b. Output Response,  $w_B$ , for the Vertical Rate Command System  
( $V_{EAS} = 100$  Knots)

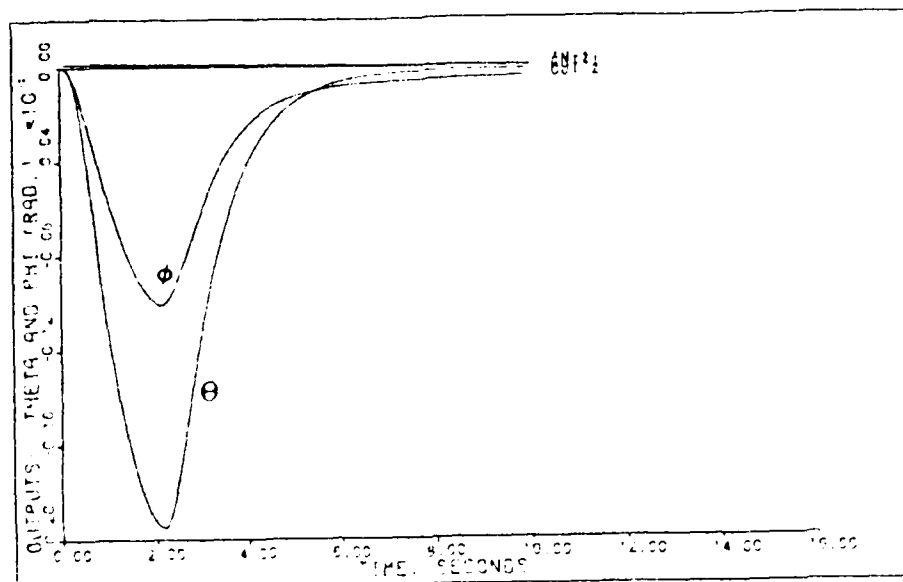


Figure 16c. Output Responses,  $\Theta$  and  $\phi$ , for the Vertical Rate Command System ( $V_{EAS} = 100$  Knots)

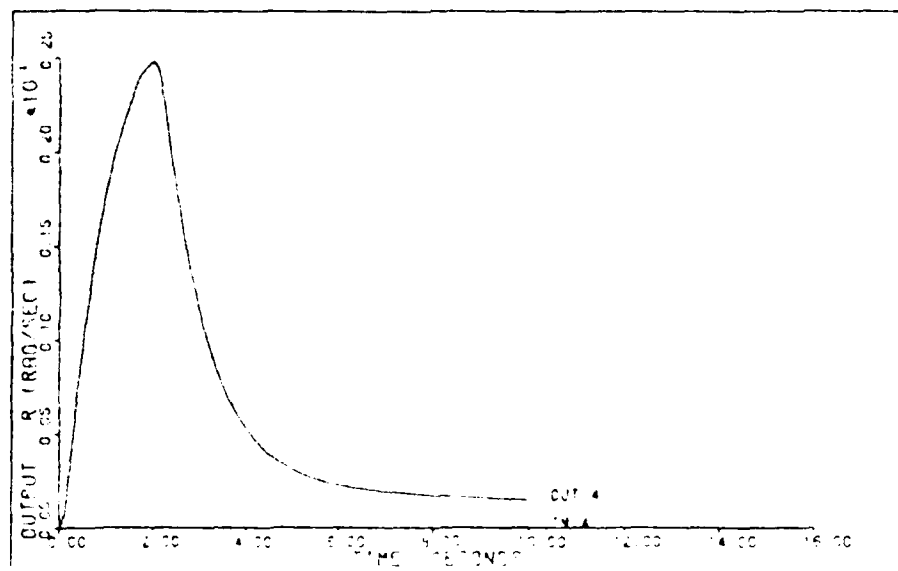


Figure 16d. Output Response,  $r_B$ , for the Vertical Rate Command System ( $V_{EAS} = 100$  Knots)

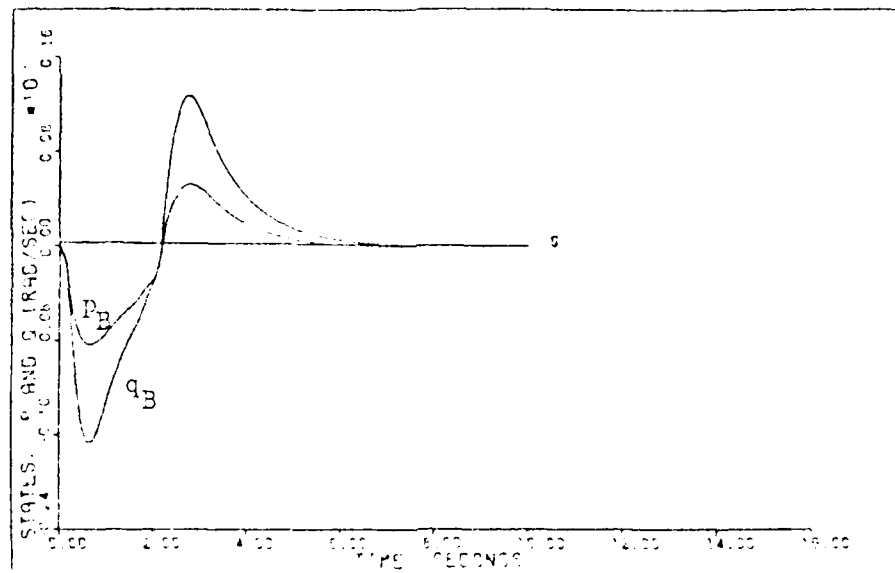


Figure 16e. State Responses,  $p_B$  and  $q_B$ , for the Vertical Rate Command System ( $V_{EAS} = 100$  Knots)

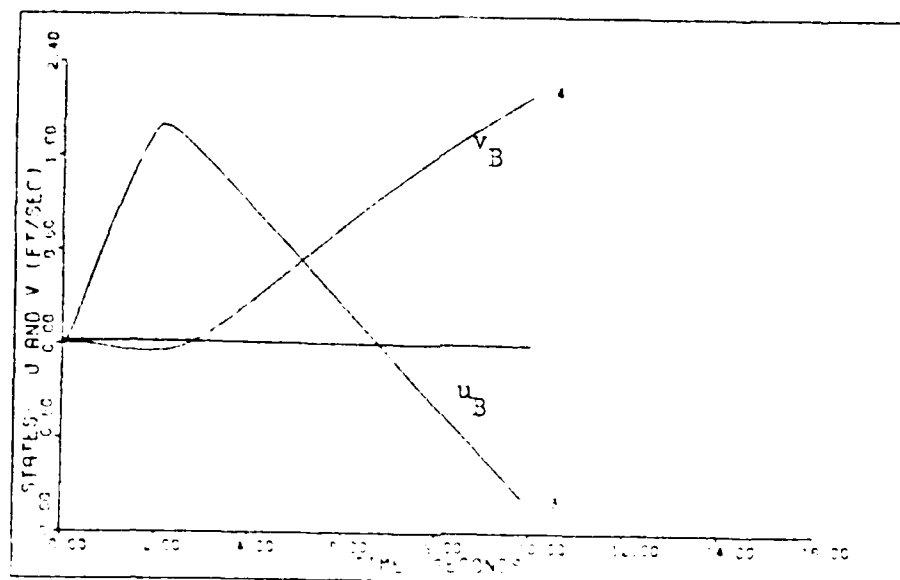


Figure 16f. State Responses,  $u_B$  and  $v_B$  for the Vertical Rate Command System ( $V_{EAS} = 100$  Knots)

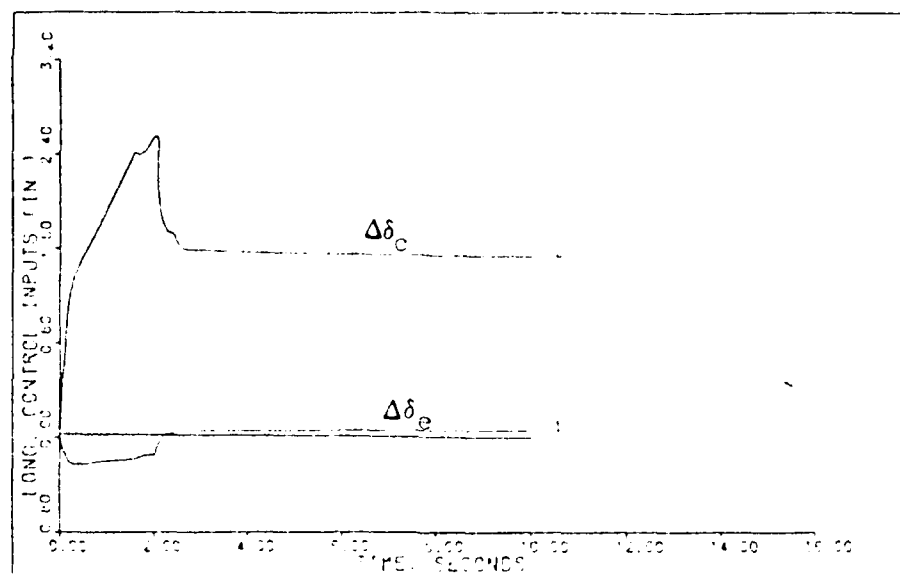


Figure 16g. Longitudinal Control Surface Responses,  $\Delta\delta_e$  and  $\Delta\delta_c$ , for the Vertical Rate Command System ( $V_{EAS} = 100$  Knots)

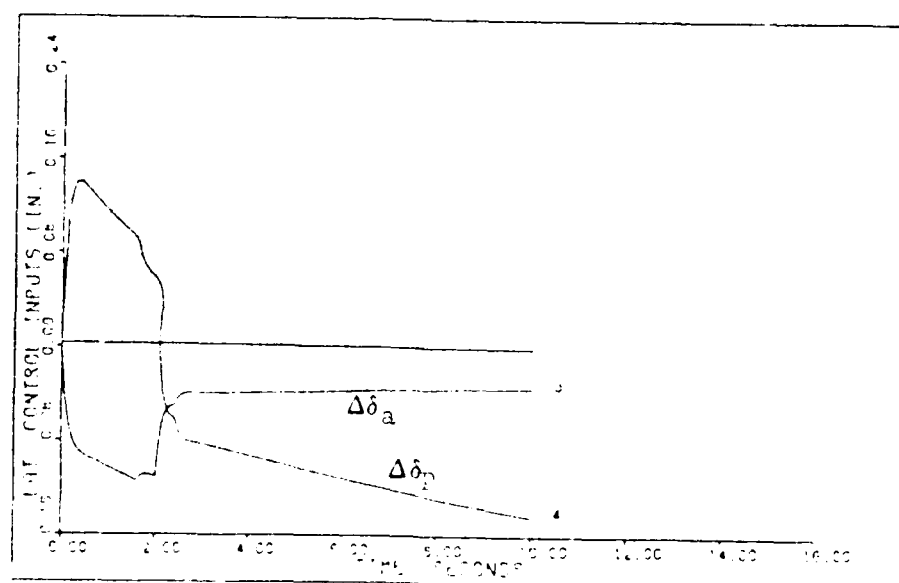


Figure 16h. Lateral Control Surface Responses,  $\Delta\delta_a$  and  $\Delta\delta_r$ , for the Vertical Rate Command System ( $V_{EAS} = 100$  Knots)

Table IV-14  
Vertical Rate Responses for the  $V_{EAS} = 100$  knots

Outputs	$M_p$	$t_p$	$M_m$	$t_m$	FV	$t_s$
$\theta$	0	0	-0.0019481	2.2	-0.0000174	9.4
$\phi$	0	0	-0.0010048	2.1	-0.0000464	9.8
$w_B$	0	0	-20.084928	2.7	-20.000272	2.2
$r_B$	0.0024778	2.0	0	0	0.00014944	9.8

Examination of the figures of merit and the time response plots reveals tight tracking of the desired outputs. Figure 16g. shows that there still might be a problem with the control surface rate limit for  $\Delta\delta_c$ . The effects of the lateral modes represented by  $v_B$ ,  $\phi$ , and  $r_B$  are present but minimal.

The denominator of the closed-loop transfer function for the  $V_{EAS} = 140$  knots flight condition is

$$\begin{aligned}
 & (.1000E+01) S^{**} 12 & (-.3730E+02) + J(0. & ) \\
 & (.1016E+03) S^{**} 11 & (-.3630E+02) + J(0. & ) \\
 & (.3733E+04) S^{**} 10 & (-.4775E+01) + J(.3324E+01) \\
 & (.6331E+05) S^{**} 9 & (-.4775E+01) + J(-.3324E+01) \\
 & (.5819E+06) S^{**} 8 & (-.1008E+02) + J(0. & ) \\
 & (.3148E+07) S^{**} 7 & (-.4023E+01) + J(0. & ) \\
 & (.1016E+08) S^{**} 6 & (-.1048E+01) + J(.1472E+00) & (4.52) \\
 & (.1926E+08) S^{**} 5 & (-.1048E+01) + J(-.1472E+00) \\
 & (.2116E+08) S^{**} 4 & (-.1176E+01) + J(0. & ) \\
 & (.1284E+08) S^{**} 3 & (-.9222E+00) + J(0. & ) \\
 & (.3757E+07) S^{**} 2 & (-.2391E-01) + J(0 & ) \\
 & (.3505E+06) S^{**} 1 & (-.1185E+00) + J(0. & ) \\
 & (.6401E+04) S^{**} 0 & \text{Denominator gain} = .1000E+01
 \end{aligned}$$

It should be noted that the closed-loop poles are all within the stable region. The figures of merit are presented in Table IV-15 and the time response plots in Figures 17a.-17h. The equation for  $\dot{h}_E$  is

$$\dot{h}_E = 236.44 \theta - 0.0161 u_B - 0.99987 w_B \quad (4.53)$$

Design Data for the Vertical Rate Command System

Flight Condition:  $V_{EAS} = 140$  knots

$T = 0.02$  seconds

$\alpha = 1.0$

$$\underline{\Sigma} = \begin{bmatrix} 0.25 & 0 & 0 & 0 \\ 0 & 1.00 & 0 & 0 \\ 0 & 0 & 0.25 & 0 \\ 0 & 0 & 0 & 1.0 \end{bmatrix}$$

$\epsilon = 0.25$

$$\underline{M} = \begin{bmatrix} 0.25 & 0 & 0 & 0 \\ 0 & 0.25 & 0 & 0 \\ 0 & 0 & 0 & 0 \\ 0 & 0 & 0 & 0 \end{bmatrix}$$

$$\underline{K}_0 = \underline{K}_1 = \begin{bmatrix} 1.387 & -0.3071 & -0.0006461 & 0.1996 \\ -1.203 & 0.3284 & -0.01706 & 0.2881 \\ -0.02173 & 2.054 & 0.001875 & 0.5624 \\ -0.1234 & -0.1624 & -0.001688 & 0.8198 \end{bmatrix}$$

Input ramp time: 2.0 seconds

Input command:  $\theta = 0.0$

$\phi = 0.0$

$w_B = 20$  ft/s step

$r_B = 0.0$

Note: Step commands are ramped to steady state over a specified time. This time is designated as the "input ramp time" given above.

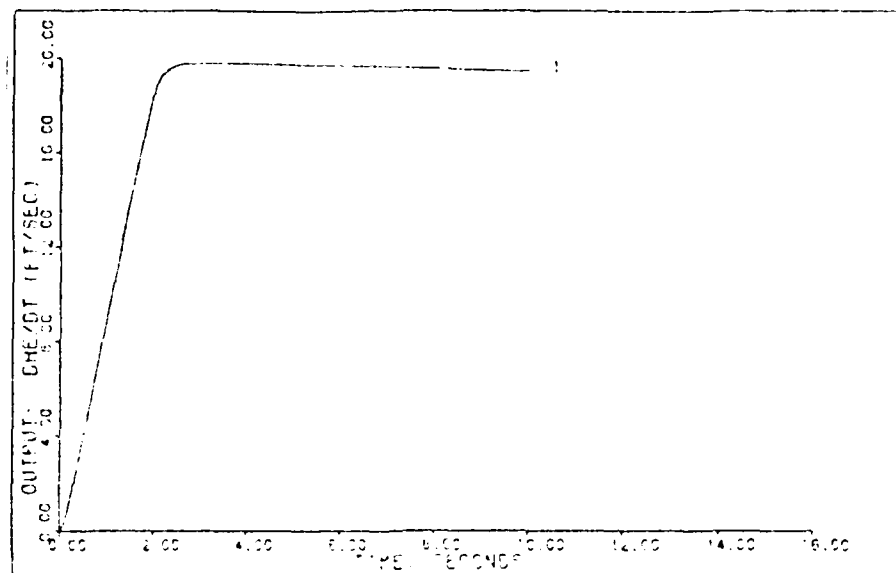


Figure 17a. Output Response,  $\dot{h}_E$ , for the Vertical Rate Command System  
( $V_{EAS} = 140$  Knots)

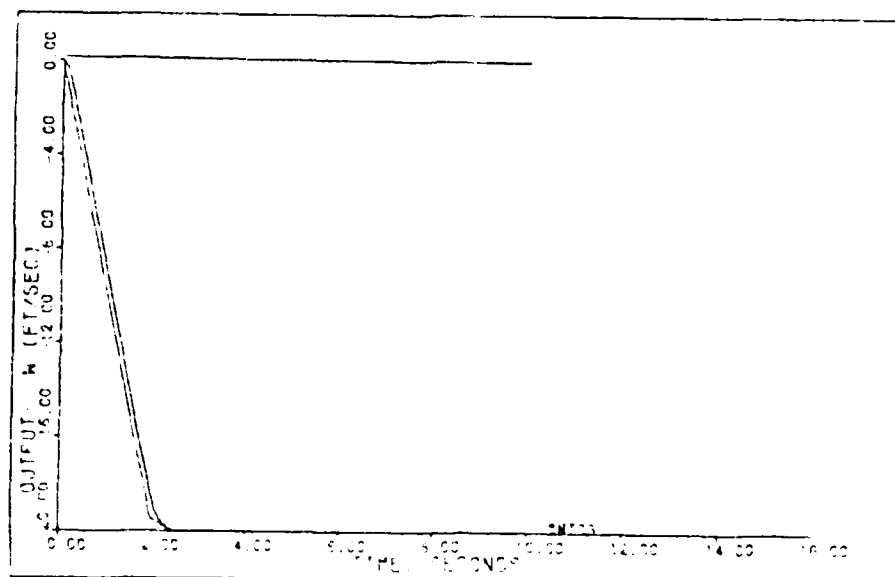


Figure 17b. Output Response,  $w_B$ , for the Vertical Rate Command System  
( $V_{EAS} = 140$  Knots)



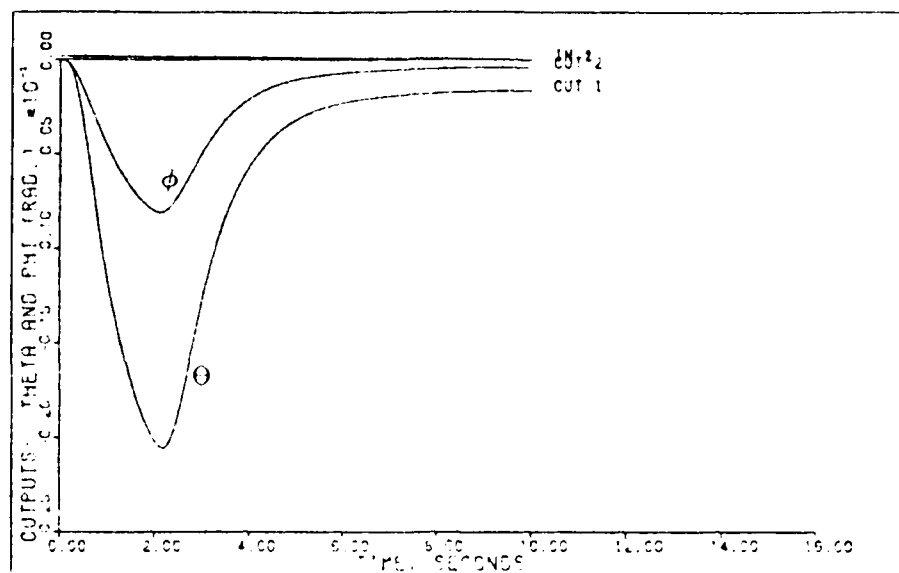


Figure 17c. Output Responses,  $\Theta$  and  $\phi$ , for the Vertical Rate Command System ( $V_{EAS} = 140$  Knots)

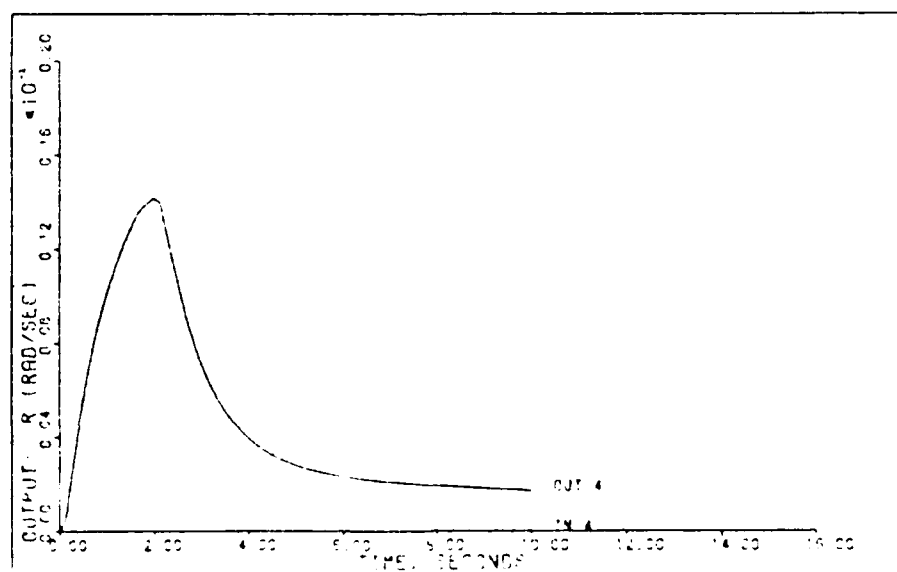


Figure 17d. Output Response,  $r_B$ , for the Vertical Rate Command System ( $V_{EAS} = 140$  Knots)

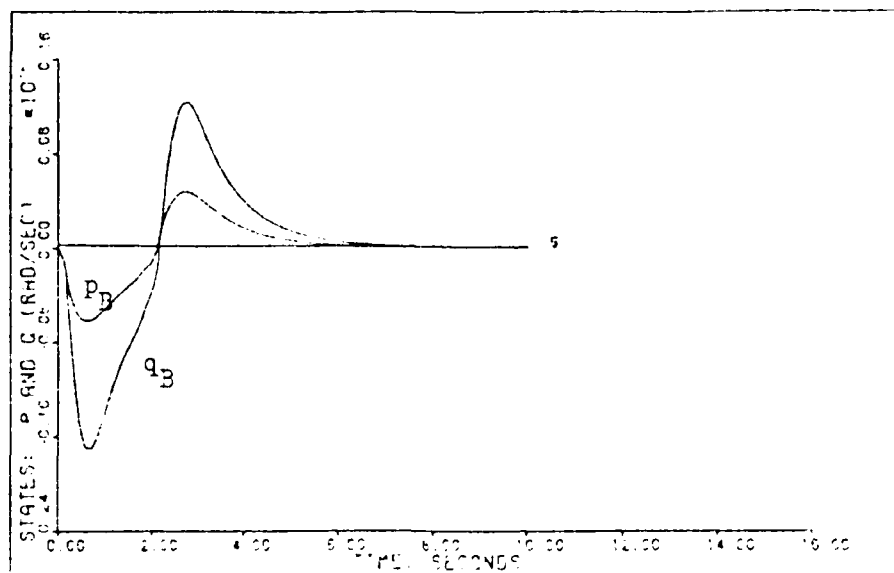


Figure 17e. State Responses,  $p_B$  and  $q_B$ , for the Vertical Rate Command System ( $V_{EAS} = 140$  Knots)

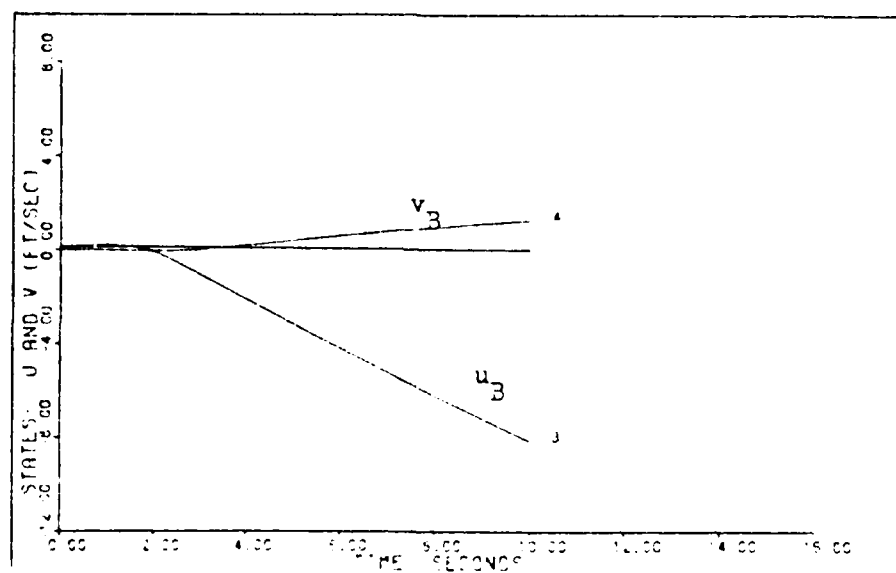


Figure 17f. State Responses,  $u_B$  and  $v_B$  for the Vertical Rate Command System ( $V_{EAS} = 140$  Knots)

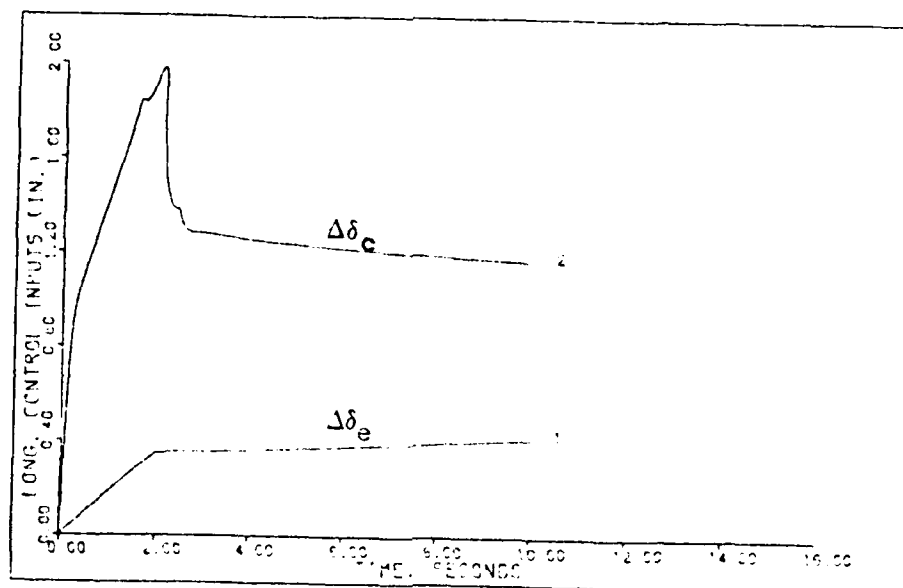


Figure 17g. Longitudinal Control Surface Responses,  $\Delta\delta_e$  and  $\Delta\delta_c$ , for the Vertical Rate Command System ( $V_{EAS} = 140$  Knots)

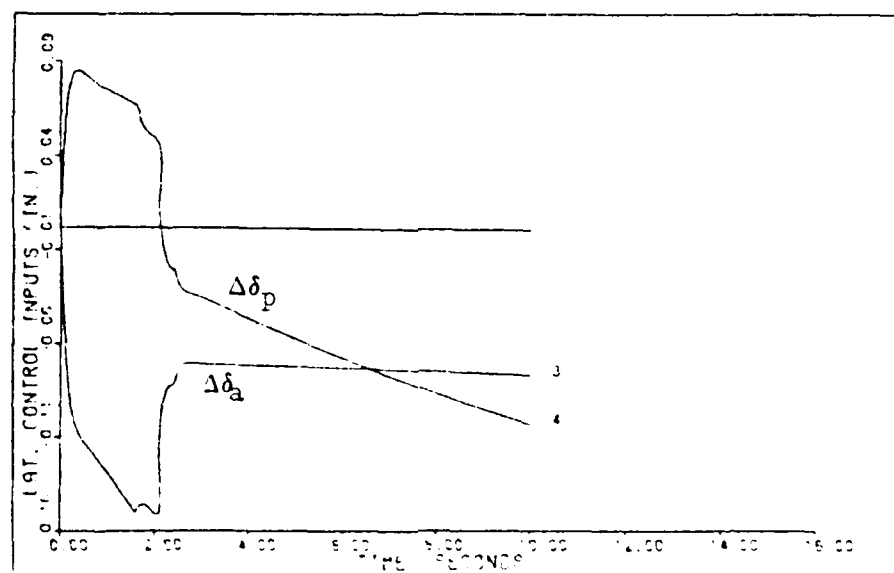


Figure 17h. Lateral Control Surface Responses,  $\Delta\delta_a$  and  $\Delta\delta_p$ , for the Vertical Rate Command System ( $V_{EAS} = 140$  Knots)

Table IV-15  
Vertical Rate Responses for the  $V_{EAS} = 140$  knots

Outputs	$M_p$	$t_p$	$M_m$	$t_m$	FV	$t_s$
$\theta$	0	0	-0.002057	2.2	-0.000161	9.6
$\phi$	0	0	-0.000810	2.1	-0.000039	9.8
$w_B$	0	0	-20.02749	2.7	-20.000063	2.2
$r_B$	0.001415	2.7	0	0	0.000172	9.7

Examination of the time response plots and the figures of merit reveals tight tracking of the desired outputs. The effects of the lateral modes represented by  $\phi$ ,  $v_B$ , and  $r_B$  are minimized for this flight condition.

In summary, tight tracking control is achieved by the individual digital control laws for the vertical rate command system at the  $V_{EAS} = 20, 40, 60, 100$ , and 140 knots flight conditions. A problem may exist with exceeding the control surface rate limit for the collective lift control. This problem is evident at the lower flight conditions. As mentioned earlier, the deflection of the collective lift control primarily performs the vertical rate response. Deflections of the cyclic pitch control and tail rotor yaw control prevent unwanted perturbations in the lateral modes represented by  $\phi$ ,  $v_B$ , and  $r_B$ . For the five flight conditions, these unwanted lateral effects are pretty well minimized. Overall, the vertical rate command system individual digital control laws perform much better than the ones developed for the yaw rate command system and the coordinated turn system.

## V. Robust Controller Design

In Chapter IV, a separate multivariable digital control law is developed at each flight condition for a particular maneuver. Each digital control law is designed to obtain the tightest tracking of the commanded maneuver. By using a digital computer, each control law could be implemented for a maneuver at a particular flight condition by gain scheduling. The advantages of gain scheduling are that it can be easily accomplished with current digital flight hardware and the update rate for gain scheduling is relatively low since flight conditions change rather slowly. In summary, eleven "best" digital control laws were developed which can be easily implemented by gain scheduling. Then the question arises, "Why develop a robust controller if the "best" performance by individual control laws has already been achieved?" The advantage of the robust controller over individual control laws is the reduction in complexity. Robust controllers require less memory which allows more storage for other data, and they require less computer time and software since gain scheduling is not required. This reduction in computer time allows more computation time for other on-board systems. As long as performance degradation is minimal, a robust controller would be better than a number of "best" individual control laws.

One measure of robustness is the ability of a control law design to yield acceptable performance for an inaccurate parameter in the aircraft model. Such an ability significantly reduces the fine tuning and redesign at later stages in the development of a new system. This test of robustness is mostly concerned with the individual control law for a particular flight condition. A second measure of robustness is the

ability of a control system design, with fixed gains, to provide acceptable performance over a wide range of flight conditions. In this study, emphasis is placed on this measure of robustness. The first measure of robustness could be an area for future research.

In this chapter, designs for robust controllers for the yaw rate command system, coordinated turn command system, and the vertical rate command system are developed and their performances compared to those achieved by the individual control laws. The three command systems are summarized below:

Yaw Rate Command System:

$$\begin{aligned}\theta &= 0.0 \\ p_B &= 0.0 \\ w_B &= 0.0 \\ r_B &= 0.1745 \text{ rad/sec, step input}\end{aligned}\tag{5.1}$$

Coordinated Turn Command System:

$$\begin{aligned}\theta &= 0.0 \\ \phi &= 0.5235 \text{ rad., step input} \\ v_B &= 0.0 \\ w_B &= 0.0\end{aligned}\tag{5.2}$$

Vertical Rate Command System:

$$\begin{aligned}\theta &= 0.0 \\ \phi &= 0.0 \\ w_B &= 20.0 \text{ ft/sec, step input} \\ r_B &= 0.0\end{aligned}\tag{5.3}$$

Note: Each step input has an input ramp time.

#### Design Methodology

The easiest method in finding a possible robust controller is to implement a digital control law developed at one flight condition at the

other flight conditions for a particular maneuver. It should be noted that when checking a robust controller, the state equations and the control limits are different for each flight condition. While developing individual digital control laws, the flight conditions that were hardest to design for were the  $V_{EAS} = 100$  knots flight condition and especially the  $V_{EAS} = 140$  knots flight condition. At these flight conditions, recurring unstable poles in the closed-loop denominator and control limit saturation were prevalent. The first attempt at robust controller design is to implement a control law developed at the lower more stable flight conditions at the higher more unstable flight conditions. The results show that even though the figures of merit are numerically acceptable, the time response plots revealed high-frequency oscillations which are very unacceptable. The second attempt is to implement the highest (in terms of  $V_{EAS}$ ) flight condition's control law at the lower, more stable flight conditions. The results obtained are both numerically acceptable as well as graphically acceptable. If this method had failed, the next step would be to adjust the gain matrix elements to achieve a robust controller. The rest of this chapter presents the results achieved by the robust controllers with comparisons to the results achieved by the individual control laws.

#### Yaw Rate Command System

As noted in Chapter IV, satisfactory stable designs at the  $V_{EAS} = 100$  knots and  $V_{EAS} = 140$  knots flight conditions could not be achieved. Therefore, the control law, shown below, for the  $V_{EAS} = 60$  knots flight condition was implemented at the  $V_{EAS} = 20$  knots and  $V_{EAS} = 40$  knots flight condition.

$$\underline{u}(kT)=[50\text{Hz}] \begin{bmatrix} 0.4388 & -0.01388 & 0.0005775 & 0.00259 \\ -0.01703 & 0.008547 & -0.002668 & 0.08984 \\ -0.00717 & 0.4855 & 0.0002487 & 0.1517 \\ 0.008557 & -0.06569 & -0.0001695 & 0.295 \end{bmatrix} \underline{e}(kT) \\ + \begin{bmatrix} 1.755 & -0.0553 & 0.00231 & 0.01036 \\ -0.6814 & 0.03419 & -0.01067 & 0.3594 \\ -0.02868 & 1.942 & 0.0009946 & 0.6068 \\ 0.03423 & -0.2628 & -0.000678 & 1.18 \end{bmatrix} \underline{z}(kT) \quad (5.4)$$

For the  $V_{EAS} = 20$  knots flight condition, the denominator of the closed-loop transfer function is:

$$\begin{aligned} & (.1000E+01) S^{**} 12 \quad (-.3474E+02) + J(0. \quad ) \\ & (.5198E+02) S^{**} 11 \quad (-.4551E+01) + J(.3805E+01) \\ & (.7471E+03) S^{**} 10 \quad (-.4551E+01) + J(-.3805E+01) \\ & (.5940E+04) S^{**} 9 \quad (-.3024E+00) + J(.3730E+01) \\ & (.3059E+05) S^{**} 8 \quad (-.3024E+00) + J(-.3730E+01) \\ & (.1159E+06) S^{**} 7 \quad (-.6162E+00) + J(.1741E+01) \\ & (.3248E+06) S^{**} 6 \quad (-.6162E+00) + J(-.1741E+01) \\ & (.6023E+06) S^{**} 5 \quad (-.4050E+01) + J(0. \quad ) \\ & (.7505E+06) S^{**} 4 \quad (-.2212E+01) + J(0. \quad ) \\ & (.5515E+06) S^{**} 3 \quad (.2377E-02) + J(.2378E-01) \\ & (.2060E+05) S^{**} 2 \quad (.2377E-02) + J(-.2378E-01) \\ & (.2084E+03) S^{**} 1 \quad (-.4361E-01) + J(0. \quad ) \\ & (.1303E+02) S^{**} 0 \quad \text{DENOMINATOR GAIN} = .1000E+01 \end{aligned} \quad (5.5)$$

It should be noted that there are two unstable poles at  $0.002377 \pm j0.02378$ , which indicates that the helicopter, with output feedback, has two unstable modes. Of course, this is an unacceptable result if only stable systems are considered. However, there are backup mechanical systems and manual pilot inputs for severe instability problems. As can be seen from the figures of merit and the response plots, the unstable pole effects are negligible. From here on, the robust controller is deemed acceptable as long as the unstable effects from right-half s-plane poles or poles outside the unit circle for the z-plane are minimal and transient responses diverge very slowly. The figures of merit for the  $V_{EAS} = 20$  knots flight conditions are presented in Table V-1 and the



time response plots in Figures 18a. - 18f. Again, it should be noted that  $\theta$  is in

Table V-1  
Yaw Rate Results ( $V_{EAS} = 20$  Knots) for the  
Robust Controller

Outputs	$M_p$	$t_p$	$M_m$	$t_m$	FV	$t_s$
$\theta$	0.00020157	0.5	-0.0027762	1.7	-0.0001351	10
$p_B$	0.0014238	1.0	-0.0000655	1.0	-0.0000655	10
$w_B$	0.33044	2.2	-0.2031981	0.9	0.0120541	10
$r_B$	0.18282	1.2	0	0	0.174541	1.5

radians and  $p_B$  and  $r_B$  are in radians/sec. As for the case of the individual control laws for the yaw rate command system,  $\phi$  in Figure 18d. is increasing at a steady rate. As explained in Chapter IV, the increasing perturbation roll angle,  $\phi$ , is due not to the perturbation roll rate  $p_B$ , but to the perturbation yaw rate,  $r_B$ . In ten seconds,  $\phi$  reaches approximately ten degrees. The side body velocity,  $v_B$ , in Figure 18c. again shows its slow oscillatory behavior.

The  $V_{EAS} = 60$  knots digital controller is also implemented at the  $V_{EAS} = 40$  knots flight condition. The closed-loop denominator is:

$$\begin{aligned}
 & (.1000E+01) S^{**} 12 \quad (-.3486E+02) + J(0. \quad ) \\
 & (.5267E+02) S^{**} 11 \quad (-.4644E+01) + J(.3764E+01) \\
 & (.7773E+03) S^{**} 10 \quad (-.4644E+01) + J(-.3764E+01) \\
 & (.6297E+04) S^{**} 9 \quad (-.3126E+00) + J(.3668E+01) \\
 & (.3289E+05) S^{**} 8 \quad (-.3126E+00) + J(-.3668E+01) \\
 & (.1256E+06) S^{**} 7 \quad (-.7555E+00) + J(.1719E+01) \\
 & (.3550E+06) S^{**} 6 \quad (-.7555E+00) + J(-.1719E+01) \\
 & (.6732E+06) S^{**} 5 \quad (-.4013E+01) + J(0. \quad ) \\
 & (.8405E+06) S^{**} 4 \quad (-.2316E+01) + J(0. \quad ) \\
 & (.8405E+06) S^{**} 3 \quad (.1727E-01) + J(.5853E-01) \\
 & (.3582E+05) S^{**} 2 \quad (.1727E-01) + J(-.5853E-01) \\
 & (.4718E+03) S^{**} 1 \quad (-.9841E-01) + J(0. \quad ) \\
 & (.2027E+03) S^{**} 0 \quad \text{DENOMINATOR GAIN} = .1000E+01
 \end{aligned} \tag{5.6}$$

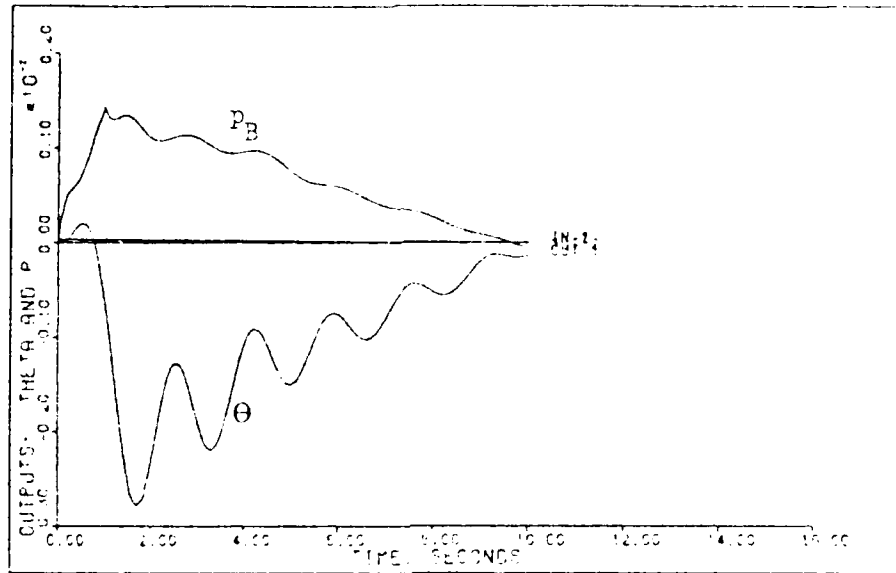


Figure 18a. Robust Controller Output Responses,  $\theta$ (rad) and  $p_B$ (rad/sec), for the Yaw Rate Command System ( $V_{EAS} = 20$  Knots)

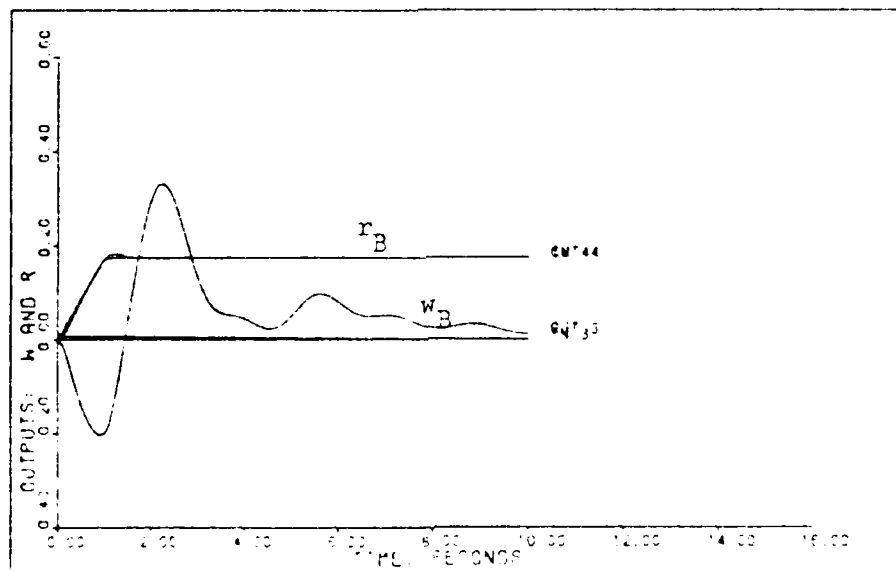


Figure 18b. Robust Controller Output Responses,  $w_B$ (ft/sec) and  $r_B$ (rad/sec), for the Yaw Rate Command System ( $V_{EAS} = 20$  Knots)

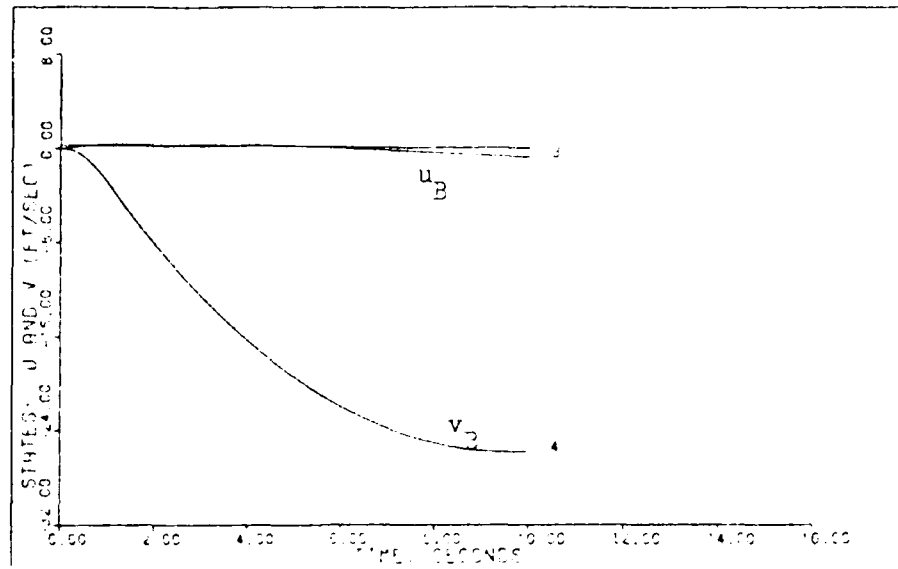


Figure 18c. Robust Controller State Responses,  $u_B$  and  $v_B$ , for the Yaw Rate Command System ( $V_{EAS} = 20$  Knots)

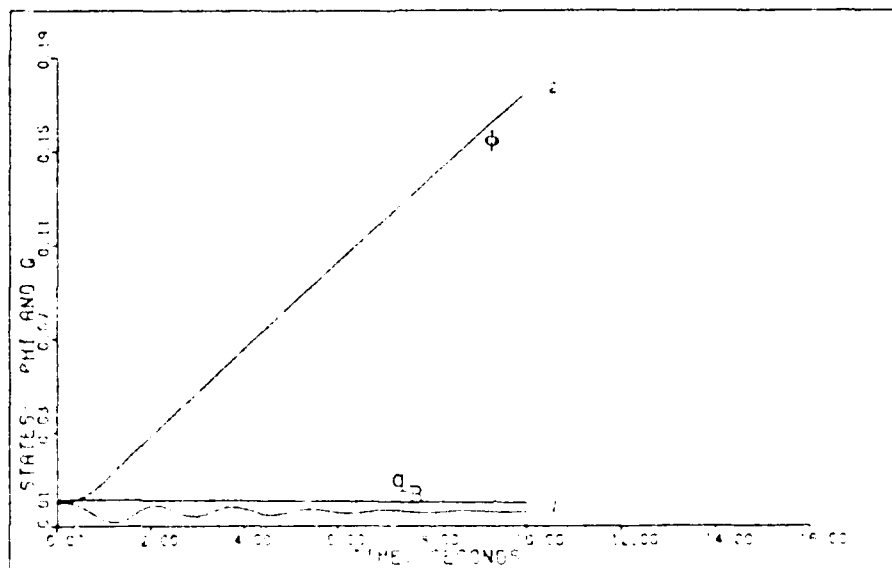


Figure 18d. Robust Controller State Responses,  $\phi$ (rad) and  $q_B$ (rad/sec) for the Yaw Rate Command System ( $V_{EAS} = 20$  Knots)

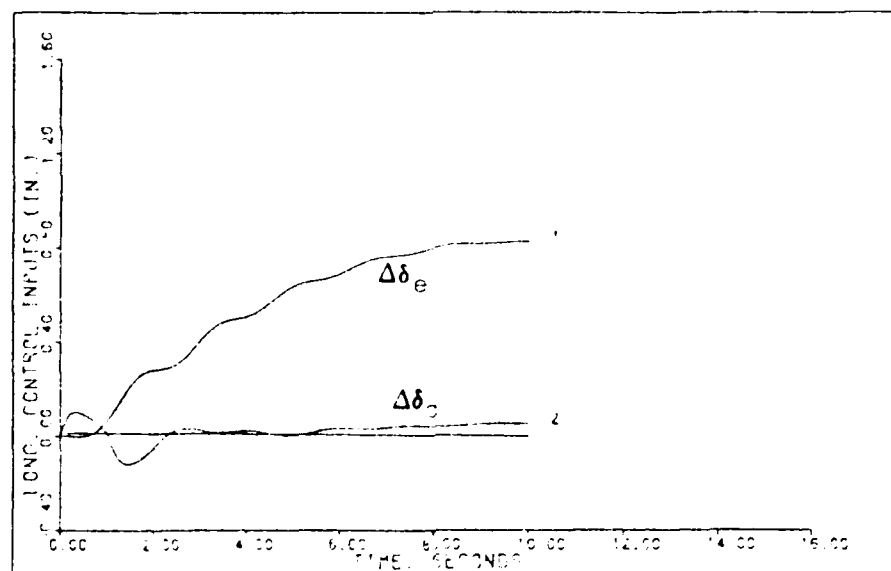


Figure 18e. Robust Controller Longitudinal Control Surface Responses,  $\Delta\delta_e$  and  $\Delta\delta_c$ , for the Yaw Rate Command System ( $V_{EAS} = 20$  Knots)

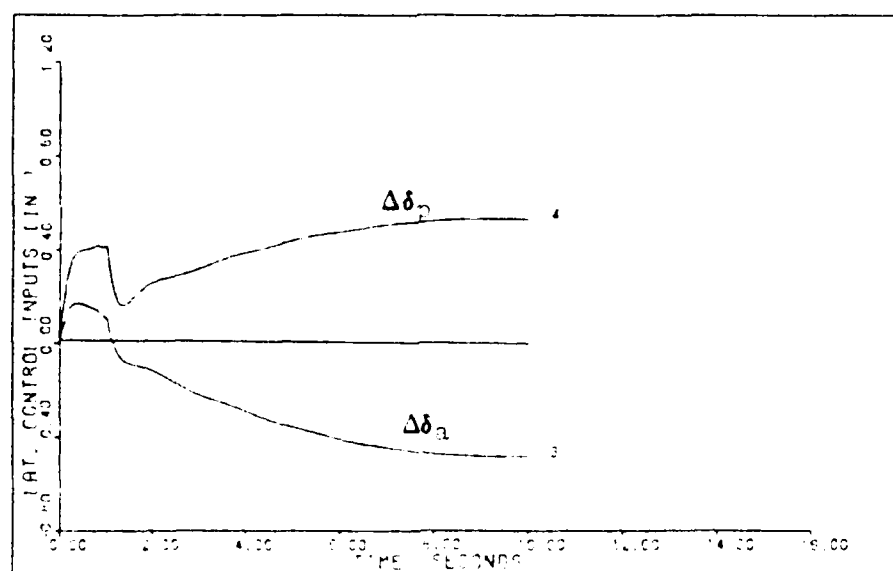


Figure 18f. Robust Controller Lateral Control Surface Responses,  $\Delta\delta_a$  and  $\Delta\delta_p$ , for the Yaw Rate Command System ( $V_{EAS} = 20$  Knots)

It should be noted that the robust controller has again produced unstable poles at  $0.01727 \pm j05853$ .

The figures of merit for this flight condition are presented in Table V-2 and the time response plots in Figures 19a. - 19f. Again, the time response plots of  $\phi$  and  $v_B$  should be examined.

Table V-2  
Yaw Rate Results ( $V_{EAS} = 40$  Knots) for the  
Robust Controller

Outputs	$M_p$	$t_p$	$M_m$	$t_m$	FV	$t_s$
$\theta$	$5.383 \times 10^{-7}$	0.1	-0.0031989	1.6	-0.00108774	9.5
$p_B$	0.002217	2.5	0	0	-0.0009121	9.9
$w_B$	0.25704	2.2	-0.188623	1.0	0.03262	9.8
$r_B$	0.1801823	1.2	0	0	0.1732855	1.5

Comparisons with the individual digital control laws are listed for a desired output response in Tables V-3 - V-6. The letter (R) after the flight condition value stands for robust controller response. The letter (A) stands for with actuators.

Table V-3  
Yaw Rate Results for the Output Response,  $\theta$

$V_{EAS}$	$M_p$	$t_p$	$M_m$	$t_m$	FV	$t_s$
20	0.00084723	8.9	-0.0041178	1.8	-0.000851	10
20R	0.00020157	0.5	-0.0027762	1.7	-0.0001351	10
40A	0	0	-0.003705	1.6	0.001085	10
40R	$5.383 \times 10^{-7}$	0.1	-0.0031989	1.6	-0.00108774	9.5
60	0	0	-0.0035923	1.5	-0.001395	9.1

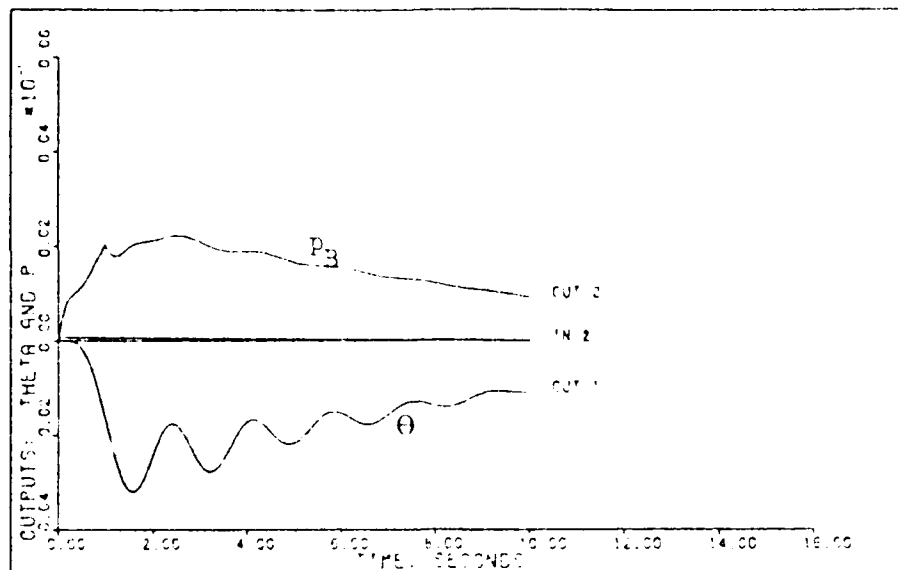


Figure 19a. Robust Controller Output Responses,  $\theta$ (rad) and  $p_B$ (rad/sec), for the Yaw Rate Command System ( $V_{EAS} = 40$  Knots)

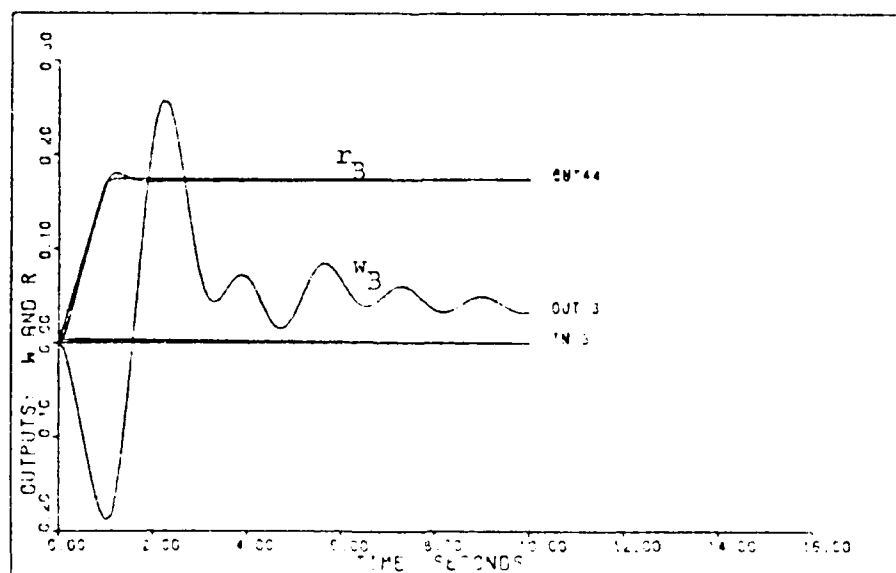


Figure 19b. Robust Controller Output Responses,  $w_B$ (ft/sec) and  $r_B$ (rad/sec), for the Yaw Rate Command System ( $V_{EAS} = 40$  Knots)

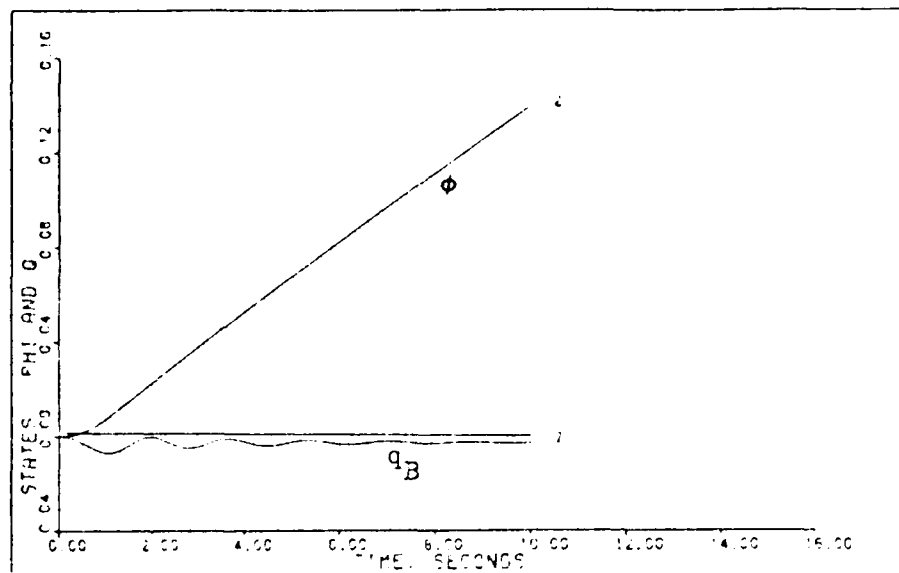


Figure 19c. Robust Controller State Responses,  $\phi$ (rad) and  $q_B$ (rad/sec), for the Yaw Rate Command System ( $V_{EAS} = 40$  Knots)

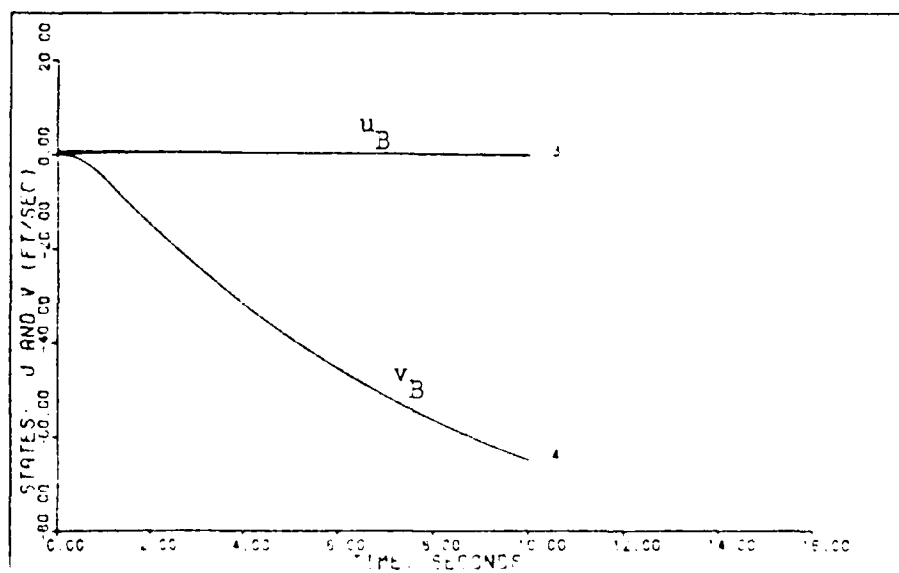


Figure 19d. Robust Controller State Responses,  $u_B$  and  $v_B$ , for the Yaw Rate Command System ( $V_{EAS} = 40$  Knots)

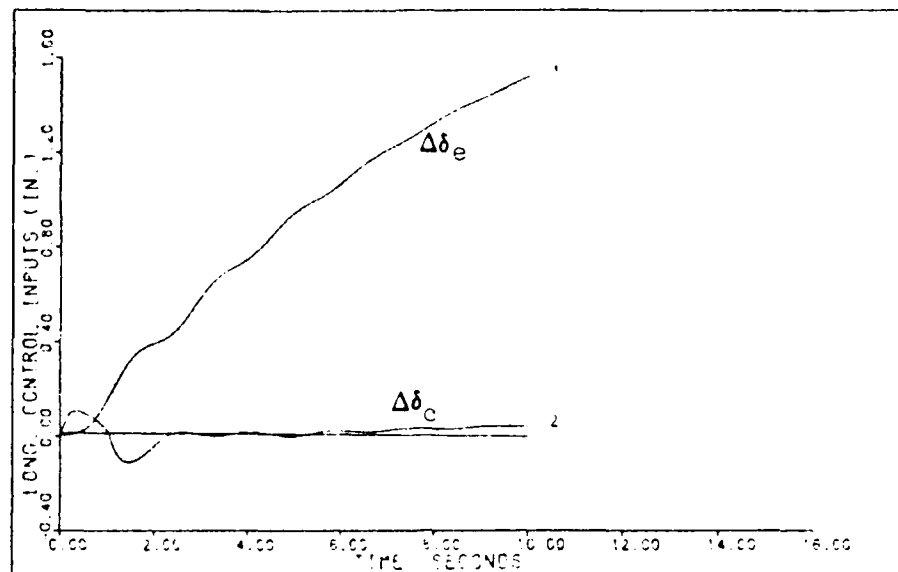


Figure 19e. Robust Controller Longitudinal Control Surface Responses,  $\Delta\delta_e$  and  $\Delta\delta_c$ , for the Yaw Rate Command System ( $V_{EAS} = 40$  Knots)

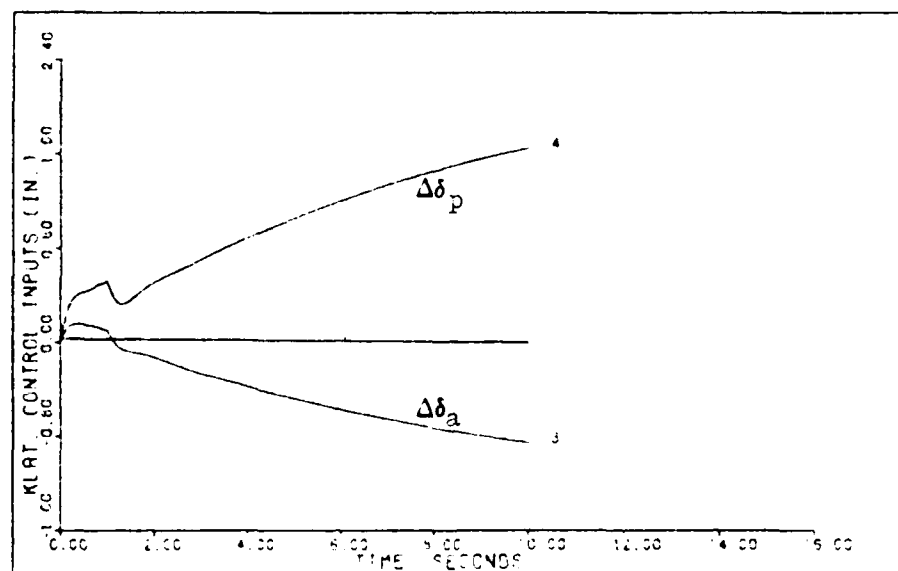


Figure 19f. Robust Controller Lateral Control Surface Responses,  $\Delta\delta_a$  and  $\Delta\delta_p$ , for the Yaw Rate Command System ( $V_{EAS} = 40$  Knots)



Table V-4  
Yaw Rate Results for the Output Response,  $p_B$

$V_{EAS}$	$M_p$	$t_p$	$M_m$	$t_m$	FV	$t_s$
20	0.0040857	1.4	-0.000631	10	-0.000631	10
20R	0.0014238	1.0	-0.0000655	10	-0.0000655	10
40A	0.003456	1.4	-0.0000607	0.1	0.0013465	10
40R	0.002217	2.5	0	0	0.0009121	9.9
60	0.0035991	1.4	0	0	0.0016613	1.9

Table V-5  
Yaw Rate Results for the Output Response,  $w_B$

$V_{EAS}$	$M_p$	$t_p$	$M_m$	$t_m$	FV	$t_s$
20	0.1865	2.7	-0.12069	1.4	-0.01753	10
20R	0.33044	2.2	-0.2031981	0.9	0.0120541	10
40A	0.180373	2.3	-0.151656	1.1	0.013948	10
40R	0.25704	2.2	-0.188623	1.0	0.03262	9.8
60	0.256420	2.2	-0.134232	1.2	0.0105276	9.9

Table V-6  
Yaw Rate Results for the Output Response,  $r_B$

$V_{EAS}$	$M_p$	$t_p$	$M_m$	$t_m$	FV	$t_s$
20	0.18666	1.3	0	0	0.17435	1.6
20R	0.18282	1.2	0	0	0.174541	1.5
40A	0.18058	1.2	0	0	0.173435	1.5
40R	0.1801823	1.2	0	0	0.1732855	1.5
60	0.1766397	1.2	0	0	0.1714144	1.4

The tables show that except for the z-axis body velocity,  $w_B$ , the robust controller performs better than the individual counterparts. The one obvious drawback, of course, is that the robust controller produced two unstable modes. The time response plots for the robust controller are similar to those for the individual control laws.

#### Coordinated Turn Command System

The coordinated turn command system is given by Equation (5.2). The three flight conditions for the coordinated turn are  $V_{EAS} = 60, 100$  and 140 knots. Since the  $V_{EAS} = 140$  knots is the highest (in terms of  $V_{EAS}$ ), it is chosen as the robust controller to be implemented at the other flight conditions. The control law for the  $V_{EAS} = 140$  knots flight condition is

$$\begin{aligned} \underline{u}(kT) = [50\text{Hz}] & \begin{bmatrix} 1.2438 & 0.005929 & -0.00609 & -0.0001509 \\ -1.197 & 0.04457 & -0.008789 & -0.003228 \\ -0.1649 & 0.1529 & -0.01716 & 0.0002646 \\ -0.3259 & 0.0756 & -0.02501 & -0.0004396 \end{bmatrix} \underline{e}(kT) \\ & + \begin{bmatrix} 0.7103 & 0.003388 & -0.00348 & -0.00008624 \\ -0.6838 & 0.02547 & -0.005022 & -0.001845 \\ -0.09423 & 0.0874 & -0.009803 & 0.0001512 \\ -0.1862 & 0.04321 & -0.01429 & -0.0002512 \end{bmatrix} \underline{z}(kT) \end{aligned} \quad (5.7)$$

For the  $V_{EAS} = 60$  knots flight condition, the closed-loop denominator is:

$$\begin{aligned} & (.1000E+01) S^{**} 12 & (-.6415E+00) + J(.9269E+01) \\ & (.1608E+02) S^{**} 11 & (-.6415E+00) + J(-.9269E+01) \\ & (.2076E+03) S^{**} 10 & (-.2677E+01) + J(-.3078E+01) \\ & (.1817E+04) S^{**} 9 & (-.2677E+01) + J(-.3078E+01) \\ & (.1034E+05) S^{**} 8 & (-.7606E+00) + J(.5527E+00) \\ & (.3798E+05) S^{**} 7 & (-.7606E+00) + J(-.5527E+00) \\ & (.8856E+05) S^{**} 6 & (-.3180E+01) + J(.1126E+01) \\ & (.1271E+06) S^{**} 5 & (-.3180E+01) + J(-.1126E+01) \\ & (.1127E+06) S^{**} 4 & (-.1085E-01) + J(0.) \\ & (.5981E+05) S^{**} 3 & (-.4949E+00) + J(.3192E-01) \end{aligned} \quad (5.8)$$

```

( .1738E+05) S** 2    (-.4949E+00) + J(-.3192E-01)
( .2168E+04) S** 1    (-.5587E+00) + J(0.          )
( .2155E+02) S** 0    DENOMINATOR GAIN = .1000E+01

```

It should be noted that unlike the robust controller for the yaw rate command system, the coordinated turn robust controller produces all stable poles. This means that the closed-loop poles are all in the left-half s-plane or within the unit circle in the z-plane.

The figures of merit for the  $V_{EAS} = 60$  knots flight conditions are presented in Table V-7 and the time response plots in Figures 20a. - 20g.

Table V-7  
Coordinated Turn Results ( $V_{EAS} = 60$  Knots) for the  
Robust Controller

Outputs	$M_p$	$t_p$	$M_m$	$t_m$	FV	$t_s$
$\theta$	0.000349798	1.1	-0.00025436	4.1	0.00015335	10
$\phi$	0.58715576	4.5	0	0	0.5200745	7.4
$v_B$	0.27968256	4.2	-0.1859034	0.5	-0.0088153	10
$w_B$	0.5296735	5.3	-0.8855	2.1	-0.125963	9.9

Even though the figures of merit are numerically acceptable, the robust controller has introduced slow oscillations in the time responses. These oscillations, however, are small in magnitude and therefore are considered acceptable.

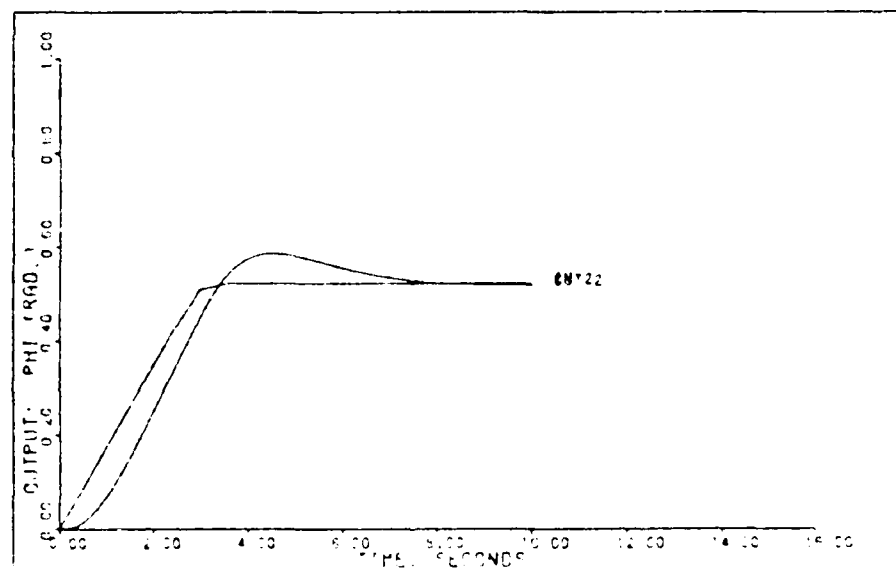


Figure 20a. Robust Controller Output Response,  $\phi$ , for the Coordinated Turn Command System ( $V_{EAS} = 60$  Knots)

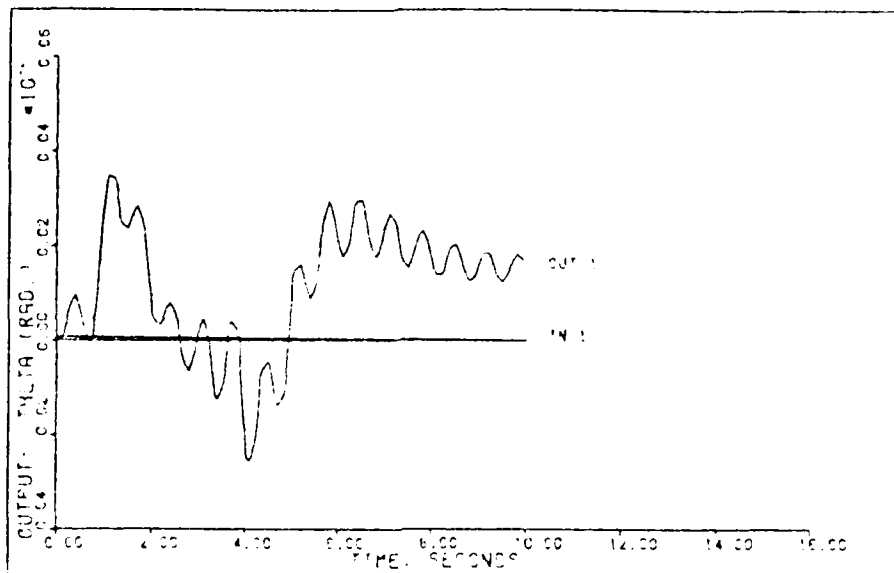


Figure 20b. Robust Controller Output Response,  $\Theta$ , for the Coordinated Turn Command System ( $V_{EAS} = 60$  Knots)

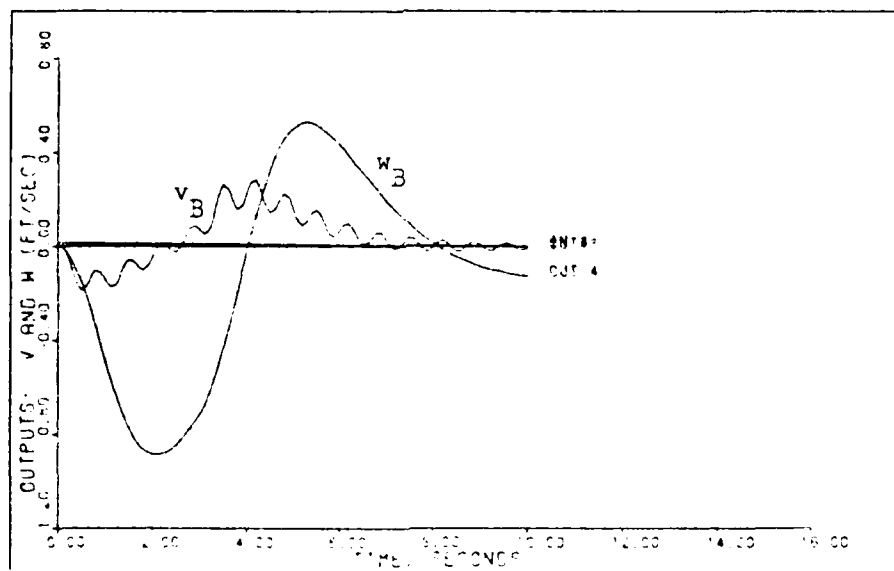


Figure 20c. Robust Controller Output Responses,  $v_B$  and  $w_B$ , for the Coordinated Turn Command System ( $V_{EAS} = 60$  Knots)

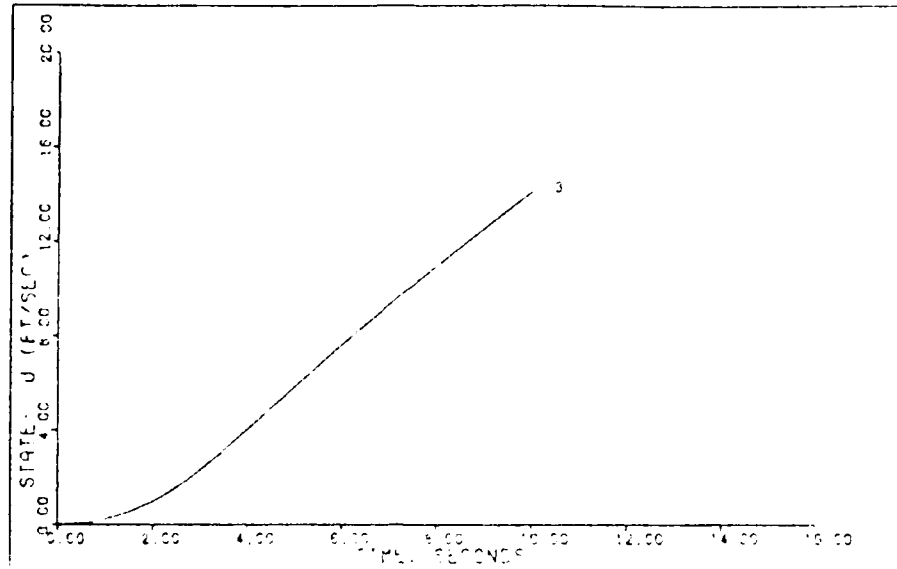


Figure 20d. Robust Controller State Response,  $u_B$ , for the Coordinated Turn Command System ( $V_{EAS} = 60$  Knots)

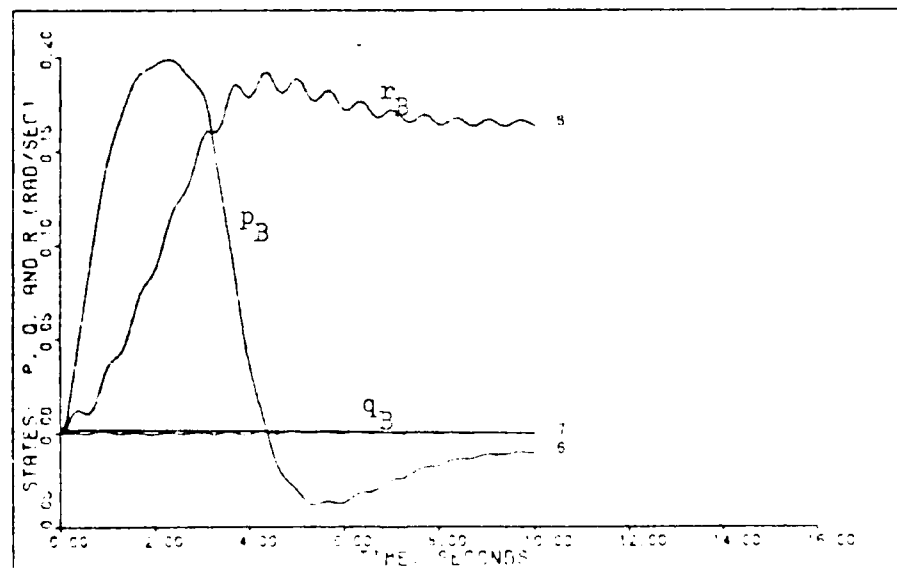


Figure 20e. Robust Controller State Responses,  $p_B$ ,  $q_B$ , and  $r_B$ , for the Coordinated Turn Command System ( $V_{EAS} = 60$  Knots)

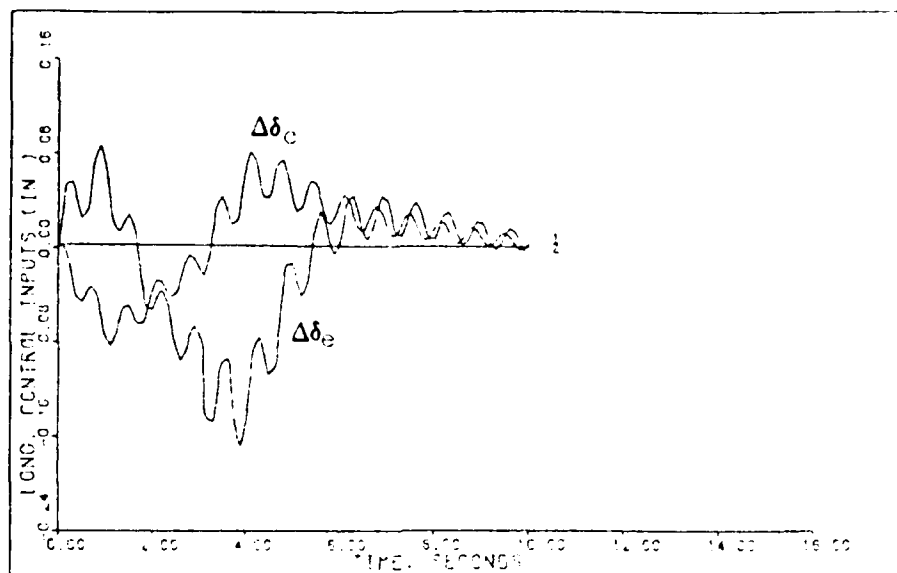


Figure 20f. Robust Controller Longitudinal Control Surface Responses,  $\Delta\delta_e$  and  $\Delta\delta_c$ , for the Coordinated Turn Command System ( $V_{EAS} = 60$  Knots)

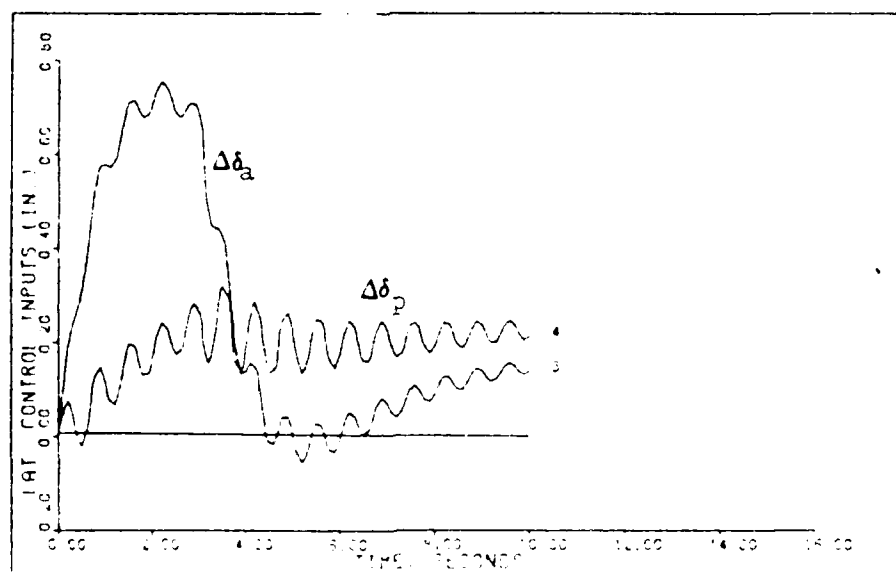


Figure 20g. Robust Controller Lateral Control Surface Responses,  $\Delta\delta_a$  and  $\Delta\delta_p$ , for the Coordinated Turn Command System ( $V_{EAS} = 60$  Knots)

For the  $V_{EAS} = 100$  knots flight condition, the closed-loop denominator is:

$$\begin{aligned}
 & (.1000E+01) S^{**} 12 \quad (-.8889E+00) + J(.1322E+02) \\
 & (.1820E+02) S^{**} 11 \quad (-.8889E+00) + J(-.1322E+02) \\
 & (.3235E+03) S^{**} 10 \quad (-.2626E+01) + J(.2490E+01) \\
 & (.3579E+04) S^{**} 9 \quad (-.2626E+01) + J(-.2490E+01) \\
 & (.2292E+05) S^{**} 8 \quad (-.3982E+01) + J(.1172E+01) \\
 & (.8926E+05) S^{**} 7 \quad (-.3982E+01) + J(-.1172E+01) \\
 & (.2159E+06) S^{**} 6 \quad (-.8191E+00) + J(-.5141E+00) \\
 & (.3189E+06) S^{**} 5 \quad (-.8191E+00) + J(.5141E+00) \\
 & (.2885E+06) S^{**} 4 \quad (-.4923E+00) + J(.3846E-01) \\
 & (.1554E+06) S^{**} 3 \quad (-.4923E+00) + J(-.3846E-01) \\
 & (.4591E+05) S^{**} 2 \quad (-.2022E-01) + J(0.) \\
 & (.5947E+04) S^{**} 1 \quad (-.5628E+00) + J(0.) \\
 & (.1027E+03) S^{**} 0 \quad \text{DENOMINATOR GAIN} = .1000E+01
 \end{aligned} \tag{5.9}$$

It should be noted that the robust controller has produced all stable poles.

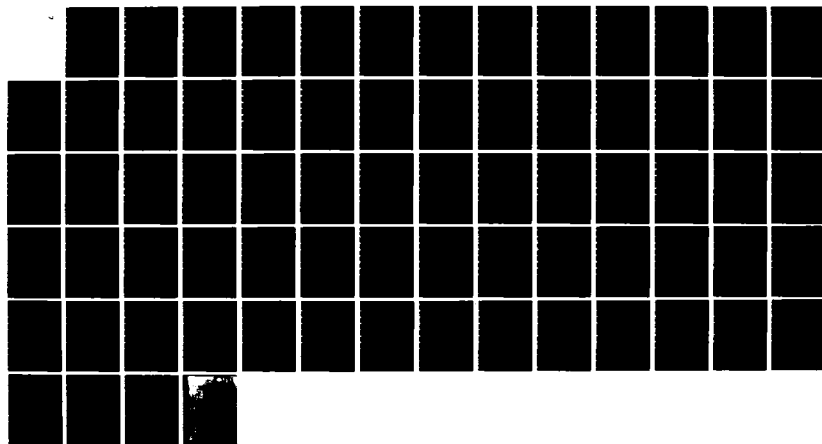
The figures of merit for the  $V_{EAS} = 100$  knots flight condition are presented in Table V-8 and the time response plots in Figures 21a. - 21g.

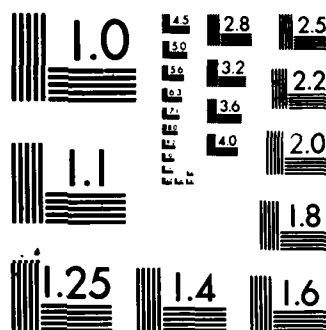
Table V-8  
Coordinated Turn Results ( $V_{EAS} = 100$  Knots) for the  
Robust Controller

Outputs	$M_p$	$t_p$	$M_m$	$t_m$	FV	$t_s$
$\theta$	0.0001901	1.3	-0.0000874	4.3	0.0000937	10
$\phi$	0.5839063	4.6	0	0	0.5226756	7.4
$v_B$	0.24791514	4.3	-0.210376	0.3	0.0407919	10
$w_B$	0.30241226	5.4	-0.436832	2.0	0.00717331	10



AD-A141 046 MULTIVARIABLE DIGITAL CONTROL LAWS FOR THE UH-60A BLACK 3/3  
HAWK HELICOPTER(U) AIR FORCE INST OF TECH  
WRIGHT-PATTERSON AFB OH SCHOOL OF ENGINEERING  
UNCLASSIFIED B H MAYHEW MAR 84 AFIT/GE/EE/84N-6 F/G 1/3 NL





MICROCOPY RESOLUTION TEST CHART  
NATIONAL BUREAU OF STANDARDS-1963-A

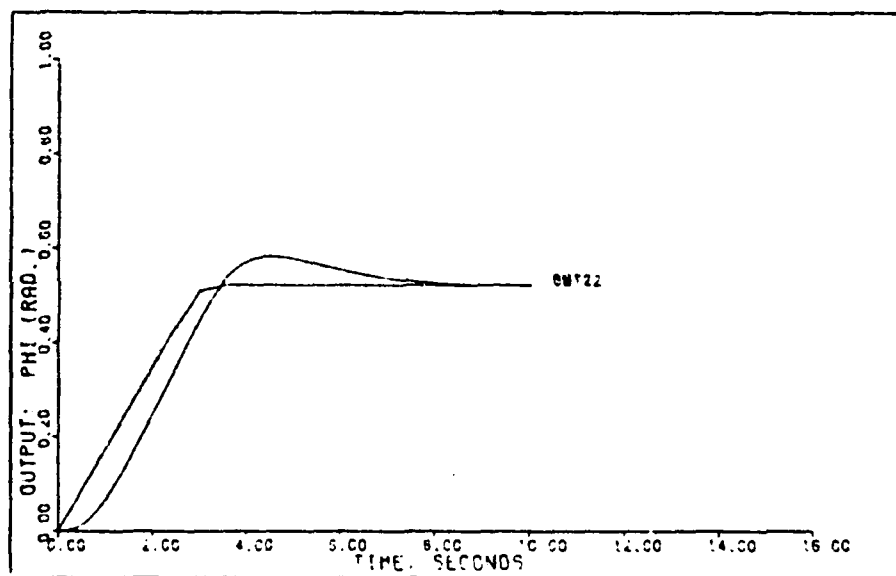


Figure 21a. Robust Controller Output Response,  $\phi$ , for the Coordinated Turn Command System ( $V_{EAS} = 100$  Knots)

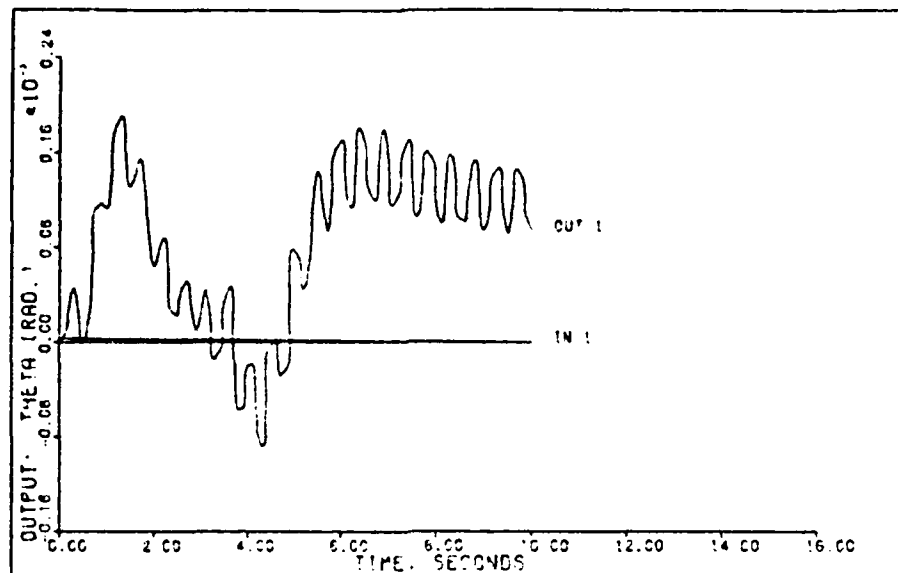


Figure 21b. Robust Controller Output Response,  $\Theta$ , for the Coordinated Turn Command System ( $V_{EAS} = 100$  Knots)

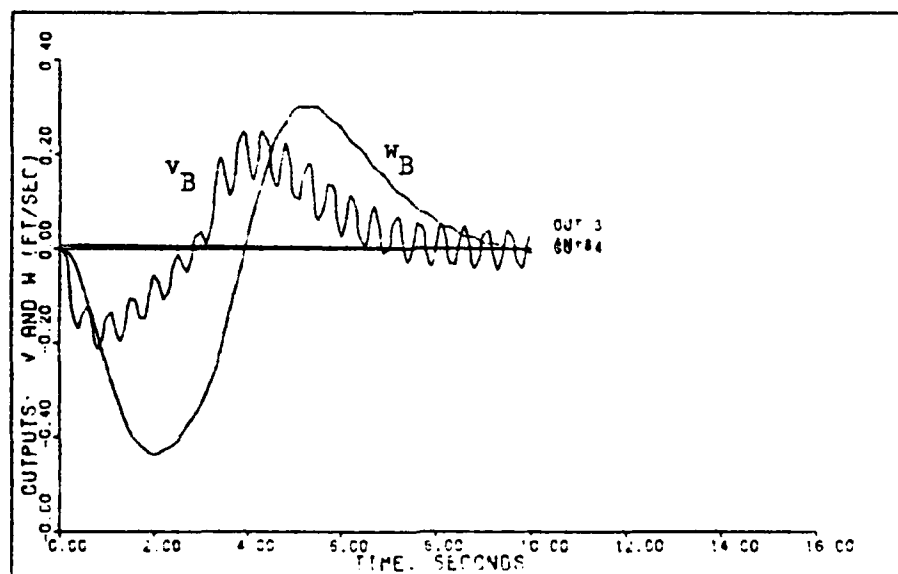


Figure 21c. Robust Controller Output Responses,  $v_B$  and  $w_B$ , for the Coordinated Turn Command System ( $V_{EAS} = 100$  Knots)

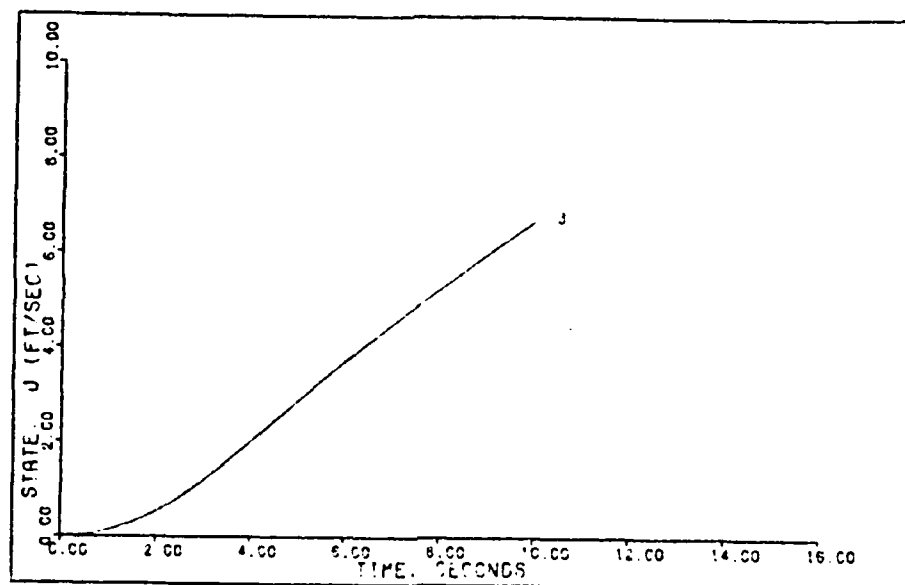


Figure 21d. Robust Controller State Response,  $u_B$ , for the Coordinated Turn Command System ( $V_{EAS} = 100$  Knots)

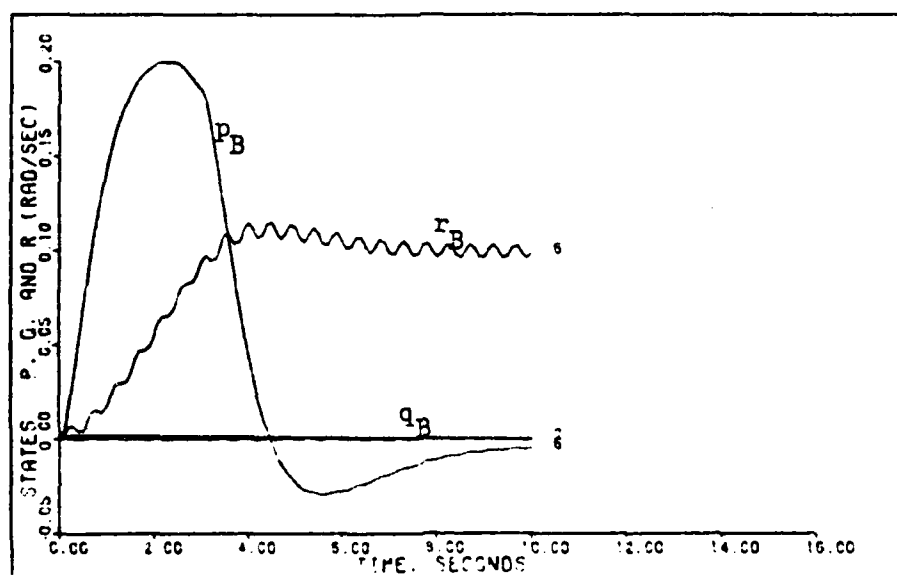


Figure 21e. Robust Controller State Responses,  $p_B$ ,  $q_B$ , and  $r_B$ , for the Coordinated Turn Command System ( $V_{EAS} = 100$  Knots)

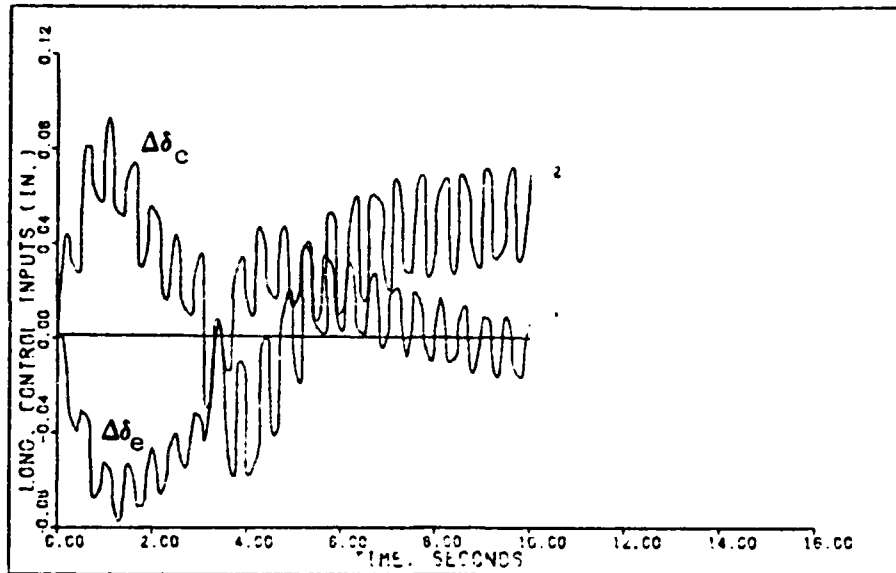


Figure 21f. Robust Controller Longitudinal Control Surface Responses,  $\Delta\delta_e$  and  $\Delta\delta_c$ , for the Coordinated Turn Command System ( $V_{EAS} = 100$  Knots)

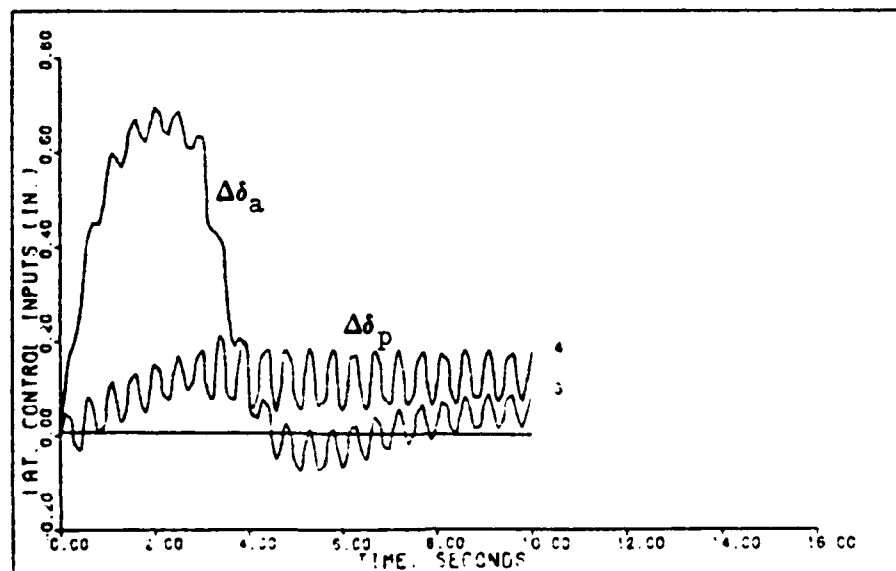


Figure 21g. Robust Controller Lateral Control Surface Responses,  $\Delta\delta_a$  and  $\Delta\delta_p$ , for the Coordinated Turn Command System ( $V_{EAS} = 100$  Knots)

Comparing Figures 21a.-21g. to Figures 9a.-9g. reveals that the robust controller reduces the magnitude and frequency of the oscillations experienced by the individual digital control law. It could be concluded that the robust controller stabilizes the system better than the individual control law.

Comparisons of the individual digital control law results to the robust controller results are listed in Tables V-9 - V-12 for the desired outputs.

Table V-9  
Coordinated Turn Results for the Output Response,  $\theta$

V EAS	M <sub>p</sub>	t <sub>p</sub>	M <sub>m</sub>	t <sub>m</sub>	FV	t <sub>s</sub>
60	0.00010521	0.9	-0.000099106	4.1	0.00002301	9.9
60R	0.000349798	1.1	-0.00025436	0	0.00015335	10
100	0.00029817	1.1	-0.0002789	4.2	0.00007846	10
100R	0.0001901	1.3	-0.0000874	4.3	0.0000937	10
140	0.000166257	6.1	-0.00002261	2.1	0.00013792	10
140A	0.0001639	6.1	-0.00002125	2.0	0.0001374	9.3

Table V-10  
Coordinated Turn Results for the Output Response,  $\phi$

V EAS	M <sub>p</sub>	t <sub>p</sub>	M <sub>m</sub>	t <sub>m</sub>	FV	t <sub>s</sub>
60	0.52641322	4.4	0	0	0.5234557	3.5
60R	0.58715576	4.5	0	0	0.5200745	7.4
100	0.545978	4.2	0	0	0.523831	5.6
100R	0.5839063	4.6	0	0	0.5226756	7.4
140	0.57912	4.5	0	0	0.523761	7.2
140A	0.57918	4.5	0	0	0.523777	7.2

Table V-11  
Coordinated Turn Results for the Output Response,  $v_B$

$V_{EAS}$	$M_p$	$t_p$	$M_m$	$t_m$	FV	$t_s$
60	0.0226923	3.1	-0.02664617	0.1	0.0004735	10
60R	0.27968256	4.2	-0.1859034	0.5	-0.0088153	10
100	0.116272	3.5	-0.1067917	0.5	0.0515887	10
100R	0.24791514	4.3	-0.210376	0.8	0.0407919	10
140	0.2335084	3.9	-0.2035789	0.7	0.09211712	10
140A	0.19958	4.0	-0.202249	0.7	0.002178	10

Table V-12  
Coordinated Turn Results for the Output Response,  $w_B$

$V_{eas}$	$M_p$	$t_p$	$M_m$	$t_m$	FV	$t_s$
60	0.02664741	3.9	-0.04513320	0.7	-0.0043384	9.9
60R	0.5296735	5.3	-0.8855	2.1	-0.125963	9.9
100	0.1093917	4.4	-0.1465897	1.3	0.0009846	10
100R	0.30241226	5.4	-0.436832	2.0	0.00717331	10
140	0.19928899	5.1	-0.27393537	1.9	0.00613385	10
140A	0.20630	5.1	-0.298619	1.8	0.006909	10

The tables show that the individual control laws perform much better than the robust controller. The robust controller, however, provides a more stable response for the  $V_{EAS} = 100$  knots flight condition than the individual control law. Even though the robust controller results are not as tight as the individual control laws, they are still acceptable.



### Vertical Rate Command System

The vertical rate command system is given by Equation (5.3). The five flight conditions for the coordinated turn are  $V_{EAS} = 20, 40, 60, 100$  and  $140$  knots. Since the  $V_{EAS} = 140$  knots is the highest (in terms of  $V_{EAS}$ ), it is chosen as the robust controller to be implemented at the other flight conditions. The control law for the  $V_{EAS} = 140$  knots flight condition is

$$\begin{aligned} \underline{u}(kT) = [50\text{Hz}] & \begin{bmatrix} 1.387 & -0.3071 & -0.0006461 & 0.1996 \\ -1.203 & 0.3284 & -0.01706 & 0.2881 \\ -0.02173 & 2.054 & 0.001875 & 0.5624 \\ -0.1234 & -0.1624 & -0.001688 & 0.8198 \end{bmatrix} \underline{e}(kT) \\ & + \begin{bmatrix} 1.387 & -0.3071 & -0.0006461 & 0.1996 \\ -1.203 & 0.3284 & -0.01706 & 0.2881 \\ -0.02173 & 2.054 & 0.001875 & 0.5624 \\ -0.1234 & -0.1624 & -0.001688 & 0.8198 \end{bmatrix} \underline{z}(kT) \end{aligned} \quad (5.10)$$

For the  $V_{EAS} = 20$  knots flight condition, the closed-loop denominator is:

$$\begin{aligned} & (.1000\text{E}+01) S^{**} 12 \quad (-.3642\text{E}+02) + J(0. \quad ) \\ & (.7817\text{E}+02) S^{**} 11 \quad (-.2976\text{E}+01) + J(.4075\text{E}+01) \\ & (.2131\text{E}+04) S^{**} 10 \quad (-.2976\text{E}+01) + J(-.4075\text{E}+01) \\ & (.2706\text{E}+05) S^{**} 9 \quad (-.2207\text{E}+02) + J(0. \quad ) \\ & (.1987\text{E}+06) S^{**} 8 \quad (-.5224\text{E}+01) + J(0. \quad ) \\ & (.9196\text{E}+06) S^{**} 7 \quad (-.4288\text{E}+01) + J(0. \quad ) \\ & (.2678\text{E}+07) S^{**} 6 \quad (-.1061\text{E}+01) + J(.2414\text{E}+00) \\ & (.4712\text{E}+07) S^{**} 5 \quad (-.1061\text{E}+01) + J(-.2414\text{E}+00) \\ & (.4817\text{E}+07) S^{**} 4 \quad (-.1280\text{E}+01) + J(0. \quad ) \\ & (.2646\text{E}+07) S^{**} 3 \quad (-.7750\text{E}+00) + J(0. \quad ) \\ & (.6275\text{E}+06) S^{**} 2 \quad (.1904\text{E}-01) + J(0. \quad ) \\ & (.1774\text{E}+05) S^{**} 1 \quad (-.5695\text{E}-01) + J(0. \quad ) \\ & (-.5840\text{E}+03) S^{**} 0 \quad \text{DENOMINATOR GAIN} = .1000\text{E}+01 \end{aligned} \quad (5.11)$$

It should be noted that the robust controller has produced an unstable pole at 0.01904.

The figures of merit for the  $V_{EAS} = 20$  knots flight condition are presented in Table V-13 and the time response plots in Figures 22a.-22e.

Table V-13  
Vertical Rate Results ( $V_{EAS} = 20$  knots) for the  
Robust Controller

Outputs	$M_p$	$t_p$	$M_m$	$t_m$	FV	$t_s$
$\theta$	0.00035173	0.5	-0.00138995	2.5	0.000087675	8.2
$\phi$	0.000159426	3.2	-0.0024429	1.1	-0.0001367	8.4
$w_B$	0	0	-20.50402	2.6	-20.0027269	3.0
$r_B$	0.00578838	0.5	-0.0016736	2.7	0.0001686	7.2

It should be remembered that the desired output response  $\dot{h}_E = -w_B$ .

For the  $V_{EAS} = 40$  knots flight condition, the closed-loop denominator is:

$$\begin{aligned}
 & (.1000E+01) S^{**} 12 \quad (-.3737E+02) + J(0. \quad ) \\
 & (.7935E+02) S^{**} 11 \quad (-.2225E+02) + J(0. \quad ) \\
 & (.2183E+04) S^{**} 10 \quad (-.2543E+01) + J(.4214E+01) \\
 & (.2776E+05) S^{**} 9 \quad (-.2543E+01) + J(-.4214E+01) \\
 & (.2036E+06) S^{**} 8 \quad (-.6387E+01) + J(0. \quad ) \\
 & (.9528E+06) S^{**} 7 \quad (-.4097E+01) + J(0. \quad ) \\
 & (.2833E+07) S^{**} 6 \quad (-.8491E+00) + J(.2160E+00) \\
 & (.5079E+07) S^{**} 5 \quad (-.8491E+00) + J(-.2160E+00) \\
 & (.5273E+07) S^{**} 4 \quad (-.1205E+01) + J(.1727E+00) \\
 & (.2954E+07) S^{**} 3 \quad (-.1205E+01) + J(-.1727E+00) \\
 & (.7366E+06) S^{**} 2 \quad (-.2270E-01) + J(.4671E-01) \\
 & (.3454E+05) S^{**} 1 \quad (-.2270E-01) + J(-.4671E-01) \\
 & (.1618E+04) S^{**} 0 \quad \text{DENOMINATOR GAIN} = .1000E+01
 \end{aligned} \tag{5.12}$$

It should be noted that the robust controller has produced all stable poles for the closed-loop system.

The figures of merit for the  $V_{EAS} = 40$  knots flight condition are presented in Table V-14 and the time response plots in Figures 23a. - 23f.

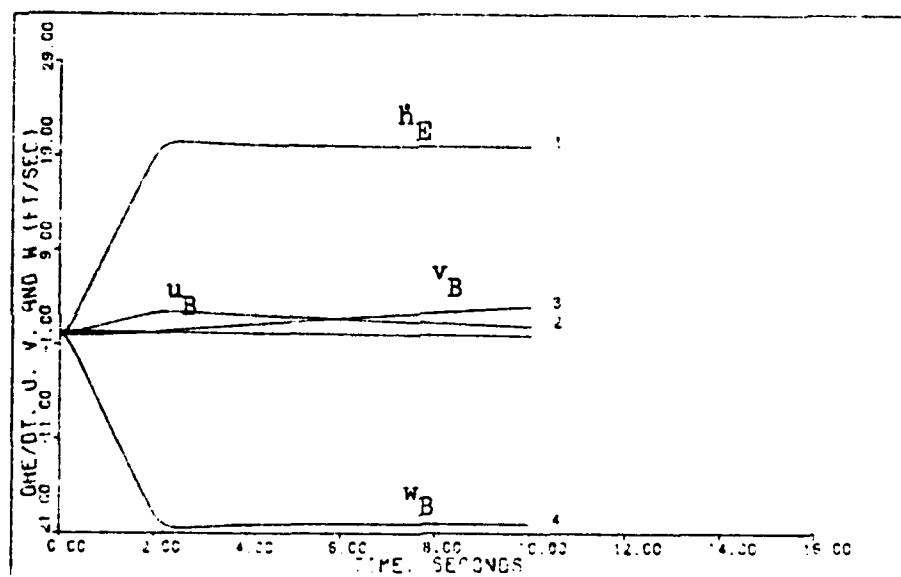


Figure 22a. Robust Controller Output Responses,  $\dot{h}_E$  and  $w_B$ , and State Responses,  $u_B$  and  $v_B$ , for the Vertical Rate Command System ( $V_{EAS} = 20$  Knots)

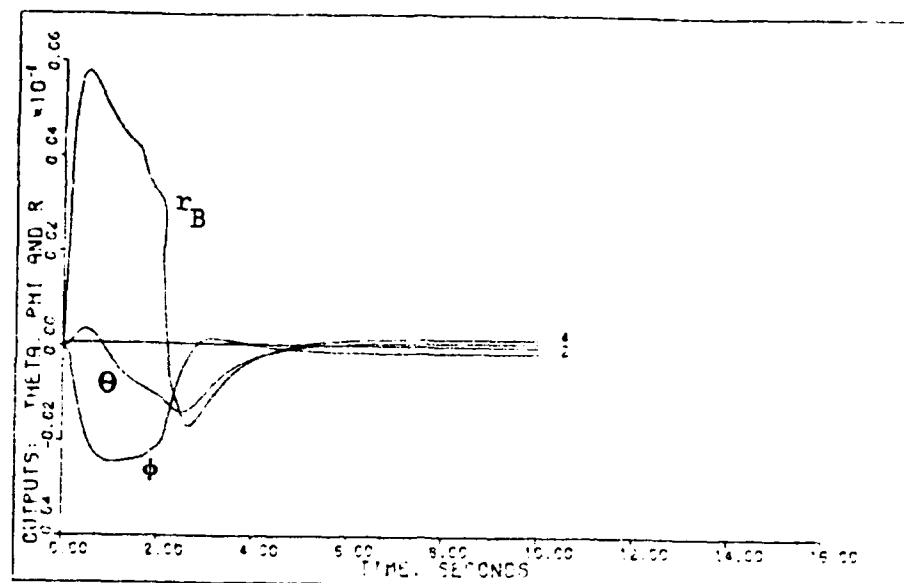


Figure 22b. Robust Controller Output Responses,  $\theta$  and  $\phi$ (rad), and  $r_B$ (rad/sec) for the Vertical Rate Command System ( $V_{EAS} = 20$  Knots)

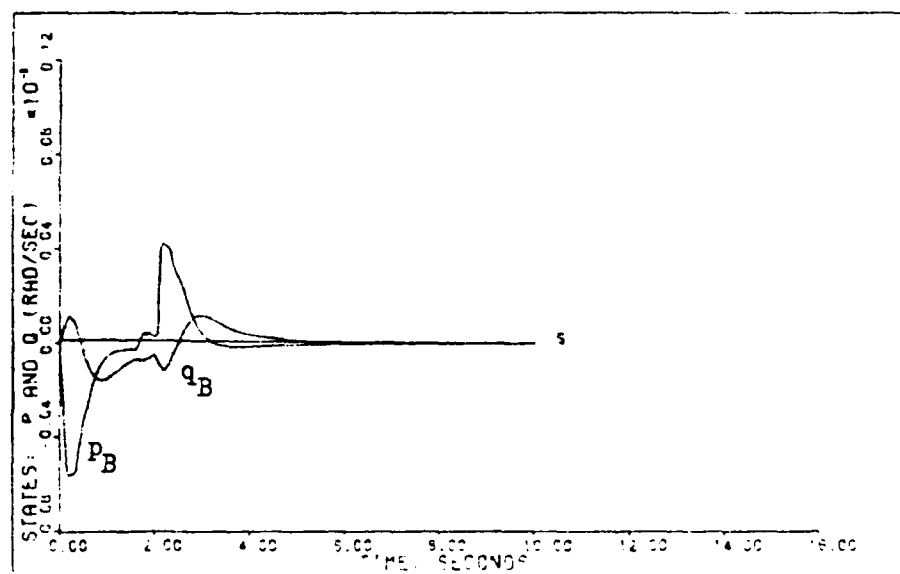


Figure 22c. Robust Controller State Responses,  $p_B$  and  $q_B$ , for the Vertical Rate Command System ( $V_{EAS} = 20$  Knots)

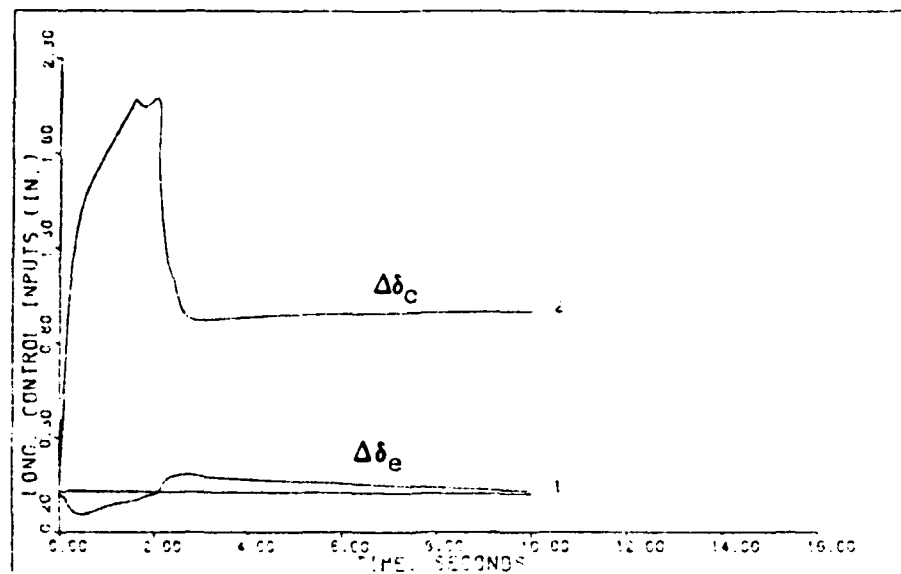


Figure 22d. Robust Controller Longitudinal Control Surface Responses,  $\Delta\delta_e$  and  $\Delta\delta_c$ , for the Vertical Rate Command System ( $V_{EAS} = 20$  Knots)

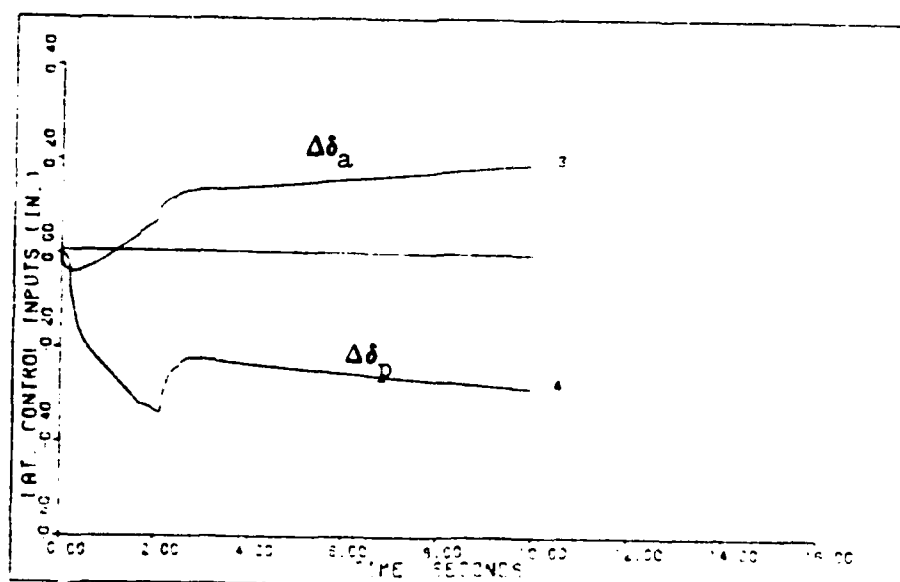


Figure 22e. Robust Controller Lateral Control Surface Responses,  $\Delta\delta_a$  and  $\Delta\delta_p$ , for the Vertical Rate Command System ( $V_{EAS} = 20$  Knots)

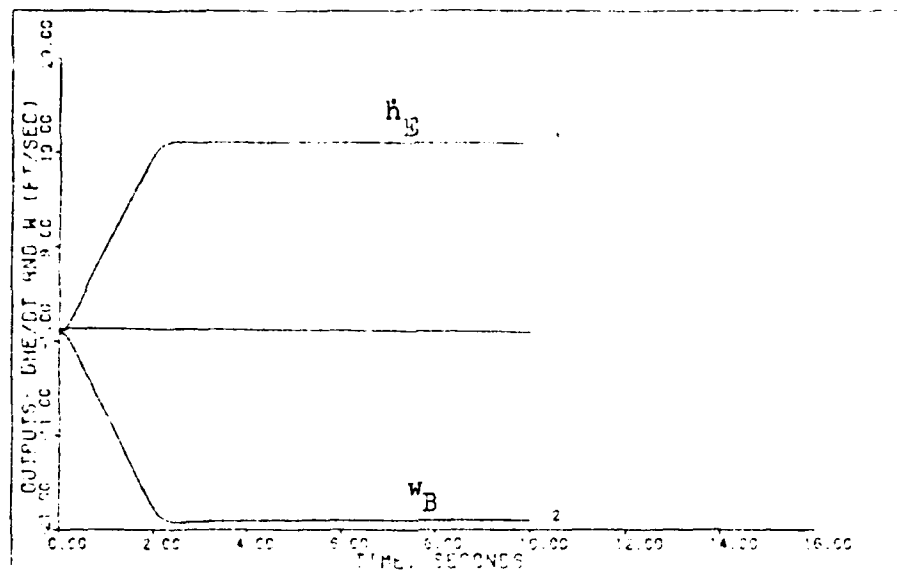


Figure 23a. Robust Controller Output Responses,  $\dot{h}_E$  and  $w_B$ , for the Vertical Rate Command System ( $V_{EAS} = 40$  Knots)

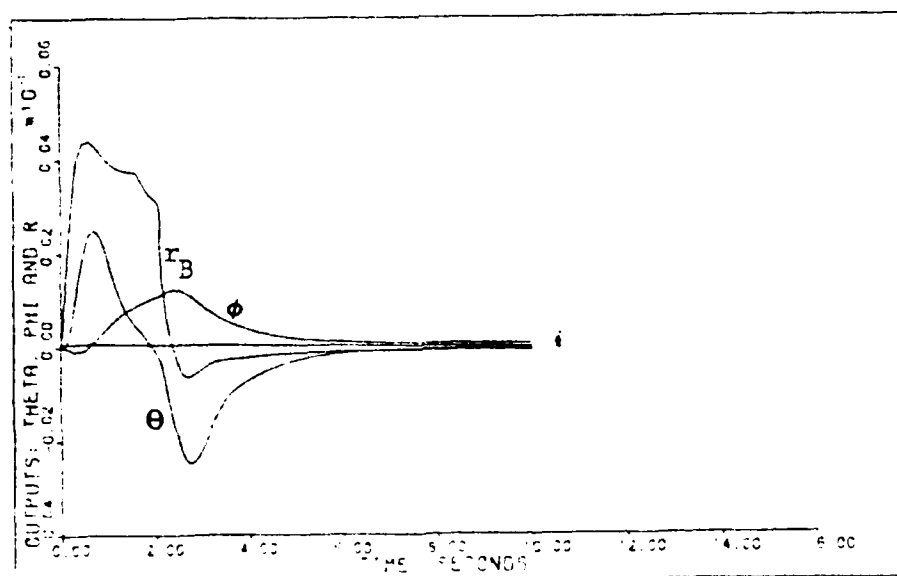


Figure 23b. Robust Controller Output Responses,  $\theta$  and  $\phi$ (rad), and  $r_B$ (rad/sec) for the Vertical Rate Command System ( $V_{EAS} = 40$  Knots)

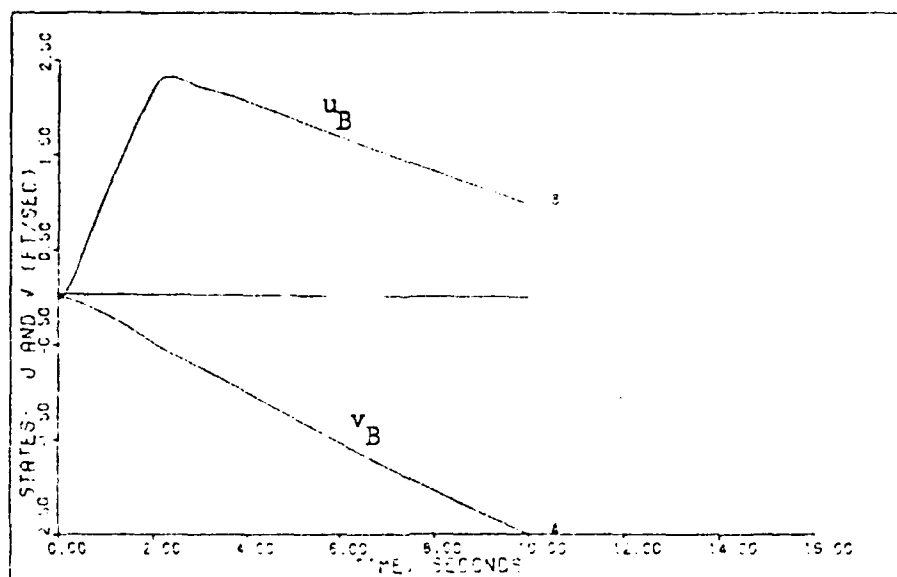


Figure 23c. Robust Controller State Responses,  $u_B$  and  $v_B$ , for the Vertical Rate Command System ( $V_{EAS} = 40$  Knots)

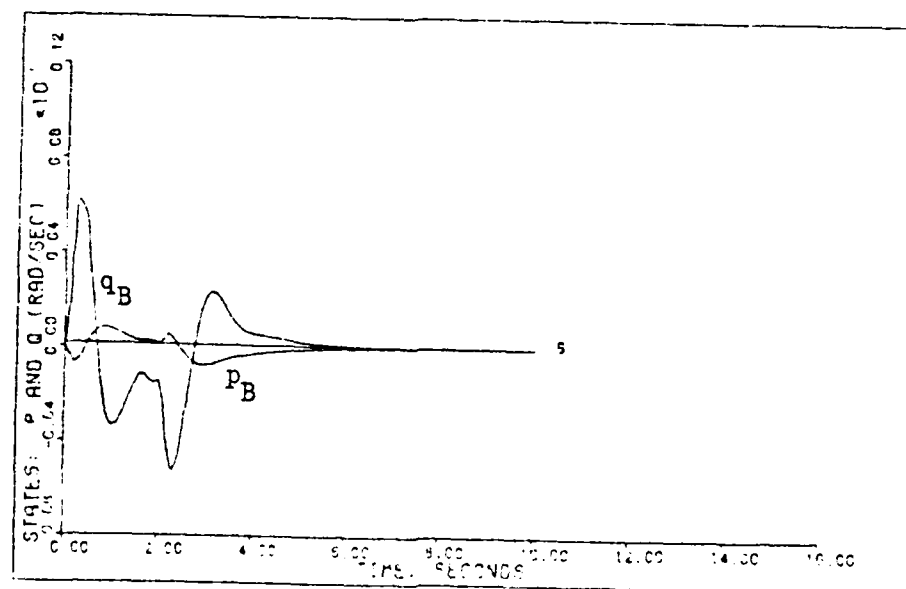


Figure 23d. Robust Controller State Responses,  $p_B$  and  $q_B$ , for the Vertical Rate Command System ( $V_{EAS} = 40$  Knots)

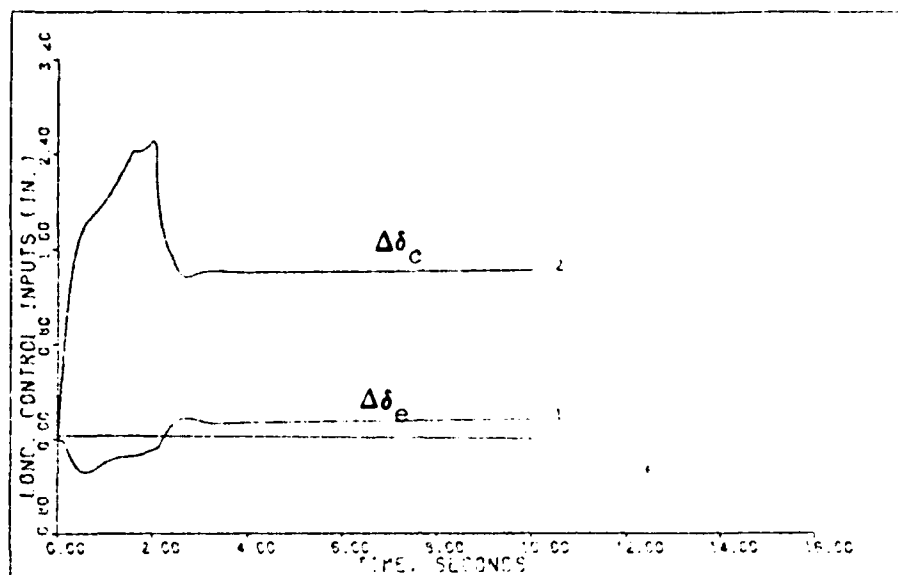


Figure 23e. Robust Controller Longitudinal Control Surface Responses,  $\Delta\delta_e$  and  $\Delta\delta_c$ , for the Vertical Rate Command System ( $V_{EAS} = 40$  Knots)

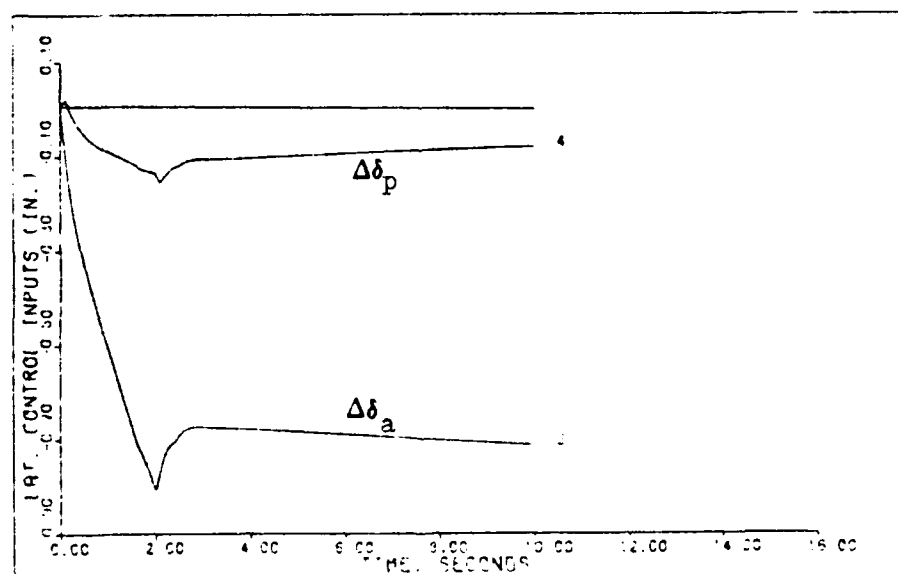


Figure 23f. Robust Controller Lateral Control Surface Responses,  $\Delta\delta_a$  and  $\Delta\delta_p$ , for the Vertical Rate Command System ( $V_{EAS} = 40$  Knots)



Table V-14  
Vertical Rate Results ( $V_{EAS} = 40$  knots) for the  
Robust Controller

Outputs	$M_p$	$t_p$	$M_m$	$t_m$	FV	$t_s$
$\theta$	0.002486216	0.7	-0.0024558	2.8	-0.000040161	9.8
$\phi$	0.001229876	2.4	-0.00009757	0.4	0.000069291	9.6
$w_B$	0	0	-20.24889	2.6	-19.9939268	2.2
$r_B$	0.00438707	0.6	-0.00063305	2.7	-0.00006738	9.7

For the  $V_{EAS} = 60$  knots flight condition, the closed-loop denominator is:

$$\begin{aligned}
 & (.1000E+01) S^{**} 12 \quad (-.3671E+02) + J(0. \quad ) \\
 & (.8377E+02) S^{**} 11 \quad (-.2619E+02) + J(0. \quad ) \\
 & (.2461E+04) S^{**} 10 \quad (-.2234E+01) + J(.4277E+01) \\
 & (.3281E+05) S^{**} 9 \quad (-.2234E+01) + J(-.4277E+01) \\
 & (.2461E+06) S^{**} 8 \quad (-.8284E+01) + J(0. \quad ) \\
 & (.1184E+07) S^{**} 7 \quad (-.3994E+01) + J(0. \quad ) \\
 & (.3641E+07) S^{**} 6 \quad (-.1018E+01) + J(.1685E+00) \\
 & (.6707E+07) S^{**} 5 \quad (-.1018E+01) + J(-.1685E+00) \\
 & (.7093E+07) S^{**} 4 \quad (-.1175E+01) + J(0. \quad ) \\
 & (.4029E+07) S^{**} 3 \quad (-.8519E+00) + J(0. \quad ) \\
 & (.1020E+07) S^{**} 2 \quad (-.3308E-02) + J(0. \quad ) \\
 & (.5114E+05) S^{**} 1 \quad (-.6064E-01) + J(0. \quad ) \\
 & (.1582E+03) S^{**} 0 \quad \text{DENOMINATOR GAIN} = .1000E+01
 \end{aligned} \tag{5.13}$$

It should be noted that the robust controller has produced all stable poles for the closed-loop system.

The figures of merit for the  $V_{EAS} = 60$  knots flight condition are presented in Table V-15 and the time response plots in Figures 24a. - 24h.

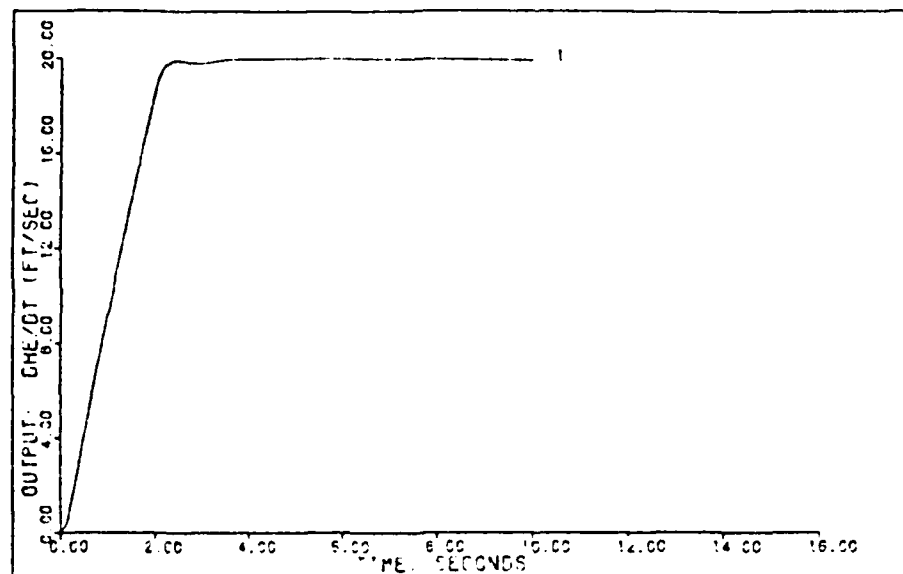


Figure 24a. Robust Controller Output Response,  $\dot{h}_E$ , for the Vertical Rate Command System ( $V_{EAS} = 60$  Knots)

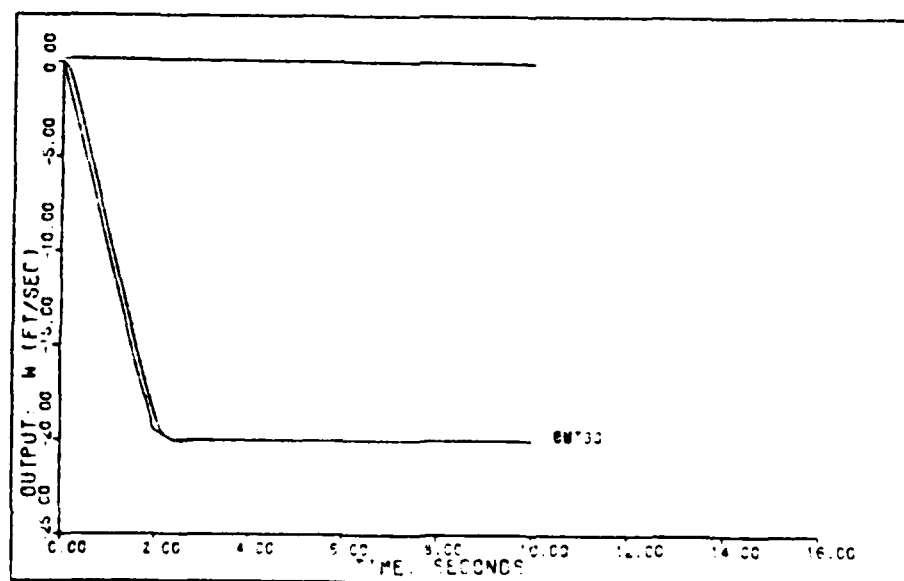


Figure 24b. Robust Controller Output Response,  $w_B$ , for the Vertical Rate Command System ( $V_{EAS} = 60$  Knots)

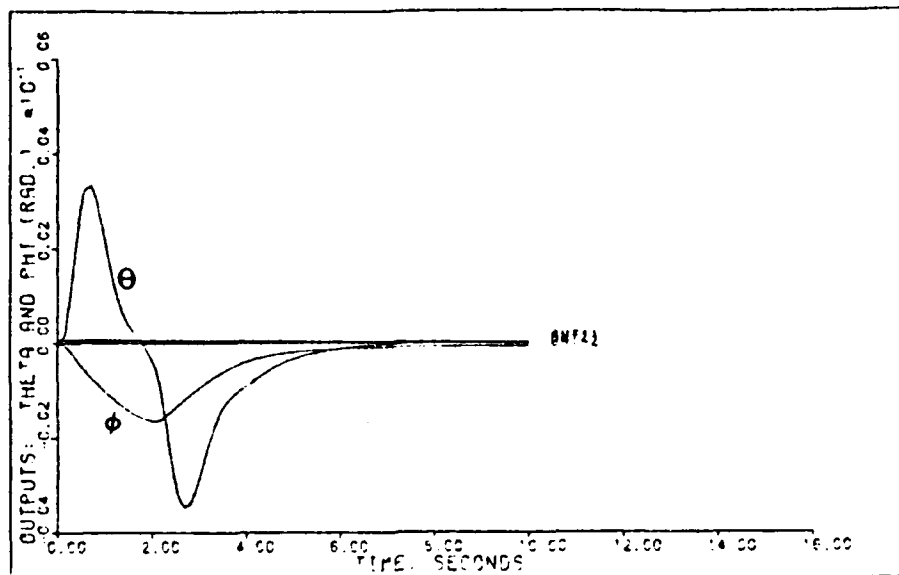


Figure 24c. Robust Controller Output Responses,  $\Theta$  and  $\phi$ , for the Vertical Rate Command System ( $V_{EAS} = 60$  Knots)

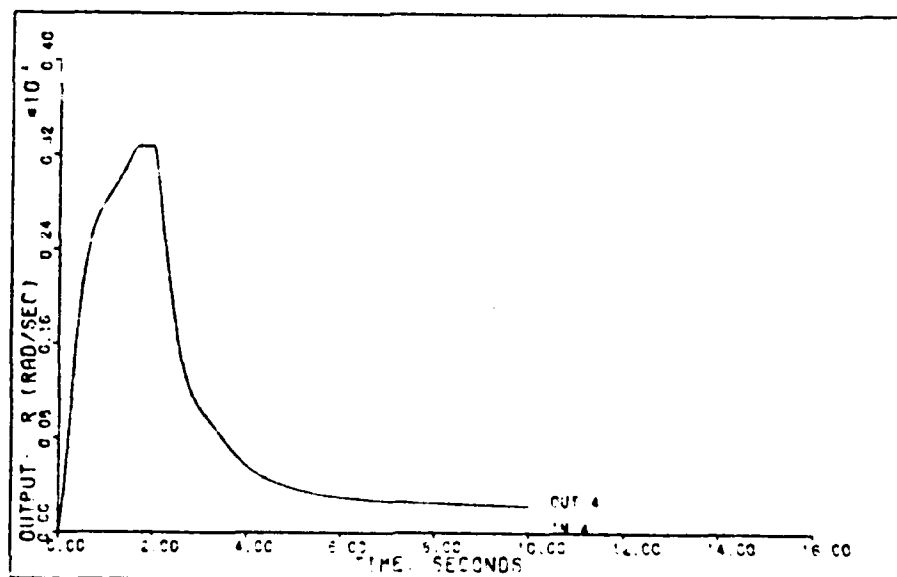


Figure 24d. Robust Controller Output Response,  $r_B$ , for the Vertical Rate Command System ( $V_{EAS} = 60$  Knots)

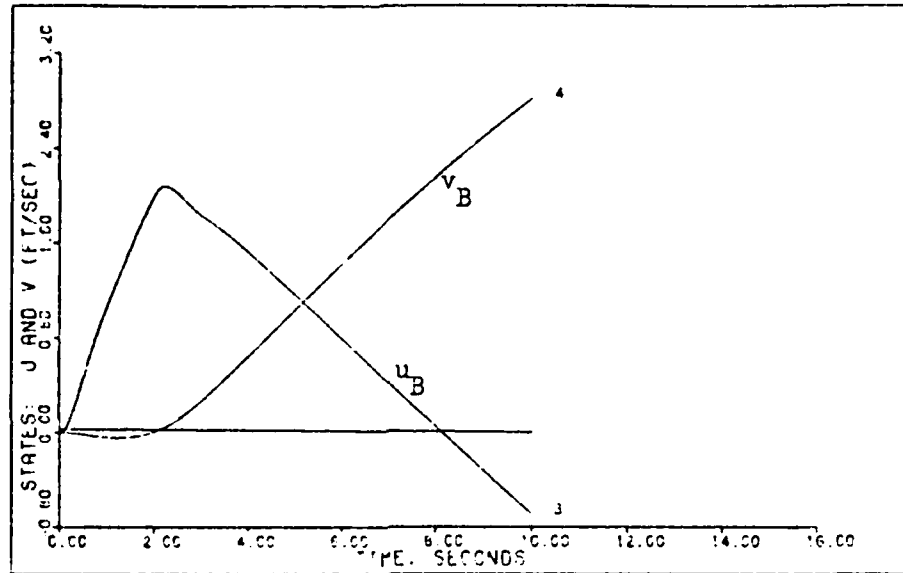


Figure 24e. Robust Controller State Responses,  $u_B$  and  $v_B$ , for the Vertical Rate Command System ( $V_{EAS} = 60$  Knots)

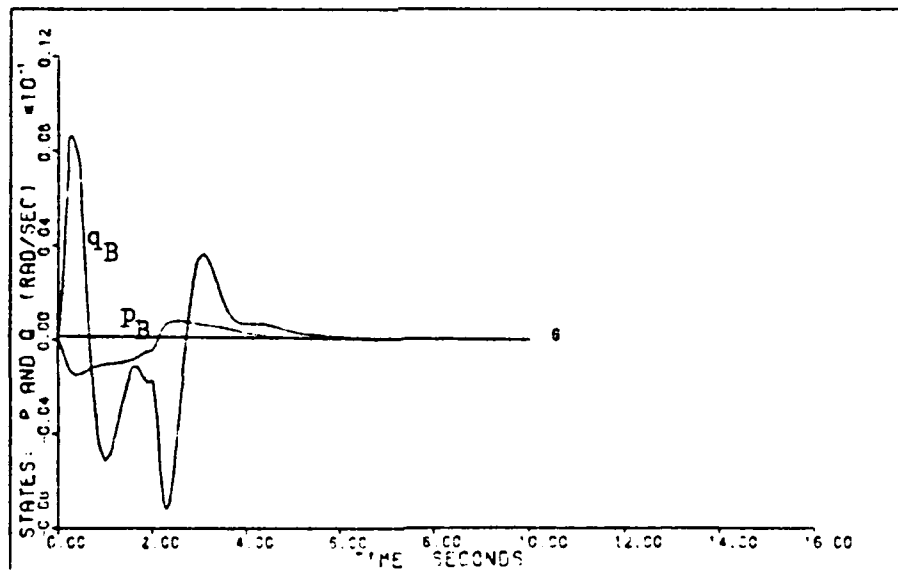


Figure 24f. Robust Controller State Responses,  $p_B$  and  $q_B$ , for the Vertical Rate Command System ( $V_{EAS} = 60$  Knots)

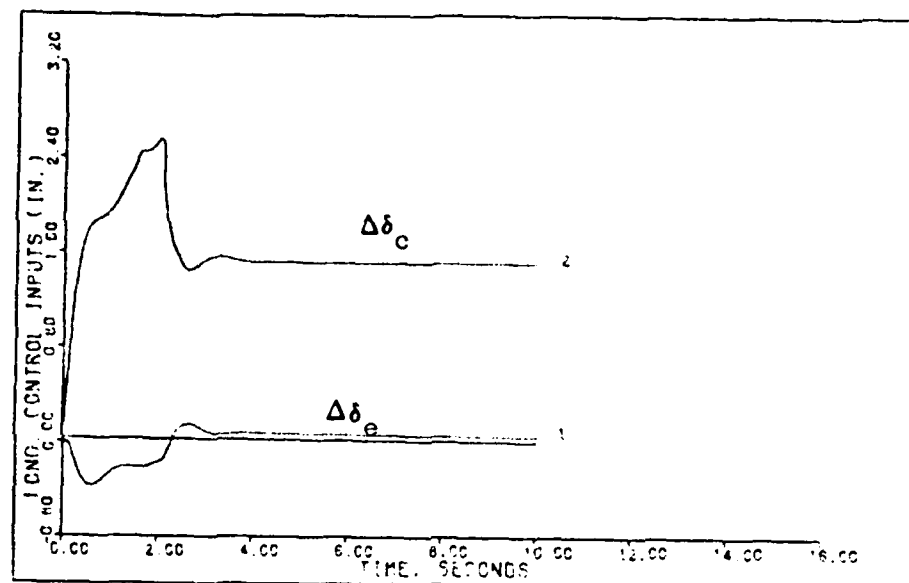


Figure 24g. Robust Controller Longitudinal Control Surface Responses,  $\Delta\delta_e$  and  $\Delta\delta_c$ , for the Vertical Rate Command System ( $V_{EAS} = 60$  Knots)

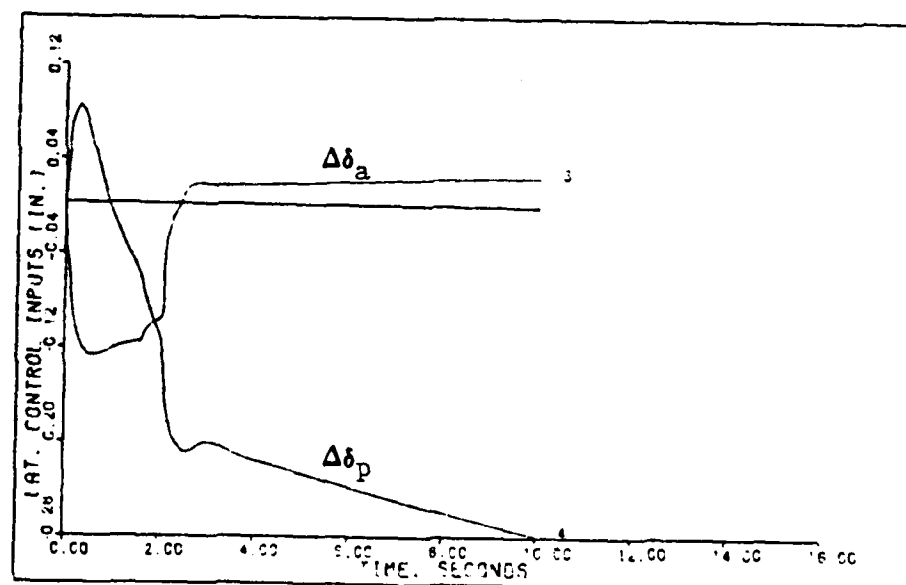


Figure 24h. Robust Controller Lateral Control Surface Responses,  $\Delta\delta_a$  and  $\Delta\delta_p$ , for the Vertical Rate Command System ( $V_{EAS} = 60$  Knots)

Table V-15  
Vertical Rate Results ( $V_{EAS} = 60$  knots) for the  
Robust Controller

Outputs	$M_p$	$t_p$	$M_m$	$t_m$	FV	$t_s$
$\theta$	0.003307	0.7	-0.0034546	2.7	0.000008605	9.9
$\phi$	0	0	-0.0016475	2.1	-0.000075719	9.7
$w_B$	0	0	-20.123626	2.6	-19.998419	2.2
$r_B$	0.0032747	1.8	0	0	0.000230178	9.6

For the  $V_{EAS} = 100$  knots flight condition, the denominator of the closed-loop transfer function is:

$$\begin{aligned}
 & (.1000E+01) S^{**} 12 \quad (-.3642E+02) + J(0. \quad ) \\
 & (.9246E+02) S^{**} 11 \quad (-.23251E+02) + J(0. \quad ) \\
 & (.3026E+04) S^{**} 10 \quad (-.2235E+01) + J(.4204E+01) \\
 & (.4424E+05) S^{**} 9 \quad (-.2235E+01) + J(-.4204E+01) \\
 & (.3487E+06) S^{**} 8 \quad (-.1089E+02) + J(0. \quad ) \\
 & (.1739E+07) S^{**} 7 \quad (-.3994E+01) + J(0. \quad ) \\
 & (.5529E+07) S^{**} 6 \quad (-.9016E+00) + J(.1419E+00) \\
 & (.1049E+08) S^{**} 5 \quad (-.9016E+00) + J(-.1419E+00) \\
 & (.1142E+08) S^{**} 4 \quad (-.1133E+01) + J(.1041E+00) \\
 & (.6749E+07) S^{**} 3 \quad (-.1133E+01) + J(-.1041E+00) \\
 & (.1852E+07) S^{**} 2 \quad (-.2711E-01) + J(0. \quad ) \\
 & (.1382E+06) S^{**} 1 \quad (-.7367E-01) + J(0. \quad ) \\
 & (.2514E+04) S^{**} 0 \quad \text{DENOMINATOR GAIN} = .1000E+01
 \end{aligned} \tag{5.14}$$

It should be noted that the robust controller produces all stable poles for the closed-loop system.

The figures of merit for the  $V_{EAS} = 100$  knots flight condition are presented in Table V-16 and the time response plots in Figure 25a. - 25h.

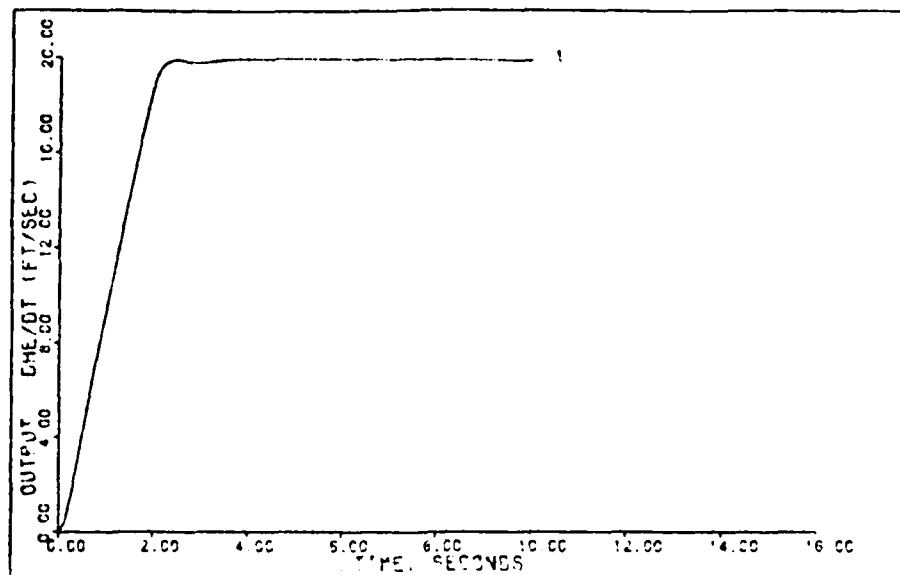


Figure 25a. Robust Controller Output Response,  $\dot{h}_E$ , for the Vertical Rate Command System ( $V_{EAS} = 100$  Knots)

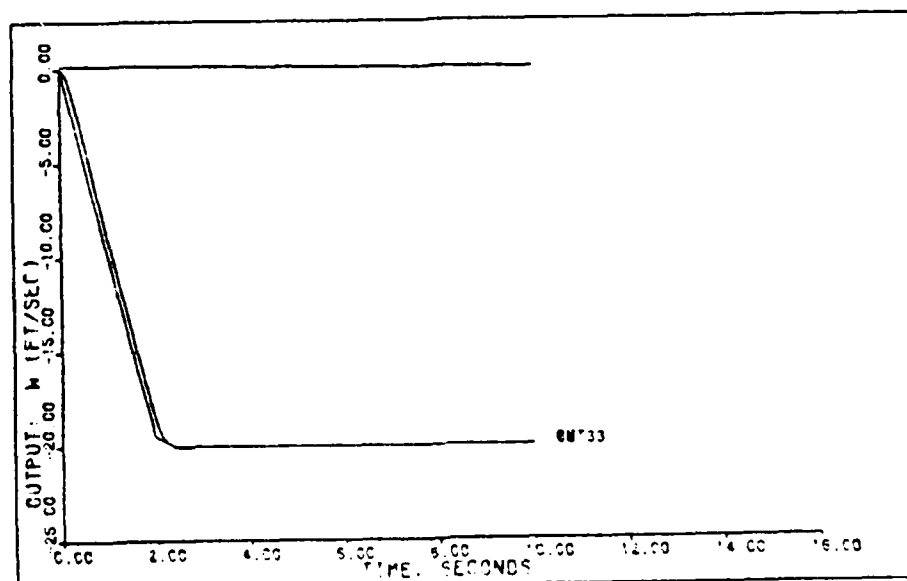


Figure 25b. Robust Controller Output Response,  $w_B$ , for the Vertical Rate Command System ( $V_{EAS} = 100$  Knots)

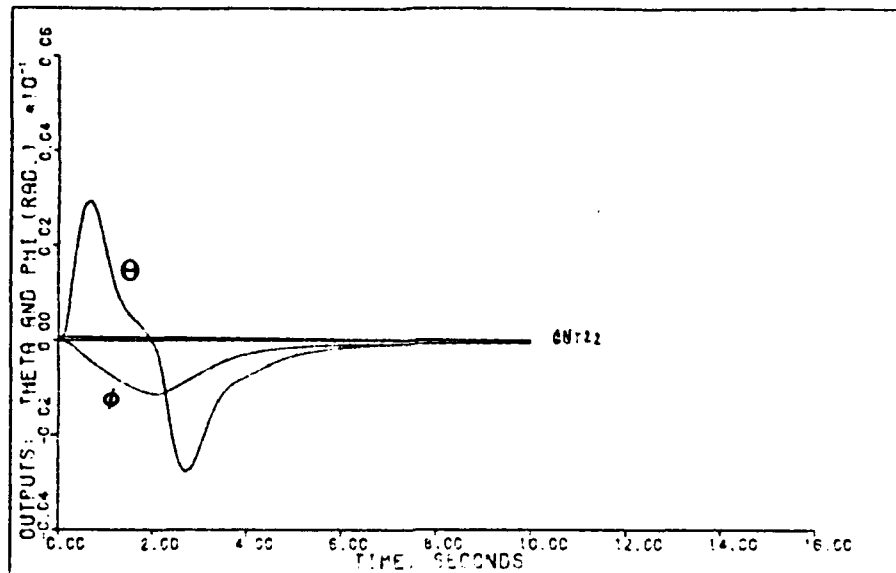


Figure 25c. Robust Controller Output Responses,  $\Theta$  and  $\phi$ , for the Vertical Rate Command System ( $V_{EAS} = 100$  Knots)

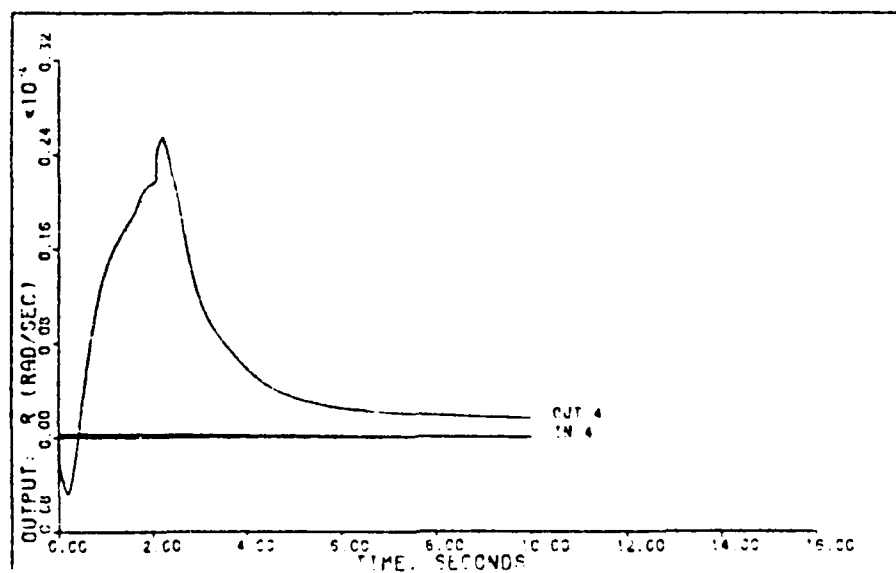


Figure 25d. Robust Controller Output Response,  $r_B$ , for the Vertical Rate Command System ( $V_{EAS} = 100$  Knots)



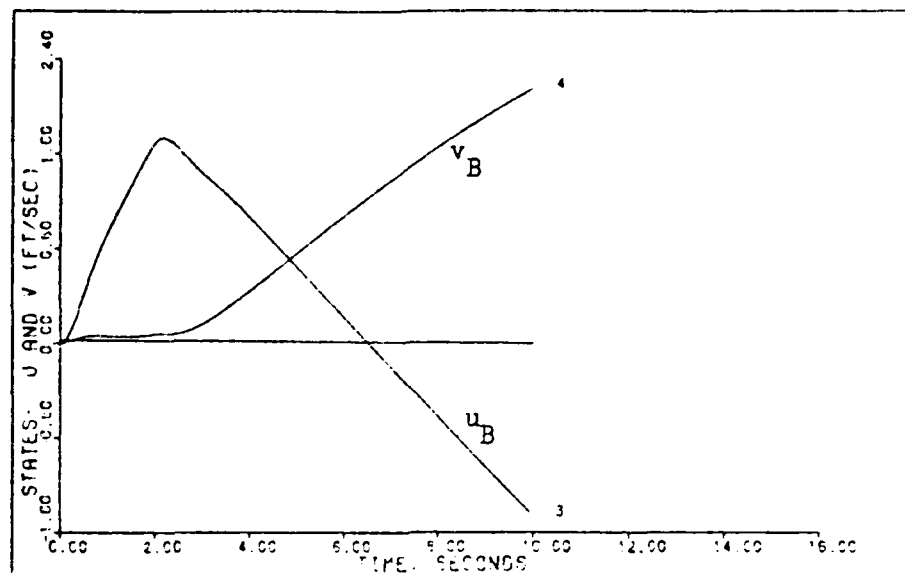


Figure 25e. Robust Controller State Responses,  $u_B$  and  $v_B$ , for the Vertical Rate Command System ( $V_{EAS} = 100$  Knots)

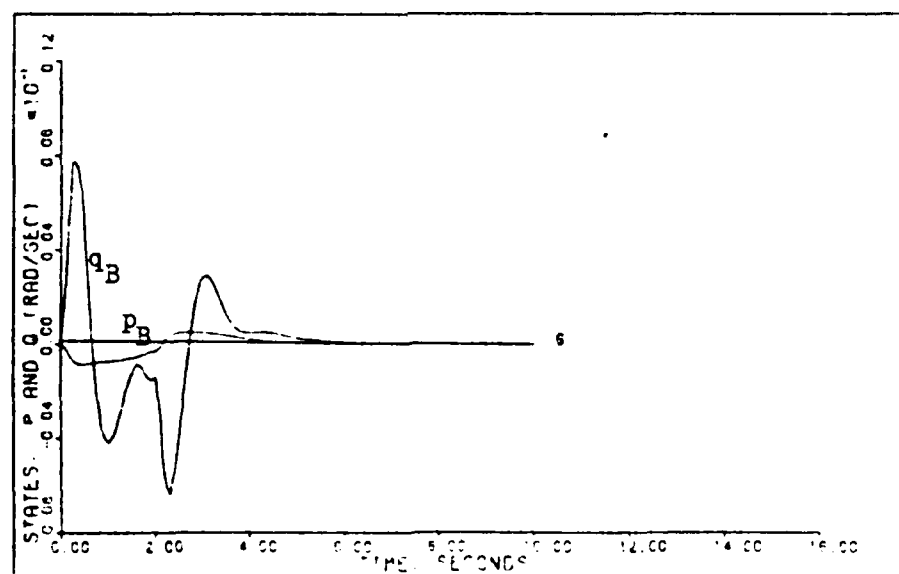


Figure 25f. Robust Controller State Responses,  $p_B$  and  $q_B$ , for the Vertical Rate Command System ( $V_{EAS} = 100$  Knots)

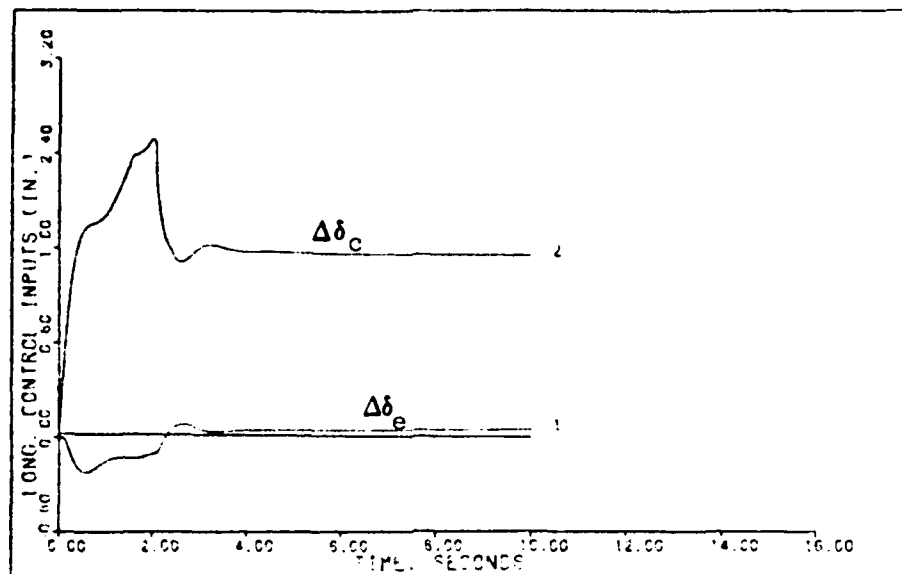


Figure 25g. Robust Controller Longitudinal Control Surface Responses,  $\Delta\delta_e$  and  $\Delta\delta_c$ , for the Vertical Rate Command System ( $V_{EAS} = 100$  Knots)

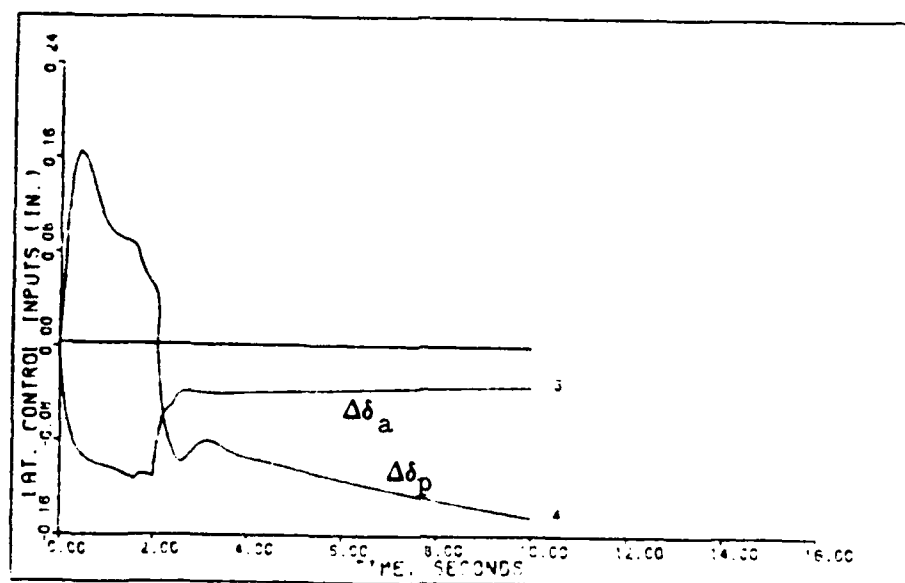


Figure 25h. Robust Controller Lateral Control Surface Responses,  $\Delta\delta_a$  and  $\Delta\delta_p$ , for the Vertical Rate Command System ( $V_{EAS} = 100$  Knots)

Table V-16  
Vertical Rate Results ( $V_{EAS} = 100$  knots) for the  
Robust Controller

Outputs	$M_p$	$t_p$	$M_m$	$t_m$	FV	$t_s$
$\theta$	0.00291965	0.7	-0.002765	2.7	-0.000049765	9.8
$\phi$	0	0	-0.0011394	2.1	-0.0000528	9.8
$w_B$	0	0	-20.103643	2.5	-19.999474	2.2
$r_B$	0.00254462	2.2	-0.0004801	0.2	0.000162637	9.8

As can be seen from Tables V-13 - V-16, the robust controller results are excellent for the four flight conditions. The one problem is the unstable pole produced by the robust controller at the  $V_{EAS} = 20$  knots flight condition.

Comparisons of the individual digital control law results to the robust controller results are listed in Tables V-17 - V-20 for the desired outputs.

Table V-19  
Vertical Rate Results for the Output Response,  $w_B$

$V_{EAS}$	$M_p$	$t_p$	$M_m$	$t_m$	FV	$t_s$
20	0	0	-20.38037	2.5	-19.998275	2.1
20R	0	0	-20.50402	2.6	-20.0027269	3.0
40	0	0	-20.253673	2.6	-19.99738	2.1
40A	0	0	-20.32646	2.8	-20.00837	2.2
40R	0	0	-20.24889	2.6	-19.9939268	2.2
60	0	0	-20.1735469	2.6	-19.999012	2.2
60R	0	0	-20.123626	2.6	-19.998419	2.2
100	0	0	-20.084928	2.7	-20.000272	2.2
100R	0	0	-20.103643	2.5	-19.999474	2.2
140	0	0	-20.027492	2.7	-20.000063	2.2

Table V-20  
Vertical Rate Results for the Output Response,  $r_B$

$V_{EAS}$	$M_p$	$t_p$	$M_m$	$t_m$	FV	$t_s$
20	0.0005902	2.0	0	0	0.00008046	9.1
20R	0.00578838	0.5	-0.0016736	2.7	0.0001686	7.2
40	0.0009603	2.0	-0.00004467	7.9	-0.00004164	9.6
40A	0.0011397	1.9	-0.00014126	0.1	-0.0000252	10
40R	0.00438707	0.6	-0.00063305	2.7	-0.00006738	9.7
60	0.00209503	2.0	0	0	0.00016207	9.6
60R	0.0032747	1.8	0	0	0.000230178	9.6
100	0.0024779	2.0	0	0	0.00014944	9.8
100R	0.00254462	2.2	-0.0004801	0.2	0.000167637	9.8
140	0.00141495	2.7	0	0	0.00017226	9.7

Table V-17  
Vertical Rate Results for the Output Response,  $\theta$

V EAS	M <sub>p</sub>	t <sub>p</sub>	M <sub>m</sub>	t <sub>m</sub>	FV	t <sub>s</sub>
20	0.00009159	8.8	-0.000613	2.1	0.00009114	7.3
20R	0.00035173	0.5	-0.00138995	2.5	0.000087675	8.2
40	0	0	-0.0014824	2.2	-0.00005151	9.7
40A	0.00016716	0.3	-0.0016025	2.4	-0.0000533	10
40R	0.002486216	0.7	-0.0024558	2.8	-0.000040161	9.8
60	0.000034546	8.9	-0.0018708	2.1	0.000033564	9.5
60R	0.00330708	0.7	-0.0034546	2.7	0.000008605	9.9
100	0	0	-0.0019481	2.2	-0.0000174	9.4
100R	0.00291965	0.7	-0.002765	2.7	-0.000049765	9.8
140	0	0	-0.0020574	2.2	-0.0001611	9.6

Table V-18  
Vertical Rate Results for the Output Response,  $\phi$

V EAS	M <sub>p</sub>	t <sub>p</sub>	M <sub>m</sub>	t <sub>m</sub>	FV	t <sub>s</sub>
20	0.000159426	0	-0.0008251	2.2	0.000104	9.0
20R	0.000159426	3.2	-0.0024429	1.1	-0.0001267	8.4
40	0.001416303	2.1	0	0	0.0000623	9.6
40A	0.00145751	2.0	-0.0000897	0.1	0.0000674	10
40R	0.001229876	2.4	-0.00009757	0.4	0.000069291	9.6
60	0	0	-0.00127329	2.1	-0.000051926	9.8
60R	0	0	-0.0016475	2.1	-0.000075719	9.7
100	0	0	-0.0010048	2.1	-0.0000464	9.8
100R	0	0	-0.0011394	2.1	-0.0000528	9.8
140	0	0	-0.00080998	2.2	-0.00003945	9.8

A close examination of Tables V-17 - V-20 reveals that the performance of the individual digital control laws has slightly tighter tracking than for the robust controller.

In general, the robust controllers show tight tracking performance slightly worse than the performances achieved by the individual digital control laws. The unstable pole encountered for the vertical rate command system at  $V_{EAS} = 20$  knots could possibly be eliminated by using the  $V_{EAS} = 60$  knots control law. The unstable poles produced by the robust controller for the yaw rate response at the  $V_{EAS} = 20$  knots and  $V_{EAS} = 40$  knots flight conditions could possibly be made stable by redesigning the  $V_{EAS} = 60$  knots control law. The tradeoff might be degraded performance at the  $V_{EAS} = 60$  knots flight condition if only one controller for all flight conditions is desired. However, as mentioned earlier, unstable systems can be further compensated by back-up mechanical systems and manual pilot inputs. Therefore, for a robust controller that provides tight tracking control over the entire flight spectrum, an unstable pole(s), which produces a very slow divergence can be overlooked.

## VI. CONCLUSIONS AND RECOMMENDATIONS

### Thesis Summary

This thesis effort is designed to show the applicability of Professor Brian Porter's control law techniques as applied to the UH-60A Black Hawk helicopter. Development of digital control laws for the yaw rate command system, the coordinated turn command system, and the vertical rate command system are considered. Each command system must perform the desired maneuver at its applicable flight conditions. The flight conditions for the UH-60A Black Hawk helicopter for this study are  $V_{EAS} = 20, 40, 60, 100, \text{ and } 140$  knots. Development of a robust controller is considered for each command system by implementing the individual digital control law developed at the highest flight condition (in terms of  $V_{EAS}$ ) at the other applicable flight conditions.

Chapter I presents an introduction to the need for a study in this area. Chapter II describes the required state space representation needed to model the helicopter's equations of motion. A brief summary of control law theory for the regular and irregular design techniques as well as the effects of transmission zeros is presented in Chapter III. Chapter IV describes the development of the control laws and presents the results achieved by the individual digital control laws for the three commanded maneuvers. Chapter V discusses the results achieved by the robust controllers with comparisons to the results achieved by the individual control laws.

Appendix A in this thesis contains the development of the equations of motion and the resulting computer program, NONSIM, which simulates a nonlinear, symmetrical aircraft at a constant flight condition. The

program NONSIM will eventually be implemented in MULTI giving the C.A.D. package a nonlinear simulation capability. The effects of adding a computational delay during the simulation for the helicopter are shown in Appendix B.

### Conclusions

This thesis concludes that digital tracker control laws can indeed be successfully designed for the UH-60A Black Hawk helicopter especially for the coordinated turn command system and the vertical rate command system. Controllers designed for the three maneuvers at their applicable flight conditions are found to tightly track the commanded inputs. However, a problem does exist in the yaw rate command system in that the dutch roll mode is present in the uncontrolled states,  $\phi$  and  $v_B$ .

Theory provides that total decoupling of outputs is achievable. However, the high-gain nature of the design technique would require large control surface deflections, unless the input vector  $\underline{u}$  is shaped to meet performance specifications. Thus the control law parameter,  $\epsilon$ , is adjusted to reduce the control surface commands and still meet the overall tracking requirements in a satisfactory manner. There is some acceptable interaction between outputs. It is acknowledged that the designs are not optimum in every sense; however, the design method is a viable alternative to other multivariable techniques. The major advantages of this design technique based on preliminary designs are:

1. The ease of design and the ability to fine tune to specific requirements.



2. The use of output feedback without the need of full state information.

3. The high degree of decoupling available.

4. The similarity in developing continuous and discrete designs.

The robust controller for each of the three maneuvers shows results slightly worse than the results achieved by the individual control laws. Robustness, in this study, is the ability of a constant gain controller, designed for a particular flight condition, to adequately perform the same maneuver at the other flight conditions. Except for the three flight conditions in which unstable poles are produced by the robust controller, the robust controller could be implemented in the digital computer instead of the individual control laws. The problem of unstable poles using a robust controller can be ignored as long as the effects of these poles are small over the time interval of interest and if there are back-up mechanical systems and manual pilot inputs. The advantage of a robust controller to avoid gain scheduling over a wide range of flight conditions is enough to neglect unstable poles that have minimal effects on the desired outputs.

#### Recommendations

There are several areas of interest which should be investigated in the future. It was noted for the coordinated turn command system that there existed high frequency oscillations in some outputs for the  $V_{EAS} = 100$  and 140 knots flight conditions. These oscillations have appeared in other theses (Ref 2), but the origin of these oscillations is still a mystery. One hypothesis suggests that the oscillations have some correlation to the sampling frequency. Therefore, one area of future

research is to find the cause of the oscillations and to remedy the problem.

Another area to be researched is the excitation of the dutch roll mode in the yaw rate command system. The limitation that the number of outputs must equal the number of control surfaces restricts satisfactory results for this maneuver. An area of future research would be the development of another approach that would be implemented when the number of desired outputs to be controlled is greater than the number of control surfaces.

Final recommendations suggest improvements in the computer program MULTI. These include, but are not limited to:

1. Implementation of anti-windup compensation to prevent saturation of the control surface limits.
2. The addition of compensation filters to handle cases in which two or more transmission zeros are located at the origin or in the right-half of the  $s$ -plane.

## Bibliography

1. Balfour, A. and D. H. Marwick. Programming in Standard Fortran 77. New York: North-Holland Inc., 1979.
2. Barfield, A. Finley. "Multivariable Control Laws for the AFIT/F-16". MS Thesis. Air Force Institute of Technology, Wright-Patterson AFB, OH; September 1983.
3. Blakelock, John H. Automatic Control of Aircraft and Missiles. New York: John Wiley and Sons, Inc., 1965.
4. D'Azzo, John J., and Constantine H. Houppis. Linear Control Systems Analysis and Design (Second Edition). New York: McGraw-Hill Book Company, 1981.
5. Etkin, Bernard. Dynamics of Atmospheric Flight. New York: John Wiley & Sons, Inc., 1972.
6. Falb, P. L. and W. A. Wolovich. "Decoupling in the Design and Synthesis of Multivariable Control Systems," IEEE Transaction on Automatic Control, AC-12(6): 651-659 (December 1967).
7. Lamont, Gary B., and Constantine H. Houppis. Digital Control System: Theory, Hardware, Software. McGraw-Hill Book Company, to be published.
8. Lewis, Tom. High-Gain Error Actuated Flight Control Systems for Continuous Multivariable Plants. MS Thesis. Air Force Institute of Technology, Wright-Patterson AFB, OH; December 1982.
9. Porter, B. "Asymptotic Properties of Linear Multivariable Continuous-Time Tracking Systems Incorporating High-Gain Error Actuated Controllers," International Journal of Systems Science, 10(12): 1433-1444 (December 1979).
10. Porter, B. "Asymptotic Properties of Linear Multivariable Discrete-Time Tracking Systems Incorporating Fast Sampling Error-Actuated Controllers," International Journal of Systems Science, 11(11): 1279-1293 (November 1980).
11. Porter, B. "Computation of the Zeros of Linear Multivariable Systems," International Journal of Systems Science, (10(12): 1427-1432 (December 1979).
12. Porter, B. and A. Bradshaw. "Design of Linear Multivariable Discrete-Time Tracking Systems Incorporating Fast-Sampling Error-Actuated Controllers," International Journal of Systems Science, 11(7): 817-826 (July 1980).

13. Porter, Douglas S. Design and Analysis of a Multivariable Digital Controller for the A-7D DIGITAC II Aircraft and the Development of an Interactive Computer Design Program. MS Thesis. Air Force Institute of Technology, Wright-Patterson AFB, OH; December 1981 (AFIT/GE/EE/81D-48)
14. Porter, B. Design of High Performance Tracking Systems. USAME/DC/120/81. Air Force Flight Dynamics Laboratory, Wright-Patterson AFB, Ohio.
15. Porter, B. "Design of Tunable Non-undershooting Servomechanism," Correspondence with Dr. J. J. D'Azzo, Wright-Patterson AFB, Ohio: Air Force Institute of Technology.
16. Porter, B. "Singular Perturbation Methods in the Design of Tracking Systems Incorporating Error-Actuated Controllers for Plants with Explicit Actuator Dynamics," International Journal of Control, 35(2): 383-389.
17. Porter, B. and A. Bradshaw. "Singular Perturbation Methods in the Design of Tracking Systems Incorporating Fast Sampling Error-Actuated Controllers," International Journal of Systems Science, 12(10): 1181-1192 (October 1981).
18. Porter, B., and J. J. D'Azzo. "Transmission Zeros of Linear Multivariable Continuous-Time System", Electronic Letters, 13(24): 753-755 (November 24, 1977).
19. Ridgely, D. Brett, Siva S. Banda, and John J. D'Azzo. "Decoupling of High Gain Multivariable Tracking Systems." Paper No. 83-0280 presented at the AIAA 21st Aerospace Sciences Conference, Reno, Nevada, 10-13 January 1983.
20. Rosenbrock, H. H. "The Zeros of a System," International Journal of Control, 18 (2): 297-299 (1973).

APPENDIX A

## Appendix A

### Nonlinear simulation of a Symmetrical Aircraft

One addition to MULTI that has been recommended by previous theses is the simulation of a nonlinear symmetrical aircraft. Appendix A contains the equations of motion needed for the simulation, the resulting program called NONSIM, and a brief output simulation of the program's capabilities. The equations of motion are written in the body-axis coordinate system. The following assumptions are made in developing the equations of motion:

1. The aircraft is a rigid body, and mass is constant.
2. The earth's surface is an inertial reference frame.
3. The atmosphere is assumed fixed with respect to the earth.
4. Aerodynamics are fixed for a particular flight condition.

The last assumption could be eliminated if a processor array could be employed. For changing flight conditions, the processor array would refer to aerodynamic tables and graphs, interpolate between points, and provide the new data to the on-going simulation.

Currently, program NONSIM is an independent program to be integrated into MULTI at a later date. Things that must be considered when integrating NONSIM into MULTI are:

1. The control surfaces of NONSIM must be the same as the u vector in MULTI.
2. NONSIM must be a separate overlay that inputs its own data file but uses MULTI's simulation option.

The program NONSIM simulates any nonlinear symmetrical aircraft that can be modeled by the following equations:

Force Equations:

$$\dot{u} = \frac{1}{m} [X_a + T_{x_B} - mg \sin \theta] + rv - qw \quad (A-1)$$

$$\dot{v} = \frac{1}{m} [Y + T_{y_B} + mg \sin \phi \cos \theta] + pw - ru \quad (A-2)$$

$$\dot{w} = \frac{1}{m} [Z_a + T_{z_B} + mg \cos \phi \cos \theta] + qu - pv \quad (A-3)$$

Moment Equations:

$$\begin{aligned} \dot{p} = & \frac{I_{yy} I_{zz}}{\Delta} [L + I_{xz} pq + (I_{yy} - I_{zz})rq] \\ & + \frac{I_{xz} I_{yy}}{\Delta} [N + I_{xx} - I_{yy})pq - I_{xz}qr] \end{aligned} \quad (A-4)$$

$$\dot{q} = \frac{I_{xx} I_{zz} - I_{xz}^2}{\Delta} [M + I_{xz}(r^2 - p^2) + (I_{zz} - I_{xx})pr] \quad (A-5)$$

$$\begin{aligned} \dot{r} = & \frac{I_{xz} I_{yy}}{\Delta} [L + I_{xz}pq + (I_{yy} - I_{zz})rq] \\ & + \frac{I_{xx} I_{yy}}{\Delta} [N - I_{xz}qr + I_{xx} - I_{yy})pq] \end{aligned} \quad (A-6)$$

where  $\Delta$  is given by

$$\Delta = I_{xx} I_{yy} I_{zz} - I_{xz}^2 I_{yy} \quad (A-7)$$

Kinemactic Equations:

$$\dot{\phi} = p + [\sin \phi \tan \theta]q + [\cos \phi \tan \theta]r \quad (A-8)$$

$$\dot{\theta} = [\cos \phi]q - [\sin \phi]r \quad (A-9)$$

$$\dot{\psi} = [\sin \phi \sec \theta]q + [\cos \phi \sec \theta]r \quad (A-10)$$

Trajectory Equations:

$$\begin{aligned} \dot{x}_E = & [\cos \theta \cos \psi]u + [\sin \phi \sin \theta \cos \psi - \cos \phi \sin \psi]v \\ & + [\cos \phi \cos \theta \cos \psi + \sin \phi \sin \psi]w \end{aligned} \quad (A-11)$$

$$\begin{aligned}\dot{y}_E = & [\cos\theta\sin\psi]u + [\sin\phi\sin\theta\sin\psi + \cos\phi\cos\psi]v \\ & + [\cos\phi\sin\theta\sin\psi - \sin\phi\cos\psi]w\end{aligned}\quad (A-12)$$

$$\dot{z}_E = [-\sin\theta]u + [\sin\phi\cos\theta]v + [\cos\phi\cos\theta]w \quad (A-13)$$

where  $u$ ,  $v$ , and  $w$  are total velocities,  $p$ ,  $q$ , and  $r$  are total angular velocities,  $\phi$ ,  $\theta$ , and  $\psi$  are total angles, and  $x_E$ ,  $y_E$ , and  $z_E$  are total trajectories. It should be noted that these states are not perturbation states.

The aerodynamic force equation along the x-body axis in terms of lift and drag is

$$X_a = L\sin\alpha - D\cos\beta \quad (A-14)$$

where the total lift is given by

$$L = QSC_L \quad (A-15)$$

and the dynamic pressure by

$$Q = 1/2 \rho V^2 = 1/2 \rho [u^2 + v^2 + w^2]^{1/2} \quad (A-16)$$

and the total drag by

$$D = QSC_D = QS(C_{D_0} + KC_L^2) \quad (A-17)$$

The constant  $K$  is a function of the configuration shape, thrust coefficient, and Mach number and is given by

$$K = \frac{1}{\pi A e} \quad (A-18)$$

where  $e$  is the configuration constant and  $A$  is the aspect ratio. The nondimensional total lift,  $C_L$ , is a function of the angle of attack, the rate of change of angle of attack, the pitch rate, the total velocity, and the control surfaces and is given by

$$C_L = C_{L\alpha_T} + C_{L\alpha} \alpha + C_{L\dot{\alpha}} \dot{\alpha} + C_{L_V} V + C_{L\delta} \delta \quad (A-19)$$



where  $\alpha_T$  is the trimmed angle of attack which gives the aircraft its trimmed lift. From Equation (A-16), the nondimensional drag is a function of  $C_L^2$ . The terms, i.e.  $C_L^2 \alpha^2$  and  $C_{L_\alpha} \alpha C_L \dot{\alpha}$  are normally omitted for simulation purposes. Therefore,  $C_D$  can be approximated by

$$C_D \approx C_{D_0} + 2KC_{L_0} [0.5C_{L_0} + C_{L_\alpha} \alpha + C_{L_\alpha} \alpha + C_{L_q} q + C_{L_V} V + C_{L_\delta} \delta] \quad (A-20)$$

where

$$C_{L_0} = C_L \alpha_T \quad (A-21)$$

An equivalent expression for the angle of attack is

$$\alpha = \tan^{-1}(w/u) \quad (A-22)$$

and is used in the simulation instead of  $\alpha$ . An expression for  $\dot{\alpha}$  can be derived by taking the derivative with respect to time of the  $\alpha$  represented by Equation (A-21) and is given for the simulation by

$$\dot{\alpha} = \frac{\dot{u}w - \dot{w}u}{u^2 + w^2} \quad (A-23)$$

It should be noted from Equation (A-15), that the expression for the true velocity,  $V$ , is given by

$$V = [u^2 + v^2 + w^2]^{1/2} \quad (A-24)$$

Therefore, great caution must be used when data is entered for  $C_{L_V}$  which is given by

$$C_{L_V} = \frac{\partial C_L}{\partial V} \quad (A-25)$$

The user should reference a book on aircraft dynamics before supplying a data value to this nondimensional coefficient.

The aerodynamic force equation along the z-body axis in terms of lift and drag is

$$Z_a = -L \cos \alpha - L \cos \beta \sin \alpha \quad (A-26)$$

where the sideslip angle  $\beta$  is given by

$$\beta = \sin^{-1}(v/V). \quad (A-27)$$

The total dimensional side-force  $Y$  along the y-body axis is given by

$$Y = QS[C_{y_\beta} \beta + C_{y_p} p + C_{y_r} r + C_{y_\delta} \delta]. \quad (A-28)$$

The total dimensional rolling moment  $L$  about the x-body axis is given by

$$L = QSb[C_{L_\beta} \beta + C_{L_p} p + C_{L_r} r + C_{L_\delta} \delta]. \quad (A-29)$$

The total dimensional pitching moment  $M$  about the y-body axis is given by

$$M = QSc[C_{M_0} + C_{M_\alpha} \alpha + C_{M_{\dot{\alpha}}} \dot{\alpha} + C_{M_V} V + C_{M_q} q + C_{M_\delta} \delta]. \quad (A-30)$$

where  $C_{M_0}$  is given by

$$C_{M_0} = C_{M_\alpha} \alpha_T. \quad (A-31)$$

The total dimensional yawing moment  $N$  about the z-body axis is given by

$$N = QSb[C_{N_\beta} \beta + C_{N_p} p + C_{N_r} r + C_{N_\delta} \delta]. \quad (A-32)$$

The current version of NONSIM assumes that the lateral control surfaces affect only lateral states and the longitudinal control surface affect only longitudinal states. Therefore,

$$C_{I_\delta} \delta = C_{I_{\delta_e}} \delta_e + C_{I_{\delta_f}} \delta_f \quad (I=L,M) \quad (A-33)$$

where the longitudinal control surfaces are nominally

$\delta_e$  = elevator

$\delta_f$  = flaperon

The control surfaces are the same as those for the AFTI/F-16 (Ref 2).

It should be noted that even though  $\delta_e$  currently infers elevator displacement, it could also be defined as something else by the user.

For the lateral case, an example is

$$C_{J\delta} \delta = C_{J\delta_a} \delta_a + C_{J\delta_{DT}} \delta_{DT} + C_{J\delta_r} \delta_r + C_{J\delta_c} \delta_c \quad (J=Y, L, N) \quad (A-34)$$

where the lateral control surfaces are nominally

$\delta_a$  = aileron

$\delta_{DT}$  = differential tail

$\delta_r$  = rudder

$\delta_c$  = vertical canard

It should be noted the assumption of decoupled control surfaces might not be valid. If this is the case, the program must be changed to reflect the case of lateral control surfaces affecting longitudinal states or vice-versa.

The flight path angle is given by

$$\gamma = \theta - \alpha \quad (A-35)$$

The rest of the features of the program NONSIM are listed in the comments that are printed when the program is run or are found by examining the example simulation. The sample data file that is listed after the program can be generated by examining the read from user's data file statements. The program can enter data interactively from the terminal or can be read from a stored file. When inputting from the terminal, the program is not user friendly.

The following is a printout of the program NONSIM, a data file listing and an example simulation exhibiting the features of NONSIM. The example simulation is for AFTI/F-16 flying at Mach=1.6 and an altitude of 30,000 feet (Ref 2).

```

PROGRAM NONSIM(OUTPUT,TAPE6=OUTPUT,DATA,TAPE3=DATA)
EXTERNAL F
INTRINSIC ATAN,SIN,COS,TAN

```

```

C*
C*THIS OPTION SIMULATES A NONLINEAR,SYMMETRICAL AIRCRAFT.
C*
C*INPUTS TO THE SIMULATION ARE:
C* BIXX- X MASS MOMENT OF INERTIA OF AIRCRAFT, SLUG-FT SQ.
C* RIXZ- XZ CROSS PRODUCT OF INERTIA OF AIRCRAFT, SLUG-FT SQ.
C* BIYY- Y MASS MOMENT OF INERTIA OF AIRCRAFT, SLUG-FT SQ.
C* BIZZ- Z MASS MOMENT OF INERTIA OF AIRCRAFT, SLUG-FT SQ.
C* ACGW- AIRCRAFT GROSS WEIGHT, POUNDS
C* VTRFPS- TRUE AIRSPEED, FEET PER SECOND
C* CBAR- WING MEAN AERODYNAMIC CHORD
C* S- WING REFERENCE AREA
C* Q- DYNAMIC PRESSURE
C* AR- ASPECT RATIO
C* EO-
C* FTXB- THRUST ALONG X-BODY
C* FTYB- THRUST ALONG Y-BODY
C* FTZB- THRUST ALONG Z-BODY
C* CLO- INITIAL COEFFICIENT OF LIFT IN THE X-DIRECTION
C* CLA- COEFFICIENT OF LIFT DUE TO ANGLE OF ANGLE
C* CLAD- COEFFICIENT OF LIFT DUE TO RATE OF CHANGE OF ALPHA
C* CLV- COEFFICIENT OF LIFT DUE TO VELOCITY INCREMENT ALONG OX
C* CLQ- COEFFICIENT OF LIFT DUE TO RATE OF CHANGE OF PITCH ANGLE
C* CLDE- COEFFICIENT OF LIFT DUE TO ELEVATOR
C* CLDF- COEFFICIENT OF LIFT DUE TO FLAPERON
C* CDMIN- INITIAL COEFFICIENT OF DRAG
C* CYBETA- FORCE DERIVATIVE DUE TO SIDESLIP
C* CYP- FORCE DERIVATIVE DUE TO RATE OF CHANGE OF ROLL ANGLE
C* CYR- FORCE DERIVATIVE DUE TO RATE OF CHANGE OF YAW ANGLE
C* CYAILR- FORCE DERIVATIVE DUE TO AILERON
C* CYRUDD- FORCE DERIVATIVE DUE TO RUDDER
C* CYDT- Y-FORCE DERIVATIVE DUE TO THE DIFFERENTIAL TAIL
C* CYDC- Y-FORCE DERIVATIVE DUE TO THE VERTICAL CANARD
C* CLBETA- ROLLING MOMENT DERIVATIVE DUE TO SIDESLIP
C* CLP-ROLLING MOMENT DERIVATIVE DUE TO RATE CHANGE OF ROLL
C* CLR-ROLLING MOMENT DERIVATIVE DUE TO RATE CHANGE OF YAW ANG
C* CLAILR- ROLLING MOMENT DERIVATIVE DUE TO AILERON
C* CLRUDD- ROLLING MOMENT DERIVATIVE DUE TO RUDDER
C* CLDT- ROLLING MOMENT DERIVATIVE DUE TO DIFF.TAIL
C* CLDC- ROLLING MOMENT DERIVATIVE DUE TO CANARD
C* CMQ- INITIAL COEFFICIENT OF PITCHING MOMENT
C* CMA- COEFFICIENT OF PITCHING MOMENT DUE TO ANGLE OF ATTACK
C* CMV- COEFFICIENT OF PITCHING MOMENT DUE TO FORWARD VELOCITY
C* CMR- COEFFICIENT OF PITCHING MOMENT DUE TO RATE OF CHANGE OF
C* PITCH ANGLE (THETA)
C* CMDE-COEFFICIENT OF PITCHING MOMENT DUE TO ELEVATOR
C* CMDF- PITCHING MOMENT DERIVATIVE DUE TO FLAPERON
C* CNBETA- YAWING MOMENT DERIVATIVE DUE TO SIDESLIP
C* CNP-YAWING MOMENT DERIVATIVE FROM RATE CHANGE OF ROLL ANGLE
C* CNR-YAWING MOMENT DERIVATIVE FROM RATE CHANGE OF YAW ANGLE
C* CNAILR- YAWING MOMENT DERIVATIVE DUE TO AILERON
C* CNRUDD- YAWING MOMENT DERIVATIVE DUE TO RUDDER

```

```

C* CNDT- YAWING MOMENT DERIVATIVE DUE TO DIFF. TAIL
C* CNDC- YAWING MOMENT DERIVATIVE DUE TO CANARD
C* DELTAE- ELEVATOR DEFLECTION
C* DELTAA- AILERON DEFLECTION
C* DELTAR- RUDDER DEFLECTION
C* DELTAF- FLAPRON DEFLECTION
C* DELTAT- DIFFERENTIAL TAIL DEFLECTION
C* DELTAC- VERTICAL CANARD DEFLECTION
C* T- INITIAL STARTING TIME OF SIMULATION
C* TOUT- STEP SIZE OF SIMULATION
C* TTOTAL- TOTAL TIME OF SIMULATION
C* PHIT- TRIM ROLL ANGLE
C* THETAT- TRIM PITCH ANGLE
C* PSIT- TRIM YAW ANGLE
C* BETAT- TRIM SIDESLIP ANGLE
C* GAMMAT- TRIM FLIGHT PATH ANGLE
C* ALPHAT- TRIM ANGLE OF ATTACK
C* TPhi- TOTAL ROLL ANGLE (=PHI+PHIT)
C* TTHETA- TOTAL PITCH ANGLE (=THETA+THETAT)
C* Tpsi- TOTAL YAW ANGLE (=PSI+PSIT)
C* TBETA- TOTAL SIDESLIP ANGLE (=BETA+BETAT)
C* TGAMMA- TOTAL FLIGHT PATH ANGLE (=GAMMA+GAMMAT)
C* TALPHA- TOTAL ANGLE OF ATTACK (=ALPHA+ALPHAT)
C*
C*OUTPUTS OF SIMULATION ARE:
C* X-X TRAJECTORY FROM BODY TO VEHICLE CARRIED FRAME
C* Y-Y TRAJECTORY FROM BODY TO VEHICLE CARRIED FRAME
C* Z-Z TRAJECTORY FROM BODY TO VEHICLE CARRIED FRAME
C* PHI- ROLL ANGLE
C* THETA- PITCH ANGLE
C* PSI- YAW ANGLE
C* UR- VELOCITY ALONG OX
C* VR- VELOCITY ALONG OY
C* WR- VELOCITY ALONG OZ
C* P- AIRCRAFT ANGULAR VELOCITY IN ROLL
C* Q- AIRCRAFT ANGULAR VELOCITY IN PITCH
C* R- AIRCRAFT ANGULAR VELOCITY IN YAW
C* BETA- SIDESLIP ANGLE
C* ALPHA- ANGLE OF ATTACK
C* GAMMA- FLIGHT PATH ANGLE
C* HEIGHT- ALTITUDE (HEIGHT=-Z)
C*
      DIMENSION G(12),GDOT(12),GD(12)
      REAL B1XX,B1XZ,B1YY,B1ZZ
      REAL ACGW,UTREPS,GRAV,MASS,CBAR,Q,S,R,A,...
      REAL CL0,CL1,CLAD,CLV,CLQ,CLDE,CLDF
      REAL CYBETA,CYF,CYR,CYAILR,CYRUDD,CYRT,CYID
      REAL CLBETA,CLF,CLR,CLAILR,CLRUDD,CLDT,CLDC
      REAL CM0,CMA,CMAD,CMV,CMR,CMTF,CMDF
      REAL CNBETA,CNF,CNR,CNADR,CNRUDD,CNDT,CNDC
      REAL FTXR,FTYR,FTZR
      REAL DELTAE,DELTAA,DELTAR,DELTAF,DELTAT,DELTAC
      REAL PSIT,THETAT,PHIT,BETAT,GAMMAT,ALPHAT
      REAL TPhi,TTHETA,Tpsi,TBETA,TGAMMA,TALPHA
      REAL T,TOUT,TTOTAL,TINIT,SAMPLE
      REAL GAMMA,ALPHA,BETA,ALPHAT

```

```

REAL HEIGHT
INTEGER NEQN, IFLAG, IWORK(5), N1, N2, N3, N4
REAL RELEERR, ABSEERR, G, GDOT, GO
REAL WORK(352)
REAL C, D, E, DET, K, J, PI
COMMON/B/BIXX, BIYY, BIZZ, BTXZ
COMMON/C/MASS, UTRFPS, GRAV, CBAR, Q, S, B
COMMON/X/CLO, CLA, CLAI, CLU, CLQ, CLIE, CLIF
COMMON/Y/CYBETA, CYP, CYR, CYAILR, CYRUDD, CYDT, CYDC
COMMON/Z/COMIN, ALPHAT, BETAT, ALPHAI, BETAI, ALPHAI
COMMON/L/CLBETA, CLP, CLR, CLATLR, CLRUDD, CLDT, CLDC
COMMON/M/CNO, CMA, CMAL, CMV, CMQ, CMDF, CMOF
COMMON/N/CNBETA, CNF, CNR, CNAILR, CNRUDD, CNDT, CNDC
COMMON/FT/FTXB, FTYR, FTZR
COMMON/DELTA/DELTAE, DELTAA, DELTAR, DELTAF, DELTAT, DELTAC
COMMON/MULTPL/C, D, E, DET, K, PI
DATA IWORK, WORK/5*0, 352*0./

```

C\*

C\* ONE PARAMETERS

```

RELEERR=0.000100
ABSEERR=0.000100
IFLAG=1
NEQN=12

```

C\*

```

PRINT*, ' '
PRINT*, 'THIS OPTION SETS UP AND RUNS A SIMULATION FOR A '
PRINT*, 'NONLINEAR, SYMMETRICAL AIRCRAFT.'
PRINT*, '      * OF INPUTS = 74 '
PRINT*, '      * OF OUTPUTS = 24 '
PRINT*, 'THE OUTPUTS OF THE SIMULATION ARE THE PERTURBATION'
PRINT*, 'ANGLES PHI, THETA, PSI, BETA, GAMMA, AND ALPHA'
PRINT*, '(DEG.), THE BODY VELOCITIES XB, YB, AND ZB '
PRINT*, '(FT/SEC), THE EARTH FRAME TRAJECTORIES X, Y, '
PRINT*, 'AND Z (FT), HEIGHT, TRUE VELOCITY, AND THE '
PRINT*, 'DERIVATIVE OF ALPHA. THE FINAL OUTPUTS ARE THE '
PRINT*, 'TOTAL ANGLES (TRIM+PERTURBATION) PHI, THETA, PSI, '
PRINT*, 'BETA, GAMMA, AND ALPHA (DEG.).'
PRINT*, ' '
PRINT*, 'CAUTION: ALL NONDIMENSIONAL FORCE AND MOMENT '
PRINT*, 'COEFFICIENTS DUE TO AN ANGLE MUST HAVE UNITS OF '
PRINT*, '(1/DEG.). ALL ANGLES WILL BE INPUTTED AND OUT-'
PRINT*, 'PUTTED IN DEGREES.'
PRINT*, ' '
PRINT*, 'WHEN TRIMMING THE AIRCRAFT (ALL PERTURBATIONS ARE '
PRINT*, 'EQUAL TO 0) THE FOLLOWING EQUATIONS MUST BE '
PRINT*, 'SATISFIED (VIRFPS = TRUE VELOCITY):'
PRINT*, '      (1) CLO = CLA*ALPHAT + CLU*UTRFPSP'
PRINT*, '      (2) CMO = CMA*ALPHAT + CMU*UTRFPSP'
PRINT*, 'WHERE ALPHAT IS THE TRIM ANGLE OF ATTACK.'
PRINT*, ' '
PRINT*, ' '
PRINT*, 'THE USER MUST INPUT THE FOLLOWING DATA:'
PRINT*, ' '
PRINT*, 'IS THE DATA STORED ON TAPE3=DATA?'
PRINT*, ' ( 1= YES , 0= NO ) > '
READ*, N1

```

```

      IF(NI,FQ.1) GO TO 500
C*
C*  ENTER DATA FROM THE USER'S TERMINAL
C*
      PRINT*, ' '
      PRINT*, 'ENTER THE MOMENTS OF INERTIA:'
      PRINT*, 'R1XX R1YY R1ZZ R1XZ > '
      READ*, R1XX,R1YY,R1ZZ,R1XZ
      PRINT*, ' '
      PRINT*, 'ENTER G VALUE (GRAVITY ,I.F. 32.2FT/SEC SQ.)'
      PRINT*, 'GRAVITY> '
      READ*,GRAV
      PRINT*, ' '
      PRINT*, 'ENTER THE AIRCRAFT WEIGHT AND THE TRUE AIRSPEED:'
      PRINT*, 'ACGW VT >'
      READ*, ACGW,VTRFPS
      PRINT*, ' '
      PRINT*, 'ENTER THE WING REFERENCE AREA, THE WING MEAN AERO-'
      PRINT*, 'DYNAMIC CHORD, AND THE DYNAMIC PRESSURE:'
      PRINT*, 'S CBAR Q > '
      READ*, S,CBAR,Q
      PRINT*, 'ENTER CONFIGURATION CONSTANT F USED IN CALCULATING'
      PRINT*, 'K > '
      READ*, FO
      PRINT*, ' '
      PRINT*, 'ENTER THE LIFT (CL) COEFFICIENTS:'
      PRINT*, 'CLO CLA CLAD CLV CLQ CLDE CLDF > '
      READ*, CLO,CLA,CLAD,CLV,CLQ,CLDE,CLDF
      PRINT*, ' '
      PRINT*, 'ENTER THE Y FORCE COEFFICIENTS:'
      PRINT*, 'BETA P R AILERON RUDDER DIFF.TAIL CANARD'
      READ*,CYBETA,CYP,CYR,CYAILR,CYRUDD,CYDT,CYDC
      PRINT*, ' '
      PRINT*, 'ENTER THE INITIAL DRAG (CDMIN) COEFFICIENT >'
      READ*, CDMIN
      PRINT*, ' '
      PRINT*, 'ENTER THE INITIAL PITCHING MOMENT COEFF.(CMO) > '
      READ*, CMO
      PRINT*, ' '
      PRINT*, 'ENTER THE ROLLING MOMENT COEFFICIENTS (CL)'
      PRINT*, 'BETA P R AILERON RUDDER DIFF.TAIL CANARD'
      READ*, CLBETA,CLP,CLR,CLAILR,CLRUDD,CLDT,CLDC
      PRINT*, ' '
      PRINT*, 'ENTER THE PITCHING MOMENT (CM) COEFFICIENTS:'
      PRINT*, 'CMA CMAD CMV CMQ CMDE CMDF >'
      READ*,CMA,CMAD,CMV,CMQ,CMDE,CMDF
      PRINT*, ' '
      PRINT*, 'ENTER THE YAWING MOMENT COEFFICIENTS (CN)'
      PRINT*, 'BETA P R AILERON RUDDER DIFF.TAIL CANARD'
      READ*, CNBETA,CNP,CNR,CNAILR,CNRUDD,CNDT,CNDC
      PRINT*, ' '
      PRINT*, 'ENTER THE FORCES DUE TO THRUST (FT)'
      PRINT*, 'XB VR WR >'
      READ*,FTXB,FTYR,FTZR
      PRINT*, ' '
      PRINT*, 'ENTER INITIAL TIME OF SIMULATION: '

```

```

READ*, TINIT
PRINT*, 'ENTER FINAL TIME OF SIMULATION> '
READ*, TTOTAL
PRINT*, 'ENTER TIME STEP SIZE OF SIMULATION> '
READ*, SAMPLE
PRINT*, ' '
PRINT*, 'ENTER THE TRIM CONDITIONS FOR:'
PRINT*, 'PHI THETA PSI BETA ALPHAT ALPHAD (DEG.) > '
READ*, PHIT, THETAT, PSIT, BETAT, ALPHAT, ALPHAD
PRINT*, 'UB VB WB > '
READ*, GO(4), GO(5), GO(6)
PRINT*, 'P Q R > '
READ*, GO(7), GO(8), GO(9)
PRINT*, 'X Y Z > '
READ*, GO(10), GO(11), GO(12)
PRINT*, ' '
PRINT*, 'ENTER COMMANDED CONTROL SURFACE DEFLECTIONS (DEG.)'
PRINT*, 'ELEVATOR AILERON RUDDER> '
READ*, DELTAE, DELTAA, DELTAR
PRINT*, 'FLAPERON DIFF. TAIL CANARD> '
READ*, DELTAF, DELTAT, DELTAC
GO TO 1000
500 CONTINUE
C*
C* ENTER DATA FROM THE USER'S DATA FILE
C*
READ(3,*) B1XX, B1YY, B1ZZ, B1XZ
READ(3,*) GRAV
READ(3,*) ACGW, VTRFPS
READ(3,*) S, CHAR, Q, R, ED
READ(3,*) CL0, CL1, CL10, CL1V, CL0, CL1E, CL1F
READ(3,*) CYBETA, CYF, CYR, CYAILR, CYRUDD, CYDT, CYUC
READ(3,*) CDMIN
READ(3,*) CLBETA, CLF, CLR, CLAILR, CLRUDD, CLDT, CLDC
READ(3,*) CM0, CMA, CMAD, CMV, CMQ, CMDE, CMDF
READ(3,*) CNBETA, CNF, CNR, CNAILR, CNRUDD, CNDT, CNDC
READ(3,*) FTXB, FTYB, FTZR
READ(3,*) TINIT, TTOTAL, SAMPLE
READ(3,*) PHIT, THETAT, PSIT, BETAT, ALPHAT, ALPHAD
READ(3,*) GO(4), GO(5), GO(6)
READ(3,*) GO(7), GO(8), GO(9)
READ(3,*) GO(10), GO(11), GO(12)
READ(3,*) DELTAE, DELTAA, DELTAR, DELTAF, DELTAT, DELTAC
1000 CONTINUE
C*
C* CALCULATION OF MATHEMATICAL COEFFICIENTS USED IN THE
C* NONLINEAR DIFFERENTIAL EQUATIONS.
C*
PI=3.14159265389793D0
AR=S/CHAR**2
K=1.0/(PI*AR*ED)
MASS=ACGW/GRAV
DET=B1XX*B1YY*B1ZZ-(B1XZ**2)*B1YY
C=B1YY*B1ZZ/DET
D=B1XZ*B1YY/DET
E=(B1XX*B1ZZ-B1XZ**2)/DET

```



```

C*      PRINT*, ' '
      PRINT*, 'THIS CONCLUDES THE INPUT OF THE DATA.'
      PRINT*, 'THE SIMULATION WILL NOW BEGIN.'
      PRINT*, ' '

C*
C*      REWRITE THE INPUT TO THE USER FOR OUTPUT CHECKS
C*
      WRITE(6,5)
5  FORMAT(1X,'*****')
      WRITE(6,10)
10  FORMAT(16X,'AIRCRAFT PARAMETERS')
      WRITE(6,15) BIXX,GRAV,S
15  FORMAT(1X,'BIXX = ',F14.6,1X,' GRAV = ',F14.6,1X
+,' S = ',F10.6)
      WRITE(6,20) BIYY,ACGW,CBAR
20  FORMAT(1X,'BIYY = ',F14.6,1X,' ACGW = ',F14.6,1X
+,' CBAR = ',F10.6)
      WRITE(6,25) BIZZ,VTRFPS,AR
25  FORMAT(1X,'BIZZ = ',F14.6,1X,' VTRFPS = ',F14.6,1X
+,' AR = ',F10.6)
      WRITE(6,30) BIXZ,Q
30  FORMAT(1X,'BIXZ = ',F14.6,1X,' Q = ',F14.6)
      WRITE(6,35)
35  FORMAT(1X,'*****')
      WRITE(6,40)
40  FORMAT(8X,'LONGITUDINAL BODY AXIS COEFFICIENTS')
      WRITE(6,42) CLO,CMO
42  FORMAT(1X,' CLO = ',1PE13.6,1X,' CMO = ',1PF13.6)
      WRITE(6,45) CLV,CMV
45  FORMAT(1X,' CLV = ',1PE13.6,1X,' CMV = ',1PF13.6)
      WRITE(6,50) CLA,CMA
50  FORMAT(1X,' CLA = ',1PF13.6,1X,' CMA = ',1PE13.6)
      WRITE(6,51) CLAD,CMAD
51  FORMAT(1X,' CLAD = ',1PE13.6,1X,' CMAD = ',1PF13.6)
      WRITE(6,55) CLQ,CMQ
55  FORMAT(1X,' CLQ = ',1PE13.6,1X,' CMQ = ',1PF13.6)
      WRITE(6,60) CLDE,CMDE
60  FORMAT(1X,' CLDE = ',1PE13.6,1X,' CMDE = ',1PF13.6)
      WRITE(6,62) CLDF,CMDF
62  FORMAT(1X,' CLDF = ',1PE13.6,1X,' CMDF = ',1PF13.6)
      WRITE(6,65) CDMIN
65  FORMAT(1X,' CDMIN = ',1PE13.6)
      WRITE(6,70)
70  FORMAT(1X,'*****')
      WRITE(6,75)
75  FORMAT(8X,'LAT-TWR BODY AXIS COEFFICIENTS')
      WRITE(6,80) CYBETA,CLBETA,CNBETA
80  FORMAT(1X,' CYBETA = ',1PF13.6,1X,' CLBETA = ',1PE13.6,1X,
+,' CNBETA = ',1PE13.6)
      WRITE(6,85) CYP,CLP,CNP
85  FORMAT(1X,' CYP = ',1PE13.6,1X,' CLP = ',1PE13.6,1X,
+,' CNP = ',1PF13.6)
      WRITE(6,90) CYR,CLR,CNR
90  FORMAT(1X,' CYR = ',1PE13.6,1X,' CLR = ',1PE13.6,1X,
+,' CNR = ',1PE13.6)

```

```

WRITE(6,95) CYAILR,CLAILR,CNAILR
95  FORMAT(1X,' CYAILR = ',1PE13.6,1X,' CLAILR = ',1PE13.6,1X,
+ ' CNAILR = ',1PE13.6)
WRITE(6,100) CYRUDD,CLRUDU,CNRUDU
100 FORMAT(1X,' CYRUDD = ',1PE13.6,1X,' CLRUDU = ',1PE13.6,1X,
+ ' CNRUDD = ',1PE13.6)
WRITE(6,102) CYDT,CLDT,CNDT
102 FORMAT(1X,' CYDT = ',1PE13.6,1X,' CLDT = ',1PE13.6,1X,
+ ' CNDT = ',1PE13.6)
WRITE(6,104) CYDC,CLDC,CNDC
104 FORMAT(1X,' CYDC = ',1PE13.6,1X,' CLDC = ',1PE13.6,1X,
+ ' CNDC = ',1PE13.6)
WRITE(6,105)
105 FORMAT(1X,'*****')
WRITE(6,107)
107 FORMAT(8X,'THRUST COEFFICIENTS')
WRITE(6,108) FTXB,FTYB,FTZB
108 FORMAT(1X,'FTXB = ',1PE13.6,1X,'FTYB = ',1PE13.6,1X,
+ 'FTZB = ',1PE13.6)
WRITE(6,109)
109 FORMAT(1X,'*****')
WRITE(6,110)
110 FORMAT(8X,'COMMANDED CONTROL SURFACE DEFLECTIONS:')
WRITE(6,111) DELTAE,DELTA A,DELTA R
111 FORMAT(1X,'DELTAE = ',1PE13.6,1X,' DELTA A = ',1PE13.6,1X,
+ ' DELTA R = ',1PE13.6)
WRITE(6,1110) DELTAF,DELTA T,DELTA C
1110 FORMAT(1X,'DELTAF = ',1PE13.6,1X,' DELTA T = ',1PE13.6,1X,
+ ' DELTA C = ',1PE13.6)
WRITE(6,112)
WRITE(6,211)
211 FORMAT(8X,'THE TRIM ANGLES OF THE AIRCRAFT:')
WRITE(6,212) PHIT,THETAT,PSIT
212 FORMAT(1X,' PHIT = ',1PE13.6,2X,' THETAT = ',1PE13.6,2X,
+ ' PSIT = ',1PE13.6)
GAMMAT=THETAT-ALPHAT
WRITE(6,214) BETAT,ALPHAT,GAMMAT
214 FORMAT(1X,'BETAT = ',1PE13.6,2X,' ALPHAT = ',1PE13.6,2X,
+ ' GAMMAT = ',1PE13.6)
WRITE(6,112)

C*
C* CONVERT FROM TRIM ANGLES TO PERTURBATION ANGLES
C*
TALPHA=ATAN(GO(6)/GO(4))*180.0/PI
ALPHA=TALPHA-ALPHAT
TBETA=ASIN(GO(5)/VTRFES)*180.0/PI
BETA=TBETA-BETAT
GO(1)=0
GO(2)=0
GO(3)=0
GAMMA=THETAT-ALPHAT

C*
112 FORMAT(1X,'*****')
WRITE(6,113) TINIT
113 FORMAT(1X,'THE OUTPUTS AT T = ',F5.2,' SECONDS ARE:')
WRITE(6,115) GO(1),GO(2),GO(3)

```

```

115  FORMAT(1X,' PHT = ',1PE13.6,1X,' THETA = ',1PE13.6,1X,
+ ' PSI = ',1PE13.6)
    WRITE(6,120) GO(4),GO(5),GO(6)
120  FORMAT(1X,' UB = ',1PE13.6,1X,' VB = ',1PE13.6,1X,
+ ' WR = ',1PE13.6)
C*
C* ERROR CHECK ON INITIAL UR (UB CANNOT EQUAL 0)
C*
    IF (GO(4).EQ.0.000) THEN
        PRINT*, 'THE INITIAL UR CANNOT BE ZERO AS IT WILL'
        PRINT*, 'CAUSE ALPHA=ATAN(WR/UB) TO BLOW UP.'
    END IF
C*
    WRITE(6,125) GO(7),GO(8),GO(9)
125  FORMAT(1X,' P = ',1PE13.6,1X,' Q = ',1PE13.6,1X,
+ ' R = ',1PE13.6)
    WRITE(6,130) GO(10),GO(11),GO(12)
130  FORMAT(1X,' X = ',1PE13.6,1X,' Y = ',1PE13.6,1X,
+ ' Z = ',1PE13.6)
    WRITE(6,135) ALPHA,GAMMA,BETA
135  FORMAT(1X,' ALPHA = ',1PE13.6,1X,' GAMMA = ',1PE13.6,1X,
+ ' BETA = ',1PE13.6)
    HEIGHT=-GO(12)
C*
C* CHECK ON THE VALUE OF HEIGHT FOR A POSSIBLE CRASH
C*
    IF (HEIGHT.LT.0.0) THEN
        PRINT*, '
        PRINT*, '*****'
        PRINT*, '*  CCCC RRRR  AA  SSSS  HH  HH  * *'
        PRINT*, '* CC CC RR RR  AAAA  SS  SS  HH  HH  * *'
        PRINT*, '* CC  RR RR  AA  AA  SSS  HH  HH  * *'
        PRINT*, '* CC  RRRR  AAAAAAA  SSSS  HHHHHHH  * *'
        PRINT*, '* CC  RR RR  AA  AA  SSS  HH  HH  * *'
        PRINT*, '* CC CC RR RR AA  AA  SS  SS  HH  HH  * *'
        PRINT*, '*  CCCC RR RR AA  AA  SSSS  HH  HH  * *'
        PRINT*, '*****'
        PRINT*, '
        STOP
    END IF
    WRITE(6,136) HEIGHT,VTRFPS,ALPHA
136  FORMAT(1X,'HEIGHT = ',1PE13.6,1X,'VTRFPS = ',1PE13.6,1X,
+ 'ALPHA = ',1PE13.6)
C*
C* INITIALIZATIONS OF THE STATES
C*
    GO(1)=PHIT*PI/180.0
    GO(2)=THETA*PI/180.0
    GO(3)=PSIT*PI/180.0
    DO 200 N=1,12
        G(N)=GO(N)
200  CONTINUE
C*
    TTOTAL=TTOTAL-SAMPLE
2000 CONTINUE
    PRINT*, '

```

```

C*
C* CALLS TO ODE, OUTPUTS FROM ODE, AND CHECKS FOR ERROR MESSAGES
C*
      DO 999 J=TINIT,TTOTAL,SAMPLE
      TOUT=TINIT+SAMPLE
9999  CALL ODE(F,NEQN,G,TINIT,TOUT,RELERR,ABSERR,IFLAG,WORK,
+      IWORK)
      WRITE(6,137) TOUT
137   FORMAT(1X,'THE OUTPUTS AT T = ',F5.2,' SECONDS ARE:')
C*
C* CONVERT PHI, THETA, PSI, ALPHA, AND BETA FROM RADIANS
C* TO DEGREES FOR PRINTING PURPOSES. CONVERT PHI, THETA, AND
C* PSI TO PERTURBATION ANGLES FROM TOTAL ANGLES.
C*
      G(1)=G(1)*180.0/PI-PHIT
      G(2)=G(2)*180.0/PI-THETAT
      G(3)=G(3)*180.0/PI-PSIT
      ALPHA=ALPHA*180.0/PI
      BETA=BETA*180.0/PI
      GAMMA=G(2)-ALPHA
C*
      WRITE(6,140) G(1),G(2),G(3)
140   FORMAT(1X,'   PHI = ',1PE13.6,1X,' THETA = ',1PE13.6,1X,
+   '   PSI = ',1PE13.6)
      WRITE(6,145) G(4),G(5),G(6)
145   FORMAT(1X,'   UR = ',1PE13.6,1X,'   UB = ',1PE13.6,1X,
+   '   WB = ',1PE13.6)
C*
C* ERROR CHECK ON UB (UB CANNOT EQUAL 0)
C*
      IF (G(4).EQ.0.000) THEN
        PRINT*, 'ERROR IN UB (UB=0.0) CAUSES ALPHA=ATAN'
        PRINT*, '(WB/UR) TO BLOW UP.'
      END IF
C*
      WRITE(6,150) G(7),G(8),G(9)
150   FORMAT(1X,'   P = ',1PE13.6,1X,'   Q = ',1PE13.6,1X,
+   '   R = ',1PE13.6)
      WRITE(6,155) G(10),G(11),G(12)
155   FORMAT(1X,'   X = ',1PE13.6,1X,'   Y = ',1PE13.6,1X,
+   '   Z = ',1PE13.6)
      WRITE(6,160) ALPHA,GAMMA,BETA
160   FORMAT(1X,' ALPHA = ',1PE13.6,1X,' GAMMA = ',1PE13.6,1X,
+   ' BETA = ',1PE13.6)
      HEIGHT=-G(12)
      IF (HEIGHT.LT.0.0) THEN
        PRINT*, '
        PRINT*, '*****'
        PRINT*, '*  CCCC  RRRR   AA   SSSS  HH  HH  * *'
        PRINT*, '* CC  CC RR  RR  AAAA  SS  SS  HH  HH  * *'
        PRINT*, '* CC      RR RR  AA  AA  SSS   HH  HH  * *'
        PRINT*, '* CC      RRRR  AAAAAAA  SSSS  HHHHHHH  * *'
        PRINT*, '* CC      RR RR  AA   AA   SSS   HH  HH  * *'
        PRINT*, '* CC  CC RR  RR AA   AA  SS  SS  HH  HH  * *'
        PRINT*, '*  CCCC  RR  RR AA   AA  SSSS  HH  HH  * *'
        PRINT*, '*****'
      END IF

```

```

      PRINT*, ' '
      STOP
      END IF
      WRITE(6,162) HEIGHT,VTRFPS,ALPHAD
162  FORMAT(1X,'HEIGHT = ',1PE13.6,1X,'VTRFPS = ',1PE13.6,1X,
+    'ALPHAD = ',1PE13.6)
      PRINT*, ' '
      WRITE(6,1632)
1632  FORMAT(1X,'THE TOTAL ANGLES (TRIM + PERTURBATION):')
      TALPHA=ALPHA+ALPHAD
      TGAMMA=GAMMA+GAMMA1
      TBETA=BETA+BETAD
      TPHI=G(1)+PHI1
      TTHETA=G(2)+THETA1
      TPSI=G(3)+PSI1
      WRITE(6,1634) TALPHA,TGAMMA,TBETA
1634  FORMAT(1X,'TALPHA = ',1PE13.6,1X,' TGAMMA = ',1PE13.6,1X,
+    ', TBETA = ',1PE13.6)
      WRITE(6,1636) TPHI,TTHETA,TPSI
1636  FORMAT(1X,' TPHI = ',1PE13.6,1X,' TTHETA = ',1PE13.6,1X,
+    ', TPSI = ',1PE13.6)

C*
C*  CONVERT ANGLES FROM DEGREES TO RADIANS FOR SIMULATION
C*
      G(1)=TPHI*PI/180.0
      G(2)=TTHETA*PI/180.0
      G(3)=TPSI*PI/180.0

C*
      IF(IFLAG.NE.2) THEN
        PRINT*, ' '
        IF(IFLAG.EQ.3) THEN
          PRINT*, 'INTEGRATION DID NOT REACH TOUT BECAUSE'
          PRINT*, 'ERROR TOLERANCES TOO SMALL. RELEERR,ABSERR'
          PRINT*, 'INCREASED APPROPRIATELY FOR CONTINUING.'
          PRINT*, ' '
          PRINT*, 'DOES THE USER WANT ONE TOLERANCE PARAMETERS'
          PRINT*, 'RELEERR = ',RELEERR,' AND ABSERR = ',ABSERR
          PRINT*, 'INCREASED?'
          PRINT*, 'ENTER (1=YES 0=NO) > '
          READ*,N3
          IF(N3.EQ.1) THEN
            PRINT*, 'ENTER NEW RELEERR AND ABSERR:'
            PRINT*, 'RELEERR ABSERR >'
            READ*, RELEERR,ABSERR
            GO TO 9999
          END IF
        END IF
        IF(IFLAG.EQ.4) THEN
          PRINT*, 'INTEGRATION DID NOT REACH TOUT BECAUSE'
          PRINT*, 'MORE THAN 500 STEPS NEEDED.'
          PRINT*, ' '
          PRINT*, 'DOES THE USER WANT TO CONTINUE?'
          PRINT*, 'ENTER (1=YES 0=NO) >'
          READ*,N4
          IF(N4.EQ.1) THEN
            GO TO 9999
          END IF
        END IF
      END IF

```

```

        END IF
    END IF
    IF(IFLAG.EQ.5) THEN
        PRINT*, 'INTEGRATION DID NOT REACH TOUT BECAUSE'
        PRINT*, 'EQUATIONS APPEAR TO BE STIFF.'
    END IF
    IF(IFLAG.EQ.6) THEN
        PRINT*, 'INVALID INPUT PARAMETERS(FATAL ERROR)'
    END IF

C*
C* END PROGRAM DUE TO ERROR MESSAGES FROM ODE
C*

        PRINT*, ' '
        PRINT*, 'THE PROGRAM HAS BEEN TERMINATED DUE TO ERROR'
        PRINT*, 'MESSAGE FROM ODE.'
        PRINT*, ' '
        STOP
    END IF

C*
        PRINT*, ' '
999 CONTINUE
    PRINT*, 'DOES THE USER WANT TO CONTINUE THE SIMULATION?'
    PRINT*, 'ENTER 0 IF SIMULATION ENDS.'
    PRINT*, 'ENTER 1 IF SIMULATION CONTINUES WITH THE SAME'
    PRINT*, '        CONTROL SURFACE DEFLECTIONS.'
    PRINT*, 'ENTER 2 IF SIMULATION CONTINUES WITH NEW '
    PRINT*, '        CONTROL SURFACE DEFLECTIONS.'
    PRINT*, 'ENTER 3 IF SIMULATION CONTINUES WITH NEW FORCES'
    PRINT*, '        DUE TO THRUST VALUES.'
    PRINT*, 'ENTER 4 IF SIMULATION CONTINUES WITH BOTH NEW'
    PRINT*, '        CONTROL SURFACE DEFLECTIONS AND NEW '
    PRINT*, '        FORCES DUE TO THRUST.'
    PRINT*, 'ENTER #> '
    READ*, N2
    IF(N2.NE.0) THEN
        PRINT*, 'ENTER NEW FINAL SIMULATION TIME > '
        READ*, TTOTAL
        PRINT*, 'ENTER NEW SAMPLING TIME > '
        READ*, SAMPLE
        IF(N2.EQ.2) THEN
            PRINT*, ' '
            PRINT*, 'ENTER NEW CONTROL SURFACE DEFLECTIONS:'
            PRINT*, 'DELTAE DELTAA DELTAR > '
            READ*, DELTAE, DELTAA, DELTAR
            PRINT*, 'DELTAF DELTAT DELTAC > '
            READ*, DELTAF, DELTAT, DELTAC
            WRITE(6,305)
            WRITE(6,307)
            WRITE(6,310) DELTAE, DELTAA, DELTAR
            WRITE(6,312) DELTAF, DELTAT, DELTAC
            WRITE(6,305)
        END IF
        IF(N2.EQ.3) THEN
            PRINT*, ' '
            PRINT*, 'ENTER THE NEW FORCES DUE TO THRUST (FT):'
            PRINT*, 'XB YR ZR >'

```

```

      READ*, FTXB,FTYB,FTZB
      WRITE(6,305)
      WRITE(6,320)
      WRITE(6,325) FTXB,FTYB,FTZB
      WRITE(6,305)
    END IF
    IF(N2.EQ.4) THEN
      PRINT*, ' '
      PRINT*, 'ENTER THE CONTROL SURFACE DEFLECTIONS:'
      PRINT*, 'DELTAE DELTAA DELTAR >'
      READ*, DELTAE,DELTAA,DELTAR
      PRINT*, 'DELTAF DELTAT DELTAC >'
      READ*, DELTAF,DELTAT,DELTAC
      PRINT*, ' '
      PRINT*, 'ENTER THE NEW FORCES DUE TO THRUST (FT):'
      PRINT*, 'XB YB ZB >'
      READ*, FTXB,FTYB,FTZB
      WRITE(6,305)
305      FORMAT(1X,'*****')
      WRITE(6,307)
307      FORMAT(8X,'COMMANDED CONTROL SURFACE DEFLECTIONS:')
      WRITE(6,310) DELTAE,DELTAA,DELTAR
310      FORMAT(1X,'DELTAE = ',1PE13.6,1X,'DELTAA = ',1PE13.6,
      +      1X,'DELTAR = ',1PE13.6)
      WRITE(6,312) DELTAF,DELTAT,DELTAC
312      FORMAT(1X,'DELTAF = ',1PE13.6,1X,'DELTAT = ',1PE13.6,
      +      1X,'DELTAC = ',1PE13.6)
      WRITE(6,315)
315      FORMAT(1X,'*****')
      WRITE(6,320)
320      FORMAT(8X,'THE NEW FORCES DUE TO THRUST (FT) ARE:')
      WRITE(6,325) FTXB,FTYB,FTZB
325      FORMAT(1X,'FTXB = ',1PE13.6,1X,' FTYB = ',1PE13.6,1X,
      +      ' FTZB = ',1PE13.6)
      WRITE(6,305)
    END IF
    GO TO 2000
  ELSE
    STOP
  END IF
END

C*
C* THIS SUBROUTINE FORMS THE NONLINEAR DIFFERENTIAL
C* EQUATIONS OF THE SYMMETRICAL AIRCRAFT.
C*
C* THE VARIABLE EQUIVALENTS ARE:
C*   G(1)=PHI
C*   G(2)=THETA
C*   G(3)=PSI
C*   G(4)=WR
C*   G(5)=VR
C*   G(6)=WB
C*   G(7)=P
C*   G(8)=Q
C*   G(9)=R
C*   G(10)=X

```

```

C*      G(11)=Y
C*      G(12)=Z
C*
SUBROUTINE F(T,G,GDOT)
REAL BIXX,BIXZ,BIYY,BIZZ
REAL MASS,VTRFPS,GRAV,S,CBAR,Q
REAL CLA,CLAD,CLV,CLQ,CLDE,CLDF,CLO
REAL CYBETA,CYP,CYR,CYATLR,CYRUDD,CYDT,CYDC
REAL COMIN,ALPHAT,BETAT,ALPHAD,BETA,ALPHA
REAL CLBETA,CLP,CLR,CLATLR,CLRUDD,CLDT,CLDC
REAL CMA,CMU,CMQ,CMDE,CMDF,CMO
REAL CNBETA,CNP,CNR,CNATLR,CNRUDD,CNDT,CNDC
REAL FTXB,FTYB,FTZB
REAL T
REAL DELTAE,DELTA,DELTAR,DELTAF,DELTAT,DELTAC
REAL C,D,E,DET,K,PI
DIMENSION G(12),GDOT(12)
COMMON/B/BIXX,BIYY,BIZZ,BIXZ
COMMON/C/MASS,VTRFPS,GRAV,CBAR,Q,S,B
COMMON/X/CLO,CLA,CLAD,CLV,CLQ,CLDE,CLDF
COMMON/Y/CYBETA,CYP,CYR,CYATLR,CYRUDD,CYDT,CYDC
COMMON/Z/COMIN,ALPHAT,BETAT,ALPHAD,BETA,ALPHA
COMMON/I/CLBETA,CLP,CLR,CLATLR,CLRUDD,CLDT,CLDC
COMMON/M/CMO,CMA,CMU,CMQ,CMDE,CMDF
COMMON/N/CNBETA,CNP,CNR,CNATLR,CNRUDD,CNDT,CNDC
COMMON/FT/FTXB,FTYB,FTZB
COMMON/DELTA/DELTAE,DELTA,DELTAR,DELTAF,DELTAT,DELTAC
COMMON/MULTPL/C,D,E,DET,K,PI
VTRFPS=(G(4)**2+G(5)**2+G(6)**2)**(1.0/2.0)
ALPHA=ATAN(G(6)/G(4))-ALPHAT*PI/180.0
BETA=ASIN(G(5)/VTRFPS)-BETAT*PI/180.0
CLD=CLDE*DELTAE+CLDF*DELTAF
CMQ=CMDF*DELTAE+CMDE*DELTAF
CNU=CNATLR*DELTA+CNRUDD*DELTAR+CNDT*DELTAT+CNDC*DELTAC
CLLD=CLATLR*DELTA+CLRUDD*DELTAR+CLDT*DELTAT+CLDC*DELTAC
CYD=CYATLR*DELTA+CYRUDD*DELTAR+CYDT*DELTAT+CYDC*DELTAC

C*
C*      PHI DERIVATIVE EQUATION
C*
      GDOT(1)=G(7)+(SIN(G(1))*TAN(G(2)))*G(8)+(COS(G(1))*
      +TAN(G(2)))*G(9)

C*
C*      THETA DERIVATIVE EQUATION
C*
      GDOT(2)=COS(G(1))*G(8)-SIN(G(1))*G(9)

C*
C*      PSI DERIVATIVE EQUATION
C*
      GDOT(3)=SIN(G(1))*G(8)/COS(G(2))+COS(G(1))*G(9)/COS(G(2))

C*
C*      U BODY DERIVATIVE EQUATION
C*
      GDOT(4)=(Q*S*(CLO+CLA*ALPHA*180.0/PI+CLAD*ALPHAD+
      +CLQ*G(8)+CLV*VTRFPS+CLD)*SIN(ALPHA)-Q*S*(COMIN+2*B*CLQ*
      +(0.5*CLD+CLA*ALPHA*180.0/PI+CLAD*ALPHAD+CLQ*G(8)+CLV*

```



```

      +VTRFPS+CLD))*COS(BETA)*COS(ALPHA)+FTXB-MASS*GRAV*
      +SIN(G(2)))/MASS+G(9)*G(5)-G(8)*G(6)
C*
C* V BODY DERIVATIVE EQUATION
C*
      GDOT(5)=(Q*S*(CYBETA*BETA*180.0/PI+CYP*G(7)+CYR*G(9)+
      +CYD)+FTYB+MASS*GRAV*SIN(G(1))*COS(G(2)))/MASS+G(7)*G(6)-
      +G(9)*G(4)
C*
C* W BODY DERIVATIVE EQUATION
C*
      GDOT(6)=(-Q*S*(CLO+CLA*ALPHA*180.0/PI+CLAD*ALPHAD+
      +CLO*G(8)+CLV*VTRFPS+CLD))*COS(ALPHA)-Q*S*(CDM(N+2)*CLO*
      +(0.5*CLO+CLA*ALPHA*180.0/PI+CLAD*ALPHAD+CLQ*G(8)+CLV*
      +VTRFPS+CLD))*COS(BETA)*SIN(ALPHA)+FTZB+MASS*GRAV*
      +COS(G(1))*COS(G(2)))/MASS+G(8)*G(4)-G(7)*G(5)
C*
C* CALCULATION OF THE DERIVATIVE OF ALPHA
C*
      ALPHAD=(GDOT(4)*G(6)-GDOT(6)*G(4))/(G(4)**2+G(6)**2)
C*
C* P DERIVATIVE EQUATION
C*
      GDOT(7)=C*(Q*S*B*(CLBETA*BETA*180.0/PI+CLP*G(7)+CLR*G(9)+
      +CLLD)+BIXZ*G(7)*G(8)+(BIYY-BIZZ)*G(8)*G(9))+H*(Q*S*B*
      +(CNBETA*BETA*180.0/PI+CNF*G(7)+CNR*G(9)+CND)+(BIXX-BIYY)*
      +G(7)*G(8)-BIXZ*G(9)*G(8))
C*
C* Q DERIVATIVE EQUATION
C*
      GDOT(8)=E*(Q*S*CBAR*(CMO+CMA*ALPHA*180.0/PI+CMQ*G(8)+
      +CMA*ALPHAD+CMV*VTRFPS+CND)+BIXZ*(G(9)**2-G(7)**2)+
      +(BIZZ-BIXX)*G(9)*G(7))
C*
C* R DERIVATIVE EQUATION
C*
      GDOT(9)=D*(Q*S*B*(CLBETA*BETA*180.0/PI+CLP*G(7)+CLR*G(9)+
      +CLLD)+BIXZ*G(7)*G(8)+(BIYY-BIZZ)*G(9)*G(8)+BIXX*BIYY*
      +(Q*S*B*(CNBETA*BETA*180.0/PI+CNF*G(7)+CNR*G(9)+CND)+
      +(BIXX-BIYY)*G(7)*G(8)-BIXZ*G(8)*G(9))/DET
C*
C* X DERIVATIVE EQUATION
C*
      GDOT(10)=COS(G(2))*COS(G(3))*G(4)+(SIN(G(1))*SIN(G(2))*
      +COS(G(3))-COS(G(1))*SIN(G(3)))*G(5)+(COS(G(1))*
      +SIN(G(2))*COS(G(3))+SIN(G(1))*SIN(G(3)))*G(6)
C*
C* Y DERIVATIVE EQUATION
C*
      GDOT(11)=COS(G(2))*SIN(G(3))*G(4)+(SIN(G(1))*SIN(G(2))*
      +SIN(G(3))+COS(G(1))*COS(G(3)))*G(5)+(COS(G(1))*
      +SIN(G(2))*SIN(G(3))-SIN(G(1))*COS(G(3)))*G(6)
C*
C* Z DERIVATIVE EQUATION
C*

```

```

      GDOT(12)=(-SIN(G(2)))*G(4)+(SIN(G(1))*COS(G(2)))*G(5)+
      +(COS(G(1))*COS(G(2)))*G(6)
C*
      RETURN
      END
--EOR--
--EOR--
--EOF--
END OF FILE
?? END
AERO    IS A LOCAL FILE
/

```

```

      XEDIT,DATA
      XEDIT 3.1.00
      ?? T
      ?? F*
      10033.429 53876.269 61278.452 282.13217
      32.2
      21018.0 1591.75
      300.0 11.32 1129.3126 30.0 0.8
      0.06202943 0.066129 -2.974699 0.0 3.458724 0.006180 0.004004
      -0.019192 0.026463 0.516864 0.000362 0.000552 0.000281 0.001541
      0.0449031142
      -0.001702 -0.257331 0.018261 -0.00025 0.000077 -0.000811 0.000232
      0.0010042202 -0.010705 0.501981 0.0 -1.869366 -0.008061 -0.001432
      0.00088 0.004371 -0.246367 0.000236 -0.000349 0.000281 0.001541
      15778.98151 0.0 0.0
      0.0 5.0 1.0
      0.0 0.9380064 0.0 0.0 0.9380064 0.0
      1591.5367 0.0 26.057853
      0 0 0
      0.0 0.0 -30000.0
      0.0 0.0 0.0 0.0 0.0 0.0
      --EOR--
      --EOF--
      END OF FILE
      ?? END
      DATA    IS A LOCAL FILE
      /

```

```

      GET.L1=ODE
      /LIBRARY(L1)
      LIBRARY(L1)
      /REWIND,AERO,DATA
      REWIND,AERO,DATA.
      /FINIS,T=AERO,B=1 GO,I=0,ANSI=0
      1.706 CP SECONDS COMPIATION TIME.
      /1 GO

```

THIS OPTION SETS UP AND RUNS A SIMULATION FOR A  
NONLINEAR, SYMMETRICAL AIRCRAFT.

# OF INPUTS = 74

# OF OUTPUTS = 24

THE OUTPUTS OF THE SIMULATION ARE THE PERTURBATION  
ANGLES PHI, THETA, PSI, BETA, GAMMA, AND ALPHA  
(DEG.), THE BODY VELOCITIES XR, VR, AND WR  
(FT/SEC), THE EARTH FRAME TRAJECTORIES X, Y,  
AND Z (FT), HEIGHT, TRUE VELOCITY, AND THE  
DERIVATIVE OF ALPHA. THE FINAL OUTPUTS ARE THE  
TOTAL ANGLES (TRIM+PERTURBATION) PHI, THETA, PSI,  
BETA, GAMMA, AND ALPHA (DEG.).

CAUTION: ALL NONDIMENSIONAL FORCE AND MOMENT  
COEFFICIENTS DUE TO AN ANGLE MUST HAVE UNITS OF  
(1/DEG.). ALL ANGLES WILL BE INPUTTED AND OUT-  
PUTTED IN DEGREES.

WHEN TRIMMING THE AIRCRAFT (ALL PERTURBATIONS ARE  
EQUAL TO 0) THE FOLLOWING EQUATIONS MUST BE  
SATISFIED (VTRFPS = TRUE VELOCITY):

(1)  $CLO = CLA * ALPHAT + CLV * VTRFPS$

(2)  $CMD = CMA * ALPHAT + CMV * VTRFPS$

WHERE ALPHAT IS THE TRIM ANGLE OF ATTACK.

THE USER MUST INPUT THE FOLLOWING DATA:

IS THE DATA STORED ON TAPE3-DATA?

( 1= YES , 0= NO )

? 1

THIS CONCLUDES THE INPUT OF THE DATA.  
THE SIMULATION WILL NOW BEGIN.

\*\*\*\*\*

#### AIRCRAFT PARAMETERS

R1XX = 10033.429000 GRAV = 32.200000 S = 300.000000  
R1YY = 53876.269000 ACGW = 21018.000000 CBAR = 11.320000  
R1ZZ = 61278.452000 VTRFPS = 1591.750000 AR = 2.341145  
R1XZ = 282.132170 Q = 1129.312600

\*\*\*\*\*

#### LONGITUDINAL BODY AXIS COEFFICIENTS

CLO = 6.202943E-02 CMD = 1.004220E-03  
CLV = 0. CMV = 0.  
CLA = 6.612900E-02 CMA = -1.070500E-02  
CLAD = -2.974699E+00 CMAD = 5.019810E-01  
CLQ = 3.458724E+00 CMQ = -1.83936E+00  
CLDE = 6.180000E-03 CLDE = -8.061000E-03  
CLDF = 4.004000E-03 CLDF = -1.432000E-03  
CLMIN = 4.490311E-02

\*\*\*\*\*

#### LAT-DIR BODY AXIS COEFFICIENTS

CYBETA = -1.919200E-02 CLBETA = -1.702000E-03 CNBETA = 8.800000E-04

CYP = 2.646300E-02    CLP = -2.573310E-01    CNP = 4.371000E-03  
 CYR = 5.168640E-01    CLR = 1.826100E-02    CNR = -2.463670E-01  
 CYAILR = 3.620000E-04    CLAILR = -2.500000E-04    CNAILR = 2.360000E-04  
 CYRUDD = 5.520000E-04    CLRUDD = 7.700000E-05    CNRUDD = -3.490000E-04  
 CYDT = 2.810000E-04    CLDT = -8.110000E-04    CNDT = 2.810000E-04  
 CYDC = 1.541000E-03    CLDC = 2.320000E-04    CNDc = 1.541000E-03

\*\*\*\*\*

#### THRUST COEFFICIENTS

FTXB = 1.577898E+04    FTYB = 0.    FTZB = 0.

\*\*\*\*\*

#### COMMANDED CONTROL SURFACE DEFLECTIONS:

DELTAE = 0.    DELTAA = 0.    DELTAK = 0.  
 DELTAF = 0.    DELTAT = 0.    DELTAC = 0.

\*\*\*\*\*

#### THE TRIM ANGLES OF THE AIRCRAFT:

PHIT = 0.    THETAT = 9.380064E-01    PSIT = 0.  
 BETAT = 0.    ALPHAT = 9.380064E-01    GAMMAT = 0.

\*\*\*\*\*

#### THE OUTPUTS AT T = 0.00 SECONDS ARE:

PHI = 0.    THETA = 0.    PSI = 0.  
 UB = 1.591537E+03    VB = 0.    WB = 2.605785E+01  
 P = 0.    Q = 0.    R = 0.  
 X = 0.    Y = 0.    Z = -3.000000E+04  
 ALPHA = 1.448921E-09    GAMMA = 0.    BETA = 0.  
 HEIGHT = 3.000000E+04    VTRFPS = 1.591750E+03    ALPHAD = 0.

#### THE OUTPUTS AT T = 1.00 SECONDS ARE:

PHI = 0.    THETA = 3.044688E-02    PSI = 0.  
 UB = 1.591496E+03    VB = 0.    WB = 2.603781E+01  
 P = 0.    Q = 8.450937E-04    R = 0.  
 X = 1.591731E+03    Y = 0.    Z = -3.000044E+04  
 ALPHA = -7.461600E-04    GAMMA = 3.119304E-02    BETA = 0.  
 HEIGHT = 3.000044E+04    VTRFPS = 1.591709E+03    ALPHAD = 1.650258E-04

#### THE TOTAL ANGLES (TRIM + PERTURBATION):

TALPHA = 9.372602E-01    TGAMMA = 3.119304E-02    TBETA = 0.  
 TPHI = 0.    TTHETA = 9.684533E-01    TPSI = 0.

#### THE OUTPUTS AT T = 2.00 SECONDS ARE:

PHI = 0.    THETA = 6.231936E-02    PSI = 0.  
 UB = 1.591435E+03    VB = 0.    WB = 2.597282E+01  
 P = 0.    Q = 4.454864E-04    R = 0.  
 X = 3.183410E+03    Y = 0.    Z = -3.000178E+04  
 ALPHA = -3.008699E-03    GAMMA = 6.532806E-02    BETA = 0.  
 HEIGHT = 3.000178E+04    VTRFPS = 1.591647E+03    ALPHAD = 2.677518E-05

#### THE TOTAL ANGLES (TRIM + PERTURBATION):

TALPHA = 9.349977E-01    TGAMMA = 6.532806E-02    TBETA = 0.  
 TPHI = 0.    TTHETA = 1.000326E+00    TPSI = 0.

#### THE OUTPUTS AT T = 3.00 SECONDS ARE:

PHI = 0.    THETA = 9.399488E-02    PSI = 0.  
 UB = 1.591357E+03    VB = 0.    WB = 2.595281E+01  
 P = 0.    Q = 5.302806E-04    R = 0.  
 X = 4.775018E+03    Y = 0.    Z = -3.000404E+04  
 ALPHA = -3.668222E-03    GAMMA = 9.766310E-02    BETA = 0.

HEIGHT = 3.000404E+04 VTRFPS = 1.591568E+03 ALPHAD = -2.671253E-05

THE TOTAL ANGLES (TRIM + PERTURBATION):

TALPHA = 9.343382E-01 TGAMMA = 9.766310E-02 TTHETA = 0.  
TFPHI = 0. TTHETA = 1.032001E+00 TPSI = 0.

THE OUTPUTS AT T = 4.00 SECONDS ARE:

PHI = 0. THETA = 1.256336E-01 PSI = 0.  
UB = 1.591261E+03 VB = 0. WB = 2.594355E+01  
P = 0. Q = 9.594745E-04 R = 0.  
X = 6.366537E+03 Y = 0. Z = -3.000721E+04  
ALPHA = -3.971218E-03 GAMMA = 1.296048E-01 BETA = 0.  
HEIGHT = 3.000721E+04 VTRFPS = 1.591471E+03 ALPHAD = 8.045119E-05

THE TOTAL ANGLES (TRIM + PERTURBATION):

TALPHA = 9.340352E-01 TGAMMA = 1.296048E-01 TTHETA = 0.  
TFPHI = 0. TTHETA = 1.063640E+00 TPSI = 0.

THE OUTPUTS AT T = 5.00 SECONDS ARE:

PHI = 0. THETA = 1.571800E-01 PSI = 0.  
UB = 1.591147E+03 VB = 0. WB = 2.596649E+01  
P = 0. Q = 6.227530E-04 R = 0.  
X = 7.957948E+03 Y = 0. Z = -3.001124E+04  
ALPHA = -3.062427E-03 GAMMA = 1.602425E-01 BETA = 0.  
HEIGHT = 3.001124E+04 VTRFPS = 1.591359E+03 ALPHAD = 1.239335E-05

THE TOTAL ANGLES (TRIM + PERTURBATION):

TALPHA = 9.349440E-01 TGAMMA = 1.602425E-01 TTHETA = 0.  
TFPHI = 0. TTHETA = 1.095186E+00 TPSI = 0.

DOES THE USER WANT TO CONTINUE THE SIMULATION?

ENTER 0 IF SIMULATION ENDS.

ENTER 1 IF SIMULATION CONTINUES WITH THE SAME  
CONTROL SURFACE DEFLECTIONS.

ENTER 2 IF SIMULATION CONTINUES WITH NEW  
CONTROL SURFACE DEFLECTIONS.

ENTER 3 IF SIMULATION CONTINUES WITH NEW FORCES  
DUE TO THRUST VALUES.

ENTER 4 IF SIMULATION CONTINUES WITH BOTH NEW  
CONTROL SURFACE DEFLECTIONS AND NEW  
FORCES DUE TO THRUST.

ENTER #>

? 2

ENTER NEW FINAL SIMULATION TIME >

? 7.0

ENTER NEW SAMPLING TIME >

? 0.5

ENTER NEW CONTROL SURFACE DEFLECTIONS:

DELTA E DELTA A DELTA R >

? -10.0,0,0

DELTA F DELTA T DELTA C >

? 0,0,0

\*\*\*\*\*

COMMANDED CONTROL SURFACE DEFLECTIONS:

DELTA E = -1.000000E+01 DELTA A = 0. DELTA R = 0.

DELTA F = 0. DELTA T = 0. DELTA C = 0.  
\*\*\*\*\*

THE OUTPUTS AT T = 5.50 SECONDS ARE:

PHI = 0. THETA = 1.703249E+00 PSI = 0.  
UB = 1.589883E+03 VB = 0. WB = 3.117252E+01  
P = 0. Q = 4.067032E-02 R = 0.  
X = 8.753298E+03 Y = 0. Z = -3.001990E+04  
ALPHA = 1.852434E-01 GAMMA = 1.118006E+00 BETA = 0.  
HEIGHT = 3.001990E+04 VTRFPS = 1.590188E+03 ALPHAD = -5.796539E-03

THE TOTAL ANGLES (TRIM + PERTURBATION):

TALPHA = 1.123250E+00 TGAMMA = 1.118006E+00 TBETA = 0.  
TPHI = 0. TTHETA = 2.241256E+00 TPSI = 0.

THE OUTPUTS AT T = 6.00 SECONDS ARE:

PHI = 0. THETA = 2.462264E+00 PSI = 0.  
UB = 1.588287E+03 VB = 0. WB = 3.497711E+01  
P = 0. Q = 4.026444E-02 R = 0.  
X = 9.547696E+03 Y = 0. Z = -3.004244E+04  
ALPHA = 3.237298E-01 GAMMA = 2.138534E+00 BETA = 0.  
HEIGHT = 3.004244E+04 VTRFPS = 1.588670E+03 ALPHAD = -4.300306E-03

THE TOTAL ANGLES (TRIM + PERTURBATION):

TALPHA = 1.261736E+00 TGAMMA = 2.138534E+00 TBETA = 0.  
TPHI = 0. TTHETA = 3.400270E+00 TPSI = 0.

THE OUTPUTS AT T = 6.50 SECONDS ARE:

PHI = 0. THETA = 3.612220E+00 PSI = 0.  
UB = 1.586389E+03 VB = 0. WB = 3.770438E+01  
P = 0. Q = 4.002324E-02 R = 0.  
X = 1.034072E+04 Y = 0. Z = -3.007930E+04  
ALPHA = 4.237598E-01 GAMMA = 3.188460E+00 BETA = 0.  
HEIGHT = 3.007930E+04 VTRFPS = 1.586831E+03 ALPHAD = -3.070267E-03

THE TOTAL ANGLES (TRIM + PERTURBATION):

TALPHA = 1.361766E+00 TGAMMA = 3.188460E+00 TBETA = 0.  
TPHI = 0. TTHETA = 4.550276E+00 TPSI = 0.

THE OUTPUTS AT T = 7.00 SECONDS ARE:

PHI = 0. THETA = 4.755843E+00 PSI = 0.  
UB = 1.584187E+03 VB = 0. WB = 3.963559E+01  
P = 0. Q = 3.985751E-02 R = 0.  
X = 1.113193E+04 Y = 0. Z = -3.013079E+04  
ALPHA = 4.954742E-01 GAMMA = 4.260369E+00 BETA = 0.  
HEIGHT = 3.013079E+04 VTRFPS = 1.584673E+03 ALPHAD = -2.200380E-03

THE TOTAL ANGLES (TRIM + PERTURBATION):

TALPHA = 1.433481E+00 TGAMMA = 4.260369E+00 TBETA = 0.  
TPHI = 0. TTHETA = 5.693850E+00 TPSI = 0.

THE OUTPUTS AT T = 7.50 SECONDS ARE:

PHI = 0. THETA = 5.895095E+00 PSI = 0.  
UB = 1.581681E+03 VB = 0. WB = 4.098331E+01  
P = 0. Q = 3.962666E-02 R = 0.  
X = 1.192087E+04 Y = 0. Z = -3.019708E+04

ALPHA = 5.466607E-01 GAMMA = 5.348434E+00 BETA = 0.  
HEIGHT = 3.019708E+04 VTRFPS = 1.582190E+03 ALPHAD = -1.600524E-03

THE TOTAL ANGLES (TRIM + PERTURBATION):

TALPHA = 1.484667E+00 TGAMMA = 5.348434E+00 TBETA = 0.  
TPHI = 0. TTHETA = 6.833101E+00 TPSI = 0.

DOES THE USER WANT TO CONTINUE THE SIMULATION?

ENTER 0 IF SIMULATION ENDS.

ENTER 1 IF SIMULATION CONTINUES WITH THE SAME  
CONTROL SURFACE DEFLECTIONS.

ENTER 2 IF SIMULATION CONTINUES WITH NEW  
CONTROL SURFACE DEFLECTIONS.

ENTER 3 IF SIMULATION CONTINUES WITH NEW FORCES  
DUE TO THRUST VALUES.

ENTER 4 IF SIMULATION CONTINUES WITH BOTH NEW  
CONTROL SURFACE DEFLECTIONS AND NEW  
FORCES DUE TO THRUST.

ENTER #>

? 2

ENTER NEW FINAL SIMULATION TIME >

? 9.0

ENTER NEW SAMPLING TIME >

? 0.5

ENTER NEW CONTROL SURFACE DEFLECTIONS:

DELTA E DELTA A DELTA R >

? 0,5,0

DELTA F DELTA T DELTA C >

? 0,0,0

\*\*\*\*\*

COMMANDED CONTROL SURFACE DEFLECTIONS:

DELTA E = 0. DELTA A = 5.000000E+00 DELTA R = 0.

DELTA F = 0. DELTA T = 0. DELTA C = 0.

\*\*\*\*\*

THE OUTPUTS AT T = 8.00 SECONDS ARE:

PHI = -1.057936E-01 THETA = 5.901053E+00 PSI = 1.244022E-01  
UB = 1.580099E+03 VB = -2.287607E+00 WB = 3.687502E+01  
P = -3.944181E-03 Q = -5.539928E-04 R = 4.436074E-03  
X = 1.270799E+04 Y = 2.749679E-01 Z = -3.027205E+04  
ALPHA = 3.983940E-01 GAMMA = 5.502659E+00 BETA = -8.322300E-02  
HEIGHT = 3.027205E+04 VTRFPS = 1.580525E+03 ALPHAD = 4.417483E-03

THE TOTAL ANGLES (TRIM + PERTURBATION):

TALPHA = 1.336400E+00 TGAMMA = 5.502659E+00 TBETA = -8.322300E-02  
TPHI = -1.057936E-01 TTHETA = 6.839059E+00 TPSI = 1.244022E-01

THE OUTPUTS AT T = 8.50 SECONDS ARE:

PHI = -1.989566E-01 THETA = 5.890140E+00 PSI = 2.487845E-01  
UB = 1.578505E+03 VB = -4.186078E+00 WB = 3.382194E+01  
P = -3.522863E-03 Q = -2.484852E-04 R = 4.194383E-03  
X = 1.349413E+04 Y = 1.250917E+00 Z = -3.034848E+04  
ALPHA = 2.892193E-01 GAMMA = 5.600921E+00 BETA = -1.520653E-01  
HEIGHT = 3.034848E+04 VTRFPS = 1.578869E+03 ALPHAD = 3.211058E-03

THE TOTAL ANGLES (TRIM + PERTURBATION):  
TALPHA = 1.227226E+00 TGAMMA = 5.600921E+00 TBETA = -1.520653E-01  
TPHI = -1.989566E-01 TTHETA = 6.828146E+00 TPSI = 2.487845E-01

THE OUTPUTS AT T = 9.00 SECONDS ARE:

PHI = -2.816624E-01 THETA = 5.886945E+00 PSI = 3.670051E-01  
UR = 1.576894E+03 VR = -5.649249E+00 WR = 3.157795E+01  
P = -3.631460E-03 Q = -2.355208E-05 R = 4.006654E-03  
X = 1.427933E+04 Y = 3.070341E+00 Z = -3.042603E+04  
ALPHA = 2.091374E-01 GAMMA = 5.677807E+00 BETA = -2.052766E-01  
HEIGHT = 3.042603E+04 VTRFPS = 1.577209E+03 ALPHAD = 2.455374E-03

THE TOTAL ANGLES (TRIM + PERTURBATION):

TALPHA = 1.147144E+00 TGAMMA = 5.677807E+00 TBETA = -2.052766E-01  
TPHI = -2.816624E-01 TTHETA = 6.824951E+00 TPSI = 3.670051E-01

THE OUTPUTS AT T = 9.50 SECONDS ARE:

PHI = -3.565240E-01 THETA = 5.887429E+00 PSI = 4.804443E-01  
UR = 1.575244E+03 VR = -6.779127E+00 WR = 2.992809E+01  
P = -2.983431E-03 Q = 1.125403E-04 R = 3.862821E-03  
X = 1.506361E+04 Y = 5.841438E+00 Z = -3.050442E+04  
ALPHA = 1.492644E-01 GAMMA = 5.740164E+00 BETA = -2.473753E-01  
HEIGHT = 3.050442E+04 VTRFPS = 1.575504E+03 ALPHAD = 1.716483E-03

THE TOTAL ANGLES (TRIM + PERTURBATION):

TALPHA = 1.087271E+00 TGAMMA = 5.740164E+00 TBETA = -2.473753E-01  
TPHI = -3.565240E-01 TTHETA = 6.827435E+00 TPSI = 4.804443E-01

DOES THE USER WANT TO CONTINUE THE SIMULATION?

ENTER 0 IF SIMULATION ENDS.

ENTER 1 IF SIMULATION CONTINUES WITH THE SAME  
CONTROL SURFACE DEFLECTIONS.

ENTER 2 IF SIMULATION CONTINUES WITH NEW  
CONTROL SURFACE DEFLECTIONS.

ENTER 3 IF SIMULATION CONTINUES WITH NEW FORCES  
DUE TO THRUST VALUES.

ENTER 4 IF SIMULATION CONTINUES WITH BOTH NEW  
CONTROL SURFACE DEFLECTIONS AND NEW  
FORCES DUE TO THRUST.

ENTER #>

? 0

3.513 CP SECONDS EXECUTION TIME.

/BYE

UN=T841028 LOG OFF 13.29.21.

JSN=SCHQ SRU-S 15.219

TAF CONNECT TIME 00.22.33.

LOGGED OUT.

HOST DISCONNECTED CONTROL CHARACTER=(ESC)

ENTER INPUT TO CONNECT TO HOST



APPENDIX B

## Appendix B

### Coordinated Turn With Computational Delay

This appendix contains responses for the coordinated turn command system with a computational delay modelled in the system for the  $V_{EAS} = 60$  knots flight condition.

A delay in the time response can be modelled by the following block diagrams:

$$x(s) \rightarrow \boxed{e^{-sT}} \rightarrow y(s) \quad (B-1)$$

$$u(t) \rightarrow \boxed{\text{DELAY}} \rightarrow u(t+T_1) \quad (B-2)$$

where  $T_1$  is the computational delay factor to be implemented in the system. The idea of the computational delay is to model the amount of time allotted to computations in the digital computer and the time it takes the resulting electrical signal to reach the control inputs. The previous designs were based on instantaneous control which is not a realistic situation. The time response plots for  $T_1 = 0.02$  seconds are presented in Figures B-1a.-B-1g. It is evident from the time response plots, that the addition of the computational delay has destabilized the system. These results correspond well to what was expected from theory in that a delay destabilizes the plant. Further design efforts reduced the magnitude of the growing oscillations only.

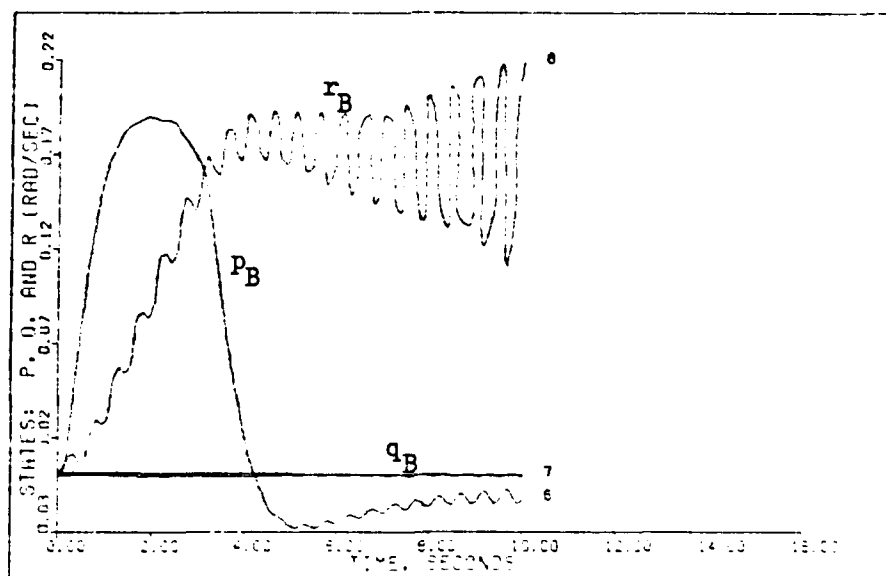


Figure B-1a. State Responses,  $p_B$ ,  $q_B$ , and  $r_B$ , for the Coordinated Turn Command System With Computational Delay ( $V_{EAS}=60$  knots)

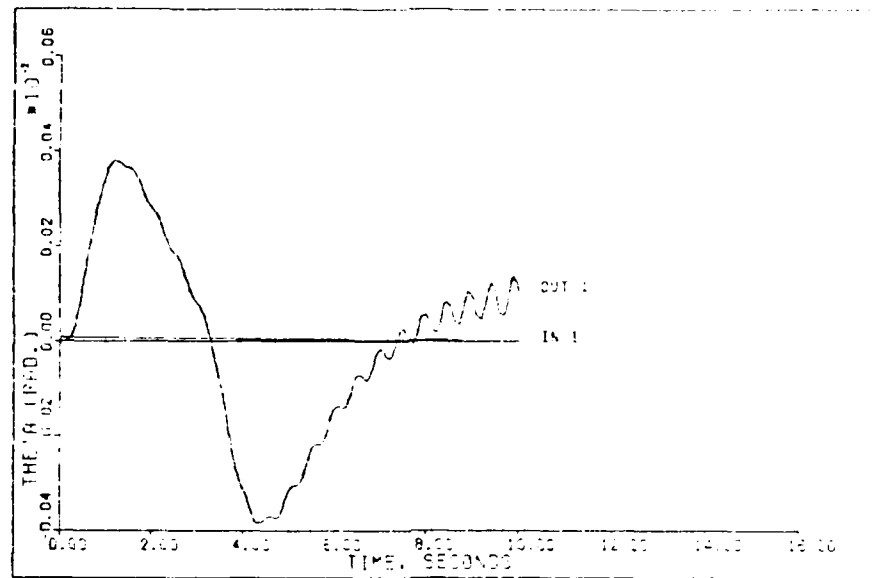


Figure B-1b. Output Response,  $\Theta$ , for the Coordinated Turn Command System With Computational Delay ( $V_{EAS} = 60$  knots)

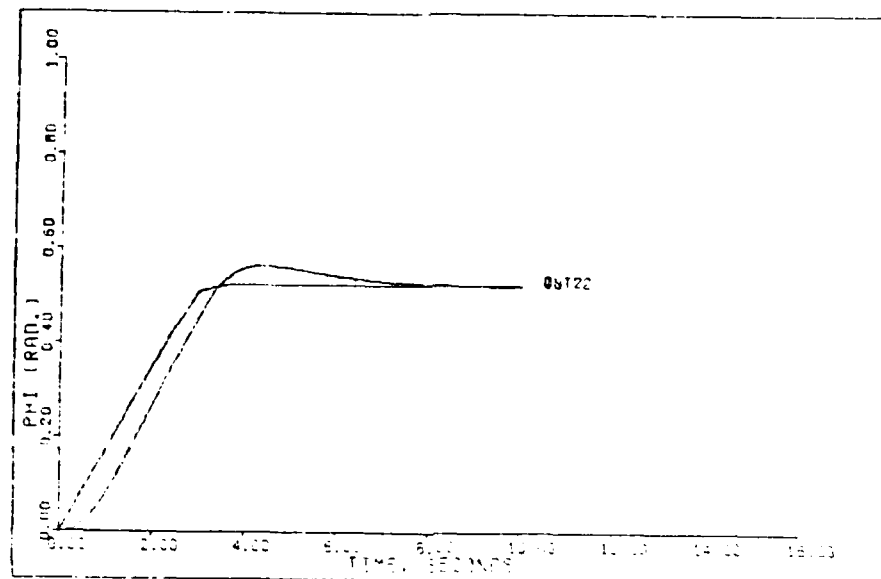


Figure B-1c. Output Response,  $\phi$ , for the Coordinated Turn Command System With Computational Delay ( $V_{EAS}=60$  knots)

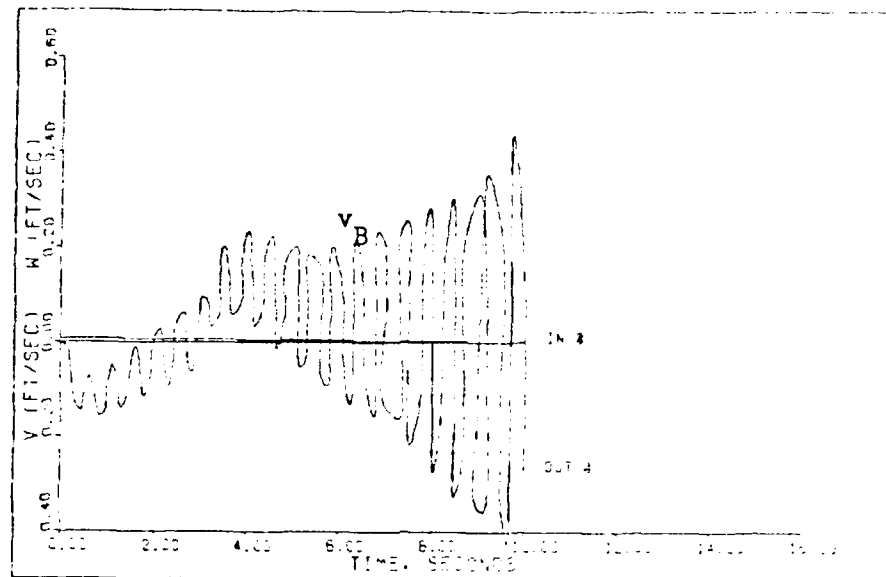


Figure B-1d. Output Responses,  $v_B$  and  $w_B$ , for the Coordinated Turn Command System with Computational Delay ( $V_{EAS}=60$  knots)

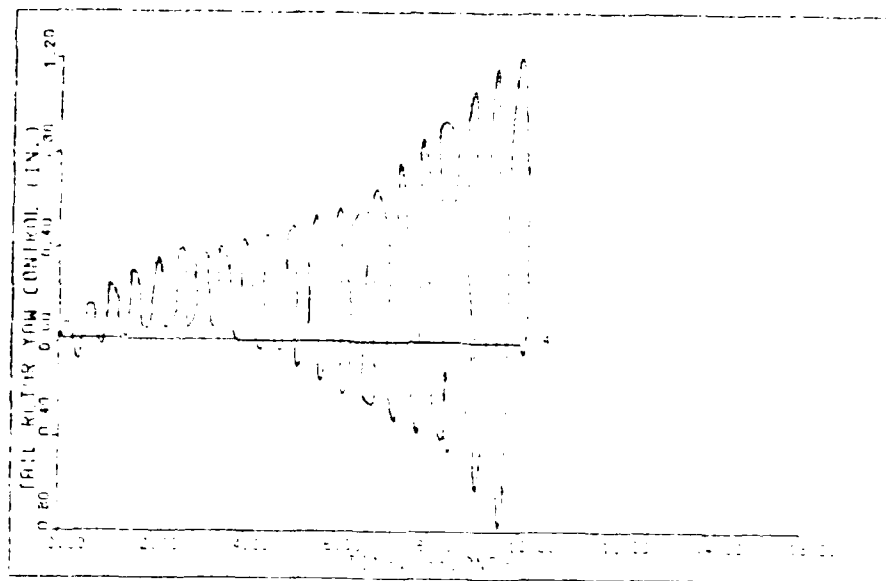


Figure B-1e. Cyclic Roll Control Response,  $\Delta\delta_a$ , for the Coordinated Turn Command System with Computational Delay ( $V_{EAS}=60$  knots)

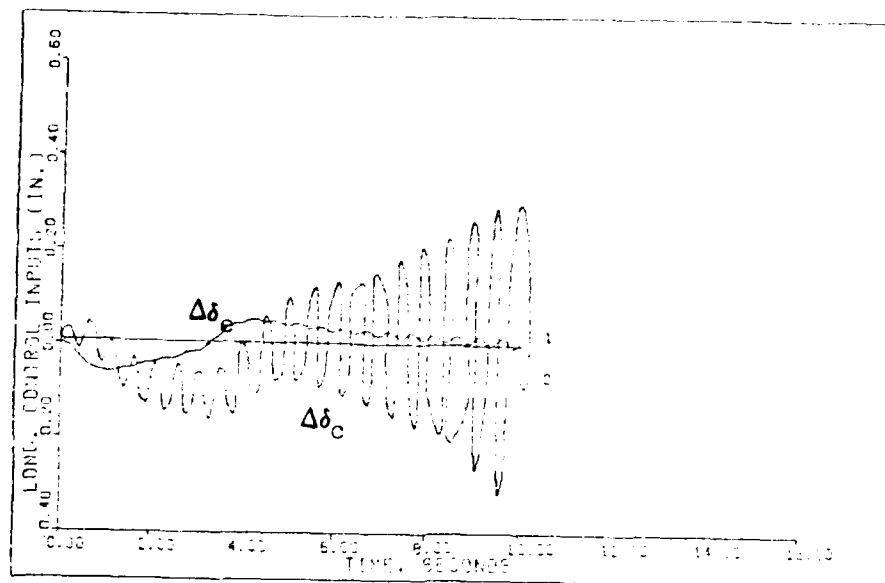


Figure B-1f. Longitudinal Control Surface Responses,  $\Delta\delta_e$  and  $\Delta\delta_c$ , for the Coordinated Turn Command System With Computational Delay ( $V_{EAS} = 60$  knots).

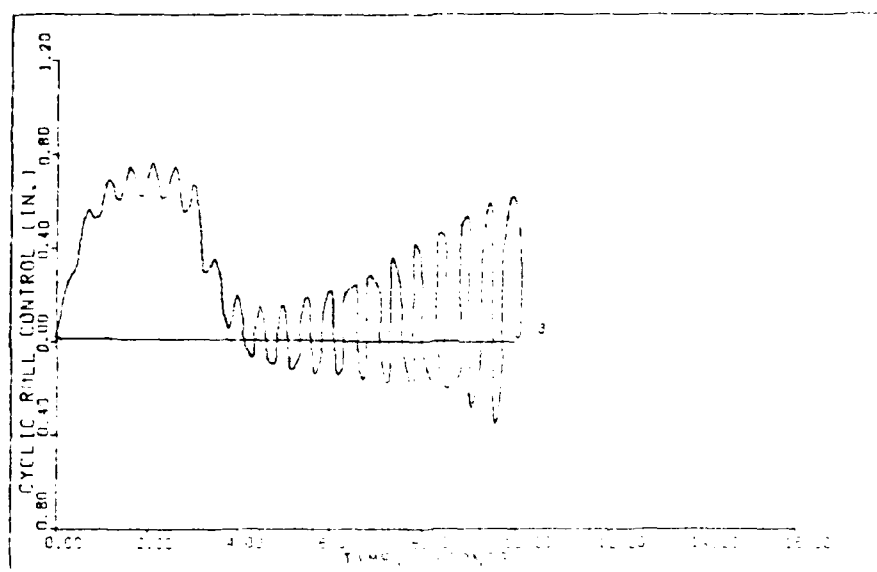


Figure B-1g. Tail Rotor Yaw Control Response,  $\Delta\delta_p$ , for the Coordinated Turn Command System With Computational Delay ( $V_{EAS} = 60$  knots)

## VITA

Brian Harold Mayhew was born on 17 May 1960 at Dyess Air Force Base, Texas. He graduated from high school in Peru, New York in 1978 and attended Washington University in St. Louis, Missouri from which he received a Bachelor of Science of Systems Science and Mathematics in May 1982. Upon graduation, he received a commission in the USAF through the ROTC program. After graduation, he entered the School of Engineering, Air Force Institute of Technology, in June 1982. His next assignment is with the Simulation/Validation Branch, Foreign Technology Division, Wright-Patterson AFB, Ohio.

Permanent Address: 7 Deepdale Rd.

Plattsburgh, New York 12901

UNCLASSIFIED

SECURITY CLASSIFICATION OF THIS PAGE

## REPORT DOCUMENTATION PAGE

1. REPORT SECURITY CLASSIFICATION UNCLASSIFIED		1d. RESTRICTIVE MARKINGS	
2a. SECURITY CLASSIFICATION AUTHORITY		3. DISTRIBUTION/AVAILABILITY OF REPORT Approved for public release; distribution unlimited.	
2b. DECLASSIFICATION/DOWNGRADING SCHEDULE			
4. PERFORMING ORGANIZATION REPORT NUMBER(S) AFIT/GE/EE/84M-6		5. MONITORING ORGANIZATION REPORT NUMBER(S)	
6a. NAME OF PERFORMING ORGANIZATION Air Force Institute of Technology	6b. OFFICE SYMBOL (If applicable) AFIT/EN	7a. NAME OF MONITORING ORGANIZATION	
6c. ADDRESS (City, State and ZIP Code) Wright-Patterson AFB, Ohio 45433		7b. ADDRESS (City, State and ZIP Code)	
8a. NAME OF FUNDING/SPONSORING ORGANIZATION E. Robert Lemble Aeromechanics Laboratory	8b. OFFICE SYMBOL (If applicable)	9. PROCUREMENT INSTRUMENT IDENTIFICATION NUMBER	
8c. ADDRESS (City, State and ZIP Code) Research & Technology Laboratories U.S. Army Aviation R&D Command Ames Research Center Moffett Field, CA 94035		10. SOURCE OF FUNDING NOS.	
11. TITLE (Include Security Classification) MULTIVARIABLE DIGITAL CONTROL LAWS FOR THE UH-60A BLACK HAWK HELICOPTER (UNCLASSIFIED)		PROGRAM ELEMENT NO.	PROJECT NO.
		TASK NO.	WORK UNIT NO.
12. PERSONAL AUTHOR(S) Brian Harold Mayhew, 2Lt, USAF			
13a. TYPE OF REPORT MS Thesis	13b. TIME COVERED FROM Mar 83 TO Mar 84	14. DATE OF REPORT (Yr., Mo., Day) 1984, March 14	15. PAGE COUNT 232
16. SUPPLEMENTARY NOTATION Approved for public release. LAW AFM 184-17. BYN/E. WOLVER Dept. for Research and Professional Development Air Force Institute of Technology (AFIT) Wright-Patterson AFB, OH 45433			
17. COSATI CODES		18. SUBJECT TERMS (Continue on reverse if necessary)	
FIELD	GROUP	SUB. GR.	
19. ABSTRACT (Continue on reverse if necessary and identify by block number) This thesis investigates the application of multivariable design techniques developed by Professor Brian Porter of the University of Salford, England to design digital control laws for the UH-60A Black Hawk helicopter. In the study, designs were developed for five longitudinally and laterally, strongly coupled plants with control inputs of cyclic roll control, cyclic pitch control, collective lift control, and tail rotor yaw control. An improved computer-aided design package called "MULTI" was used in refining the control laws. Separate controllers were developed to perform three flight maneuvers. The maneuvers performed were a coordinated turn, a yaw rate response, and a vertical rate response. Since each maneuver is flown at a different airspeed, a uniquely specified linearized plant model was required. The methods employed to obtain a design are presented along with the evaluations of the final control laws. After successful designs of the individual control laws for the three maneuvers were developed, tests were performed to find a single controller to			
20. DISTRIBUTION/AVAILABILITY OF ABSTRACT UNCLASSIFIED/UNLIMITED <input checked="" type="checkbox"/> SAME AS RPT. <input type="checkbox"/> DTIC USERS <input type="checkbox"/>		21. ABSTRACT SECURITY CLASSIFICATION UNCLASSIFIED	
22a. NAME OF RESPONSIBLE INDIVIDUAL Dr. J. J. D'Azzo		22b. TELEPHONE NUMBER (Include Area Code) (513) 255-2024	22c. OFFICE SYMBOL AFIT/EN



UNCLASSIFIED

SECURITY CLASSIFICATION OF THIS PAGE

19. (cont.)

perform each maneuver for its applicable flight conditions. Finally, the evaluation of the robustness of the single controllers is presented.

UNCLASSIFIED

SECURITY CLASSIFICATION OF THIS PAGE

END

FILMED

6-84

DTIC